

# Journal of Engineering and Technology for Industrial Applications



**ISSN 2447-0228**

**August 2021**

**Volume 07 / No 30**

**Editor-in-Chief: J. C. Leite**

**[www.itegam-jetia.org](http://www.itegam-jetia.org)**



O **ITEGAM-JETIA: Journal of Engineering and Technology for Industrial Applications** is a publication of the Galileo Institute of Technology and Education of the Amazon (ITEGAM), located in the city of Manaus since 2008. JETIA publishes original scientific articles covering all aspects of engineering. Our goal is the dissemination of research original, useful and relevant presenting new knowledge on theoretical or practical aspects of methodologies and methods used in engineering or leading to improvements in professional practice. All the conclusions presented in the articles It should be state-of-the-art and supported by current rigorous analysis and balanced assessment. Public magazine scientific and technological research articles, review articles and case studies.

**JETIA** will address topics from the following areas of knowledge: Mechanical Engineering, Civil Engineering, Materials and Mineralogy, Geosciences, Environment, Information and Decision Systems, Processes and Energy, Electrical and Automation, Mechatronics, Biotechnology and other Engineering related areas.

**Publication Information:**

**ITEGAM-JETIA** (ISSN 2447-0228), (online) is published by Galileo Institute of Technology and Education of the Amazon on a every two months (February, April, June, August, October and December).

**Contact information:**

Web page: [www.itegam-jetia.org](http://www.itegam-jetia.org)

Email: [editor@itegam-jetia.org](mailto:editor@itegam-jetia.org)

Galileo Institute of Technology and Education of the Amazon (ITEGAM).

Joaquim Nabuco Avenue, No. 1950. Center. Manaus, Amazonas. Brazil.

Zip Code: 69020-031. Phone: (92) 3584-6145.

**Copyright 2014. Galileo Institute of Technology and Education of the Amazon (ITEGAM)**

The total or partial reproduction of texts related to articles is allowed, only if the source is properly cited. The concepts and opinions expressed in the articles are the sole responsibility of the authors.

**Previous Notice**

All statements, methods, instructions and ideas are the sole responsibility of the authors and do not necessarily represent the view of ITEGAM -JETIA. The publisher is not responsible for any damage and / or damage to the use of the contents of this journal. The concepts and opinions expressed in the articles are the sole responsibility of the authors.

**Directory**

Members of the ITEGAM Editorial Center - Journal of Engineering and Technology for Industrial Applications (ITEGAM-JETIA) of the Galileo Institute of Technology and Education of the Amazon (ITEGAM). Manaus-Amazonas, Brazil.

**Jandecy Cabral Leite**, CEO and Editorial Editor-in-Chief

**Ivan Leandro Rodriguez Rico**, Editorial Assistant

**Ricardo Silva Parente**, Information Technology Assistant

ITEGAM-JETIA. v.7, n.30. August of 2021. Manaus - Amazonas, Brazil. ISSN 2447-0228 (ONLINE)  
<https://www.itegam-jetia.org>

## SUMMARY

- FINANCIAL AND ENVIRONMENTAL EFFICIENCY ASSESSMENT MODEL OF SEVEN IRANIAN CHEMICAL INDUSTRIES** 4  
*Malek Hassanpour*
- DISPERSION AND TURBULENCE: A CLOSE RELATIONSHIP UNVEILED BY MEANS OF STATE FUNCTION** 18  
*Alfredo Jose Constain, Gina Peña Olarte and Carlos Peña Guzman*
- DETECTION OF PLANT LEAF DISEASES USING RECENT PROGRESS IN DEEP LEARNING-BASED IDENTIFICATION TECHNIQUES** 29  
*Jency Rubia J and Babitha Lincy R*
- DESIGN AND ANALYSIS OF QCA ADDER CIRCUITS FOR EFFICIENT COMPUTATION** 37  
*Jency Rubia J and Babitha Lincy R*
- DETERMINATION OF NATURALLY OCCURRING RADIOACTIVE MATERIALS-NORM (RA-226, RA-228) IN SYNTHETIC FLOWBACK DEVELOPED AT LABORATORY SCALE FROM ROCKS OF THE LA LUNA-1 WELL, COLOMBIA, AND BENCHMARKING WITH MARCELLUS AND EAGLE FORD SHALE PLAYS** 45  
*Jenny Paola Rueda, Javier Perez, Alvaro Villar Garcia and Jose Manuel Usuriaga*
- ISOLATION, MOLECULAR IDENTIFICATION AND ENZYME ACTIVITY OF AMYLASE PRODUCING THERMOPHILIC BACTERIA FROM HOT SPRINGS** 62  
*Edy Fachrial, Vincentia Ade Rizky, Harmileni, I Nyoman Ehrich Lister, Chrismis Novalinda Ginting, Titania T Nugroho and Saryono*
- CATCHMENT SCALE ASSESSMENT OF POLLUTION THREATS TO WATER QUALITY IN RELATION TO PREVALENCE OF WATER-BORNE DISEASES IN SOME COMMUNITIES IN Omu-ARAN, NIGERIA** 69  
*Omotoso Toyin and O. Ibitoye*
- LIFE-CYCLE COST ANALYSIS (LCCA) COMPARISON OF PAVEMENTS (FLEXIBLE, RIGID AND RIGID-ADMIXED WITH COW BONE ASH)** 75  
*Ariyo Adanikin, Funsho Falade, Adewale Olutaiwo, Temi Ajibade and Itunuoluwa Adeoye*





## FINANCIAL AND ENVIRONMENTAL EFFICIENCY ASSESSMENT MODEL OF SEVEN IRANIAN CHEMICAL INDUSTRIES

Malek Hassanpour\*<sup>1</sup>

<sup>1</sup> Department of Environmental science, UCS, Osmania University, Telangana State, India.

<sup>1</sup> <http://orcid.org/0000-0001-9662-0623>

Email: \*malek.hassanpour@yahoo.com

### ARTICLE INFO

#### Article History

Received: July 16<sup>th</sup>, 2021

Accepted: August 23<sup>th</sup>, 2021

Published: August 31<sup>th</sup>, 2021

#### Keywords:

Financial assessment,  
Industries technologies,  
EIA,  
Screening of projects,  
MCDM models.

### ABSTRACT

The chemical industries commercially emerged to be the type of prominent techniques in handling and generating a variety of valuable products. The present research included the description of technologies, energy and materials streams, facilities exploited in generation lines of industries. The main source of the present study refers to the screening of industrial projects in project identification steps of the Environmental Impact Assessment (EIA) plan in Iran. The initial data of assessment estimated by the evaluator team was taken into further processing in both environmental and financial issues via the Data Envelopment Analysis (DEA) model. The conventional DEA model was integrated with 4 weighing systems of Multi-Criteria Decision-Making (MCDM) models to assess the performance of seven Iranian chemical industries in both environmental and currency issues empirically. The findings classified the industries in financial and environmental efficiency scores. The conclusion of the research can be summarized in developing two types of classification based on the screening step of project identification and with good compliance between findings in the integration of DEA-weighting systems.



Copyright ©2016 by authors and Galileo Institute of Technology and Education of the Amazon (ITEGAM). This work is licensed under the Creative Commons Attribution International License (CC BY 4.0).

### I. INTRODUCTION

Energy is one of the most expensive inputs to industries worldwide. But energy prices have been somewhat low until a few years ago due to decline the government subsidies for energy stream have been increased in Iran. Now, with the lack of government's targeted subsidies and price liberalization, energy prices are expected to rise sharply. This increase in price has led to an increase in production costs in industries, especially industries with high energy consumption, such as steel, automobiles, cement, petrochemicals, etc. [1].

The purpose of energy analysis is to replace high energy inputs with renewable sources and lower energy consumption alternatives. Regular measurement of efficiency will lead to the proper exploitation of resources and prevent an unbalanced increase in energy consumption. With the increase in energy consumption in the industrial sector, various indicators are used, the most important of which is energy efficiency, which is equal to the ratio of total output energy to total input energy. Added net

energy equal to the energy produced minus the input energy. Energy efficiency is equivalent to dividing the quantity of product generated by the total input energy or the quantity of product released per unit of energy consumed [2].

Efficiency means creating the least amount of waste and spending the least amount of money while maintaining quantity and quality. Energy efficiency refers to the use of less energy to produce a certain amount of goods or services. Performance is measured based on parametric and non-parametric variables or a combination of them. The parametric method is based on econometric models (financial statements, financial ratios, and a variety of models defined), in this case, the production function is defined by several independent variables, and then using observational data, the coefficients of the production function and the production function itself are estimated, and therefore it is used to determine efficiency [3]. Although the description of non-parametric methods is out of the framework sought by the present study but the main definition falls into models configured with statistical and mathematical relationships with certain variables.



The DEA method is a mathematical programming method to evaluate the performance of decision-making units. This method evaluates decision-making units with an input-output approach. In this method, decision-making units are divided into two groups of efficient and inefficient units (efficient units are units whose efficiency score is relatively equal to one). High performance is a goal that organizations pursue. A logical and scientific method of performance appraisal can not only effectively evaluate the organization's past performance, but also lead to decisions made to improve and achieve the desired performance position in the future. The DEA method uses mathematical programming and it is possible to use a large number of variables and there is no limit to the number of inputs and outputs available in other methods [4][5].

In industry, if producers are able to generate a certain amount of product with a minimum amount of factors of production or the maximum possible amount of different products with a certain amount of factors of production, other manufacturers of this industry will be efficient if to be able to act like these manufacturers. The DEA model is a method to evaluate the efficiency of homogeneous decision-making units. Units in which identical inputs are used to achieve identical outputs. In this method, the efficiency of a decision-making unit can be compared with itself (individually) over time and with other alternatives too. Therefore, the decision-making unit can be considered time and growth rates. It identified it over different time periods and then is compared the performance of the decision-making unit at different times by examining growth rate. The importance of this study refers to select a homogenous group of 7 chemical industries to be assessed by the DEA model in both financial and environmental reports [6].

The objectives devised to achieve by the current study refer to (1) classification of 7 chemical industries based on financial and environmental issues (2) determining the values of weights in weighing systems for all variables (3) ranking of 7 industries based on efficiency score in both financial and environmental issues (4) conducting a sensitivity analysis to prove the precision and accuracy applied in computations. A comparison between the classification of industries in both environmental and financial issues can fill the existing gap in science for either equal or different classes exhibited. To the best of my knowledge, this is the first research of efficiency assessment based on the screening step of chemical industries projects across Iran. Also, this study has taken into consideration the financial performance assessment based on recent prices of materials and energy streams in the market of Tehran, Iran.

## II. LITERATURE REVIEW

The research introduced a new DEA model to select the best supplier consist of 4 inputs, 3 outputs, and 1 undesirable output. The results of the research were about efficiencies of aggregate, overall, and bundle in the case of sustainability of suppliers [7]. The efficiency of greenhouse farmers has been assessed via the slack-based DEA model in the sultanate, Oman. The results proved the inefficiency of 79% of alternatives due to a huge quantity of energy consumption. To improve the efficiency level has been recommended to confer subside of government organizations along with water consumption regulations [8]. The loyalty and intellectual capital of staff have been investigated via DEA-Principal component analysis for distinguishing the efficiency of organizations with regard to 3 inputs and one output variable. The ranking of alternatives ended up in the classification of them along with a sensitivity analysis to prove the precision and accuracy in

findings [9]. The two-stage DEA model configured with fuzzy ambient has been used for 15 ammonia-manufacturing with a list of inputs (4 variables), outputs (3 variables), and undesirable outputs (2 variables). The minimum and maximum efficiency scores reported between 0.45-1 respectively [10].

The energy and carbon (for 4 different fuels) efficiency scrutinized via radial chance-constrained DEA model in 3 regions (18 states) of china from 2013-2017. The high-quality fuel consumption generated efficient transportation performance and vice versa. In the performance assessment of regions, east china reported dominance over central china [11]. To assess the performance of 28 banking systems of Iran utilized the dynamic DEA model during 2018-2019. By the way, lots of financial indicators have been taken into attention to find the efficiency score. The efficiency score has been released between 0.6245- 1 [12]. To assess the energy efficiency of agricultural products (maize) an integrated DEA-CCR-SBM model assigned to rank the alternatives in Pakistan. The efficiency score expressed to be around 59.67% [13].

The government of China tried to handle and mitigate the carbon emissions and introduced a DEA model of integrated cooperative game data to assess the performance of units in provinces. The obtained results proved that over ten percent's of total emissions allocated for 2 provinces and 5 sub-industries [14]. The 18 liquor manufactories of china have been assessed based on two models of DEA-CCR and DEA-BCC and an integrated model of both from 2016 to 2018. The methodology of research encompassed labor efficiency, Wastewater treatment efficiency, Poverty alleviation efficiency, Revenue efficiency, Net profit efficiency, and Intangible assets efficiency. The minimum and maximum efficiency scores reported being around 0.1848-1 respectively [15]. The financial assessment of 44 Iranian cement industries has been carried out via the regional DEA model, Anderson Peterson method along with a regression analysis from 2012-2016. The industries classified from the highest efficiency to the lowest one [16]. The Energy (E1), Economic (E2), Environmental (E3), and efficiency in 26 enrich nations of the world has been scrutinized via both the traditional DEA model and bargaining game cross-efficiency DEA approach regarding lots of variables from 2015 to 2017. The findings of performance analysis in currency reported to be medium around 0.77, 0.8, and 0.26 for E1 to E3 with various efficiency levels for each country respectively [17].

The sustainability of 353 marine cage lobsters has been investigated using a material balance principle-based DEA model by an initial matrix of one output and 3 input variables in Vietnam. The findings emphasized reducing environmental costs to get better performance of units investigated [18]. To assess the energy, economic and environmental performance in OECD countries (30 nations) applied the non-radial DEA model. The research classified the countries for 3 classes of mentioned cases by conferring certain scores for nations individually [19]. The studies of the author classified 405 Iranian industries based on the energy stream (5 main criteria of the number of employees, water, fuel, the power consumed, land area occupied by each industry) and material flow introduced into industrial cycles. It used an integrated model of DEA- Additive Ratio ASsessment (ARAS) to classify the industries [6]. Also, the studies of the author developed to classify the same industries based on financial assessment via conventional DEA model united with 4 weighing systems of MCDM models. The energy stream assumed as input variables and sold products as revenue in this regard.

### III. METHODOLOGY

The data were collected from the database of both the Iranian environment protection agency and the Iranian industries organization initially. The original resource of data refers to the screening step of project identification in the EIA plan [20, 21]. Then the processing of initial data has been accomplished in conventional DEA connected to weighing systems of MCDM. To calculate the energy stream (number of stuff, water, fuel, power consumed) in industries was used a period of 300 working days per year. Figure 1 displays the evaluation steps of EIA and followed work for current research.

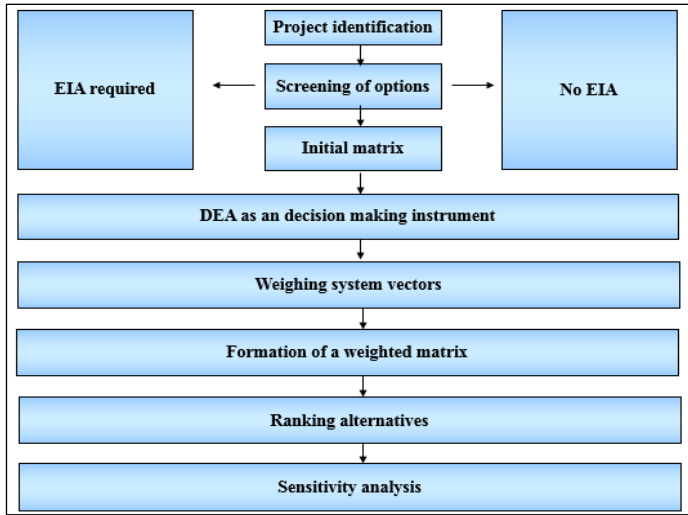


Figure 1: The evaluation steps of EIA and followed work for current research.

Source: Author, (2021).

#### III.1 WEIGHING SYSTEM OF FRIEDMAN TEST

The Friedman test is a non-parametric statistical test employed to compare the central indicators of several societies. This test is similar to a one-way analysis of variance performed in a non-parametric environment. An American economist first studied such a method in 1937. First of all, it is better to determine how the Friedman test works and its test statistics must be determined. To perform this test, an information table is considered, then the Friedman test statistic is calculated based on the rank of the values in each row with weights of the column. Thus this test is widely used in "complete block designs". The weights of the variables are calculated based on the values entered in the SPSS worksheet. Note that the rank of each value is determined by the values in the same row [22, 23]. To calculate the values of weights by Friedman test was used the SPSS software.

#### III.2 ENTROPY SHANNON

Shannon entropy method has been used as one of the most famous methods for calculating the weights of criteria. In information theory, entropy is the measurement of the amount of information needed to describe a random variable. First, we form the decision matrix. In the following, we normalize the matrix of data that is called each normalized drive  $p_{ij}$ . Normalization is by dividing the value of each column by the sum of the columns. The entropy of  $E_j$  is calculated as follows and  $k$  as a constant value holds the value of  $E_j$  between 0 and 1. A rise in Shannon entropy increases uncertainty and decreases knowledge of random variable. Another interesting aspect of Shannon entropy is its maximum

entropy property for uniform distribution. Next, the value of  $d_j$  (degree of deviation) is calculated, which states how much relevant information ( $d_j$ ) provides the decision-maker with useful information for decision making. The closer the measured values of the index are to each other, the more likely it is that competing options will not differ much in terms of that index. Therefore, the role of that indicator in decision making should be reduced equally. Then the value of weight ( $W_j$ ) is calculated for each criterion. In fact, the standard weight ( $W_j$ ) is equal to each  $d_j$  divided by the total number of  $d_j$ s [24].

$$P_{ij} = \frac{X_{ij}}{\sum_{i=1}^m X_{ij}} \quad j = 1, \dots, n \quad (1)$$

$$E_j = -k \sum_{i=1}^m P_{ij} \times \ln P_{ij} \quad i = 1, 2, \dots, m \quad (2)$$

$$k = \frac{1}{\ln m} \quad (3)$$

$$d_j = 1 - E_j \quad (4)$$

$$W_j = \frac{d_j}{\sum d_j} \quad (5)$$

#### III.3 WEIGHING SYSTEM OF CRITIC

In the CRITIC method, the importance of criteria is based on the internal correlation of criteria. It is a very convenient and practical method for determining the weight of criteria. The first step is to form a decision matrix. A decision matrix is a matrix in which there is an option in each row and a criterion in each column. This matrix contains  $m$  options and  $n$  criteria and is generally written as follows: Equation 6 is used to measure the correlation of data. Equation 7 is used to determine the initial weight of the criteria. Finally, the final weights of the criteria are determined using Equation 8 in a linear manner. In this way, the weight of each criterion is calculated with the same decision matrix of data and according to the data scatter and correlation. In this method, unlike the entropy method, only data scatter is not the decision criterion. In determining the final weights of the criteria, the sum of the weights of the criteria will be 1 because it is calculated by the linear method [25]. The symbol of  $\sigma_j$  denotes the standard deviation.

$$r_{ij} = \frac{X_{ij} - \min(X_{ij})}{\max(X_{ij}) - \min(X_{ij})} \quad (6)$$

$$C_j = \sigma_j \sum_{j=1}^m (1 - r_{ij}) \quad (7)$$

$$W_j = \frac{C_j}{\sum_{j=1}^m C_j} \quad (8)$$

#### III.4 WEIGHING SYSTEM OF AHP

In this method after making the matrix of data, it was used the multiplication of the existing values ( $a_{ij}$ ) in rows each other and division of inverse of the number of alternatives ( $1/k$ ). Finally, using the arithmetic mean ( $p_{ij}$ ) was provided the values of weights for criteria [26].

$$X_{ij} = \left( \prod_{l=1}^k a_{ij}^l \right)^{1/k}, \quad i = 1, 2, \dots, K \quad i, j = 1, 2, \dots, n, i \neq j \quad (9)$$

$$P_{ij} = \frac{X_{ij}}{\sum_{i=1}^m X_{ij}} \quad j = 1, \dots, n \quad (10)$$

### III.5 CONVENTIONAL DEA

To estimate the performance of industries by DEA model, it was employed inputs (water, fuel, the power consumed, and the number of staff), and outputs variables (products of industries based on nominal capacity) in the currency for the financial assessment. The vector of weights assigned to release the productivity of industries and then the highest productivity was assumed as benchmarking value and was estimated the efficiency score. But in the environmental issue, we have encountered quantities reported in various dimensions. Therefore the DEA model was integrated with the ARAS model to find the efficiency score. The reason for uniting traditional DEA with the ARAS model refers to the possibility of normalization of criteria in various dimensions. First, normalization was conducted according to equation 11. Then, it was assigned the vectors of weights according to equation 12. The division of weighted outputs to weighted inputs made the framework of efficiency assessment in environmental issue. The final weights were obtained according to equation 14 [6].

$$p_{ij} = \frac{X_{ij}}{\sum_{i=1}^m X_{ij}} \quad (11)$$

$$\tilde{i} = p_{ij} \times W_j, \quad i = o, m \quad (12)$$

$$S_i = \sum_{j=1}^n \text{normalized values of } X_{ij}, \quad i = o, m \quad (13)$$

$$DEA = \frac{S_i \text{ output}}{S_i \text{ input}} \quad (14)$$

## IV. RESULTS AND DISCUSSION

### IV.1 ELECTROSTATIC COATING

The basis of electrostatic coating refers to the coverage of the dye on the desired surfaces by the electric field between the dye

powder sprayer and the desired surfaces. Applications of this method comprised in the coating of metal and plastic parts, steel and cast iron pipes and driving signals, industrial machinery, electrical appliances, and in the body of car parts. The main disadvantages of this method can be mentioned difficulties in creating coatings above 200 microns and long coating time. Coverage includes the following steps, respectively: (1) Preparation of surfaces; (1.1) De-greasing: At this stage, the desired metal surfaces are prepared for coating. These operations are de-greasing, which is done by immersing the relevant part of the coating agent or the degreasing agent. Depending on the type of fat, the fat decomposition method may be performed by hydrocarbon solvents such as trichloroethylene, perchloroethylene, or petroleum. Then solvents are then removed by heating the surface. It can be employed some chemical compounds such as sulfonic acid, detergents, and alkaline solutions in this regard (1.2) De-colorization; Decolonization of metal surfaces can be done physically and chemically by immersing the part in sulfuric acid or hydrochloric acid or phosphoric acid. (1.3) Surface preparation: Depending on the type of surface, the surface is made resistant to corrosion by immersing in a chemical bath, a layer and a thin film of chemicals are placed on them. for example on steel, iron, and phosphate, or iron phosphate, on zinc metal, zinc phosphate or a layer of chromium, or reaction with chromic acid or phosphoric acid covers thin layers. (2) Washing and drying: To remove excess material from the metal surface, it is washed with water and then is dried in a furnace. In direct flame furnaces, the temperature generally is 150 to 170°C. (3) Electrostatic coating: By creating an electric field of 30 to 90 kV between the dye powder spray system and the desired plate for ionizing the air between the acid gun and the dye powder plate. The coating is accomplished by ionic bombardment on the plate. (4) Baking: The coated parts are heated to 200°C for more strength and for 10 to 20 minutes withstand to a temperature of around 120°C. (5) Cooling: The final stage of this operation is cooling, it is naturally or forcibly cooled by a stream of cold air. The products of this process is a variety of coatings, epoxy, polyester, and acrylic with a thickness of 30 to 500 microns on metal surfaces. Figure 2 shows the layout of units of the electrostatic coating industry. Table 1 shows the annual requirements of industries of electrostatic coating (nominal capacity of 81000\*).

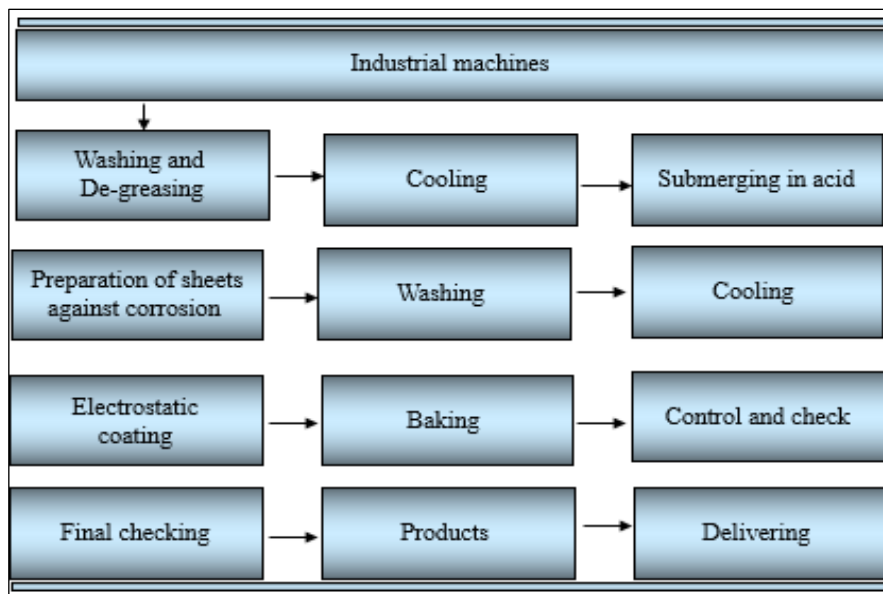


Figure 2: The layout of units of the electrostatic coating industry.  
Source: Author, (2021).



Table 1: The annual requirements of industries of electrostatic coating (nominal capacity of 81000\*).

The materials and equipment	Total annual rates
<b>Equipment and devices</b>	
A galvanized tank for solvent aeration of about 650 liters, and 100-liters steel tank for washing	1 series
An electrostatic coating line with a capacity of 300 m <sup>2</sup> /day, including an electric field generator and spray system	2 series
Heating oven with energy consumption approximately 8000 kcal per hour	1 machine
A conveyor belt (30×2 m <sup>2</sup> )	1 No
A laboratory	1 No
<b>Materials demands</b>	
De-greasing solvents (1 and 1 diethyl Chloroethane)	1000 liters
Petroleum	1000 liters
Epoxy resin	7500 kg
Polyester resin	14 tones
<b>Products</b>	
Coatings, epoxy, polyester, and acrylics 30 to 500 microns thick on metal surfaces	81000*
<b>Employees</b>	
Staff	16 persons
<b>Energy consumption</b>	
Required water	18 m <sup>3</sup> /day
Power	173 kW/day
Required fuel (Stoves)	4 Giga Joule/day
<b>Required land and landscaping</b>	
Required land	2200 m <sup>2</sup>
Construction of infrastructure (Buildings)	615 m <sup>2</sup>
* Thickness of coating 30-500 micron per 1 m <sup>2</sup> ; The fee of the electrostatic coating was assumed for each piece (financial issue); The metal pieces consists of 1 m <sup>2</sup> with 1 ton in weight like industrial machines (environmental issue)	

Source: Author, (2021).

#### IV.2 ACIDIC WATER 28% AND DISTILLED WATER

Raw water, which is the same as piped water in the city with a hardness of 300 ppm, enters the two distilled water production machines. Then raw water is converted to distilled water of 20 ppm after passing through the resin columns. The distilled water, then enter into tank number one, which is interpreted as a base with a length of 2 meters, and after controlling some of it, it is transferred to the outlet valves through a pipe and is packed in plastic bottles, ready for industrial use, and the rest is directed by the valves to tank number 3 to prepare acidic water. In addition, after each control, if the water concentration is more than twenty ppm the column needs to be regenerated, which is done by NaCl. To prepare

acidic water, sulfuric acid (98%) is transferred from tank 2 to tank 3 at the specified percentage. First, distilled water enters the tank and then acid enters. Because this tank is equipped with a stirrer, it is thoroughly mixed and acidic water is prepared and directed to tank No. 4, and after being controlled by a valve, it is directed to the acid water outlet valves to fill polyethylene bottles. Tank number one made of galvanized material, tank number 2 made of polyethylene (PE) and tank number 3 is of stainless steel 316. Figure 3 displays the layout of units of acidic water 28% and distilled water. Table 2 displays the annual requirements of industries of acidic water 28% and distilled water (nominal capacity of 600 and 1125 m<sup>3</sup> or tones).

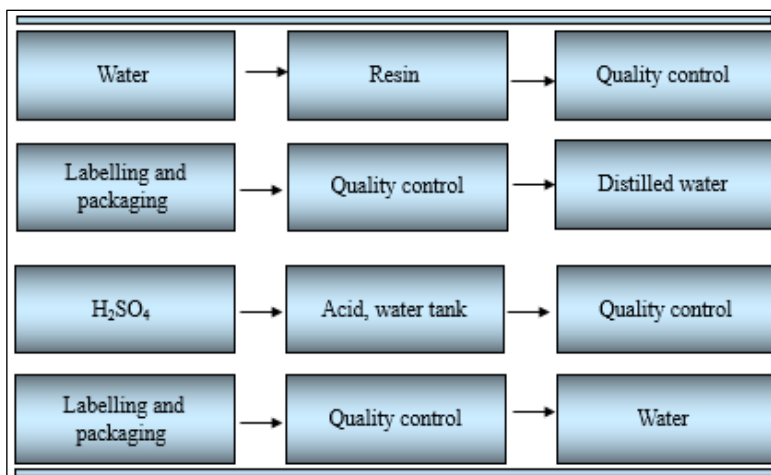


Figure 3: The layout of units of distilled water and acidic water 28% (two down diagrams).

Source: Author, (2021).

Table 2: The annual requirements of industries of acidic water 28% and distilled water (nominal capacity of 600 and 1125 t).

<b>The materials and equipment</b>	<b>Total annual rates</b>
<b>Equipment and devices</b>	
Distilled water production system, L= 3 m	2 No
Water storage tank, 2 m <sup>3</sup>	1 No
Galvanized tank of distilled water, 2 m <sup>3</sup>	2 No
PE acidic water tank, 5000 L	1 No
PE acidic water tank, 1 m <sup>3</sup>	2 No
Plumping facility	1 No
Labeling machine	1 No
Mold	2 No
Filler machine	2 No
Tank equipped to the mixer for acid water provision, 600 L	1 No
<b>Materials demands</b>	
Water	1276 m <sup>3</sup>
Paper label	1147500 No
Cardboard boxes	95625 No
Plastic bottles	1147500 No
NaCl	22032 kg
Paper labels	612000 No
Plastic bottles	612000 No
Distilled water	428400 L
H <sub>2</sub> SO <sub>4</sub>	1774480 L
Boxes	51000 No
<b>Products</b>	
Acidic water 28% for batteries applications and distilled water for industrial applications	600 and 1125 t*
<b>Employees</b>	
Staff	15 persons
<b>Energy consumption</b>	
Required water	7 m <sup>3</sup> /day
Power	32 kW/day
Required fuel (Stoves)	19 Giga Joule/day
<b>Required land and landscaping</b>	
Required land	1900 m <sup>2</sup>
Construction of infrastructure (Buildings)	541 m <sup>2</sup>
* Its density was assumed to equal with water density	

Source: Author, (2021).

### IV.3 PHTHALIC ANHYDROUS ESTERS

The production process consists of the reaction of esterification in the reactor with the help of heat and in the vicinity of the catalyst, the distillation of the product, and the separation of vapors. It also has other sectors such as product standardization, alcohol separation, neutralized excess material and water separation, purification, and filtration. Controlling the temperature in the reactor and the raw materials in terms of physical properties and the weight of the raw materials to perform the reaction, handling the pH, and the transparency and purity of the product are some of the points that should be tested and considered during production. One mole of phthalic anhydride and two moles of alcohol enter the reactor and then sulfuric acid with a concentration of 96% is added as a catalyst at a rate of 1%. Exhaust vapors from the top of the distillation tower, which contains 62% butanol and 38% water, are cooled to a temperature of 93°C after passing through the condenser and are converted to a liquid and are entered the condenser, which forms a two-phase alcohol 90%. Then it is separated as a top layer and the product after distillation for neutralization and purification enters the neutralization tank and is exposed by the caustic soda and is dehydrated using dry sodium

sulfate. Then, by passing through the filter the final product has a degree of purity of around 99%. Figure 4 denotes the step of Phthalic anhydrous esters generation. 1=sulfuric acid, 2= Phthalic anhydride, 3= alcohol Butanol or isobutanol. Table 3 includes the annual requirements of industries of Phthalic anhydrous esters.

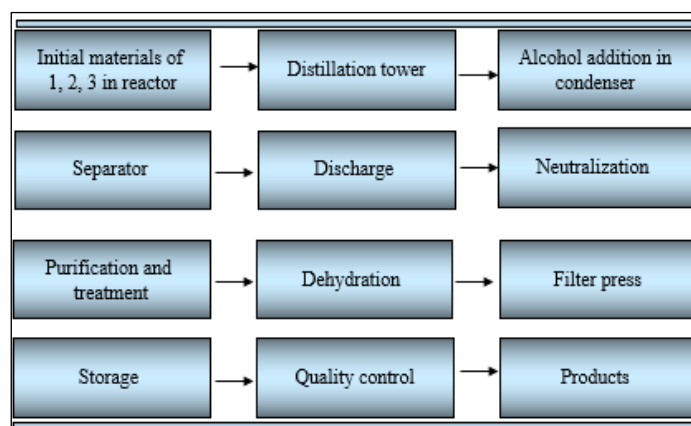


Figure 4: The steps of Phthalic anhydrous esters generation.

Source: Author, (2021).

Table 3: The annual requirements of industries of Phthalic anhydrous esters (nominal capacity of 680 and 290t).

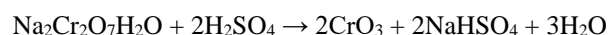
The materials and equipment	Total annual rates
<b>Equipment and devices</b>	
Stainless steel reactor, 2.2 m <sup>3</sup>	1 No
Distillation tower, stainless steel, h and d= 6 m, 450 mm	1 No
Heat exchanger, stainless steel	1 No
Naturalization tank, stainless steel, 3.5 m <sup>3</sup>	1 No
Storage tank, h and d= 4.5 and 3 m	6 No
<b>Materials demands</b>	
Phthalic anhydride 100%	590.3 t
Normal butane 98%	413.85 t
Isobutanol 98%	176.5 t
<b>Products</b>	
(1) Dibutyl phthalate 99% purity - aqueous, colorless, odorless and stable liquid - non-volatile; (2) Diisobutyl phthalate liquid with a refractive index of 1.49 and a boiling point of 327 °C - with a purity of 99%	680 and 290 t
<b>Employees</b>	
Staff	28 persons
<b>Energy consumption</b>	
Required water	13 m <sup>3</sup> /day
Power	145 kW/day
Required fuel (Stoves)	341 Giga Joule/day
<b>Required land and landscaping</b>	
Required land	5700 m <sup>2</sup>
Construction of infrastructure (Buildings)	1620 m <sup>2</sup>

Source: Author, (2021).

#### IV.4 CHROMIC ACID

Chromic acid could be prepared in two ways, dry and wet. In the dry method, concentrated sulfuric acid (98%) and dichromate sodium are simultaneously introduced into the reactor and while stirring the temperature is added to 60 °C. The sulfate Sodium hydrogen is melted and provides a suitable environment for heat transfer to melt chromic acid (at 197 °C). After the materials are completely melted, the operation is stopped. Chromic acid is separated from the bottom of the container due to its higher density. In the wet method, sulfuric acid is added to the saturated solution of sodium dichromate in water in a reaction vessel containing a fast stirrer and a stream of cold water. During the addition of acid, fine acid crystals are formed and precipitated. To separate the solid particles of chromic acid from a mixed solution is employed filtration operation. Since the wet method requires more equipment such as a cooling system, filtration, and crystallization devices, it seems that the dry method is more suitable due to the simplicity of the devices and operations. In addition, due to the moisture attraction of chromic acid, it is difficult to dry it in the wet method. Although in the dry method, it is always possible to convert some of chromium 6 to chromium 3 in the molten state, due to its relatively low energy cost in the country. Therefore, the dry method is preferred to the wet method. In addition, this method also causes less environmental pollution.

In this case, the reaction of preparing chromic acid by the discontinuous method with the presence of both concentrated sulfuric acid and sodium dichromate is as follows:



In this technique is produced about 1.2 tons of sodium hydrogen sulfate as a by-product, which is disposed of as waste if contaminated with Cr<sup>+6</sup>. Cr<sup>+6</sup> is a highly toxic and carcinogenic substance in the raw material and the product of this unit must not be entered into the environment and groundwater as leakage. The reaction reactor is made of stainless steel sheet and is equipped with a stirrer and exhaust gases to the flue and combustion chamber below. Sulfuric acid and sodium dichromate in a certain proportion are poured into the container and are gradually heated to a temperature of 197 °C. At this temperature, the resulting chromic acid is melted, then the stirrer is cut off to separate the mixture into two phases. After a few minutes, chromic acid with a density of 2.7 is placed at the bottom of the container. At this time, the chromic acid is simply discharged from the bottom of the container and is scaled and sent to the packaging section. Figure 5 presents the layout of units of the chromic acid industry. Table 4 presents the annual requirements of industries of chromic acid (nominal capacity of 270 tones).

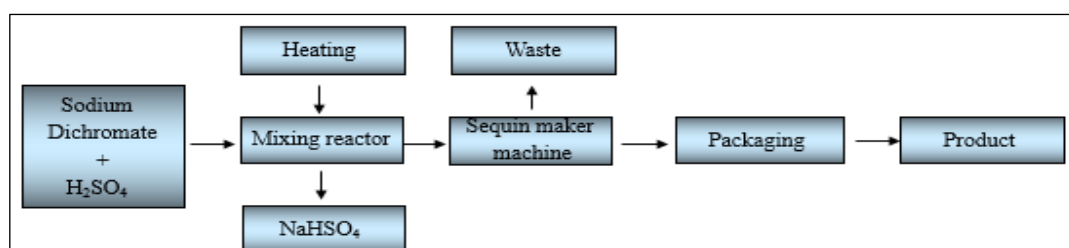


Figure 5: The layout of units of the chromic acid industry.

Source: Author, (2021).



Table 4: The annual requirements of industries of chromic acid (nominal capacity of 270 tonnes).

The materials and equipment	Total annual rates
<b>Equipment and devices</b>	
Reactor and mixer, 15 kw, 60 rpm	1 No
H <sub>2</sub> SO <sub>4</sub> tank, 30000 L	1 No
Acid measurement tank, stainless steel, 2 kW, 5 m <sup>3</sup> /h	1 No
H <sub>2</sub> SO <sub>4</sub> pump, 1 m <sup>3</sup>	2 No
Sodium Dichromate Silo, 4 kW, L= 8 m	1 No
Conveyor and elevator	1 No
Combustion chamber, d and h= 0.5 and 20 m	1 No
Chimney, 1 ton/h	1 No
Sequin maker machine, 300 kg/h	1 No
Packaging machine	1 No
Repair workshop	1 Unit
Fitted lab	1 Unit
<b>Materials demands</b>	
H <sub>2</sub> SO <sub>4</sub> 96%	270 t
Metal barrels, 20 kg	13500 No
Crystal of sodium dichromate	459 t
<b>Products</b>	
Chromic acid; 99% purity packed in purple-red 20 kg cans	270 t
<b>Employees</b>	
Staff	15 persons
<b>Energy consumption</b>	
Required water	6 m <sup>3</sup> /day
Power	61 kW/day
Required fuel (Stoves)	3 Giga Joule/day
<b>Required land and landscaping</b>	
Required land	2700 m <sup>2</sup>
Construction of infrastructure (Buildings)	785 m <sup>2</sup>

Source: Author, (2021).

#### IV.5 ZNO GENERATION INDUSTRIES

Three common methods for producing zinc oxide in industrial scale-up are as following; (1) Indirect method of preparing zinc oxide from pure zinc vapors (2) Direct method of preparing zinc oxide from zinc ore (3) Chemical reaction method for the preparation of zinc oxide. The description of the selected process (chemical reaction) for the production of zinc oxide is as follows: (1) Leaching unit: Sulfuric acid, zinc concentrate, water, and additives are mixed together inside the unit and produce high purity zinc sulfate. (2) Centrifuge: In this part, the impure solid phase is separated from the solution phase which is used for the other phase and the solution is stored in tanks to reach the cold purification stage. (3) Cold purification: In this open part, sulfuric acid and some zinc powder are added to the solution, at this stage, copper and cadmium ions are separated. (4) Centrifuge: In this step, a centrifuge is used to separate the precipitate of copper and cadmium ions from the required solution phase. (5) Hot Purification: the existing ions in the solution which are cobalt and nickel are precipitated using heat, zinc powder, arsenic oxide, and acid Sulfuric. (6) Centrifuge: The precipitate is separated from the zinc sulfate solution and is transferred to the waste section and the solution is stored in special tanks. (7) Carbonate production reactor: To prepare zinc carbonate in the next step in this reactor, we react zinc sulfate solution with sodium carbonate, and the product of this chamber is sodium carbonate. (8) Centrifuge: The resulting precipitate is required in this step, which is separated from the solution phase. (9) Furnace: The heat of the furnace causes

carbon dioxide gas to be escaped from the zinc carbonate. The product prepares zinc oxide, which includes the steps of drying the cake, crushing the lumps, and decomposing the zinc carbonate into zinc oxide. (10) Packing: The resulting zinc oxide is transferred to the packing machine and is packed in 50 kg bags. Figure 6 represents the layout of ZnO generation industries. Table 5 represents the annual requirements of industries of ZnO.

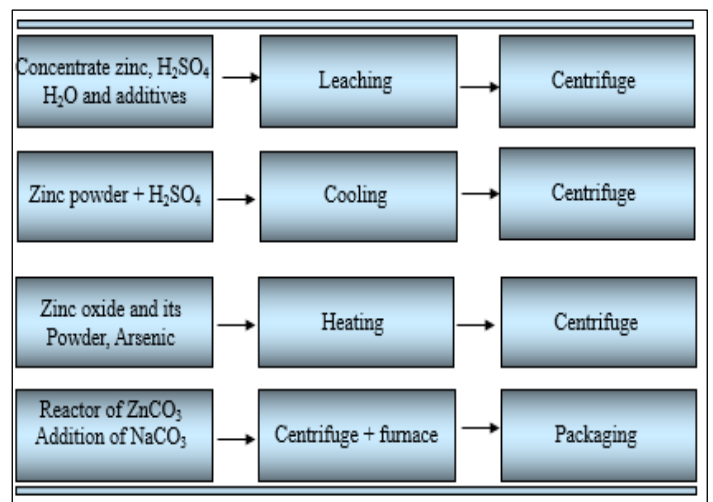


Figure 6: The layout of ZnO generation industries. Source: Author, (2021).

Table 5: The annual requirements of industries of ZnO generation (nominal capacity of 500; and 877.5 tones).

<b>The materials and equipment</b>	<b>Total annual rates</b>
<b>Equipment and devices</b>	
H <sub>2</sub> SO <sub>4</sub> Storage tank, PE, 10000 and 800 L	3 and 1 No
Conveyor	3 No
Extraction and production reactor of ZnCO <sub>3</sub> , 4500 L	2 No
Water tank made of PE, 2500 L	1 No
Centrifuge machine, d= 1.5 m and 10 hp	4 No
The storage tank of the solution, PE, 10000 L	12 No
Lime tank, 800 L	1 No
NaCO <sub>3</sub> Storage tank, 1500 L	1 No
Treatment reactor, 4 m <sup>3</sup>	2 No
Furnace	1 No
NaSO <sub>4</sub> and ZnO storage tank, steel, 10 t	2 No
Packaging machine, 50 kg	1 No
Bleach storage tank, PE, 2000 L	1 No
Centrifuge pump, 2 L/s, L= 6m	10 No
Evaporator	1 No
Temperature declining chamber	1 No
Hydro-cyclone	1 No
Dryer	1 No
Weighbridge	1 No
<b>Materials demands</b>	
Concentrate of Zn, containing moisture and purity about 50%	1012.5 t
H <sub>2</sub> SO <sub>4</sub> 98%	108 t
NaCO <sub>3</sub>	270 t
FeSO <sub>4</sub>	67.5 t
AlSO <sub>4</sub>	34.75 t
Bleach	108 t
Cao	67.5 t
PE bags of 50 kg	28000 No
Zn powder	675 kg
Arsenic oxide	270 kg
<b>Products</b>	
ZnO, white, 98% purity, in size of 0.2 μm; Sodium Sulfate	500; and 877.5t
<b>Employees</b>	
Staff	29 persons
<b>Energy consumption</b>	
Required water	32 m <sup>3</sup> /day
Power	266 kW/day
Required fuel (Stoves)	161 Giga Joule/day
<b>Required land and landscaping</b>	
Required land	5000 m <sup>2</sup>
Construction of infrastructure (Buildings)	1420 m <sup>2</sup>

Source: Author, (2021).

#### IV.6 DIETHYL ETHER

Basically, ethers are produced by the method of dehydration of alcohols or hydrogenation of alkenes in the vicinity of the catalyst. The selected process for this project is by dehydration of ethyl alcohol in the presence of sulfuric acid and aluminum catalyst, in which case by dehydration of ethyl alcohol by concentrated sulfuric acid at a temperature of 120 to 140 °C diethyl ether is produced with an efficiency of about 95%. The production process includes the following steps. First, ethyl alcohol is evaporated based on the production capacity, after passing through a heat exchanger of shell and tube type. It enters the acid-resistant

double-walled reactor in the form of steam with a temperature of about 120 to 140 °C. After passing through the sulfuric acid solution of 66 grade, it is rapidly dehydrated. Then the water vapors, sulfuric acid, and possibly peroxide are introduced into the neutralization chamber. The output of this step goes to the scrubber tower containing a soda of 5% and its acid and peroxide are removed. The neutralized solution enters the distillation tower and vapors are escaped from the top of the tower and after passing through the condenser appear as a liquid in the storage tank. Figure 7 represents the layout of units of Diethyl ether generation industries. Table 6 declares the annual requirements of industries of Diethyl ether.

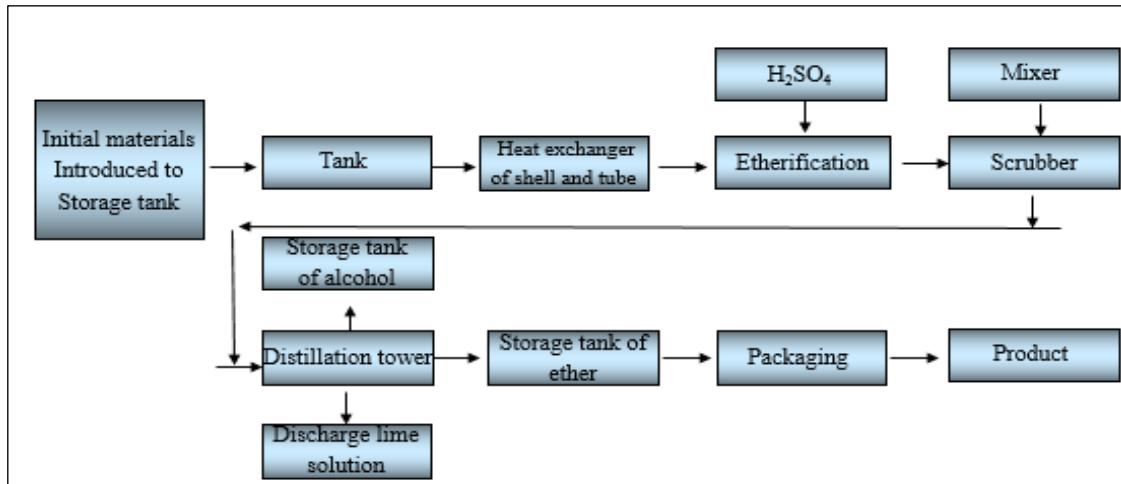


Figure 7: The layout of units of Diethyl ether generation industries.  
Source: Author, (2021).

Table 6: The annual requirements of industries of Diethyl ether (nominal capacity of 100 tones).

The materials and equipment	Total annual rates
<b>Equipment and devices</b>	
Alcohol storage tank, 30000 L, steel	1 No
Ether storage tank, 6000 L, steel 316	2 No
Noah tank, 500 L	3 No
The heat exchanger of carbon steel shell and tubing	1 No
Etherification, equipped to the mixer and 2000 L	1 No
Packed bed, steel 316, h, and d=2 m and 30 cm	1 No
Distillation tower, steel carbon, d and h= 25 cm and 3.5 m	1 No
Condenser, L and d= 1 m and 30 cm, from shell and tube type	2 No
Centrifuge pump, 8 m <sup>3</sup> /h	2 No
<b>Materials demands</b>	
Ethyl alcohol, purity of 96.5%	431.9t
H <sub>2</sub> SO <sub>4</sub> , 96-98%	367 kg
Noah, 98-99.5%	683 kg
AL dishes, 5 L	27800 No
<b>Products</b>	
Diethyl ether with a highly flammable chemical formula with a pungent odor and a scorching mass of freezing point -116.3 ° C, boiling point at atmospheric pressure 34.48 °C	100 t
<b>Employees</b>	
Staff	13 persons
<b>Energy consumption</b>	
Required water	8 m <sup>3</sup> /day
Power	131 kW/day
Required fuel (Stoves)	38 Giga Joule/day
<b>Required land and landscaping</b>	
Required land	3500 m <sup>2</sup>
Construction of infrastructure (Buildings)	1005 m <sup>2</sup>

Source: Author, (2021).

#### IV.7 NITRO-BENZENE

The nitrobenzene production process consists of the following steps:

1. Nitration unit of the present design is considered as a non-continuous process on a small scale. Therefore, the ratio of labor costs to raw materials is a small fraction. The main application of nitrobenzene is in the production of aniline and most of the produced nitrobenzene is used in the manufacturing of dye industries and the preparation of textile dyes (Azo). In addition, it can be used as a solvent and also in the role of chemical raw

material for making up rubber, photography, and medical stuff. Also, nitrobenzene is used in the military industry for preparing Nitrotoluene TNT. 2. Preparation of mixed acid: The correct proportions of both sulfuric acid 98% and nitric acid 98% are slowly mixed while the temperature is controlled. 3. The reaction of benzene and acid mixed: Considering the nitration temperature curve, the required quantities of benzene and mixed acid are entered the reactor which after the reaction, the residual acid is extracted and obtained Mono-Nitro-Benzene (MNB) is conducted towards storage tank of product. Another required amount of benzene is added to the residual acid in the extraction machine and



stirred at low temperature. Following the extraction, the benzene and nitrobenzene for use in the reaction reactor are added. It should be noted that benzene and acidic mixtures (56 to 65% by weight of sulfuric acid, 20 to 26% by weight of nitric acid, and 15 to 18% of water) are injected into the nitration reactor, which is a tube with a tubular current. The temperature of the reactor is handled around 60 to 75 °C and a pressure of about one atmosphere and a reaction time of about 15 minutes are maintained. The output mixture of the reactor which is nitrobenzene, non-combined initial materials, and some impurities are sent into a separator tank. It is returned the aqueous phase to the tower after concentration. The output mixture

from the top of this tower is sent to the distillation tower to separate nitrobenzene from benzene and water. Thus, the nitrobenzene with a purity of 99% is produced and marketed. 4. Washing: Raw MNB is washed three times with water, twice with alkaline water, and again three or more times with water. 5. Distillation: The water in the dryer is separated from the raw MNB, and the final product is stored in the storage tank. Figure 8 includes the layout of units of Nitrobenzene generation industries. Table 7 encompasses the annual requirements of industries of Nitro-benzene (nominal capacity of 1620 tones).

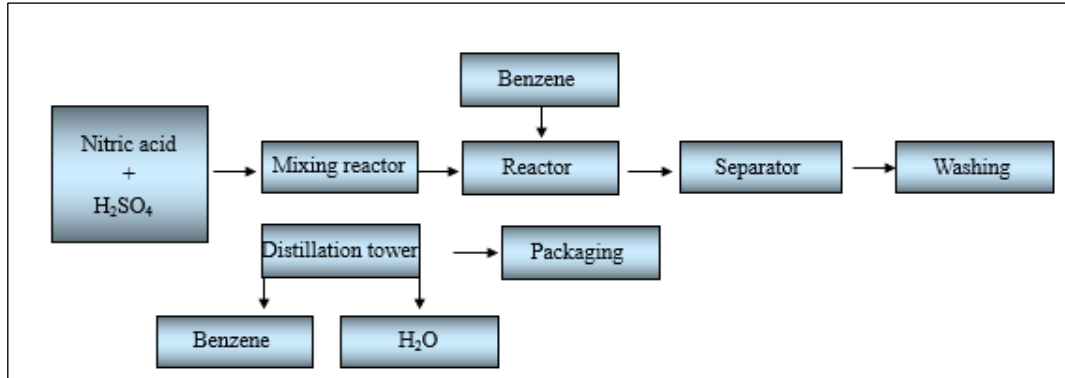


Figure 8: The layout of units of Nitrobenzene generation industries.  
Source: Author, (2021).

Table 7: The annual requirements of industries of Nitro-benzene (nominal capacity of 1620 tones).

The materials and equipment	Total annual rates
<b>Equipment and devices</b>	
The storage tank, 4 m <sup>3</sup> , steel	5 No
The reactor, 5 m <sup>3</sup> , steel	1 No
Separator, steel of 5 m <sup>3</sup>	1 No
The washing machine of 3 m <sup>3</sup>	1 No
Preheating machine	1 No
Distillation tower, 1 m <sup>3</sup>	1 No
Absorption tower, 1 m <sup>3</sup>	1 No
Boiler, 2 tons	1 No
Condenser, steel, 2 m <sup>3</sup>	1 No
Separation pump, 4 m <sup>3</sup> /h	1 No
Washing pump, 4 m <sup>3</sup> /h	1 No
Vacuum pump, 4 m <sup>3</sup> /h	1 No
Fitted lab and repair workshop	1 and 1 No
<b>Materials demands</b>	
Benzene, purity of 99.9%	1085.4 t
H <sub>2</sub> SO <sub>4</sub> 98%	923.4 t
HNO <sub>3</sub> 98% (907.2%)	907.2 t
Caustic soda 40%	12.96 t
<b>Products</b>	
Nitro-benzene, with a purity of 99.5%, density of 1.207-1.213, distillation temperature of 212-209 °C	1620 t
<b>Employees</b>	
Staff	14 persons
<b>Energy consumption</b>	
Required water	5 m <sup>3</sup> /day
Power	127 kW/day
Required fuel (Stoves)	35 Giga Joule/day
<b>Required land and landscaping</b>	
Required land	2500 m <sup>2</sup>
Construction of infrastructure (Buildings)	750 m <sup>2</sup>

Source: Author, (2021).

V. THE CALCULATION OF THE VALUES OF WEIGHTS AND EFFICIENCY SCORES AND RANKS IN DEA MODEL

The procedure assayed for finding the values of weights was declared in the methodology section. Table 8 presents the values of weights of variables in weighing systems of MCDM.

Table 8: The values of weights of variables in weighing systems of MCDM for both environmental and financial issues.

Weighing system/criteria	Friedman test	CRITIC	AHP	Entropy Shannon
<b>Financial</b>				
Employees (input)	4	0.219285877	0.015033648	0.027919688
Water (input)	3	0.200678984	0.007204305	0.109714383
Fuel (input)	1.14	0.219200316	4.02326E-05	0.390747571
Power (input)	1.86	0.144813265	0.000138423	0.07547652
Product (output)	5	0.216021559	0.977583392	0.396141838
<b>Environmental</b>				
Employees (input)	2.86	0.212312555	0.10197447	0.019712561
Water (input)	2.29	0.194297364	0.059726813	0.077463312
Fuel (input)	3.43	0.212229715	0.166772826	0.275885441
Power (input)	4.71	0.140208183	0.645518498	0.053289834
Product (output)	1.71	0.240952182	0.026007393	0.573648852

Source: Author, (2021).

To shift the environmental variables as inputs and outputs to financial issues (energy costs/revenue) was used the recent prices in the market of Tehran, Iran. Then the vectors of the values of weights were introduced into the matrix of data according to the procedure explained in the methodology. The division of weighted

outputs to weighted inputs values was given the DEA scores in financial issues. Table 9 denotes the DEA ranks in 4 weighing systems. Figure 9 displays the comparison of DEA scores in financial and environmental issues (DEAe).

Table 9: The DEA ranks in 4 weighing systems.

Industries	Friedman test	CRITIC	AHP	Entropy Shannon
<b>Financial</b>				
(1)	7	7	7	7
(2)	6	6	6	6
(3)	3	3	3	2
(4)	4	4	4	3
(5)	2	2	2	4
(6)	5	5	5	5
(7)	1	1	1	1
<b>Environmental</b>				
(1)	1	1	1	1
(2)	2	2	2	2
(3)	6	6	6	6
(4)	5	5	5	4
(5)	4	4	4	5
(6)	7	7	7	7
(7)	3	3	3	3
(1) Electrostatic coating (2) Acidic water 28% and distilled water (3) Phthalic anhydrous esters (4) Chromic acid (5) ZnO generation industries (6) Diethyl ether (7) Nitro-benzene				

Source: Author, (2021).

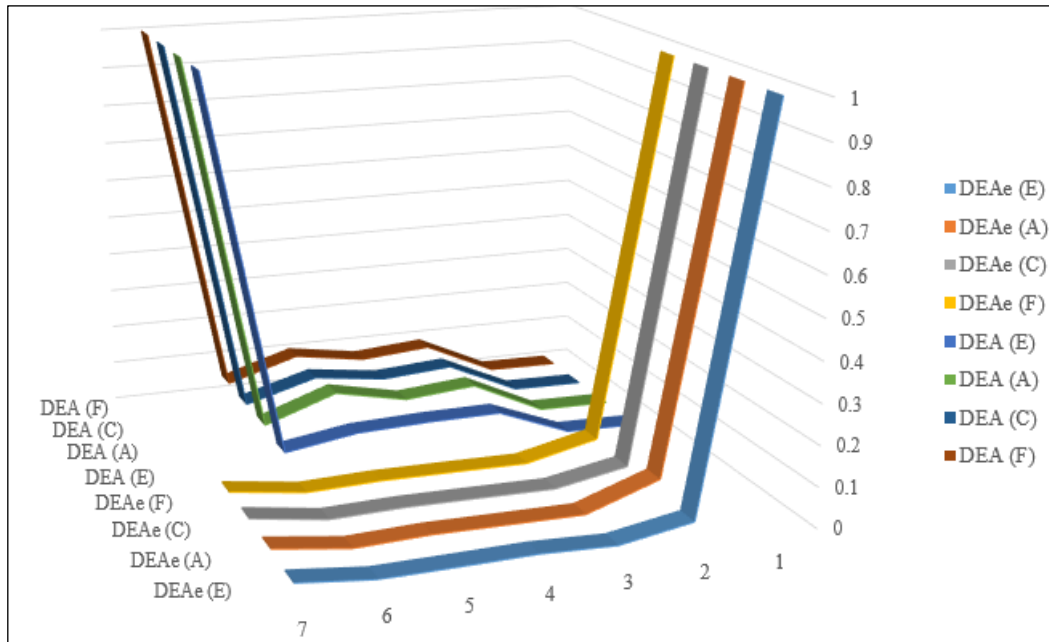


Figure 9: The comparison of DEA scores in financial and environmental issues (DEAe).

Source: Author, (2021).

In Figure 9 the F, C, A, and E are the values of weights in the DEA model based on 4 weighing systems of Friedman test, CRITIC, AHP, and Entropy Shannon respectively. According to Figure 9, the efficiency scores based on the DEA model integrated with 4 weighing systems resulted in different classifications for both environmental and financial issues that were the gap in science followed by the present research.

## VI. ANALYSIS OF MICMAC SOFTWARE

Structural analysis was introduced to allocate initially the association of ideas as an instrument. It confers the potential of describing a project or system defined and structured in a matrix with joining various dimensions. By taking into consideration the association of variables it confers to evince the prominent variables posed in developing a system in decision-making theory as either alone or in connection and integration of a complex forecasting activity (scenarios) for a maximum of 70 to 80 variables. The comparison of the obtained findings (direct, indirect, and potential classification) obviously presents the feasibility to prove the importance of employed variables but also to manifest certain variables which, because of their indirect actions, procure an overwhelming role despite the direct classification impede coming into view. Therefore, the comparison of the hierarchy of the variables in the various classifications is rich in information. The initial achievement of this kind of analysis gets back to stimulate the figuring out within the group and to initiate and sustain sparks on 'counter-intuitive' dimensions of the system's development. It was found no relations between 5 main criteria of this study using MICMAC (Matriced' Impacts Croise's Multiplication Applique'e a UN Classement) software to depict. Dewangan et al [27] used the fuzzy MICMAC method to analyze the relationship among variables of 100 companies in India. The purpose took into consideration to find which innovation enabler is dominant? MICMAC has been used to present the strength of analysis for the expert opinion for variables of urban development in Tabriz, Iran. The heat maps developed had shown influence/dependence for decision-maker in a simple view by the emergence of relations among various variables. The same role forecasted for the variables

holding the same influence/dependence. Also, the optical appearance of variables is one of the best procedures of clustering [28].

## VII. CONCLUSION

The requirements of the seven Iranian chemical industries were discussed in the present research. The demanding cases must be taken into consideration in the development stage or newly implemented plants. The criteria selection for the current alternatives can be extracted from the present content for future developments. The main aspects to be allocated for the decision-making theory can be mentioned as the parameters assessed by the Iranian evaluator team in EIA. The use of weighing systems provided the framework of a sensitivity analysis to prove the findings in the DEA model. The good compliance of results in the DEA model proved the precision and accuracy applied. The further assessment can be deployed by employing other types of weighing systems of MCDM to verify the findings. The running diagrams of industries are exploited with similar cases in other nations. With regard to developing a variety of DEA models to assess the efficiency of industries, the author recommends the use of other DEA models to expand the knowledge and compare the findings with them. Both classifications of industries can be taken into development plans by allocating a series of similar cases of chemical industries in terms of energy stream in both environmental and currency reports.

## VIII. AUTHOR'S CONTRIBUTION

**Conceptualization:** Malek Hassanpour.

**Methodology:** Malek Hassanpour.

**Investigation:** Malek Hassanpour.

**Discussion of results:** Malek Hassanpour.

**Writing – Original Draft:** Malek Hassanpour.

**Writing – Review and Editing:** Malek Hassanpour.

**Resources:** Malek Hassanpour.

**Supervision:** Malek Hassanpour.

**Approval of the final text:** Malek Hassanpour



## IX. ACKNOWLEDGMENT

This research was conducted as part of the corresponding author's Ph.D. research work (Entitled; Evaluation of 405 Iranian Industries). The tabulated data were picked up from the screening step of project identification in environmental impact assessment. The author thanked colleagues and evaluators of both the Iranian environment protection agency and Iranian industries organization for the data assessed.

## X. REFERENCES

- [1] Li, Y., Chiu, Y., Liu, Y., Lin, T.-Y., Chang, T.-H. (2020). The Impact of the Media and Environmental Pollution on the Economy and Health Using a Modified Meta 2-Stage EBM Malmquist Model. *The Journal of Health Care Organization, Provision, and Financing*, 57, 1–24. DOI: [10.1177/0046958020921070](https://doi.org/10.1177/0046958020921070).
- [2] Singh, S., Olugu, E.U., Musa, S.N. (2016). Development of sustainable manufacturing performance evaluation expert system for small and medium enterprises. *Procedia CIRP*, 40, 608 – 613. Doi: [10.1016/j.procir.2016.01.142](https://doi.org/10.1016/j.procir.2016.01.142).
- [3] Compton, M., Willis, S., Rezaie, B., Humes, K. (2018). Food processing industry energy and water consumption in the Pacific Northwest. *Innovative Food Science and Emerging Technologies*, 47, 371–383. <https://doi.org/10.1016/j.ifset.2018.04.001>.
- [4] Rahmani, M. (2017). A productivity analysis of Iranian industries using an additive data envelopment analysis. *Management Science Letters*, 7(4), 197–204. DOI: [10.5267/j.msl.2016.12.007](https://doi.org/10.5267/j.msl.2016.12.007).
- [5] Shakeri, M., Zarei, A., Azar, A., Minbash Razgah, M.M. (2020). Green Supply Chain Risk Network Management and Performance Analysis: Bayesian Belief Network Modeling. *Environmental Energy and Economic Research*, 4(3), 165-183. DOI [10.22097/eeer.2020.215399.1134](https://doi.org/10.22097/eeer.2020.215399.1134).
- [6] Hassanpour, M. (2020). Evaluation of Iranian small and medium-sized industries using the DEA based on additive ratio model-a review. *FACTA UNIVERSITATIS Series: Mechanical Engineering*, 18(3), 491 – 511 <https://doi.org/10.22190/FUME200426030H>.
- [7] Nemati, M., Saen, R.F., Matin, R.K. (2020). A data envelopment analysis approach by partial impacts between inputs and desirable undesirable outputs for sustainable supplier selection problem. *Industrial Management & Data Systems*, 121(4), 809-838. DOI [10.1108/IMDS-12-2019-0653](https://doi.org/10.1108/IMDS-12-2019-0653).
- [8] Al-Mezeini, N.K., Oukil, A., Al-Ismaili, A.M. (2020). Investigating the efficiency of greenhouse production in Oman: A twostage approach based on Data Envelopment Analysis and double bootstrapping, 247, 119160, 1-29. <https://doi.org/10.1016/j.jclepro.2019.119160>.
- [9] Rahimpour, K., Shirouyehzad, H., Asadpour, M., Karbasian M. (2020). A PCA-DEA method for organizational performance evaluation based on intellectual capital and employee loyalty a case study. *Journal of Modelling in Management*, 15(4), 1479-1513. DOI [10.1108/JM2-03-2019-0060](https://doi.org/10.1108/JM2-03-2019-0060).
- [10] Mozaffari, M.R., Mohammadi, S., Wanke, P.F., Correa, H.L. (2021). Towards greener petrochemical production: Two-stage network data envelopment analysis in a fully fuzzy environment in the presence of undesirable outputs. *Expert Systems with Applications*, 164, 113903. <https://doi.org/10.1016/j.eswa.2020.113903>.
- [11] Ren, J., Gao, B., Zhang, J., Chen, C. (2020). Measuring the Energy and Carbon Emission Efficiency of Regional Transportation Systems in China: Chance Constrained DEA Models. *Hindawi Mathematical Problems in Engineering*. Article ID 9740704, 1-12. <https://doi.org/10.1155/2020/9740704>.
- [12] Poordavoodia, A., Moazami Goudarzi, M.R., Javadic, H.H.S., Rahmani, A.M. (2021). Measuring Efficiency of Financial Cloud Services in Banking Industry Using Modified Dynamic DEA with Network Structure (Case study: Iran E-Banking). *Advances in Mathematical Finance & Applications*, 6(1), 1-28. DOI: [10.22034/amfa.2020.1898567.1416](https://doi.org/10.22034/amfa.2020.1898567.1416).
- [13] Abbas, A., Waseem, M., Yang, M. (2020). An ensemble approach for assessment of energy efficiency of agriculture system in Pakistan. *Energy Efficiency*, 13, 683-696. <https://doi.org/10.1007/s12053-020-09845-9>.
- [14] Li, F., Emrouznejad, A., Yang, G.L., Li, Y. (2020). Carbon emission abatement quota allocation in Chinese manufacturing industries: An integrated cooperative game data envelopment analysis approach. *Journal of the operational research society*, 71(8), 1259-1288. <https://doi.org/10.1080/01605682.2019.1609892>.
- [15] Li, Y., Chiu, Y.H., Wu, M., Li, Y., Lin, T.Y. (2020). Chinese liquor company management efficiency from a social responsibility perspective: a two stage dynamic directional distance function. *Economic Research-Ekonomska Istraživanja*, 1-31. DOI: [10.1080/1331677X.2020.1860797](https://doi.org/10.1080/1331677X.2020.1860797).
- [16] Oghani, A.V., Khiyabani, F.M., Farahmand, F.H.N. (2020). Data envelopment analysis technique to measure the management ability: Evidence from Iran Cement industry. *Cogent Business & Management*, 7(1), 1801960, 1-13. DOI: [10.1080/23311975.2020.1801960](https://doi.org/10.1080/23311975.2020.1801960).
- [17] Fathi, B., Ashena, M., Bahari, A.R. (2021). Energy, environmental, and economic efficiency in fossil fuel exporting countries: A modified data envelopment analysis approach. *Sustainable Production and Consumption* 26, 588–596. <https://doi.org/10.1016/j.spc.2020.12.030>.
- [18] Haia, A.T.N., Speelman, S. (2020). Economic-environmental trade-offs in marine aquaculture: The case of lobster farming in Vietnam. *Aquaculture*, 516, 734593. <https://doi.org/10.1016/j.aquaculture.2019.734593>.
- [19] Sun, H., Ikram, M., Mohsin, M., Abbas, Q. (2021). Energy security and environmental efficiency: evidence from OECD countries. *The Singapore Economic Review*, 66(2), 489-506. DOI: [10.1142/S0217590819430033](https://doi.org/10.1142/S0217590819430033).
- [20] Munn, R.E. (1979). *Environmental Impact Assessment, Principles and Procedures*. Scope 5. John Wiley and Sons, New York.
- [21] Lohani, B.N., Evans, J.W., Everitt, R.R., Ludwig, H., Richard, A.C., Shih-Liang, T.U. (1997). *Environmental Impact Assessment for Developing Countries in Asia*. Asian Development Bank. Volume 1 – Overview, 1-356.
- [22] Biju, V.G., Prashanth, C.M. (2017). Friedman and Wilcoxon evaluations comparing SVM, bagging, boosting, K-NN and decision tree classifiers. *Journal of Applied Computer Science Methods*, 9(1), 23-47. DOI [10.1515/jacsm-2017-0002](https://doi.org/10.1515/jacsm-2017-0002).
- [23] Eisinga, R., Heskes, T., Pelzer, B., Grotenhuis MT. (2017). Exact p-values for pairwise comparison of Friedman rank sums, with application to comparing classifiers. *BMC Bioinformatics*, 18, (68), 2-18.
- [24] Ijadi Maghsoodi, A., Hafezalkotob, A., Aziz Ari, I., Ijadi Maghsoodi, S., Hafezalkotob, A. (2018). Selection of Waste Lubricant Oil Regenerative Technology Using Entropy-Weighted Risk-Based Fuzzy Axiomatic Design Approach. *INFORMATICA*, 29(1), 41–7441. DOI: <https://dx.doi.org/10.15388/Informatica.2018.157>.
- [25] Küçükönder, H., Demirarslan, CP., Burgut, A., Boğa, M. (2019). A Hybrid Approach of Data Envelopment Analysis Based Grey Relational Analysis: A Study on Egg Yield. *Pakistan J. Zool*, 51(3), 903-912. DOI: <https://dx.doi.org/10.17582/journal.pjz.2019.51.3.903.912>.
- [26] Pamucar, D., Stevic, Z., Sremac, S. (2018). A New Model for Determining Weight Coefficients of Criteria in MCDM Models: Full Consistency Method (FUCOM). *Symmetry*, 10(9), 393, 1-22. DOI: [10.3390/sym10090393](https://doi.org/10.3390/sym10090393).
- [27] Dewangan, D.K., Agrawal, R., Sharma, V. (2015). Enablers for Competitiveness of Indian Manufacturing Sector: An ISM-Fuzzy MICMAC Analysis. XVIII Annual International Conference of the Society of Operations Management (SOM-14). *Procedia - Social and Behavioral Sciences*, 189, 416 – 432. DOI: [10.1016/j.sbspro.2015.03.200](https://doi.org/10.1016/j.sbspro.2015.03.200).
- [28] Ranjbar Nia B., Murgante, B., Qelichi, M.M., Rustaei, S. (2017). A Comparative Study Employing CIA Methods in Knowledge-Based Urban Development with Emphasis on Affordable Housing in Iranian Cities (Case: Tabriz). *International Conference on Computational Science and Its Applications, Part IV, LNCS 10407*, pp. 485–501. DOI: [10.1007/978-3-319-62401-3\\_35](https://doi.org/10.1007/978-3-319-62401-3_35).



ISSN ONLINE: 2447-0228

## ITEGAM-JETIA

Manaus, v.7 n.30, p. 18-28. Jul/Aug, 2021  
DOI: <https://doi.org/10.5935/jetia.v7i30.763>



RESEARCH ARTICLE

OPEN ACCESS

## DISPERSION AND TURBULENCE: A CLOSE RELATIONSHIP UNVEILED BY MEANS OF STATE FUNCTION

Alfredo Jose Constain\*<sup>1</sup>, Gina Peña Olarte<sup>2</sup> and Carlos Peña Guzman<sup>3</sup>

<sup>1,2</sup> Fluvia SAS, Bogotá, Colombia.

<sup>3</sup> Environmental and Sanitary Engineering Program, La Salle University, Bogotá, Colombia.

<sup>1</sup> <http://orcid.org/0000-0001-6442-0715> , <sup>2</sup> <http://orcid.org/0000-0002-8727-9088> , <sup>3</sup> <http://orcid.org/0000-0003-0496-9612> 

Email: \*alfredo.constain@gmail.com, carpeguz@gmail.com, ginap.olarte@fluvia.co

### ARTICLE INFO

#### Article History

Received: July 16<sup>th</sup>, 2021

Accepted: August 26<sup>th</sup>, 2021

Published: August 31<sup>th</sup>, 2021

#### Keywords:

Turbulence,  
Dispersion,  
New tracer methods,  
New measurement devices.

### ABSTRACT

This article reviews the physical conditions that natural, turbulent flows meet to be considered in "Dynamic Equilibrium", a condition that greatly facilitates the analysis of flows, thanks to the concept of "equiprobability", in such a way that the tracer dyes can give an essential information of the dynamics of the current. A general State Function is proposed for this dynamic, which allows to study Advection and Dispersion for virtually all types of river beds, achieving a series of compact and precise relationships, both in hydraulics and thermodynamics. This approach allows us to obviate the limiting use of non-linear differential equations, as "mandatory" characterization of fluid dynamics. With this new method, a practical case from the technical literature is analyzed, and it is solved in detail, comparing it with the classic method of Statistical Moments. Conclusions on results, and recommendations are made.



Copyright ©2016 by authors and Galileo Institute of Technology and Education of the Amazon (ITEGAM). This work is licensed under the Creative Commons Attribution International License (CC BY 4.0).

### I. INTRODUCTION

With the worsening of environmental problems, derived from the intense industrialization and expansion of the urban frontier, the availability of powerful methods for the interpretation and study of these issues takes on vital importance.

Paradoxically to this serious situation, since the end of the century, the methods of measurement and study of the phenomena of water pollution practically advanced a little in the theoretical part, and except for the development of increasingly advanced digital platforms, and some new ones. Ideas on how to approach turbulence from *emerging concepts* [1], far from the classical approximation of non-linear differential equations, the methods currently used are practically the same as in the 1990s. For this reason, the renewal of approaches and procedures is an important point from which you can make up for lost time.

With this optics in mind, this Article aims to question some key points about the conceptualization of the dynamics of channels, based on dispersion as a substrate of turbulence, and limited by the relative control of fluctuations (steady state), typical of the "linear" regime of non-equilibrium thermodynamics. A first basic point in

this approach is that the energetic conditions are reviewed by which it can be understood why natural, turbulent channels, in "normal" (not catastrophic) conditions, are in a low or moderately strong degree of instability, which allows the entropy production should be at a minimum value, and therefore (according to Boltzmann) present in the system, condition of "Equiprobability", leading to a "statistical constancy" of the average flow velocity.

A second point analyzed is a new Dispersion-Advection model, which basically depends on the mean velocity of the flow and on a "State function" that guides the evolution of the injected tracer cloud, and which, being also a "thermodynamic potential", indicates us when the cloud loses degrees of Freedom, of great significance when we want to calculate the situation of "Complete mixture" for water quality studies.

Turbulence in "steady state" allows the condition of "Equiprobability", which in turn allows a statistically "constant" flow rate. The subsequent dispersion can be defined very precisely.

Finally, a tracer experiment documented in detail in the technical literature is chosen, to which the new model is applied, and the results are compared with the classical Moment methodology.

## II. THEORETICAL REFERENCE

Considering the enormous difficulty that has been the deep understanding of turbulence from the Navier-Stokes non-linear differential equations, alternative approaches to the problem have emerged since the end of the last century. One of them, quite different and novel, is Emergent Analysis, in which it is recognized that, in real physical processes, the whole is not the sum of the parts, this since non-linearity and multiple feedbacks in said processes, invalidate the superposition principle, and fill the equations with multiple “incomputable” solutions. It had always been believed, as a fundamental paradigm of science, that starting from the basic processes (at the molecular level, for example) it was possible to describe phenomena of a higher level (at the human level) as “synthesis” of those previous levels. This is not possible due that “the analysis abandons us”, in line with Euler's prophetic words. As each level of reality demands its own calculation rules, it is necessary then, to formulate “emergent” approaches that cover those levels.

An analysis in this line of thought is to define the conditions in which the turbulence remains stable or not, at room temperature, without going of course to the complete analysis from the origin, via Navier-Stokes, which can be done from the thermodynamics of irreversible phenomena. From these results, anticipated by J. Frenkel in the last century, certain important conclusions can be drawn to give a useful interpretation to river hydraulics, especially considering the application of dye tracers.

### II.1 REGIMES OF CONTEMPORARY THERMODYNAMICS

Depending on the intensity of the flow of energy or substance (entering or leaving) in open real systems, its state can be placed in one of the thermodynamic stages according to the following classification [2]:

**A - Strict equilibrium**, corresponding to totally reversible processes, in which causes, and effects disappear, in response to the statistical homogeneity of the parameters associated with this state. Thus, the “Thermodynamic forces”, **F**, (temperature, concentration, free energy gradients, etc.), and their consequences, the “Thermodynamic flows”, **J**, (rates of heat transport, free energy, etc.), they are completely canceled. The fluctuations disappear quickly by the physicochemical control mechanisms. And it is proper to define “thermodynamic potentials” that allows establishing criteria for evolution towards maximums or minimums. For example, in this case, the Entropy Production,  $\sigma$ , null.

**B - Quasi-equilibrium**, or Linear Irreversibility close to equilibrium, in which the forces and thermodynamic flows are not zero, but are proportional to each other, for this reason, this stage is called “linear”, close to equilibrium. Likewise, fluctuations do not disappear completely, but they are an important aspect of instabilities, without producing catastrophic effects. In this case, when the Forces and Thermodynamic Flows are proportional to each other, the Entropy Production is set at a *minimum* value, according to a famous theorem of I. Prigogine [3]. According to the probabilistic concept of L. Boltzmann [4], a maximum entropy in a system implies that the probabilities at each point are equal [5], which is called as the “Equiprobability” condition. If the entropy according to Boltzmann is:

$$\sum_i \text{Log } p_i \sim \text{Maximo} \quad (1)$$

This implies that:

$$p_1 + p_2 + p_3 + \dots + p_n \approx 1.0 \quad (2)$$

And that:

$$p_1 = p_2 = p_3 = \dots = p_n \quad (3)$$

In other words, for a maximum entropy, the probabilities at each point in the system are equal. Now, for this maximum condition, the entropy production is a Minimum.

$$S \rightarrow \text{Max}, \sigma \rightarrow \text{Min} \quad (4)$$

**C -Dissipative Non-Equilibrium**, or distant Irreversibility, a state in which there is no proportionality between Forces and Flows and their relationship is non-linear, which is why this phase is precisely called “non-linear”. The production of entropy grows and is no longer a minimum, and the fluctuations grow to levels close to the average value of their set. In this extreme state, new structures appear in matter, combining order and disorder.

### II.2 PROBABILISTIC DISTRIBUTIONS AS A SUITABLE DESCRIPTION OF NATURAL PROCESSES

The vision of irreversible molecular phenomena has focused primarily on the “Probabilistic distributions”, or Gibbs statistical entities [6], defined as follows, for a case “j” (of “n”) possible:

$$\rho_j = \rho(p_j, q_j, t_j) \quad (5)$$

This value indicates the probability of finding the values of linear momentum, **p**, and coordinates, **q**, at time, **t**. In practice this Distribution indicates the density of points in a certain finite region of the phase space. Figure 1.

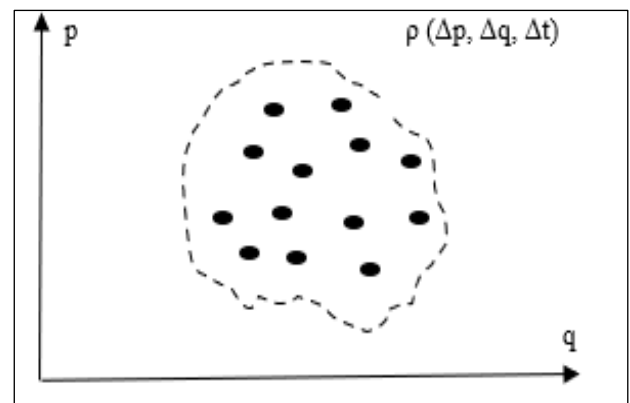


Figure 1: Probabilistic distribution in a physical system. Source: Authors, (2021).

Unlike the original conception of Gibbs and Einstein, in which the Probabilistic Distributions were fundamentally due to our ignorance regarding the inaccessible massive phenomena of the micro world, the modern view assigns them a much more fundamental role, as only coherent models of the dynamics at that level, since the “trajectories” have disappeared as their basic description, since they are “divergent” by the “Poincaré resonances” on their coupled modes for the innumerable degrees of freedom. Therefore, they are dynamic entities, inherently non-deterministic, that replace the “trajectories” of the particles, which are essentially “incomputable”, since in irreversible material assemblages, the Fourier spectral harmonic interferences, due to



the couplings between the multiple “Degrees of Freedom” lead to dividers that cancel out, giving divergence effects, which destroy these trajectories [6].

Now, for stages A-Strict Equilibrium and B - Linear Quasi-equilibrium, the compliance with the “Equiprobability” condition is of course different in each case, since only in the second case there is irreversible heat generation, increasing velocity fluctuations to a significant level. If the effect of these fluctuations is assimilated to an “absolute error” [7], which affects the value of the distribution, it can then be written for both cases:

$$\rho(A) \approx \langle \rho_A \rangle \pm \varepsilon_A \quad (6)$$

And

$$\rho(B) \approx \langle \rho_B \rangle \pm \varepsilon_B \quad (7)$$

Therefore,  $\| \varepsilon_A \| \ll \| \varepsilon_B \|$ , and the degree of inequality between these two values, will correspond to the relative deviation of the “Equiprobability” condition for the system.

Thus, by way of simplified comparison, Figure 2 shows three significant cases of flow: A) Strict equilibrium, B) “Linear” quasi-equilibrium, and C). Far from Equilibrium.

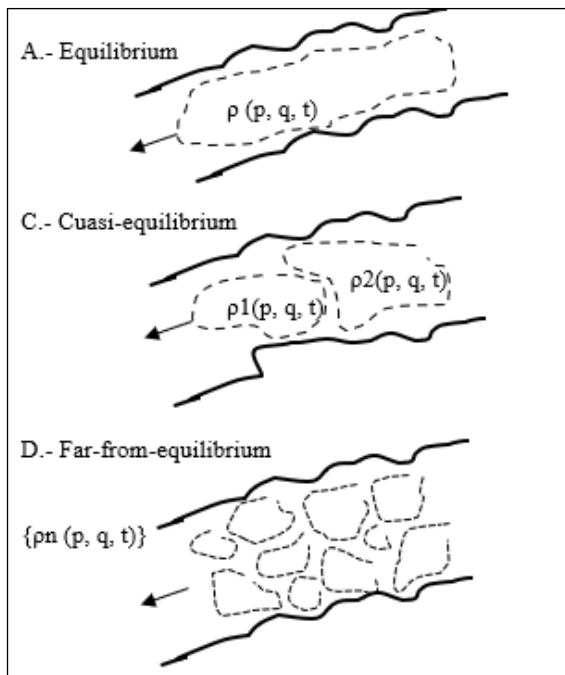


Figure 2: Different type of thermodynamic flows. Source: Authors, (2021).

In A, there is only one Probabilistic Distribution compatible with the strict Boltzmann Equivalence. In B, there are only a very few distributions. In C, there are many distributions, numbered according with “n”. The relative error increases depending on the case, from A to C.

### II.3 NATURAL WAYS AS OPEN SYSTEMS EVOLVING UNDER CONDITION OF “DYNAMIC EQUILIBRIUM

Since the “Stable State” corresponding to the irreversible, “Linear” thermodynamic stage, close to equilibrium, is important for the fluvial dynamics under usual conditions, it is necessary to establish the physical conditions that make this stage possible.

For chemical reactions, strict thermodynamic equilibrium requires that microscopic reversibility be fully met, that is, that

there is a “Detailed Balance” between contrary reactions. This condition is fulfilled when the cause of the flows, the Gibbs free energy, which in this case is defined as “Affinity”,  $A$ , is zero. In the regime close to equilibrium, for a mole of substance, this condition is slightly modified as follows:

$$\left(\frac{A}{RT}\right) \ll 1 \quad (8)$$

Here  $R \approx 8.31 \text{ J/(K * Mol)}$  is the gas constant and  $T$  is the Kelvin temperature, which for the usual cases is taken as 300 K. Therefore, the thermal molecular energy is approximately 2.5 KJoules/mol. In most chemical reactions, the molar energies involved are in the range of 10-100 KJ/mol, that is, they do not meet the “linearity” condition of expression (6), and it can be said that these types of effects, at usual temperatures, are in the non-linear regime of irreversible thermodynamics [8].

For the mechanical effects present in natural flows, the criterion of “thermodynamic linearity” must be expressed differently. If the velocity fluctuations in the fluids that make up these flows are small, it is presumable that the instabilities do not lead the turbulent system to a situation of “runaway”, which would be the way in which the system loses its stability. What is the main factor for the water to remain as “still” as possible in the presence of dynamic instabilities? This factor is undoubtedly the “fluidity” of the liquid [9], which is precisely the property of not resisting shear stress. The more “fluid” a liquid is, the more easily it will dampen the fluctuations that occur within it, and the more difficult it will be for it to move out of the “stable state” in which it is close to equilibrium.

According to the liquid model developed by J. Frenkel in socialist Russia in the 1920s and 1930s, the liquid state under normal conditions resembles crystalline solids much more than gases, as is usually the case. It is assumed. The difference between one and the other is more one of degree than of essence, the crystals being much more ordered, especially in the “long range”, where the liquids no longer present any “three-dimensional lattice” characteristics. It is therefore important to numerically characterize the “Fluidity” property from a physical-molecular point of view.

Fluidity can be defined (according to Frenkel) as the situation in which the molecules of the liquid vibrate occupying transient equilibrium positions in their quasi-crystalline lattice, jumping from time to time to a new empty neighboring position, called “hole”. For this reason, liquid molecules yield much more easily to tangential stresses, reducing external disturbances. The molecules of crystalline solids for their part remain vibrating in these equilibrium positions, much longer, almost permanently, that is, their “half-life time at equilibrium point”, called  $\tau$ , is much greater than the of the liquid. Figure 3.

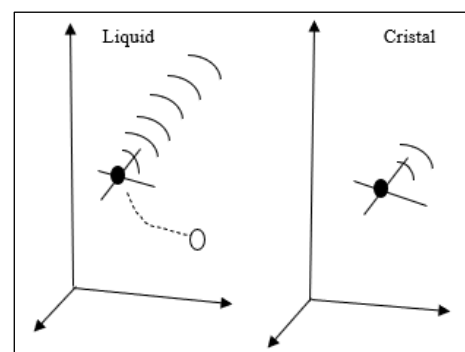


Figure 3: Mechanism of Fluidity in liquids and crystalline solids. Source: Authors, (2021).



It has been established that this "Half-life time" in equilibrium position" for quasi-crystalline liquids and solid crystals has the following molar shape, as a function of the value of the inherent period of molecular vibration,  $\tau_0 \approx 10^{-13}$  sec:

$$\tau \approx \tau_0 e^{\frac{W}{RT}} \quad (9)$$

The difference between crystalline solids and quasi-crystalline liquids (for the same ambient temperature) is of course the value of the potential energy,  $W$ , called "activation energy". For water, in a range from 300 ° K to 800 ° K, this energy per mole is between 0.57 KJ/mol, and 2.40 KJ/Mol. For crystalline solids under similar conditions, the range of this energy is between 4.8 KJ/mol and 14.4 KJ/Mol. That is, 9 times greater than for water.

It can then be said that, at room temperature (300 ° K), the water meets the following "linear" thermodynamic stability criterion:

$$\left(\frac{W}{RT}\right) \approx \left(\frac{0.57}{2.50}\right) \approx 0.23 \quad (10)$$

Namely:

$$\left(\frac{W}{RT}\right) < 1.0 \quad (11)$$

Therefore, turbulent water partially meets the numerical criterion, not as strict as in expression (8) but allowing a relatively good control of fluctuations due to a significant Fluidity effect. Turbulent water is therefore between the "linear" zone and a catastrophic zone in which this property cannot prevent runaway.

According to equations (6) and (7) in different channels there will be different errors, but it will be possible to apply without fear the concept of "Equiprobability", and consider the statistical constancy of its dynamic parameters

One way to really appreciate what is the meaning of the value expressed in equation (11) is to calculate and compare different values for equation (9) that describes the "mobility" of the water molecules from their equilibrium sites, for several cases significant of the ratio  $(W/RT)$ :

A -  $W/RT \approx 0.023$   $e^{0.023} \approx 1.023$  (12)

B -  $W/RT \approx 0.23$   $e^{0.23} \approx 1.26$  (13)

C -  $W/RT \approx 2.3$   $e^{2.3} \approx 9.97$  (14)

It is seen that the time ratio  $(\tau / \tau_0)$  varies approximately between 1.02, 1.3 and 10.0, that is, that this ratio for the conditions  $(W/RT) \approx 0.01$  and  $(W/RT) \approx 0.23$ , changes only 23% and it remains well within the same order, close to unity, justifying the great "mobility" of the water molecules at room temperature, and its facility to dampen turbulent fluctuations, to the extent that  $(W/RT)$  decreases. Figure 4.

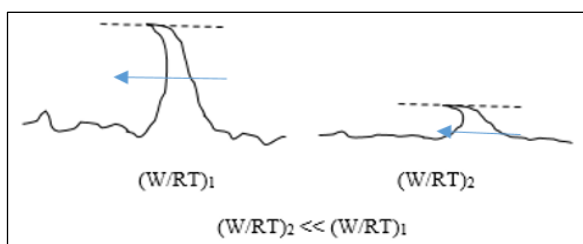


Figure 4: Control of turbulent fluctuations by means of the ratio  $(W/RT)$ . Source: Authors, (2021).

#### II.4 EQUIPROBABILITY CONDITION IN THE NATURAL WAYS AND STATISTICAL CONSTANCY OF DYNAMIC PARAMETERS IN "DYNAMIC EQUILIBRIUM"

Based on what was explained in the previous Section, and considering numerous experimental results, the researchers of river hydraulics have warned that, under "normal" conditions (not catastrophic), natural channels evolve as open systems, (exchanging energy and substance with its environment), within the thermodynamic regime of "Quasi-equilibrium", or of "linear" irreversibility. Therefore, the "Dynamic Equilibrium" or "Stable State" will be the thermodynamic regime that is chosen to analyze its physical dynamics, regarding the contemporary study of turbulence [10][11].

The condition of "Equiprobability" in natural channels can be translated as a situation of constancy of the mass transport rate since this transfer from one point to another will be between points of equal dynamic probability. In Figure 5 the local mass transfers are shown as red paths.

The global (integral) result of these local mass transfers, between equiprobable points, entails the constancy of the mean flow velocity [12]. This speed coincides with the value that defines the Chezy-Manning equation, since the tracer absorbs and expels heat from friction processes in the flow, with "n" as Roughness, R, as Hydraulic Radius, and S, as Longitudinal slope.

$$U \approx \frac{2}{n} R^{2/3} \sqrt{S} \quad (15)$$

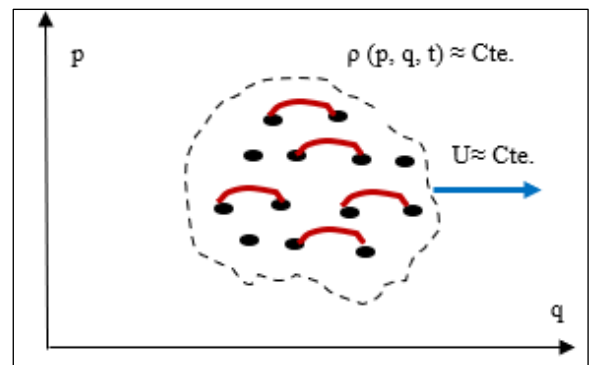


Figure 5: Statistical constancy of mass transfer. Source: Authors, (2021).

#### II.5 TRACERS AND THEIR DYNAMICS IN A TURBULENT FLOW

The tracers are inks with special properties that are poured into natural flows to measure and interpret the flow parameters, injecting a certain mass at a point "upstream" of the channel, and measuring the cloud or "plume" of the solute, passing through the "downstream" monitoring point. Once injected into the flow, the mass of the tracer substance is mixed by the effect of turbulence and shear forces that depend on the average flow velocity.

The dynamics of the tracer pen is therefore consistent with the Law of Conservation of Energy, that is, it is a "non-localized" measurement, unlike other measurement methods (such as the Pinwheel or the ultrasound profiler). They operate by means of the Law of Conservation of Momentum and are therefore a more restricted measure of the "local" type. From this perspective, the density of information provided by tracers is important since it depends on a broad set of laws that condition advection and dispersion in natural flows.

The dye tracer substance used must have certain characteristics, such as: **A** - Be soluble in water, **B** - Be environmentally neutral, **C** - Have a physicochemical characteristic that allows it to be detected (measured) by an instrument, **D** - Have a cost compatible with the amounts to be used, and **E** - Have a simple protocol for handling and interpretation of the substance and the technology to measure it. Figures 6, 7 and 8.



Figure 6: Rhodamine WT as a fluorescent dye substance. Source: Authors, (2021).



Figure 7: Fluorometric tracer advancing in a river. Source: Authors, (2021).



Figure 8: Tracer Measurement “real-time” Instrument. Source: Authors, (2021).

The tracer ink that is usually used in field experiments is Rhodamine WT (RWT), which is fluorescent, and therefore can be detected with a special optical sensor. The equipment shown measures RWT and common salt in “real time”, saving field tasks in memory, or transmitting them over the internet to the cloud.

Modern tracer technologies and methodologies allow accurate and fast measurements even in large rivers. From the information contained in the flared curve (Fickian Curve) that results from the measurement, with convenient values of mass,  $M$ , and cross-sectional area  $A$ .  $C_0$  is the background concentration of the flow, and  $E$  is the longitudinal coefficient of dispersion:

$$C(t, X) \approx \frac{M}{A\sqrt{4\pi E t}} e^{-\frac{(X_0 - Ut)^2}{4 E t}} + C_0 \quad (16)$$

Experimenters in the 1960s and after found that the actual tracer curves had a “bias” that was not consistent with the equation above. This bias was significant at the beginning of injection to flow and decreases over time.  $C_0$  is the basic concentration of the tracer in the flow. Figure 9.

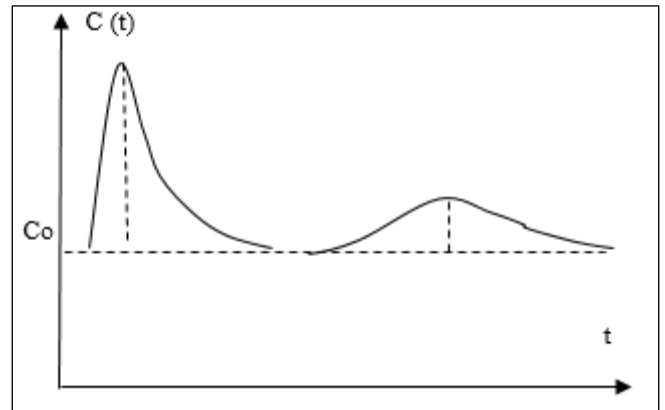


Figure 9: Characteristic Fickiana curve of a tracer. Source: Authors, (2021).

The bias is a deformation of its symmetry, showing an extended “tail”, the explanation of which has taken over a good number of theories of all kinds, but without providing a complete justification that satisfies everyone.

A successful theory to describe this variable bias has been formulated by the authors [13][14], insofar as it provides appropriate quantitative answers to various questions, without having to resort to “Ad-hoc” formulations, such as some of the most common models [15] [16]. This new theory is based on the definition of a State Function,  $\Phi(U, E, t)$ , which describes the thermodynamic evolution of the tracer plume in turbulent flow. This function depends on the mean flow velocity,  $U$ , of the Longitudinal Dispersion Coefficient,  $E$ , of the Feingenbaum Constant,  $\delta \approx 4.6692$ , and of time,  $t$ .

$$\Phi \approx \frac{1}{U} \sqrt{\frac{2 * E * \delta}{t}} \quad (17)$$

It should be noted that clearing the average velocity;  $U$ , from the previous equation, there remains a second-order algebraic definition of a formal nature like the Chezy-Manning equation. The classical expression, equation (15), is a function of mechanical forces, while the new equation (18), is a function of electrochemical forces.

$$U \approx \frac{1}{\Phi} \sqrt{\frac{2 * E * \delta}{t}} \quad (18)$$

The magnitudes  $U$ ,  $E$ , and  $t$  are state parameters, and therefore the Schwartz condition is satisfied:

$$\oint d\Phi(U, E, t) = 0 \quad (19)$$

Notable values of the state function are:  $(t_p, 2.16)$  and  $(t_0, 0.38)$ , corresponding to the concentration peak,  $t_p$ , and now when the tracer loses the transverse degree of freedom,  $t_0$ , and homogeneously fills the cross section of the stream tube through which the tracer advances (“Complete Mix” Condition). Figures 10 and 11.

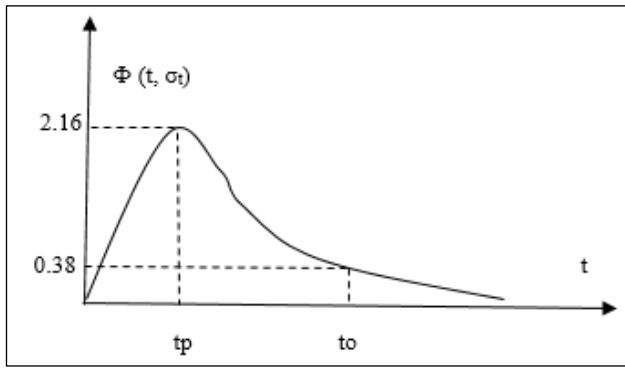


Figure 10: Graph of  $\Phi(U, E, t)$  at notable times.  
Source: Authors, (2021).

The State Function,  $\Phi(t)$ , in its evolution, describes the loss of “Degrees of freedom” of the system, but it also corresponds to the decrease of “Free Energy” in that system.

It must be remembered that when a tracer is injected into the turbulent flow, this mass carries a certain “Energy of formation”, which is a potential energy that can be transformed into useful work.

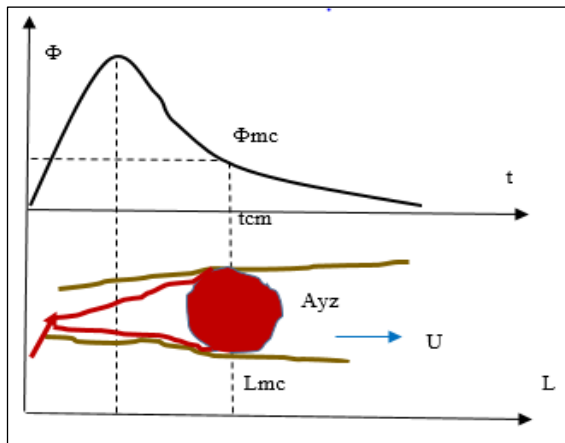


Figure 11: “Complete Mix” condition in flow cross section.  
Source: Authors, (2021).

This “Free Energy”,  $G$ , is gradually used up as the tracer plume advances, generating heat due to the irreversible friction processes in the liquid. Likewise, the principle of entropy increase must be met, and the consequent decrease in entropy production,  $\sigma$ , which tends to a minimum value, when the tracer pen has vanished, and the system is thermodynamically connected with its environment, in the “Dynamic Equilibrium”. Figure 12.

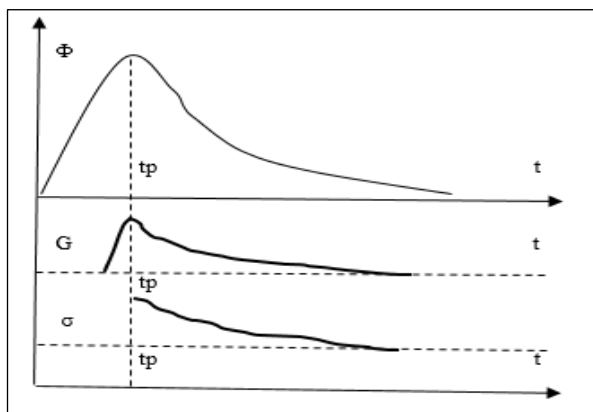


Figure 12: Correspondence between  $\Phi$  and  $G$  and  $\sigma$ .  
Source: Authors, (2021).

The state function,  $\Phi(t)$ , then describes the transition between the “pure” dispersion, at the beginning of the injection of the tracer, until the moment of thermodynamic coupling, when there is “pure” turbulence.

A somewhat general model of this “tracer-turbulence coupling”, in condition of Dynamic equilibrium of the flow, can be made from the thermodynamic analysis of the tracer plume, from the instant of injection:

$$G = H - T * S \tag{20}$$

Where  $H$  is the so-called enthalpy of formation of the tracer solute (constant value depending on the type of substance and its mass), and  $G$  is the Gibbs Free Energy, which decreases as the entropy increases. It must be understood that the tracer plume itself, when evolving in the turbulent flow, does not differ essentially from its environment, except for containing that decreasing Free Energy. Figure 13.

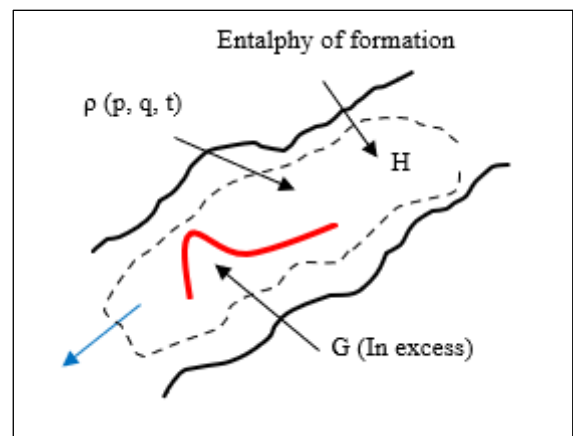


Figure 13: Tracer plume evolving on turbulent flow with an excess of free energy.  
Source: Authors, (2021).

In the previous figure, under the condition of a linear “steady state” in the flow, Equiprobability entails a single probabilistic distribution, to which the tracer plume is quite close, until it is completely integrated with its environment, and participates exactly in all its thermodynamic characteristics.

On the other hand, entropy,  $S$ , and entropy production,  $\sigma$ , are inverse values, while the former increases monotonically to a maximum value, the latter gradually decreases to a minimum value. Figure 14.

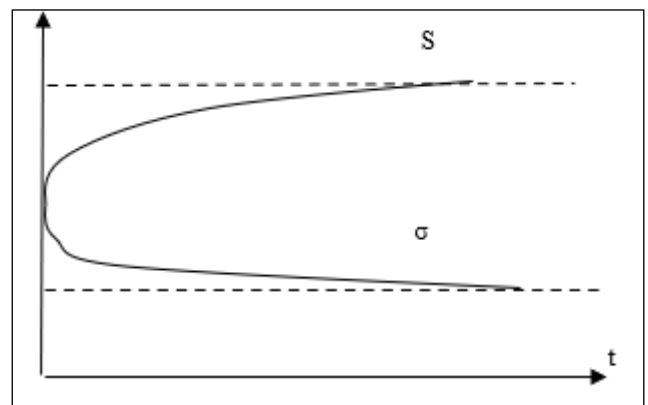


Figure 14: Relationship between Entropy and Entropy production in a linear system.  
Source: Authors, (2021).

Therefore, if “a” is a constant of proportionality, it can be established approximately that:

$$S(t) \approx \frac{a}{\sigma(t)} \tag{21}$$

On the other hand, both the state function,  $\Phi(t)$  and the free energy, decrease monotonically, and it can be said that they are proportional, by means of the constant “b”:

$$G(t) \approx b * \Phi(t) \tag{22}$$

Then, equation (20) becomes:

$$b * \Phi(t) \approx H - T * \left(\frac{a}{\sigma(t)}\right) \tag{23}$$

From this equation in general, it can be verified that the State Function and the Entropy Production are related.

### II.6 A NEW MODEL OF TRACER EVOLUTION IN A TURBULENT FLOW

Starting from the classic Fick equation, clearing the value of the Coefficient E, from equation (18) and replacing it in the classic Fick equation, equation (16), with Q, as discharge, it holds:

$$C(t, X) \approx \frac{M}{Q * \Phi * t * 1.16} e^{-\frac{(t_p - t)^2}{\left(\frac{2}{8}\right) * (\Phi * t)^2}} + C_0 \tag{24}$$

It is useful with respect to the previous equation, to define a “dilution factor” corresponding to the decrease of the peak concentration (the first factor of the right limb) with time.

$$Cp \approx \frac{M}{Q * \Phi * t * 1.16} \tag{25}$$

The subsequent analysis of the basic equation of the State Function,  $\Phi(t)$ , equation (17), the following expression can be established, which relates  $\Phi$  with  $\sigma t$  (standard deviation in time), and with  $t_p$ , the time of the peak:

$$\Phi \approx 2.16 \left(\frac{\sigma t}{t_p}\right) \tag{26}$$

An important characteristic of the State Function Application Method is that its computations are made based on the Peak Time,  $t_p$ , and not based on the “Centroid Time”,  $t_s$ , as is the case with most of current methods. As is known, this time corresponds to the center of gravity of a physical system, that is, where the center of mass is located. Figure 15.

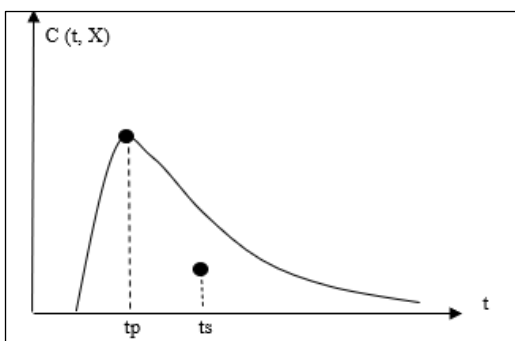


Figure 15: Peak time, and Centroid time. Source: Authors, (2021).

Now, although apparently this value has a remarkable physical significance for a dynamic system, it has the problem that, in general, there is only one statistical formula for its calculation, which makes it difficult to use in practice. A detailed analysis of this parameter indicates that the difference between the Peak Time and the Centroid Time decreases as the tracer pen advances, indicating that in a certain way this concept reflects that the bias of the curve Fickiana is eliminated at the end, so that she can actively join the dispersal [17].

This non-availability of mass is maintained in practice until the moment in which the tracer homogeneously covers the cross section of the stream tube through which the pen advances, that is, when the State function is equal to  $\Phi \approx 0.38$ , as shown in Figure 10. In this case the Centroid Time is only 13% greater than the Peak Time.

Now, with the remarkable values of the curve in Figure 6, it is possible to draw the two approximate real Fickiana curves, with different data, as shown in Figure 16.

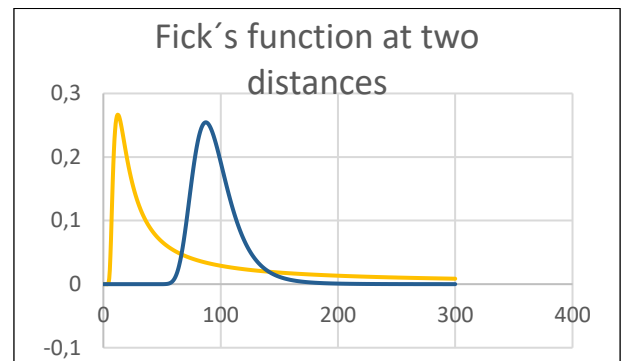


Figure 16: Tracer curves with different skew. Source: Authors, (2021).

Two important aspects should be noted: A - The bias of the first curve is much more accentuated than that of the second curve, and B.- That the concentration of the second curve is slightly lower than that of the first, as expected since the mass of the tracer is expanding.

The initial curve (yellow) corresponds to the immediate injection point, when  $\Phi \approx 2.16$ , its maximum value, here it is fulfilled that  $\sigma t \approx t_p$ ; the second curve (blue) corresponds to a further point, when  $\Phi \approx 0.382$ , the value for "Complete Mix" on the flow cross section.

The reason for the decreasing bias in the tracer Fickian curves is that the state function,  $\Phi(t)$ , decreases with time, and suppressing sequentially degrees of freedom in the system, releasing mass from its initial cohesive volume. Simultaneously the free energy of the tracer is spent, and the production of entropy is tending to a minimum. In this way, the tracer is coupling with its environment, which is in a "stable state" condition of the thermodynamic linear region.

### III. APPLICATION TO AN EXPERIMENTAL CASE: COOPER CREECK, VA. USA (1963)

To apply and adjust various river measurement methodologies in the 1950s, the United States Geological Survey (USGS) performed tracer measurements at selected sites, including the Cooper Creek River near Gage City, Virginia. The river flow when the measurements were made (1959) was in a range of 10 to 15 m<sup>3</sup>/s [18].

To analyze the data from this experiment, Godfrey & Frederick made an initial analysis of the field data, and Thackston,



Hays & Krenkel then carried out a detailed analysis of the possible theoretical alternatives to calculate the Longitudinal Coefficient of Dispersion, since the curves obtained experimentally, they showed some bias (of the Pearson-III type), and the conventional methods of the time did not allow adequate accuracy. For this reason, it was preferred to use the Moments method, which does not recognize the so-called “convective period” (recognized by most other methods), which prevented its application in the early phase of the tracer's evolution. This method only requires that the velocity be approximately constant [19].

To apply and adjust various river measurement methodologies in the 1950s, the United States Geological Survey (USGS) performed tracer measurements at selected sites, including the Cooper Creeck River near Gage City, Virginia. The river flow when the measurements were made (1959) was in a range of 10 to 15 m3/s [20].

To analyze the data from this experiment, Godfrey & Frederick made an initial analysis of the field data, and Thackston, Hays & Krenkel then carried out a detailed analysis of the possible theoretical alternatives to calculate the Longitudinal Coefficient of Dispersion, since the curves obtained experimentally, they showed some bias (of the Pearson-III type), and the conventional methods of the time did not allow adequate accuracy. For this reason, it was preferred to use the Moments method, which does not recognize the so-called “convective period” (recognized by most other methods), which prevented its application in the early phase of the tracer's evolution. This method only requires that the velocity be approximately constant [21].

To compare the results of the classical Method of Moments and the Method based on the application of the State Function, presented in this Article, the experiment in the Cooper Creek River, VA is analyzed. USA, previously documented. Thus, pouring tracer at an “upstream” point, and measuring the passage of the tracer “downstream”, at X1≈2.40 Km, and X≈4.10 Km. The data were shown in Table 1.

Table 1: Concentration data. Source: Prepared by the authors based on (McCutcheon & Martin, 1999). Source: Prepared by the authors based on (McCutcheon & Martin, 1999).

Tiempo (s)	Concentración 1 (ppb)	Concentración 2 (ppb)
0		
600		
1200		
1800	0,02	
2400	3,92	
3000	39,5	
3600	97,3	0,01
<b>4200</b>	<b>107</b>	<b>0,41</b>
4800	71,9	5,11
5400	34,6	24,1
6000	13,2	57,1
<b>6600</b>	<b>4,24</b>	<b>82</b>
7200	1,2	80,9
7800	0,31	59,8
8400	0,01	35,3
9000		17,4
9600		7,4
10200		2,79
10800		0,95
11400		0,3
12000		0,09
12600		0,02
13200		0,01
13800		
14400		
15000		

Source: Authors, (2021).

The next Figure 17 presents the graphing of the sequential curves corresponding to the data in Table 1.

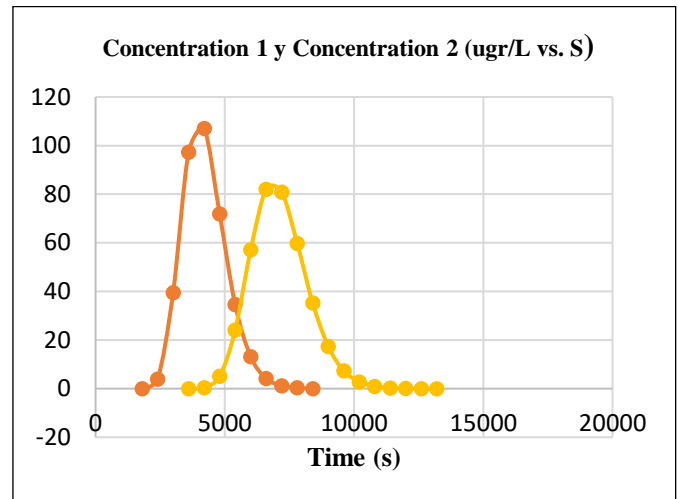


Figure 17: Plotting of the tracer data over time. Source: Authors' elaboration.

Source: Authors, (2021).

The statistical technique of Moments, operates under the assumption that the flared tracer curve can be assimilated to a Gaussian curve, in an approximate way, and thus the Longitudinal Dispersion Coefficient, E.

$$E \approx 0.5 \left( \frac{d\sigma_x^2}{dt} \right) \quad (27)$$

As the discrete experimental data are normally available as a function of time, the above equation can be transformed as follows:

$$E \approx \frac{U^2}{2} \left[ \frac{\sigma_{t2}^2 - \sigma_{t1}^2}{\langle t_2 \rangle - \langle t_1 \rangle} \right] \quad (28)$$

That is, the reason for the differences in the temporal variances at the two measurement points, and the mean times at those points.

Properly manipulating the experimental data and applying the corresponding equations to this method, we have for the two points considered, both the centroid times of the curves, as well as the variances. For these calculations, usual statistical formulas are applied [22].

$$tc1 = \frac{\int t \cdot C dt}{\int C dt} = \frac{26298 \text{ min} \cdot \text{ug/l}}{373,2 \text{ ug/l}} \approx 70,47 \text{ min} \quad (29)$$

$$tc2 = \frac{\int t \cdot C dt}{\int C dt} = \frac{45581 \text{ min} \cdot \text{ug/l}}{373,7 \text{ ug/l}} \approx 118,8 \text{ min} \quad (30)$$

And:

$$\sigma t^2 = \frac{\int t^2 \cdot C dt}{\int C dt} - t_c^2 = \frac{1926000 \text{ m}^2 \cdot \frac{\text{ug}}{\text{l}}}{373,2 \frac{\text{ug}}{\text{l}}} - (70,47 \text{ min})^2 \approx 195,0 \text{ min}^2 \quad (31)$$

$$\sigma t^2 = \frac{\int t^2 \cdot C dt}{\int C dt} - t_c^2 = \frac{5537766 \text{ m}^2 \cdot \frac{\text{ug}}{\text{l}}}{373,7 \frac{\text{ug}}{\text{l}}} - (118,2 \text{ min})^2 \approx 319,8 \text{ min}^2 \quad (32)$$

Now, the average flow velocity is calculated in this method by the following formula:



$$U = \frac{X_2 - X_1}{t_{c_2} - t_{c_1}} \approx \frac{(4100 - 2400)m}{(118,8 - 70,47)min} \approx 35,17 \text{ m/min} \quad (33)$$

Therefore, the Longitudinal Coefficient of dispersion in this case is:

$$E = \frac{U^2}{2} * \frac{(\sigma_{t_2}^2 - \sigma_{t_1}^2)}{(t_2 - t_1)} \approx \frac{(35,17 \text{ m/min})^2}{(118,8 - 70,47)min} * (319,8 - 195)m^2 \approx 1595 \text{ m}^2/min \quad (34)$$

Transforming this expression from minutes to seconds we have:

$$E \approx 27,0 \text{ m}^2/s \quad (35)$$

This is then the average value of the Longitudinal Dispersion Coefficient in the section studied, obtained with the classic statistical method of Moments.

The next step is to apply the method that includes the State function and compare the results with the previous data. This analysis is part based on the following Figure 18.

For this figure, tv1 and tv2 are the times for the peak of each distribution, and tpp1 and tpp2 are the times of the first particles of each distribution. Likewise, δ'1 and δ'2 are the standard deviations of each distribution in time, multiplied by two.

For the concrete calculations of the State Function theory, we have the following approximate formulas, based on the properties of the Gaussian function.

$$\Phi(t) \approx (\delta')/tv \quad (36)$$

It is now possible to calculate the values of the State Functions at each time of interest.

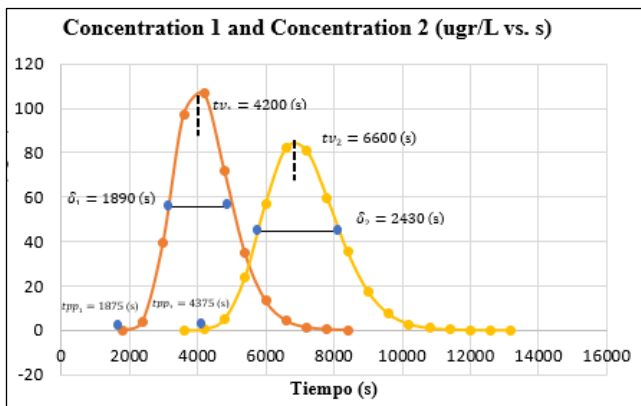


Figure 18: Data for corresponding calculations. Source: Authors, (2021).

$$\Phi_1(4200) = \frac{\delta'_1}{tv_1} = \frac{1890}{4200} = 0,45 \quad (37)$$

$$\Phi_2(6600) = \frac{\delta'_2}{tv_2} = \frac{2430}{6600} = 0,37 \quad (38)$$

Note that the available documentation of this experiment does not report neither the mass nor the flow, data that are needed to model tracer curves, equation (24). To solve this fault, the ratio "M / Q" is calculated. For the first curve:

$$Cp1 \sim 107.0 \text{ (ugr/L)}, \Phi1 \sim 0.45 \text{ and } tv1 \sim 4200 \text{ s}$$

$$\left(\frac{M}{Q}\right)_1 \approx 107 \left(\frac{ugr}{l}\right) * 0,45 * 4200 * 1,16 \approx 234587 \quad (39)$$

**Curve 1 modeling:**

With these data, the first tracer curve can be modeled, applying equation (24). The blue curve is the experimental data, while the built model is the green curve. Figure 19.

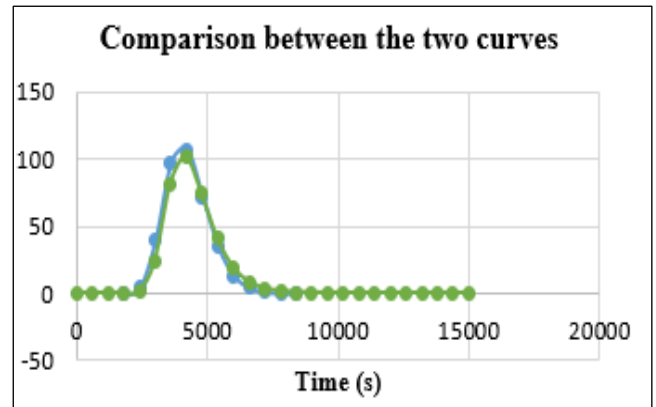


Figure 19: Experimental curve 1 and model with Φ (t). Source: Authors, (2021).

Now, the slight lag observed in the modeling of the experiment in curve 1 can be improved with changes in the time of the peak, and in the data of the state function, for that specific point, like this:

$$Cp1 \sim 108.9 \text{ ug/L}, \Phi1 \sim 0.41, \text{ and } tv1 \sim 4100 \text{ s.}$$

These changes are included in equation (24), which describes the Fickian curve 1, shown below. Figure 20:

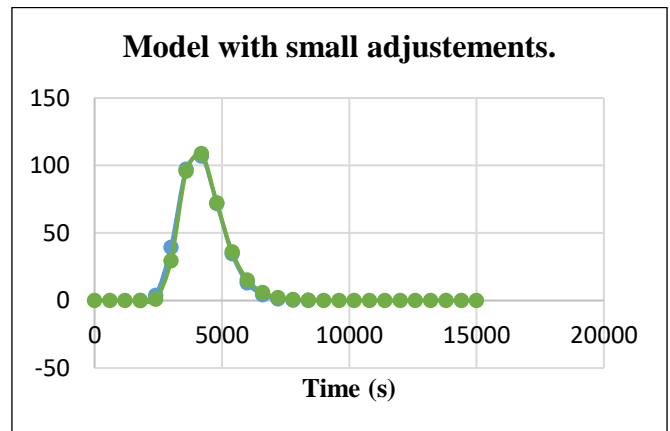


Figure 20: New modelling of first curve with small changes. Source: Authors, (2021).

**Curve 2 modeling:**

We now proceed to model the curve at point 2, considering the corresponding data:

$$Cp \sim 82.0 \text{ (ugr/l)}, \Phi \sim 0.37, \text{ and } tv \sim 6600 \text{ s.}$$

For this new curve, the ratio "M / Q" must be recalculated, from the attenuation factor that is valid there. For this new curve, the ratio "M/Q" must be recalculated, from the attenuation factor that is valid there.

$$\left(\frac{M}{Q}\right)_2 \approx 82 \left(\frac{ugr}{l}\right) * 0,37 * 6600 * 1,16 \approx 232283 \quad (40)$$

This value for the second curve is virtually the same as that calculated for the first curve, indicating good precision for the

implicit value of the flow rate (whatever it is). For the modeling of curve 2, the procedure used in curve 1 is repeated. Figure 21.

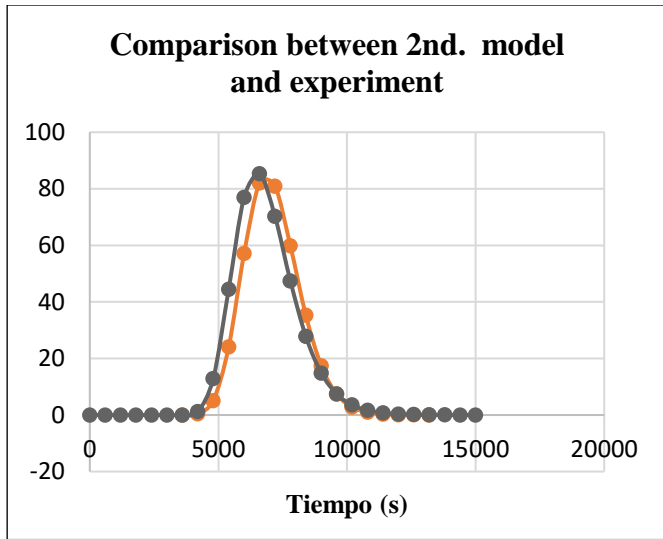


Figure 21: Experimental curve and model with  $\Phi(t)$ .  
Source: Authors, (2021).

Again, it is seen that between the theoretical model (gray) and the experimental data (orange) there is an evident lag between the curves. Now, if the data in table 1 is analyzed in detail, it can be observed that in this area of the peak (of abrupt variation), the temporal separation of the sequential measurements is “greater” than the required temporal resolution. So, the “true” time of the peak (for the model) is a little further to the right in time. We then have the following characteristic set:

$$Cp2 \sim 82.0 \text{ (ugr/L)}, \Phi2 \sim 0.344, \text{ and } tv \sim 6650 \text{ s}$$

With these values in equation (24), we have that quite coincident curves are obtained. Figure 22.

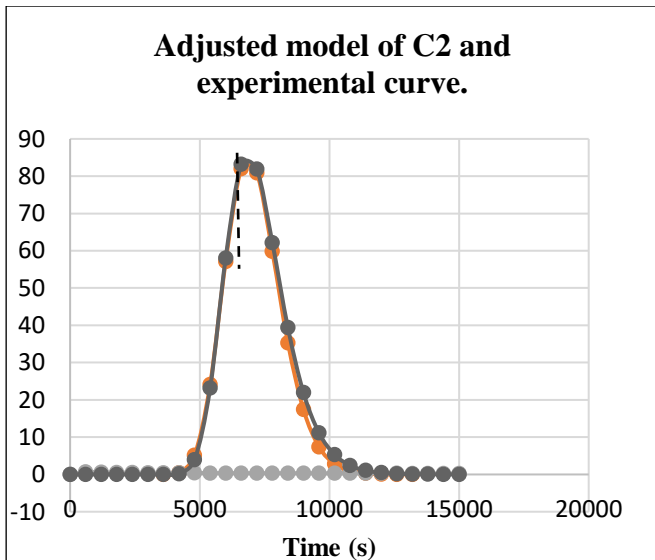


Figure 22: Refined curve with better data.  
Source: Authors, (2021).

From the “optimal” data (which corresponds to the curves in Figures 20 and 22), previously established for the section under study, the value of the Longitudinal Dispersion Coefficient is calculated and compared with the original data established by the Method of Moments.

**Curve 1:**

The optimal data set is:

$$Cp1 \sim 108.9 \text{ ug/L}, \Phi1 \sim 0.41, \text{ and } tv1 \sim 4100 \text{ s.}$$

Therefore:

$$E1 \approx \frac{\varphi^2 * U^2 * \beta * tv}{2} \approx \frac{0.41^2 * 0.59^2 * 0.214 * 4100}{2} \approx 25,7 \text{ m}^2/\text{s} \quad (41)$$

**Curve 2:**

The optimal data set is:

$$Cp2 \sim 82.0 \text{ (ugr/L)}, \Phi2 \sim 0.344, \text{ and } tv \sim 6650 \text{ s}$$

Therefore:

$$E2 \approx \frac{\varphi^2 * U^2 * \beta * tv}{2} \approx \frac{0.344^2 * 0.62^2 * 0.214 * 6650}{2} \approx 32.4 \text{ m}^2/\text{s} \quad (42)$$

An average value for the two curves 1 and 2 is:

$$\langle E \rangle \approx \frac{25.7 + 32.4}{2} \approx 26,7 \text{ m}^2/\text{s} \quad (43)$$

As can be seen, the value of the Longitudinal Dispersion Coefficient calculated with the State Function Method is remarkably close to that calculated with the classical Method of Moments, with a relative error of 1%. The State Function Method works with the velocity of the peak of the concentration and does not recognize an initial period in which Fickian physical theories cannot be applied for its interpretation. Nor does it need the concept of “Centroid” (difficult to calculate) which is explained in a natural way, because of the unavailability of mass for dispersion, which is measured by the decaying values of the State Function.

It also offers a direct explanation of the skew characteristic of these curves. Finally, calculating the peak velocities for the two measurement points,  $U1 \approx 0.59 \text{ m/s}$  and  $U2 \approx 0.62 \text{ m/s}$ , the established by L. Leopold [23] is verified in that the average velocities of a natural channel in “Dynamic equilibrium” are approximately constant, as already explained, ensuring in a certain way, the accuracy of the Moments method.

**IV. RESULTS, DISCUSSIONS AND RECOMMENDATIONS**

1 - As analyzed in detail in this Article, the “linear” nature of turbulence responds to a relatively small value of the notable factor (W/RT), which defines the “fluidity” of liquid water at room temperature and facilitates attenuation. of speed fluctuations. This condition allows the application of Prigogine’s theorem of the minimum entropy production, and therefore of the fulfillment of the “equiprobability” in the system.

In this circumstance, what is described in Figure 4, about the statistical constancy of the mass transfer between points of the system, and consequently of a “constant” average flow velocity along the course of the channel, is approximately fulfilled. The real degree of compliance with this condition is reflected in a lower or greater absolute error, equations (6) and (7).

2 - The dynamics of the tracers in turbulent flows is not independent of the turbulence itself. With the injection of the tracer to the flow, the local thermodynamic condition of the same is disturbed, since the plume carries a certain amount of Free Energy, which is spent by irreversible effects, as the plume advances in time and space, as in Figure 13.

3 - The above indicates that said irreversible evolution of the tracer in turbulent flow is governed by the general laws of

thermodynamics, and therefore it is essential to determine a "State function" that describes said evolution. The authors have presented a model of such a function in this regard. This function is applied to a specific case of a tracer experiment, taken from the technical literature, and is compared with the classical numerical results of the Statistical Moments method. The comparison between the two methods is completely satisfactory, supporting the theoretical assumptions on which the new method was based.

4 - A hardware-software tracer device is presented that operates in "real time" and incorporates the new tracer evolution state function.

5 - Further research should determine the values of the constants "a" and "b" of the equations that link the state function and the production of entropy.

## V. AUTHOR'S CONTRIBUTION

**Conceptualization:** Alfredo Jose Constain, Gina Peña Olarte and Carlos Peña Guzman.

**Methodology:** Alfredo Jose Constain, Gina Peña Olarte and Carlos Peña Guzman.

**Investigation:** Alfredo Jose Constain, Gina Peña Olarte and Carlos Peña Guzman.

**Discussion of results:** Alfredo Jose Constain, Gina Peña Olarte and Carlos Peña Guzman.

**Writing – Original Draft:** Alfredo Jose Constain, Gina Peña Olarte and Carlos Peña Guzman.

**Writing – Review and Editing:** Alfredo Jose Constain, Gina Peña Olarte and Carlos Peña Guzman.

**Resources:** Alfredo Jose Constain, Gina Peña Olarte and Carlos Peña Guzman.

**Supervision:** Alfredo Jose Constain, Gina Peña Olarte and Carlos Peña Guzman.

**Approval of the final text:** Alfredo Jose Constain, Gina Peña Olarte and Carlos Peña Guzman.

## VI. ACKNOWLEDGMENTS

Our thanks to the "Fluvia" company and to the "Universidad de la Salle", in Bogota, Colombia, for their permanent support to these research tasks.

## VII. REFERENCES

- [1] P. W. Anderson, «Physics: the opening to complexity.», Proc. Natl. Acad. Sci. U. S. A., vol. 92, n.o 15, pp. 6653-6654, jul. 1995.
- [2] I. Prigogine and G. Nicolis, "La estructura de lo complejo". Alianza Editorial. Madrid, 1987.
- [3] D. Kondepudi and I. Prigogine, "Modern Thermodynamics". Wiley, USA, 1996.
- [4] L.B. Leopold and W. Langbein, "The concept of entropy in landscape evolution". USGS Paper 502-A, 1962.
- [5] I. Prigogine, "The end of certainty". Free Press, USA. 1997.
- [6] I. Prigogine, "Las leyes del caos". Critica, Barcelona, 1997.
- [7] R. Penrose, "The Cycles of time". Random House, Barcelona.2010.
- [8] D. Kondepudi and I. Prigogine I., Ibid, 1996.
- [9] J. Frenkel, "Kinetic theory of liquids". Dover, USA, 1955.
- [10] A. Christofolletti, "Geomorfología fluvial". Edgard Blucher, Sao Paulo. 1981.
- [11] T. Ochoa, "Hidraulica de rios y procesos morfológicos". ECOE Ediciones, Bogota, 2011.

[12] A. Constain, C. Peña-Guzman and D. Mesa, "Equivalence of local and general mass transport rates in natural beds in dynamic equilibrium", Aqualac, Montevideo, 2015. V7. 1-02.

[13] A. Constain and R. Lemos, «Una ecuacion de la velocidad media del flujo en regimen no uniforme, su relacion con el fenomeno de dispersion como funcion del tiempo y su aplicacion a los estudios de calidad de agua», Ing. Civ., vol. 164, pp. 114-135, 2011.

[14] A. Constain, «Definición y análisis de una función de evolución de solutos dispersivos en flujos naturales», Dyna, vol. 175, pp. 173-181, 2012.

[15] H.B. Fischer "Dispersion predictions in Natural streams". Journal of Sanitary Engineering division, ASCE, october, 1968.

[16] H.B. Fischer. "Longitudinal dispersion in laboratory and natural streams". Report No. KH-R-12, June 1966, USA.

[17] T. Makela. and A. Annala, "Natural patterns of energy dispersal". Physics of life review. 7 (2010)

[18] R Godfrey. and B. Frederick, "Stream dispersion at selected sites". USGS 433-K Paper. 1070.

[19] L. B Leopold, «Downstream change of velocity in rivers», Am. J. Sci., vol. 251, n.o 8, pp. 606-624, ago. 1953.

[20] J.L. Martin and S.C McCutcheon, "Hydrodynamics and transport for wáter quality modeling". Lewis. Boca ratón. 1999.

[21] H.B. Fischer. Ibid. 1966

[22] J.L Martin and S.C McCutcheon. ibid. 1999.

[23] L. B. Leopold. Ibid 1953.



ISSN ONLINE: 2447-0228

## ITEGAM-JETIA

Manaus, v.7 n.30, p. 29-36. Jul/Aug, 2021  
DOI: <https://doi.org/10.5935/jetia.v7i30.768>



RESEARCH ARTICLE

OPEN ACCESS

## DETECTION OF PLANT LEAF DISEASES USING RECENT PROGRESS IN DEEP LEARNING-BASED IDENTIFICATION TECHNIQUES

Jency Rubia J\*<sup>1</sup> and Babitha Lincy R<sup>2</sup>

<sup>1</sup> Asst. Prof. Department of ECE, M.A.M College of Engineering and Technology, Tiruchirappalli, India.

<sup>2</sup> Research Scholar, Department of ECE, Sri Venkateswara College of Engineering, Sriperumbudur, India.

<sup>1</sup> <http://orcid.org/0000-0002-0088-3611> , <sup>2</sup> <http://orcid.org/0000-0003-2520-2410> 

Email: \*jencyrubia@gmail.com, rblincy@gmail.com

### ARTICLE INFO

#### Article History

Received: August 06<sup>th</sup>, 2021

Accepted: August 23<sup>th</sup>, 2021

Published: August 31<sup>th</sup>, 2021

#### Keywords:

Plant Leaf Diseases Detection,  
Deep Learning Models,  
Image Processing,  
AlexNet,  
GoogleNet.

### ABSTRACT

Mostly economy profoundly depends on farming efficiency. The farming crops are commonly affected by the disease. Since the economy depends on agriculture, this is one of the core reasons that infection identification in plants assumes a significant job in the horticulture field. On the off chance that legitimate consideration isn't taken here, at that point, it causes natural consequences for plants and because of which particular item quality, amount, or efficiency are influence. Crop misfortune because of ailments considerably influences the economy and undermines food accessibility. Quick and precise plant ailment location is essential to expanding farming efficiency in a supportable manner. In any case, plant location by human specialists is costly, tedious, and sometimes unrealistic. To counter these difficulties, Plant pathologists want an exact and dependable plant sickness conclusion framework. The on-going utilization of deep learning procedure with image processing methods for plant sickness acknowledgment has become a hot examination subject to give programmed analysis. This research provides a productive plant illness distinguishing proof technique dependent on pre-prepared deep learning models, such as AlexNet and GoogleNet designs. We trust that this work will be a significant asset for analysts in the area of ailment acknowledgment utilizing image handling strategies with deep learning architectures.



Copyright ©2016 by authors and Galileo Institute of Technology and Education of the Amazon (ITEGAM). This work is licensed under the Creative Commons Attribution International License (CC BY 4.0).

### I. INTRODUCTION

In India, tomatoes and potatoes are the significant crop plant after the main crops such as rice and wheat. Leaf blight and bacterial spot are the most predominant maladies of the tomatoes and potatoes. Plant infections have consistently been a noteworthy worry in agribusiness since they cause a decrease in crop quality. The crop plant diseases might make generous monetary misfortunes since the rural Indian economy exceptionally based on agricultural productivity efficiency. The impacts of plant ailments extend from minor manifestations to the genuine harm of whole zones of planted harvests, which causes major budgetary expenses and effects vigorously on the horticultural economy, particularly in creating nations [1]. If these maladies distinguish at an underlying stage and therapeutic measures take at that starting point, crop yield and grain quality

might be protected. At the beginning phase, the side effects of plant diseases show on various pieces of infected plants, especially leaves, in terms of perceptible change in shading and spots. To distinguish a plant malady in the starting stage, utilization of the programmed illness identification method is useful. In this manner, there is an incredible interest in exact recognizable proof strategies for plant leaf maladies.

The current strategy for plant malady recognition is by eye perception of specialists through which distinguishing proof and discovery of plant sicknesses [2]. In doing so, a large group of specialists just as constant observing of the plant requires, which costs extremely high when doing with vast ranches of area. In such conditions, the proposed automatic plant leaf disease strategy ends up being valuable in checking vast fields of yields. Automatically recognizing the plant's weaknesses by merely



spotting the side effects on the crop leaves makes it more straightforward and less expensive. Plant sickness by expert's visual way is more relentless assignment and, at the same time, less precise and should be conceivable just in reserved zones. If an automatic recognition procedure utilizes, it will take fewer endeavors, less time, and become more accurate. In the new era, machine learning strategies have gained some attention in leaf malady detection [3]. The machine learning-based strategies have been fruitful in recognizable proof of plant diseases. Different explores such as neural network and support vector machine algorithms have occurred under the field of machine learning for plant malady location detection.

Upgrades in machine learning procedures lately have made them the best in class among different computer vision approaches for image processing applications. A deep learning strategy is another pattern in the artificial intelligence-based machine learning approach, and it accomplishes best in image

classification fields. Deep learning empowers the immediate utilization of crude information without utilizing carefully assembled highlight features [4]. A customary machine learning-based computer vision tactic for crop illness identification requires manual determination of characteristics. Interestingly, profound deep learning strategy based convolutional neural systems naturally learn the most significant feature highlights by multilayer [5-6]. So deep learning-based mechanized location procedures gives an open door in the field of accuracy farming. Preparing a deep convolution neural system requires a gigantic measure of information and elite processing assets. The primary point of the deep learning technique is successfully distinguishing the sickness of a plant leaf and improves the acknowledgment rate [7-8]. In the deep learning strategy, there are lots of pre-trained models presented, such as CNN, AlexNet, GoogleNet, and so on. Some of the existing research related to plant disease recognition shown in Table 1.

Table 1: Existing research related to plant diseases recognition.

S. No	Author and Year	Model name	Comments
1.	Mrunalini R Badnakhe, 2011 [5]	K-means clustering algorithm	Neural network use the K-means clustering algorithm for plant diseases recognition. Accuracy level can increase.
2.	Kulkarni Anand H, Ashwin Patil RK, 2012 [6]	Artificial Neural Network	Artificial Neural Network used for classification with the Gabor filter based feature extraction. Recognition level can better.
3.	Arivazhagan S, Newlin Ananthi S, 2013 [7]	Support Vector Machine	Support Vector Machine used for classification. The dataset amount can be increased.
4.	Amara, J.; Bouaziz, B.; Algergawy, A, 2017[8]	Modified LeNet	CNN based Modified LeNet used for recognition. Error rate can be reduce.
5.	Cruz, A.C.; Luvisi, A.; De Bellis, L.; Ampatzidis, 2017[9]	Modified LeNet	CNN based Modified LeNet used for recognition. Accuracy rate can be increase.

Source: Authors, (2021).

This research paper's principal goal is to manage the food productivity by earlier observing of crop health like leaf symptoms. The vital aim is to generate an automatic deep learning-based crop disease detection system. This paper deliberates on Alexnet and GoogleNet based model for healthy and defected leaf classification. Generally, out-dated machine learning-based image classification includes preprocessing, segmentation, highlighted feature information extraction and classification. But advanced, deep learning approach includes preprocessing, segmentation, and grouping with automatic feature extraction.

## II. MATERIAL AND METHODS

### II.1 DATASET

This work uses the PlantVillage dataset, which consists of 15 different plant classes with the images of pepper bell, tomato, and potato diseases. The PlantVillage dataset includes leaf disease image samples for disease identification. This dataset contains approximately 3700 samples and which is freely available. This research selected the image of the pepper bell, tomato, and potato leaves from the data set for analysis [9]. The pepper bell leaf dataset was composed of symptom images of healthy pepper bell leaf and pepper bell leaf bacterial spot. The potato leaf dataset was composed of symptom images of healthy potato leaf, potato early blight and potato Late blight affected leaf [10]. The tomato dataset contains healthy leaf image with target spot affected leaf, mosaic virus affected leaf, yellow leaf curl virus affected leaf,

bacterial spot affected leaf, early and late blight affected leaf, spot affected leaf, spider mites, and two-spotted spider mite disease affected leaf images. In this paper, each class utilizes the 200 e samples for each category. Some of the corresponding images show in Figure 1.

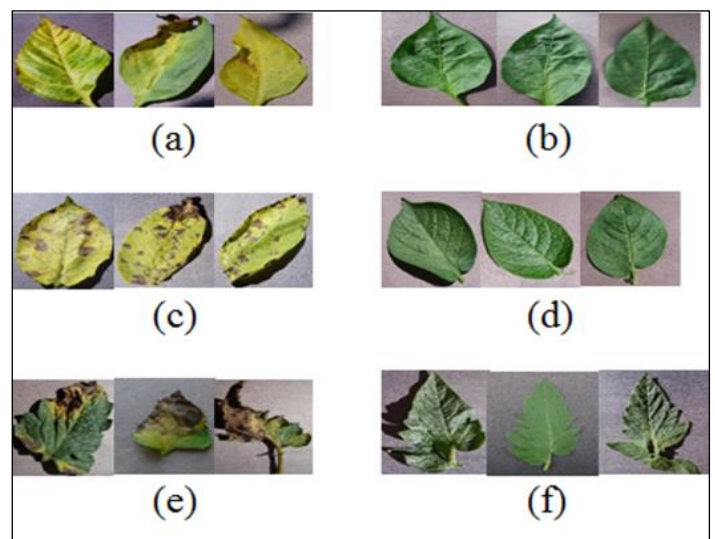


Figure 1: (a) Pepper bell Bacterial spot (b) Pepper bell healthy (c) Potato early blight (d)Potato healthy (e) Tomato Early blight (f) Tomato healthy.

Source: Authors, (2021).



**II.2 BACKGROUND**

CNN generally utilizes deep learning models in taking care of pictures related to assignments like identification, detection, classification, and so on [11-13]. These systems commonly blend convolution layers, pooling layers, and completely associated (fully connected) layers. These three squares utilize to build a CNN model by changing the number of layers, including or erasing a layer. CNN picture classification takes an information picture as input, processes it, and characterizes it under specific classes (Example: healthy leaf and disease affected leaf). When using Deep learning-based CNN models to train and test, each informative image samples will go through a progression of convolution layers with channels (Kernals), pooling, completely associated layers (FC). Finally applies to Softmax capacity to arrange an item with probabilistic qualities somewhere in the assortment of zero and one [14].

Convolution is the first layer to extricate highlight feature information from an input sample image. Convolution saves the association between pixel values by learning image feature highlights utilizing little squares of information. The pooling layers segment would diminish the number of boundaries when the image samples are excessively huge [15]. Spatial pooling, also called subsampling or downsampling, reduces each guide's dimensionality yet holds essential data. The layer called as FC layer straightened the grid into the vector and fed it into a wholly associated layer like a neural system. Different models have created since 2012 Imagenet rivalry, which had decreased the misclassification rate from 15.6% to 3.7% more than four years. Every model had shifting hyper boundaries or had utilized new strategies like Drop out, Image augmentation, regularization, normalization, Batch standardization, and so on. In this research,

the plant disease classification model is using the AlexNet and GoogleNet model [16-18].

**II.3 ALEXNET**

Even though CNN based, LeNet was notable in the PC vision and AI model group, which accomplished excellent outcomes on new little datasets. The presentation and practicality of preparing convolutional systems on more significant, more sensible datasets still couldn't seem set up. AlexNet is one of the CNN based models for image characterization. It broadly won the 2012 ImageNet LSVRC-2012 rivalry by a large margin in second place with 15.3% VS 26.2% error rates [Krizhevsky et al., 2012]. The structures of AlexNet and LeNet are fundamentally the same. AlexNet utilized an 8-layer convolutional neural system. This system demonstrated that just because the feature highlights got by learning can rise above physical configuration feature highlights, breaking the past worldview in PC vision [19].

Even though the AlexNet system had a fundamentally the same as design as LeNet, however, was more profound with more channels per layer, and with stacked convolutional layers. It comprises 11x11, 5x5, 3x3, convolutions, max pooling, dropout, information expansion technique by image augmentation, ReLU activations, and SGD with momentum. It joined the ReLU function after each convolutional and completely associated fully connected layer. In AlexNet's first layer, the convolution window shape is 11x11. Subsequently, a bigger convolution window expects to catch the item. The convolution window shape in the subsequent layer is diminished to 5x5, trailed by 3x3. Likewise, after the principal, second, and fifth convolutional layers, the system includes the most significant pooling layers with a window state of 3x3 and a stride of 2. Additionally, AlexNet has multiple times more convolution channels than LeNet.

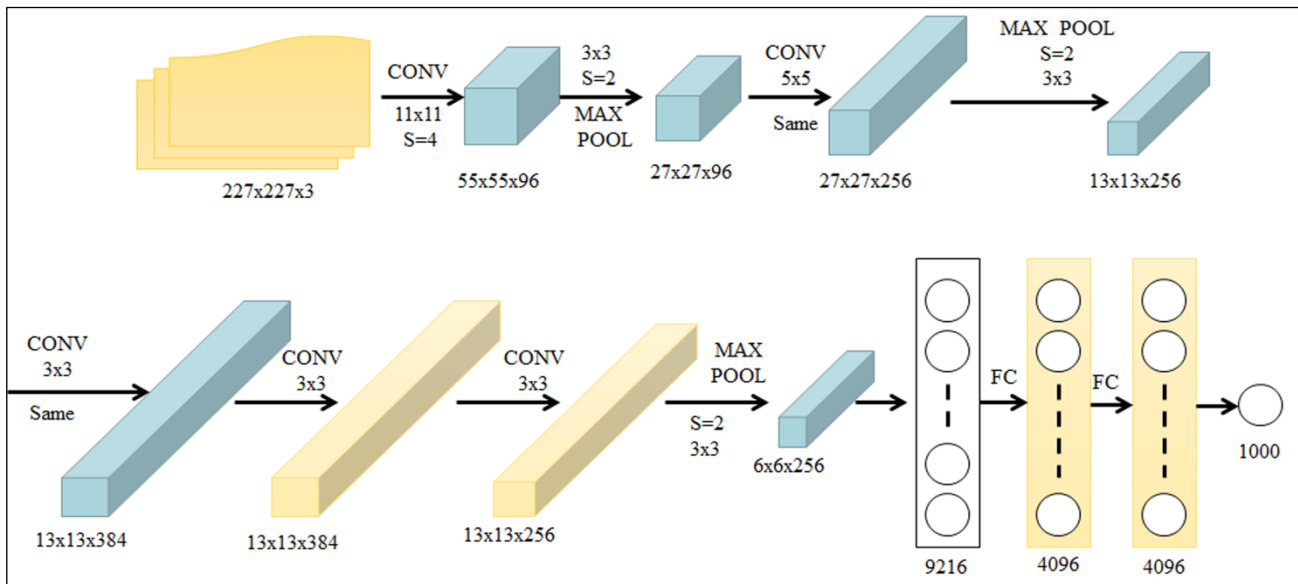


Figure 2: AlexNet architecture. Source: [10].

After the last convolutional layer, there are two wholly associated FC layers with 4096 yields. These two gigantic completely associated layers produce model parameters of about 1 GB. AlexNet changed the sigmoid function to a more accessible ReLU initiation work. From one perspective, the calculation of the ReLU enactment work is more straightforward [20-22]. For instance, it doesn't have the exponentiation activity found in the

sigmoid activation work. Relu actuation work utilizes rather than Tanh to include non-linearity. It quickens the speed by multiple times at a similar exactness. The AlexNet model uses dropout rather than regularization to manage to overfit. Be that as it may, the preparation time multiplies with the dropout pace of 0.5. It decreases the top 1 and top-5 mistake rates by 0.4% and 0.3%, individually. The AlexNet model display in Figure 2.

### II.4 GOOGLNET

GoogLeNet is the victor of the ILSVRC 2014, an image characterization rivalry, which has vast improvement over LeNet and AlexNet deep learning models and has a moderately lower mistake rate contrasted than the VGGNet. GoogLeNet is from Google. It additionally called as Inception v1 model. It contains  $1 \times 1$  convolution at the center of the system. Global pooling also utilizes toward the finish of the system as opposed to using completely associated FC layers. Another strategy used in the GoogLeNet model, called the inception module, is to have various sizes/sorts of convolutions for similar information and to stack all the yields. In GoogLeNet,  $1 \times 1$  convolution is utilized as a measurement decrease module to lessen the calculation. Already, completely associated (FC) layers are used toward the end of the system, for example, in AlexNet. In GoogLeNet, global pooling utilizes toward the end of the system by averaging each component map from  $7 \times 7$  to  $1 \times 1$ . The model found that a move

from FC layers to average pooling improved the top-1 accuracy by about 0.6%. There are 22 layers altogether.

It is now a profound model contrasted and past AlexNet, ZFNet, and VGGNet. Furthermore, can see that there are various inception modules associated together to go further. There are some transitional softmax branches at the center. On the off chance that a system workes with numerous profound layers, it may confront overfitting. To tackle this issue, going further with convolutions idea is proposed the GoogleNet engineering with having channels with different sizes that can work on a similar level [23]. With this thought, the system becomes more extensive as opposed to more profound. A maximum pooling activity is likewise performed with the convolutions and then sent into the following inception module. Since neural systems are tedious and costly to prepare, an extra  $(1 \times 1)$  convolution used before the  $(3 \times 3)$  and  $(5 \times 5)$  convolutions to diminish the elements of the system and perform quick calculations. The GoogleNet model appears in Figure 3.

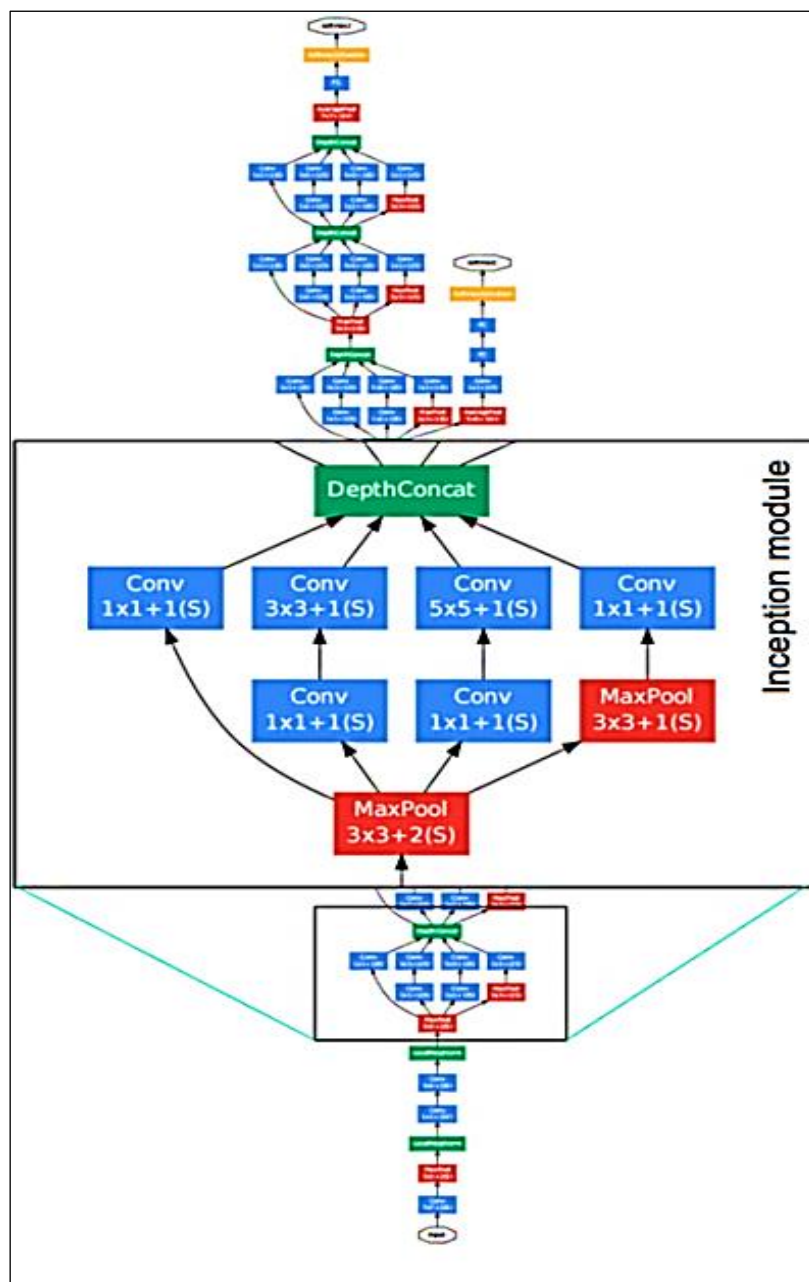


Figure 3: GoogleNet architecture.  
Source: [11].

### III. EXPERIMENTAL SETUP

The proposed research work utilized the AlexNet and GoogleNet pre-prepared model for plant leaf sicknesses recognizable proof. The plant village dataset isolates into the train, validate and test plant samples. In this exploratory arrangement, all the 15 classes utilize, where each class has around 200 examples. An aggregate of nearly 3,700 samples was available in the dataset, which was part of the train and valid samples during the run time on 80:20 proportions. For preparing and testing the neural systems, Keras consider as a deep learning structure with Tensorflow as a backend. The whole preparation and testing performed on a Windows 64-piece work area PC. The training sets are going into the pre-preparing step, such as resizing, noise removal, etc. As indicated by the information appropriation of the train set and test set idea, the plant town preparing dataset incorporates the picture expansion process.

Likewise, the plant village dataset is in uneven condition. This paper utilized random translation, cropping for information upgrades during the training process, to reduce the possibility of overfitting [24].

The initial learning rate for leaf illnesses identification is 0.001. The proposed ailment discovery model improves with the assistance of Adam analyzer with the loss of cross-entropy [25]. A few hyper boundaries are required to run the proposed model; Diverse hyper boundaries, such as padding, strides, and channels, are utilized at every one of the layers that could be tuned to manufacture a superior model. This arranged model used Xavier's initialization for weight introduction for the training process. This examination work runs the investigation up to 30 epochs to accomplish the best outcome model [26]. Diverse batch sizes tested; however, a notable volume of 32 utilizes for the training process. The arranged model gives in Figure 4.

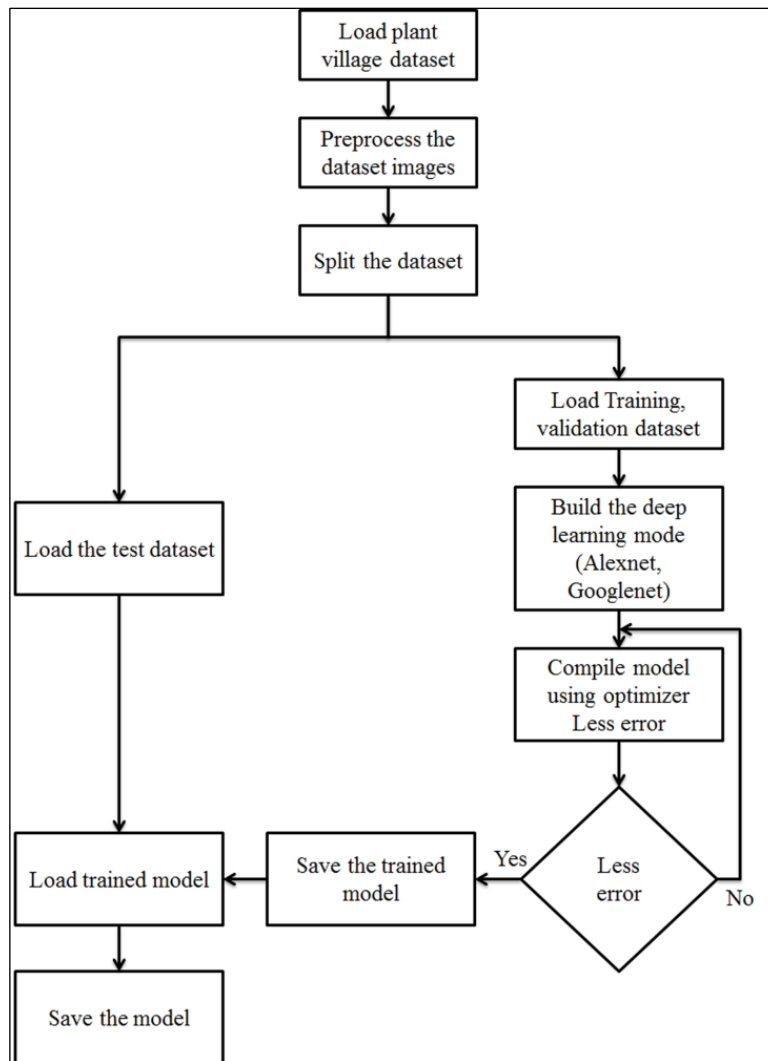


Figure 4: Experimental model design.

Source: Authors, (2021).

The model trains with the planned hyperparameter features such as learning rate, optimizers, epochs, and batch size. The arranged examination has utilized Adam enhancer with a learning rate of 0.001. When the model arranges, the pre-prepared dataset enters into the model [27]. The preparation accomplishes 30 epochs after every epoch approval done on the validation part, in the development of tuning the hyperparameter boundaries for

different quantities of channels, batch size, and the last model with ideal precision spares. The spared model utilizes for testing new information that is not found in the train and test set. During fine-tuning, fluctuated learning rates apply for the model [28-29]. After the training process, the model assesses with the probabilities that each sample has a place with a particular class was determined.

IV. RESULT AND DISCUSSION

In this paper, the utilization of Deep Convolutional Neural Networks has detail architecture to detect ailment on leaf image. The proposed philosophy tries on 15 classes of three kinds of yields. The exploratory outcomes show that the GoogleNet model performs better than the AlexNet model as far as exactness and

loss value. The training and validation based precision, loss value esteem for AlexNet, and GoogleNet show in Figure5. From the outcomes, it tends to see that lone not many examples leave misclassifies. So the proposed model is prepared legitimately with appropriate hyperparameter boundary esteems.

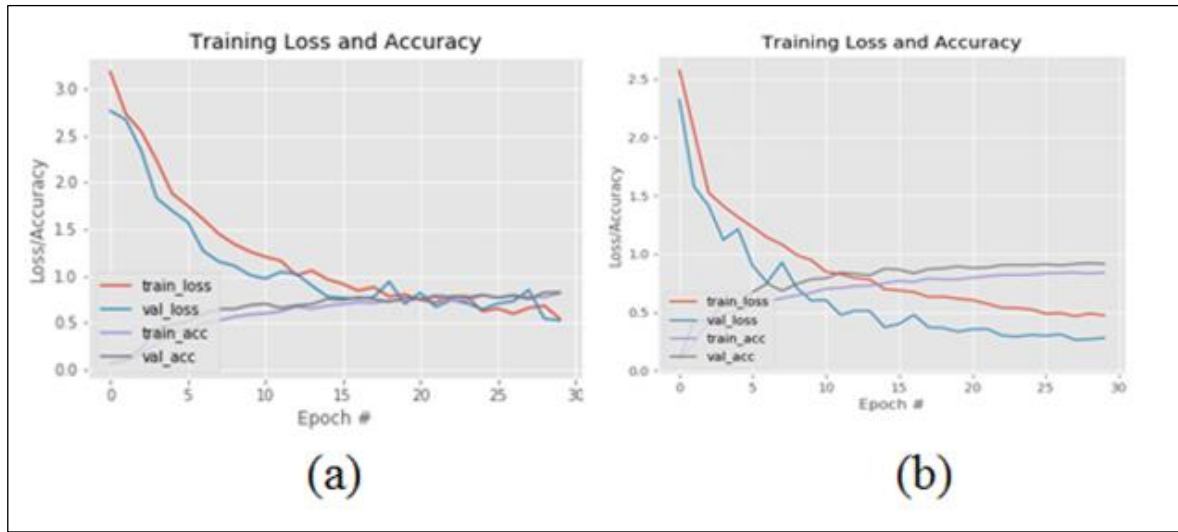


Figure 5: Training and validation result (a) AlexNet (b) GoogleNet  
Source: Authors, (2021).

In this area, results, and perceptions of the experimentation performed on both models reference. If there should be an occurrence of testing for the discovery of harvest infection, according to Figure 5, both AlexNet and GoogleNet models perform well with 83.62% and 85.74% exactness separately. A

noteworthy development inexactness shows in starting stages that get met at convergence later on. Exponential drop in loss work indicates that quicker learning in the underlying stage. It suggests that the GoogleNet model performs better than AlexNet in the assignment of yield identification.

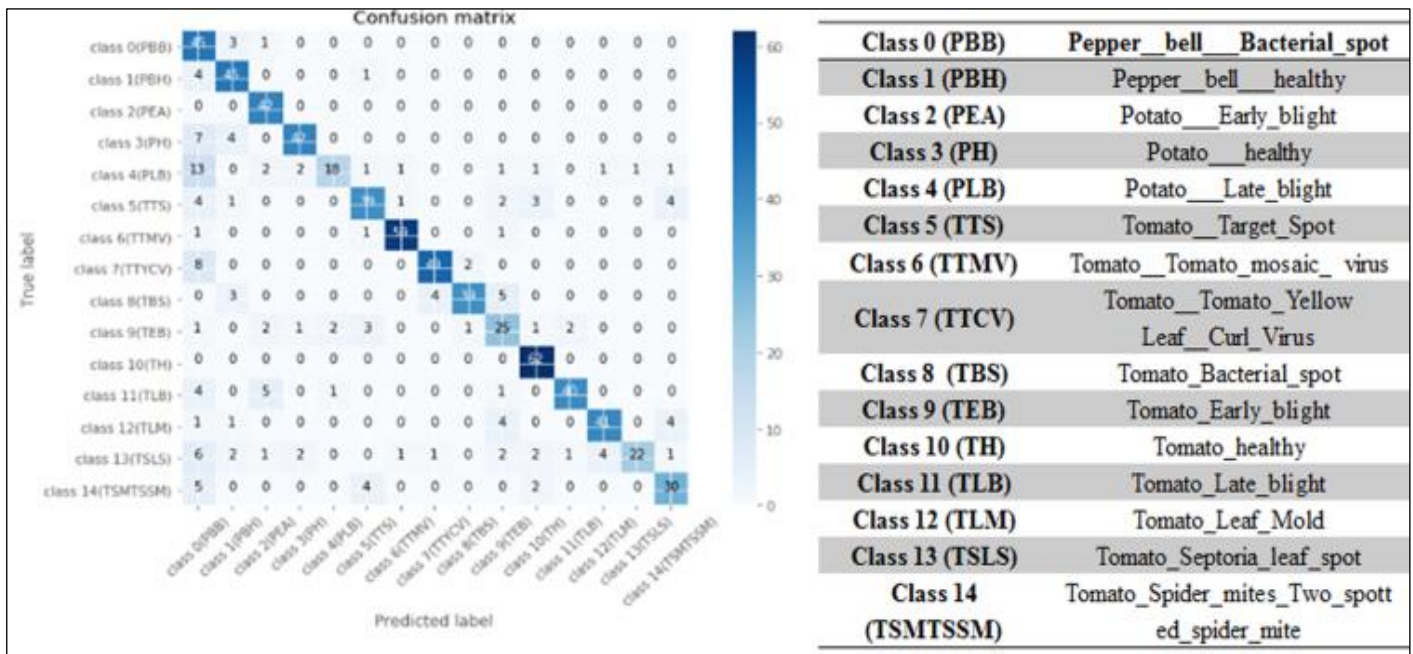


Figure 6: Confusion matrix.  
Source: Authors, (2021).

The proposed model's planned architecture gave 84.37% training based precision and 82.3% validation based exactness, which unmistakably means the overfitting. So the proposed model actualized scarcely any strategies to defeat the equivalent. One such approach is a dropout, a sort of regularization procedure

presented in every one of the convolution layer present in the system, beginning with a likelihood of 0.1 and expanding by 0.1 in each layer. With dropout, the model had the option to lessen the overfitting with a compromise. The test set was feed into the already saved trained model, which gave a test based precision of



81.7%. The confusion matrix framework and test image confirmation for the proposed model appear in Figures 6 and 7.

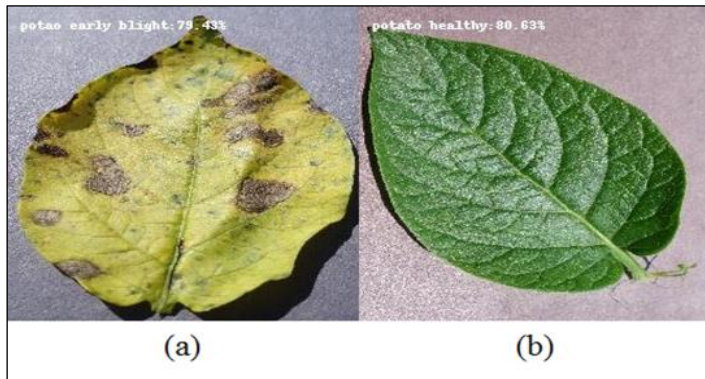


Figure 7. Test image analysis.  
Source: Authors, (2021).

## V. CONCLUSION

Based on deep convolution models, two models, such as AlexNet and GoogleNet of classification and aim on exactness rate, were proposed to distinguish leaf maladies, including pepper ball, potato, and tomato. Quantitative investigations demonstrated that the above strategies accomplish better acknowledgment results on the unequal informational index, contrasted, and the customary AI-based machine learning-based calculations. The exactness of the proposed techniques on the train based dataset was 83.62% and 85.74% individually. The strategies for this paper could reach out to other plant infection recognizable proof. It recommends that in-plant ailment acknowledgment, the approach proposed in this paper can view as when oversampling and under-sampling can't conquer the effect of data imbalance. Augmentation of this work will incorporate the number of classes of harvests, and its sicknesses can expand.

## VI. AUTHOR'S CONTRIBUTION

**Conceptualization:** Jency Rubia J and Babitha Lincy R  
**Methodology:** Jency Rubia J and Babitha Lincy R  
**Investigation:** Jency Rubia J  
**Discussion of results:** Jency Rubia J and Babitha Lincy R  
**Writing – Original Draft:** Babitha Lincy R  
**Writing – Review and Editing:** Jency Rubia J  
**Resources:** Jency Rubia J  
**Supervision:** Jency Rubia J  
**Approval of the final text:** Jency Rubia J and Babitha Lincy R

## VII. ACKNOWLEDGMENTS

The authors would like to thank the VLSI & DSP laboratory at M.A.M College of Engineering and Technology for providing a suitable environment & facilities, which was very helpful to us in research.

## VIII. REFERENCES

[1] DeChant, Chad, Tyr Wiesner-Hanks, Siyuan Chen, Ethan L. Stewart, Jason Yosinski, Michael A. Gore, Rebecca J. Nelson, and Hod Lipson (2017) "Automated identification of northern leaf blight-infected maize plants from field imagery using deep learning." *Phytopathology*, Vol.107, no. 11,pp.1426-1432

[2] Jency Rubia and Bibin Lawrence, "Analysis, Design and Implementation of 4 bit Full Adder Using FinFET", *Journal of Convergence Information Technology*, vol. 10, no. 2, March 2015, pp. 71-77.

[3] QI, Zhao, Zhaohui JIANG, Chunhe YANG, Lianzhong LIU, and Yuan RAO (2016) "Identification of maize leaf diseases based on image technology" *Journal of Anhui Agricultural University*, Vol.43, no. 2:pp.325-330.

[4] Jayme Garcia Arnal Barbedo (2019) "Plant disease identification from individual lesions and spots using deep learning," *Biosystems Engineering*, Volume 180, Pages 96-107.

[5] Jency Rubia and Babitha Lincy, "Design of Low power 4 bit ALU using 32nm FinFET technology", *International Journal Of Pure And Applied Mathematics*, vol. 120, no. 6, July 2018, pp. 8089-8099.

[6] Al-Bashish D, Braik M, Bani-Ahmad S (2011) "Detection and classification of leaf diseases using K-means-based segmentation and neural networks based classification." *Inform Technol J* 10(267-275):2011. <https://doi.org/10.3923/ijtj.2011.267.275>

[7] Jency Rubia and Bibin Lawrence, "Review of Fin FET Technology and Circuit Design Challenges", *International Journal of Engineering Research and Applications*, vol. 5, no. 12, December 2015, pp. 1-4.

[8] Mrunalini R Badnakhe, Deshmukh Prashant R. (2011) "An application of K-means clustering and artificial intelligence in pattern recognition for crop diseases," *Int Conf Adv Inf Technol* 2011; IPCSIT.

[9] Kulkarni Anand H, Ashwin Patil RK (2012), "Applying image processing technique to detect plant diseases," *Int J Mod Eng Res* 2012;2(5):3661-4.

[10] Arivazhagan S, Newlin Shebiah R, Ananthi S, Vishnu Varthini S. (2013), "Detection of unhealthy region of plant leaves and classification of plant leaf diseases using texture features." *Agric Eng Int CIGR* 2013;15(1):211-19.

[11] J JencyRubia, BG Gopal, V Prabhu, "An analysis, Design and implementation of 4 bit full adder using FinFET, *Journal of Convergence Information Technology*, vol 10, Issue 2, PP 71-77.

[12] Amara, J.; Bouaziz, B.; Algergawy, A. (2017), "A deep learning-based approach for banana leaf disease classification." *Gesellsch. Inf. Bonn*, 2017, 79-88.

[13] Cruz, A.C.; Luvisi, A.; De Bellis, L.; Ampatzidis, Y. X-FIDO (2017): "An effective application for detecting olive quick decline syndrome with deep learning and data fusion." *Front. Plant Sci.* 2017, 8, 1741.

[14] Rubia J Jency, Sathish Kumar GA, "A survey paper on modern technologies in fixed-width multiplier," 2017 Fourth International Conference on Signal Processing, Communication and Networking (ICSCN), IEEE Publisher, PP1-6.

[15] AlexNet: <https://neurohive.io/en/popular-networks/alexnet-imagenet-classification-with-deep-convolutional-neural-networks/>.

[16] Rubia JJ, Sathish Kumar G. A high-speed fixed width floating-point multiplier using residue logarithmic number system algorithm. *The International Journal of Electrical Engineering & Education*. 2020;57(4):361-375. doi:10.1177/0020720918813836.

[17] Yeon-Gyu Kim · Eui-young Cha, (2016) "Streamlined GoogLeNet Algorithm Based on CNN for Korean Character Recognition," *J. Korea Inst. Inf. Commun. Eng.* Vol. 20, No. 9: 1657~1665 Sep. 2016.

[18] Rubia JJ, GA SK. Fir filter design using floating point radix 4 algorithm. *The International Journal of Electrical Engineering & Education*. November 2019. doi:10.1177/0020720919891064.

[19] Jency RUBIA J, Babitha Lincy r, Al-Heety, "Moving vehicle detection from video sequences for Traffic Surveillance System," *ITEGAM-JETIA*, Vol 7, Issue 27, PP 41-48.

[20] Barbedo JGAB (2016) "A review on the main challenges in automatic plant disease identification based on visible range images." *Biosys Eng* 144:52-60.

[21] Jency Rubia J., Babitha Lincy R. (2021) Digital Image Restoration Using Modified Richardson-Lucy Deconvolution Algorithm. In: Chen JZ., Tavares J., Shakya S., Iliyasu A. (eds) *Image Processing and Capsule Networks*. ICIPCN 2020. *Advances in Intelligent Systems and Computing*, vol 1200. Springer, Cham. [https://doi.org/10.1007/978-3-030-51859-2\\_10](https://doi.org/10.1007/978-3-030-51859-2_10).

[22] Barbedo JGA (2013) "Digital image processing techniques for detecting, quantifying and classifying plant diseases." *SpringerPlus*2(1):660-672



Jency Rubia, Sathish Kumar, "Design and analysis of low power fixed-width multiplier using reduced precision redundancy block," IOSR J. VLSI Sig. Process, Vol 9, Issue 6, pp 1-8.

[23] S. Phadikar, J. Sil, "Rice disease identification using pattern recognition techniques." In: Proceedings of the IEEE International Conference on Computer and Information Technology (ICCIT), Khulna, Bangladesh, 2008, pp 420–423.

[24] Jency Rubia J, Sathish Kumar G.A, "FIR Filter Design Using Floating point Column Bypassing Technique," International Journal of Recent Technology and Engineering (IJRTE), , Volume-8 Issue-2S4,pp 409-413, July 2019.

[25] Afindas A and Naveenkumar S Jency Rubia J, Salim A, " Diagnosis of COVID-19 using ADAM Optimization technique in Convolutional Neural Network (CNN)," Tierärztliche Praxis, Vol 41, pp 415-425.

[26] Asfarian A, Herdiyeni Y, Rauf A, Mutaqin KH (2014) "A computer vision for rice disease identification to support integrated pest management." Crop Prot 61:103–104.

[27] Khairmar K, Dagade R (2014) "Disease detection and diagnosis on plant using image processing—a review." Int J Comput Appl 108(13):36–39.

[28] Chai Y, Wang XD (2013) "Recognition of greenhouse tomato disease based on image processing technology." Tech Autom Appl 9:83–89.



ISSN ONLINE: 2447-0228



## DESIGN AND ANALYSIS OF QCA ADDER CIRCUITS FOR EFFICIENT COMPUTATION

Jency Rubia J\*<sup>1</sup> and Babitha Lincy R<sup>2</sup>

<sup>1</sup> Asst. Prof. Department of ECE, M.A.M College of Engineering and Technology, Tiruchirappalli, India.

<sup>2</sup> Research Scholar, Department of ECE, Sri Venkateswara College of Engineering, Sriperumbudur, India.

<sup>1</sup> <http://orcid.org/0000-0002-0088-3611> , <sup>2</sup> <http://orcid.org/0000-0003-2520-2410> 

Email: \*jencyrubia@gmail.com, rblincy@gmail.com

### ARTICLE INFO

#### Article History

Received: August 07<sup>th</sup>, 2021

Accepted: August 23<sup>th</sup>, 2021

Published: August 31<sup>th</sup>, 2021

#### Keywords:

QCA (Quantum-dot Cellular Automata),  
Quantum Mechanics,  
Half adder,  
Full adder.

### ABSTRACT

QCA technology is considered a viable alternative for CMOS technology since it solves most of the CMOS implications. The Quantum dot Cellular Automata is a computer software program that relates a discrete dynamical system with quantum mechanics. Quantum mechanics is a kind of physics about subatomic particles and which has many interesting properties. The QCA offers very great switching speed and consumes power dissipation extensively. The logic circuits play an essential role in the branch of computer arithmetic. In this paper, the adder circuits have been designed using the novel transistor-free technology called QCA. In addition to that, the planned work has been investigated with CMOS technology. The proposed work is simulated and synthesized by QCA designer suit 2.0.3.



Copyright ©2016 by authors and Galileo Institute of Technology and Education of the Amazon (ITEGAM). This work is licensed under the Creative Commons Attribution International License (CC BY 4.0).

### I. INTRODUCTION

Recently, CMOS technology has confronted many physical challenges due to the shrinking gate length in a transistor. To overcome such shortcomings of the conventional CMOS technology, there is a need for effective alternative technology. The ITRS listed some technologies; among them, QCA has many mesmerizing features [1][2]. The scientist Craig S. Lent first proposed this fascinating technique in the year 1993 [3]. QCA is a new computing tool that can signify binary information depends on the spatial sharing of electron charge arrangement in chemical molecules [4]. The computation of cellular automata consists of an array of quantum dots. The Columbic interaction between the QCA cells is only the source of computational power. Otherwise, there is no current movement among cells and no additional outer source of current to the internal cells [5]. Thus, the interconnection between the cells is possible due to the reorganization the electron positions [6]. Since QCA was introduced in 1993, various experimental devices and logic circuits have been developed [7-11]. Though, these devices are not in practical yet, current research evidence that the QCA

may eventually attain high density [12], fast switching speed [13], and room heat operation [14].

In this research work, the adder circuit has been designed using QCA technology. The addition is the basic arithmetic operation and is essential in all digital supercomputers and calculators. To enhance the QCA adder cell performance and optimization of the QCA cell, here, Majority Gate (MG) logic structure has been used. There are many types of logic styles for designing circuits in QCA, such as majority gate (MG), and-or-inverter (AOI) and nand-nor-inverter (NNI), logics [15-17]. The subsequent design instructions are considered for the QCA implementation of the proposed adder circuit. The size of the cell is twenty nm by twenty nm. Also, the cell's width and height are assumed to be 18 nm and 5 nm diameter of quantum dots. The cell-to-cell distance is considered as 20 nm between each cell on the grid. These design rules are beneficial to achieve minimum propagation delay due to the cell-to-cell reactions, since there is a limit on the supreme cell amounts in a clock zone. This ensures proper propagation and reliable signal transmission. The proposed QCA adder circuit in this paper has been planned and performed using the QCA designer tool type 2.0.3 with a coherence

simulation engine [18]. The article is prearranged as charts: in section 2, the background of QCA technology and the design approaches are presented. Section 3 describes the design of the adder circuit based on the majority gate logic structure. Chapter 4 shows that the proposed QCA adder and implementation of that. Then section 5 discusses the simulation results, and lastly, the conclusion and future scope are explained in section 6.

## II. BACKGROUND OF QCA

### II.1 QCA CELL

A QCA cell is a square nanostructure of electron wells restraining free electrons. Every cell contains of four quantum dots that can accommodate a single atom per dot. The four dots are located at the four edges of the QCA cell, and two electrons are infusing into the cell. The two particles are located at the contrary corners of the cell because of the Columbic repulsion principle [19-21]. Thus, this structure provides two conceivable polarizations, as revealed in Figure 1. These elementary QCA

cells are beneficial for designing inverter, logic gates, and circuits, memory elements, etc.

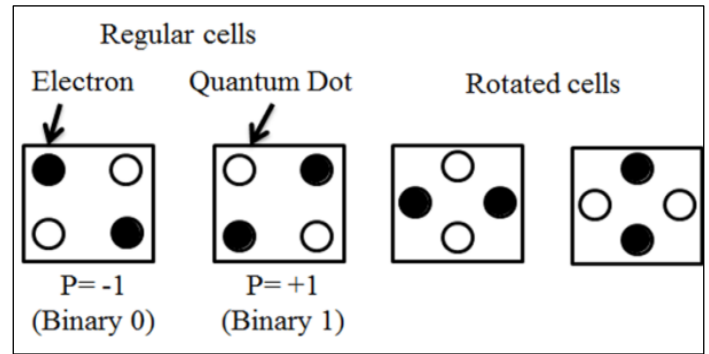


Figure 1: Basic QCA cell and two possible polarizations. Source: Authors, (2021).

### II.2 LOGIC GATES

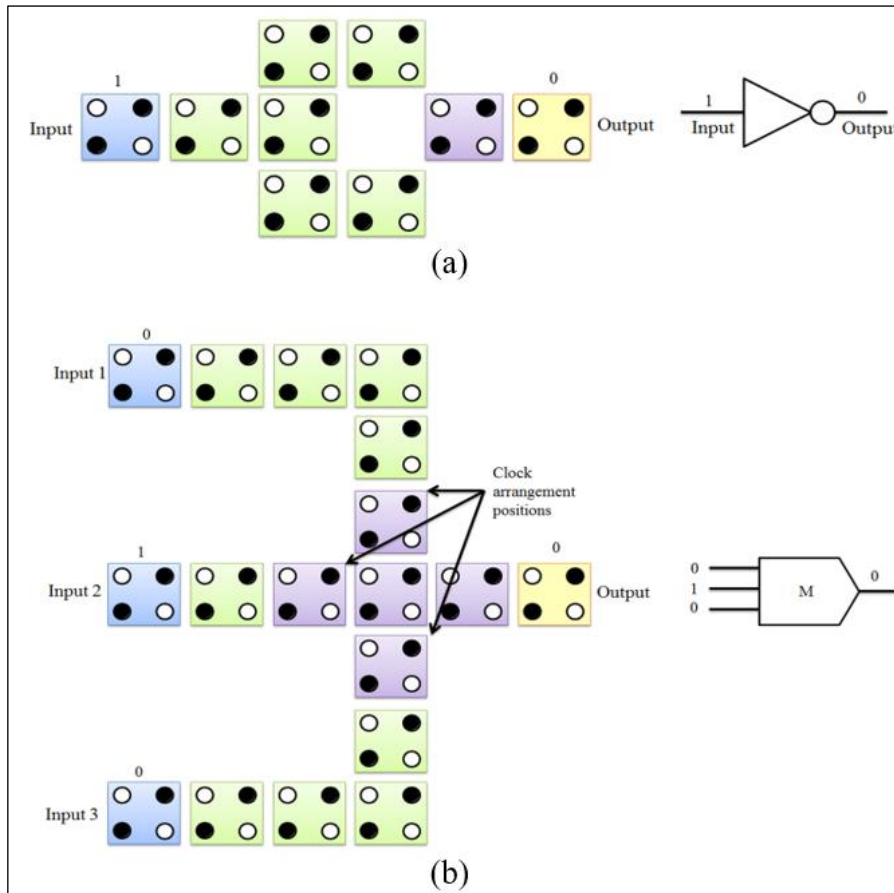


Figure 2: (a) QCA Inverter; (b) Majority gate. Source: Authors, (2021).

Combination of arithmetic and logical operation. Thus, Logic gates are the elementary building blocks of several arithmetic circuits. In the QCA context, inverters and three-input mainstream gates assisted as an essential gate. Because any logic circuits can be designed using the basic QCA gates. The first equation of the majority gate with inputs a, b, and c in  $M(a, b, c) = ab + bc + ca$ . Figure 2 illustrates the QCA inverter and the majority gate symbol and layout [22]. Two input AND gate and OR gate can be implemented using the majority gate by

making the third input constant. Therefore, utilizing AND, OR, and inverter gates, any logic functions can be achieved. The realization of AND and OR gates are as follows:

$$a \cdot b = M(a, b, 0) \quad (1)$$

$$a + b = M(a, b, 1) \quad (2)$$

### II.3 SIGNAL FLOW AND CONTROL

The consecutive QCA cells are acting like a wire. For a given one clock cycle, the half of the QCA wire is active for signal transmission, but the other half wire is in unpolarized form. During the next clock cycle, the previous active wire portion turned to an inactive state, but the remaining active zone triggers the newly activated cells to be polarized. Like this, signal transfers from one clock zone to another [23]. In general, the circuit area is split into four parts, and four-phase clock signals drive them. Each clock zone consists of four different clock signal stages, such as high-to-low, low, low-to-high, and high. The computation is begun when the clock signal in the high-to-low step and holds the value during the little clock stage. The calculation has also been released when the clock signal at the low-to-high state and inactive during the high state.

### III. PROPOSED WORK

#### III.1 DESIGN OF ADDERS USING MG

Digital computers and other gadgets perform various kinds of arithmetic operations. Among them, addition operation is considered as a most fundamental computation. The proposed work consists of designing adder circuits such as half adder and full adder using the majority gate (MG) logic style [24]. The majority gate plans the suggested work since it reduces the number of gates that required designing an adder circuit. Here, the half adder is designed using four mainstream gates and two inverters, and the full adder is developed directly by using half adders. The full adder's direct design is realized by the QCA addition algorithm, which was proposed by the researcher Walus et al. [25]. This design required two types of wiring of QCA cells. Then the designed adders are implemented with the cell minimization techniques. Hence, the proposed adders consume area and also circuit complexity. The adders are simulated and verified the results according to the truth tables. In the end, the performance analysis of the proposed work has been compared with the common techniques.

#### III.2 DESIGN OF HALF-ADDER

The half adder is a modest combinational circuit that executes the addition of two bits. The half adder circuit is traditionally designed using EXOR and AND gates. The addition of two numbers A and B processed and the respective outputs are Sum and Carry. From the concept of truth table of the half adder as in Table 1, one can recognize that the Sum output is 1 when either of the inputs (A or B) is 1, and the Carry output is 1 when both the inputs (A and B) are 1. Figure 3 shows the general diagram and Table 1 truth table of the half adder circuit [26].

The logic function of the half adder is,

$$\text{Sum} = A'B + AB' \tag{3}$$

$$\text{Carry} = AB \tag{4}$$

The QCA representation for the above equation based on MG is,

$$\text{Sum} = M(M(A, B', 0), M(A', B, 0), 1) \tag{5}$$

$$\text{Carry} = M(A, B, 0) \tag{6}$$

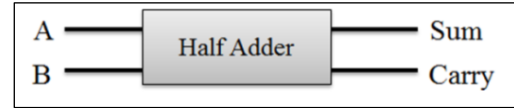


Figure 3: Schematic diagram of Half-adder. Source: Authors, (2021).

Table 1: Truth table of the Half-adder.

Inputs		Outputs	
A	B	SUM	CARRY
0	0	0	0
0	1	1	0
1	0	1	0
1	1	0	1

Source: Authors, (2021).

#### III.3 DESIGN OF FULL-ADDER

A full adder is created since there is no facility in a half adder to add carry bits from the lower bits during more than two bits presented in an addition operation [27]. For this purpose only, a full adder circuit has emerged. A full adder is a combinational circuit that achieves the addition of three inputs and produces Sum and Carry as outputs. The block diagram and truth table of the full adder is shown in Figure 4 and Table 2.



Figure 4: Schematic diagram of full-adder. Source: Authors, (2021).

Table 2: Truth table for full adder.

Inputs			Outputs	
A	B	Cin	SUM	CARRY
0	0	0	0	0
0	0	1	1	0
0	1	0	1	0
0	1	1	0	1
1	0	0	1	0
1	0	1	0	1
1	1	0	0	1
1	1	1	1	1

Source: Authors, (2021).

#### III.4 QCA ADDITION ALGORITHM

The design of QCA circuits involves two processes, one is physical design, and another is algorithmic design. For low-level design, it requires any one of the approaches [28]. But, for high-level design, both physical design and algorithmic design needs. Further, more complicated circuit design uses logic design in addition to both the design techniques. Though the QCA circuit design requires physical interactions that are unpleasant and troublesome, the algorithmic design is also a significant aspect of large circuit design. The representation of Carry using Majority Gate logic:

$$\begin{aligned} C_{out} &= AB + BC + AC \\ &= M(M(B, M(A, C, 1), 0), M(A, C, 0), 1) \\ &= M(A, B, C) \end{aligned}$$



The representation of Sum using Majority Gate logic:

$$\text{Sum} = ABC + A'B'C + A'BC' + AB'C'$$

The plan of full-adder can be implemented in two different approaches. The first technique is direct implementation, a conventional method that requires a lot of area and hardware [29]. The second approach is the Majority gate reduction, this model is simple, and it needs very few hardware requirements. In this work, the majority logic has been used for constructing QCA adders [30, 31]. The planned adders are applied with QCA cells, and the quantity of cells can be reduced by using cell minimization methods. Thus, the implementation further decreases the area and calculation complexity. The direct implementation method of full adder is,

$$\text{Sum} = M(M(A, M(M(B, C, 0), M(B', C', 0), 1, 0), M(A'M(M(B'C, 0), 1), 0), 1) \longrightarrow 11$$

Majority Gates

The implementation of full adder using reduction technique:

$$\begin{aligned} \text{Sum} &= ABC_{in} + A'B'C_{in} + A'BC'_{in} + AB'C'_{in} \\ &= (A.B + A'.B')C_{in} + (A'.B + A.B')C'_{in} \\ &= [A.B + A'.B' + A.C'_{in} + A'.C'_{in} + B.C'_{in} + B'.C'_{in}]C_{in} \\ &\quad + (A'.B + A.B')C'_{in} \\ &= [(A'.B' + A'.C'_{in} + B'.C'_{in}) + (A.B + A.C'_{in} + B.C'_{in})]C_{in} \\ &\quad + (A'.B + A.B')C'_{in} \\ &= [(A'.B' + A'.C'_{in} + B'.C'_{in}) + (A.B + A.C'_{in} + B.C'_{in})]C_{in} \\ &\quad + (A'.C'_{in} + B.C'_{in}) + (A'.C'_{in} + B'.C'_{in}) \\ &= [(A'.B' + A'.C'_{in} + B'.C'_{in})C_{in} + (A.B + A.C'_{in} \\ &\quad + B.C'_{in})]C_{in} + (AB + A'.C'_{in} \\ &\quad + B.C'_{in})(A'.C'_{in} + B'.C'_{in} + A'B') \end{aligned}$$

$$\begin{aligned} &= M(A', B', C'_{in}).C_{in} + M(A, B, C'_{in}).C_{in} \\ &\quad + M(A', B', C'_{in})M(A, B, C'_{in}) \\ &= M[M(A', B', C'_{in}), C_{in}, M(A, B, C'_{in})] \end{aligned}$$

Therefore,

$$\text{Sum} = \text{Sum} = M[C'_{out}, C_{in}, M(A, B, C'_{in})] \longrightarrow 3 \text{ majority gates.}$$

gates.

This reduction technique reduces the majority gates from 11 to 3.

#### IV. QCA IMPLEMENTATION OF ADDERS

The initial step of QCA implementation of adders is designing the adder circuit by the majority gate style. Again, the designed QCA adder circuit has large area and hardware requirements. Thus, cell minimization technique helps to reduce the circuit complexity. Finally, implement the designed adder circuit by QCA cells and compiled by QCA designer.

##### IV.1 HALF ADDER IMPLEMENTATION

Figure 5 (a) shows that the schematic diagram of the designed QCA half adder requires four common gates and two inverters. The particular QCA implementation of the half adder is illustrated in Figure 5(b). The implementation of half adder is by cell reduction techniques, and it lessens the inverter cells to two, which is designated by the circle in the layout diagram. This proposed work requires implementing the half adder is 77 cells, with a total area of 83160 nm<sup>2</sup>, which is much lesser than the existing designs. The previous implementation consists of 105 cells with an area of 108000 nm<sup>2</sup>.

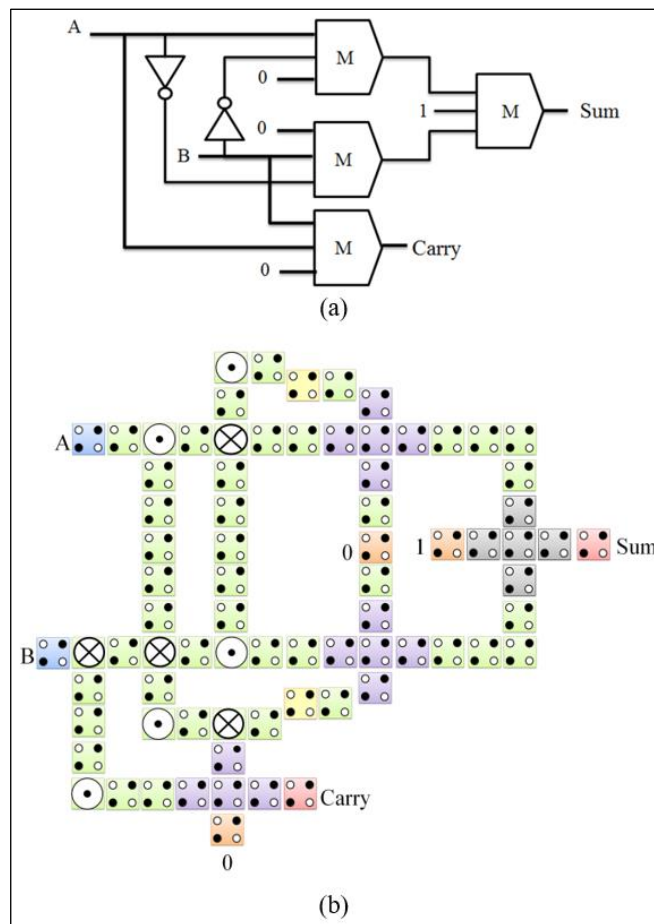


Figure 5: (a) Half adder schematic; (b) Layout of half adder. Source: Authors, (2021).

IV.2 FULL ADDER IMPLEMENTATION

The full adder can be designed by direct form and by using half adders. The full adder's straightforward implementation is based on the QCA addition algorithm, which was introduced by Zhang et al. [32][33]. The full adder's design using the direct method requires three majority gates and two inverters, as shown in Figure 6(a). Moreover, this type of implementation needs two kinds of wiring methods, such as coplanar and multilayer crossings [34]. These are known as wire crossings. From the two types of crossovers, mainly the coplanar crossover is simple to realize, and it can be used with a slight modification to the basic design. The QCA implementation of a full adder with coplanar crossover is presented in Figure 6(b). The proposed QCA full adder requires 111 QCA cells, and it consumes a total area of 114300 nm<sup>2</sup> which is comparably smaller than the previous implementations. This reduced design is achieved by using two inverter cells and some specific rules for proper cell alignment. The significant QCA design rules are (1) the number of column cells need not be the same, and (2) the minimum distance between the adjacent rows of cells is the width of two cells.

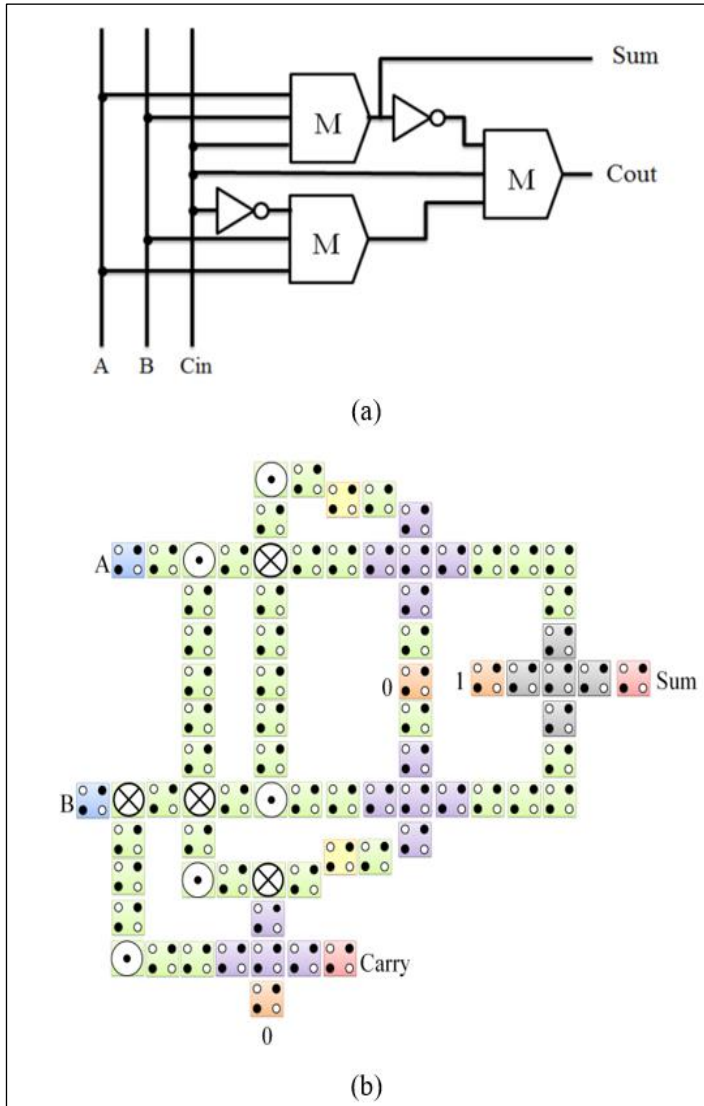


Figure 6: (a) Full adder schematic; (b) Layout of full adder. Source: Authors, (2021).

Figure 7(a) illustrates the same design of QCA full adder but the position of majority gates and inverters are modified for

simple realization. In this method of implementation multilayer crossover has involved which is very straightforward. As the name suggests, it uses more than one layer of cells like a bridge. The equivalent QCA cell implementation is shown in Figure 7(b). This kind of QCA implementation requires 98 cells with a total area of 100800 nm<sup>2</sup> and this also needs less number of cells than the existing implementations.

Another procedure for designing of full adder is using by two half adder circuits and an OR gate. This design consists of 9 majority gates and 4 inverters as presented in Figure 8(a). The respective QCA implementation of the full adder is given in Figure 8(b). Further, this design requires 192 QCA cells, with an area of 208000 nm<sup>2</sup>. The Existing implementation needs 218 cells and it consumes an area of 286880 nm<sup>2</sup>. At the end, the direct implementation with cell minimization technique provides better performance than this method.

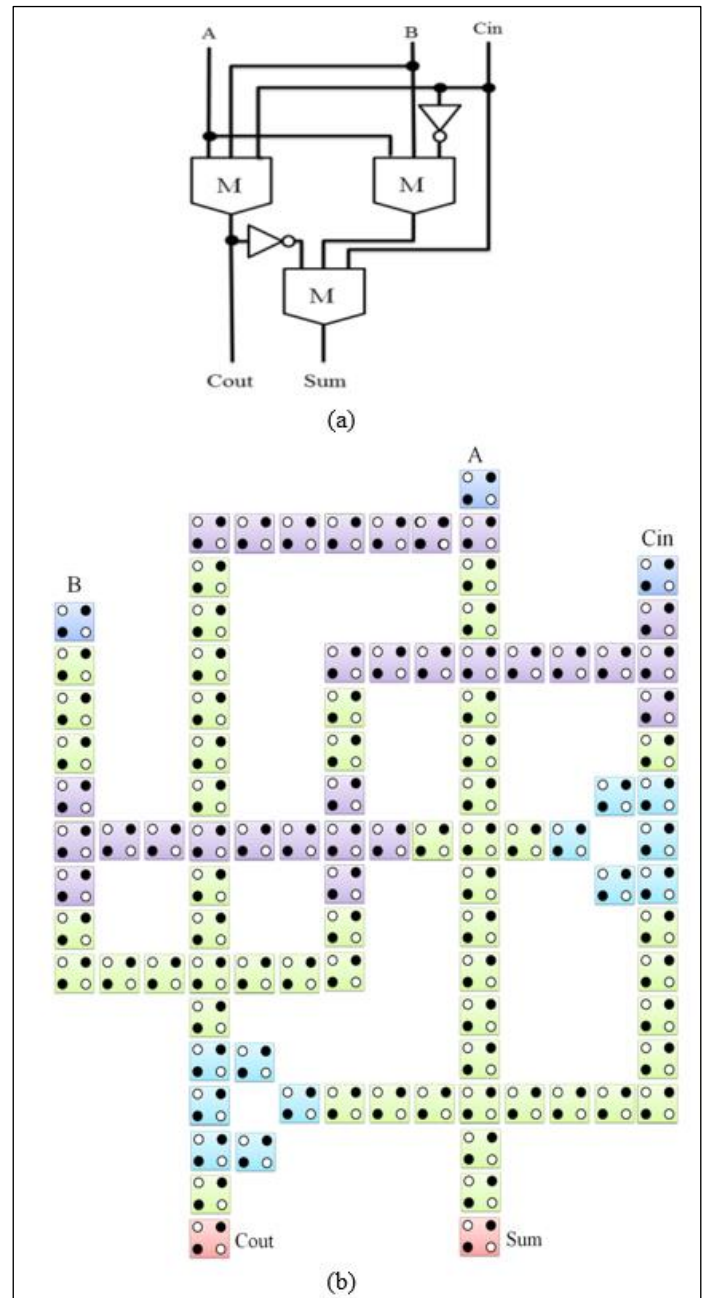


Figure 7: (a) Half adder schematic; (b) Layout of half adder. Source: Authors, (2021).

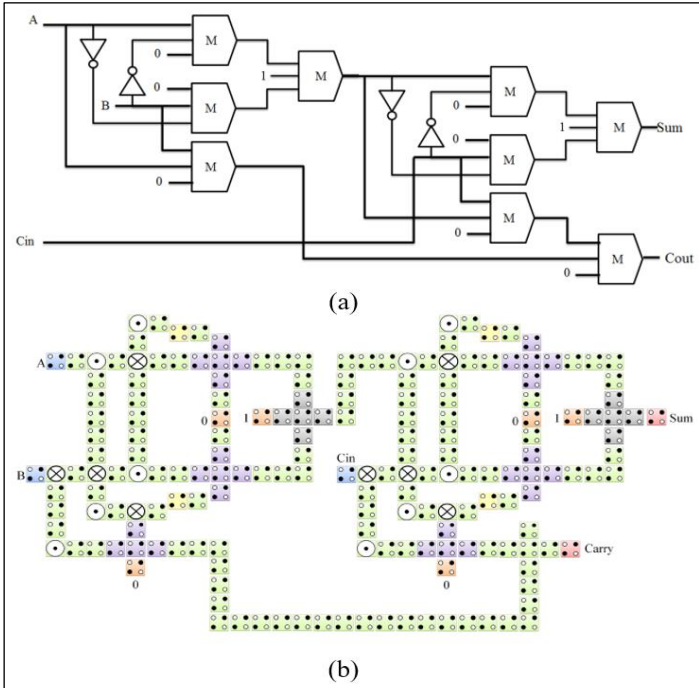


Figure 8: (a) full adder schematic using half adder; (b) Layout of full adder using half adder. Source: Authors, (2021).

## V. SIMULATION RESULTS AND DISCUSSION

### V.1 SIMULATION WAVEFORMS

The QCA implementation of half adder and full adder is simulated and synthesized by the QCADesigner 2.0.3 software, and the simulated outputs are shown in 9 and 10. Figure 9 illustrates the QCA simulated waveform of the proposed half adder. The proposed implementation requires four clock phases. Initially, the clock 0 is used to get the inputs, and the clock 1 is used to route the inputs for the majority gate logic. Then, clock 2 is used to process the majority logic gate, and clock 3 used to compute the output. Finally, the output is available in clock 0 again. The sequence of clock 1 to 3 does the following operations, such as setup for hold, relax, and release phase. These phases are used to control the flow of data in the QCA circuits. The same four clock phases are required for operating the QCA full adder and also to produce the output. The simulated results of the QCA full adder are presented in Figure 10.

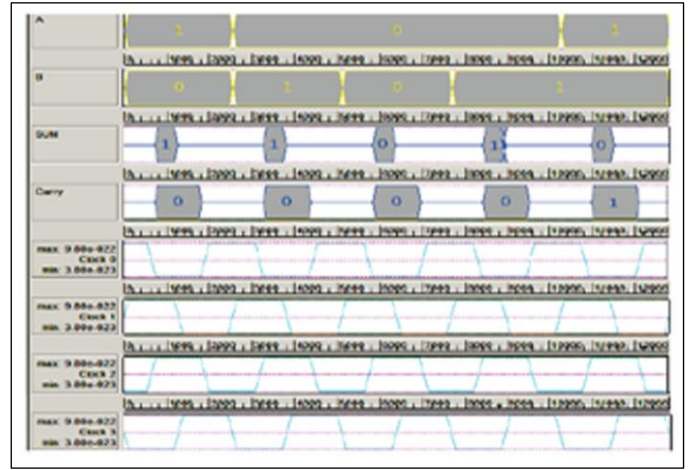


Figure 9: Half adder simulation output. Source: Authors, (2021).

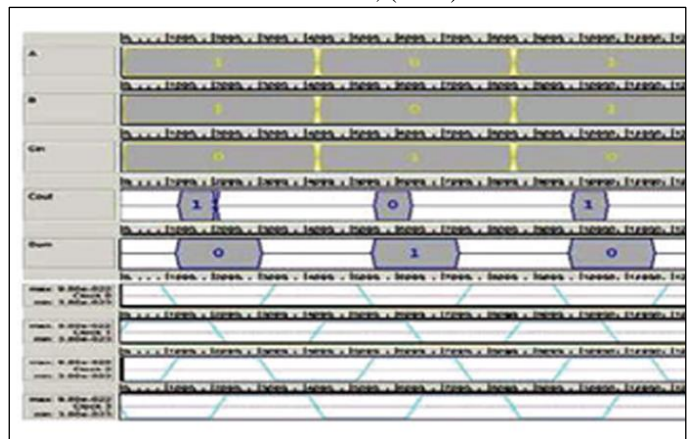


Figure 10: Full adder simulation Output. Source: Authors, (2021).

### V.2 COMPARATIVE ANALYSIS OF QCA ADDERS

The performance analysis of the different types of adders using majority gates is compared with the existing implementations, and CMOS technology is shown in Table 3. The performance analysis of the proposed work compared against factors such as area, complexity, and a number of clock cycles. Moreover, the proposed QCA adders are compared with the previous implementation and existing technology.

Table 3: Comparative performance analysis of proposed technology.

ADDERS		HALF ADDER	FULL ADDER (COPLANAR CROSSOVER)	FULL ADDER (MULTILAYER CROSSOVER)	FULL ADDER USING HALF ADDERS
CMOS	COMPLEXITY	203 CELLS	302 CELLS	-	257 CELLS
	AREA	527 NM×568 NM	652 NM×692 NM	-	450 NM×560NM
PREVIOUS DESIGN	COMPLEXITY	105 CELLS	145 CELLS	137 CELLS	218 CELLS
	AREA	300 NM×360 NM	439 NM×367 NM	435 NM× 300 NM	652 NM×440 NM
Proposed design	COMPLEXITY	77 CELLS	111 CELLS	98 CELLS	192 CELLS
	AREA	297 NM×280 NM	297 NM×280 NM	360 NM×280 NM	650 NM×320 NM
	NUMBER OF CLOCK CYCLES	1	1	1	2

Source: Authors, (2021).

## VI. CONCLUSION

In this paper, half/full adder circuits were designed and analyzed by QCA implementation. The adder circuit is the most basic circuit for any arithmetic computation. By using the Quantum dot-Cellular automata technique, the circuit complexity and area requirement is extensively curtailed. Thereby the

performance has been enhanced compared to other technology. The layout and functionality verification has been performed using the software QCADesigner, and the proposed work has compared with the parameters such as complexity, area, and the number of clock cycles. The computation of these adder circuits has been confirmed according to the truth table. From the comparative performance analysis, the proposed layouts are



suggestively smaller than the circuits using CMOS approach. In addition to that, it reduces the required area and complexity for the circuit than the previous QCA circuits. The other arithmetic circuits might be designed using these adder circuits such as subtractors, multipliers, and so on in the future. The designed circuit can be used for image processing, communication, and cryptographic applications.

## VI. AUTHOR'S CONTRIBUTION

**Conceptualization:** Jency Rubia J and Babitha Lincy R.

**Methodology:** Babitha Lincy R.

**Investigation:** Jency Rubia J.

**Discussion of results:** Jency Rubia J and Babitha Lincy R.

**Writing – Original Draft:** Jency Rubia J and Babitha Lincy R.

**Writing – Review and Editing:** Jency Rubia J.

**Resources:** Babitha Lincy R.

**Supervision:** Jency Rubia J.

**Approval of the final text:** Jency Rubia J and Babitha Lincy R.

## VII. ACKNOWLEDGMENTS

The authors would like to thank the VLSI & DSP laboratory at M.A.M College of Engineering and Technology for providing a suitable environment & facilities, which was very helpful to us in research.

## VIII. REFERENCES

- [1] Cellular Automata Inverters”, International Journal of Computer Applications, Volume 58, No.20, 2012.
- [2] C. Lent & P. D. Young, “A Device Architecture for Computing with Quantum Dots”, Proceedings of the IEEE 85, 541, 1997.
- [3] Jency Rubia and Bibin Lawrence, “Analysis, Design and Implementation of 4 bit Full Adder Using FinFET”, Journal of Convergence Information Technology, vol. 10, no. 2, March 2015, pp. 71-77.
- [4] M. A. Peer, K. A. Khan & R. A. Khan “Cellular Automata for Nanoscaled Biological Assemblies”, Proceedings of the International Conference on Nanomaterials, NANO, 2005.
- [5] Jency Rubia and Babitha Lincy, “Design of Low power 4 bit ALU using 32nm FinFET technology”, International Journal Of Pure And Applied Mathematics, vol. 120, no. 6, July 2018, pp. 8089-8099.
- [6] C. S. Lent and P. D. Tougaw, “Lines of interacting quantum-dot cells: a binary wire,” Journal of Applied Physics, vol. 74, no. 10, pp. 6227–6233, 1993.
- [7] M. Askari, M. Taghizadeh, and K. Fardad, “Digital design using quantum-dot cellular automata (a nanotechnology method),” in Proceedings of the International Conference on Computer and Communication Engineering (ICCCE '08), pp. 952–955, IEEE, Kuala Lumpur, Malaysia, May 2008.
- [8] Jency Rubia and Bibin Lawrence, “Review of Fin FET Technology and Circuit Design Challenges”, International Journal of Engineering Research and Applications, vol. 5, no. 12, December 2015, pp. 1-4.
- [9] M. Askari, M. Taghizadeh, and K. Fardad, “Design and analysis of a sequential ring counter for QCA implementation,” in Proceedings of the International Conference on Computer and Communication Engineering (ICCCE '08), pp. 933–936, May 2008.
- [10] A. Orlov et al., “Experimental Demonstration of a Binary Wire for Quantum-Dot Cellular Automata,” Applied Physics Letters, vol. 74, no. 19, pp. 2875-2877, May 1999.
- [11] Jency Rubia, BG Gopal, V Prabhu, "An analysis, Design and implementation of 4 bit full adder using FinFET, Journal of Convergence Information Technology, vol 10, Issue 2, PP 71-77.
- [12] I. Amlani et al., “Experimental Demonstration of a Leadless Quantum-Dot Cellular Automata Cell,” Applied Physics Letters, vol. 77, no. 5, pp. 738-740, July 2000.
- [13] Rubia J Jency, Sathish Kumar GA, "A survey paper on modern technologies in fixed-width multiplier," 2017 Fourth International Conference on Signal Processing, Communication and Networking (ICSCN), IEEE Publisher, PP1-6.
- [14] R.P. Cowburn and M.E. Welland, “Room Temperature Magnetic Quantum Cellular Automata,” Science, vol. 287, no. 5457, pp. 1466- 1468, Feb. 2000.
- [15] Rubia JJ, Sathish Kumar G. A high-speed fixed width floating-point multiplier using residue logarithmic number system algorithm. The International Journal of Electrical Engineering & Education. 2020;57(4):361-375. doi:10.1177/0020720918813836
- [16] H. Qi et al., “Molecular Quantum Cellular Automata Cells. Electric Field Driven Switching of a Silicon Surface Bound Array of Vertically Oriented Two-Dot Molecular Quantum Cellular Automata,” J. Am. Chemical Soc., vol. 125, pp. 15250-15259, 2003.
- [17] R.K. Kumamuru et al., “Operation of a Quantum-Dot Cellular Automata (QCA) Shift Register and Analysis of Errors,” IEEE Trans. Electron Devices, vol. 50, no. 9, pp. 1906-1913, Sept. 2003.
- [18] Rubia JJ, GA SK. Fir filter design using floating point radix 4 algorithm. The International Journal of Electrical Engineering & Education. November 2019. doi:10.1177/0020720919891064
- [19] Jency Rubia, Sathish Kumar, "Design and analysis of low power fixed-width multiplier using reduced precision redundancy block," IOSR J. VLSI Sig. Process, Vol 9, Issue 6, pp 1-8.
- [20] Kunal Das and Debashis De, "A novel approach of And-Or-Inverter (AOI) gate design for QCA," 2009 4th International Conference on Computers and Devices for Communication (CODEC), Kolkata, 2009, pp. 1-4.
- [21] Lee Ai Lim, A. Ghazali, S. C. T. Yan and Chau Chien Fat, "Sequential circuit design using Quantum-dot Cellular Automata (QCA)," 2012 IEEE International Conference on Circuits and Systems (ICCS), Kuala Lumpur, 2012, pp. 162-167, doi: 10.1109/ICCCircuitsAndSystems.2012.6408320.
- [22] QCADesigner, Micro Systems and Nanotechnology group (Mina), 2012, <http://www.mina.ubc.ca/qcadesigner>.
- [23] Walus, K., Dysart, T., Jullien, G. and Budiman, R. “QCADesigner: A rapid design and simulation tool for QCA”, IEEE Trans. Nanotechnol., Vol. 3, no.1, pp. 26–29, Mar. 2004.
- [24] Jency Rubia J, Sathish Kumar G.A, "FIR Filter Design Using Floating point Column Bypassing Technique," International Journal of Recent Technology and Engineering (IJRTE), Volume-8 Issue-2S4, pp 409-413, July 2019
- [25] A. DeHon and M.J. Wilson, “Nanowire-Based Sublithographic Programmable Logic Arrays,” Proc. Int’l Symp. Field-Programmable Gate Arrays, pp. 123-132, 2004.
- [26] Walus, K., Schulhof, G., Jullien, G. A., Zhang, R. and Wang, W. “Circuit design based on majority gates for applications with quantumdot cellular automata,” in Conf. Rec. 38th Asilomar Conf. Signals, Systems and Computers, Vol. 2, pp. 1354-1357, 2004.
- [27] Wang, W., Walus, K. and Jullien, G. A. “Quantum-dot cellular automata adders”, Third IEEE Conference on Nanotechnology, pp. 461-464, 2003.
- [28] Afindas A and Naveenkumar S Jency Rubia J, Salim A, " Diagnosis of COVID-19 using ADAM Optimization technique in Convolutional Neural Network (CNN)," Tierärztliche Praxis, Vol 41, pp 415-425
- [29] Rubia, J. J., & Sathish Kumar, G. (2020). A high-speed fixed width floating-point multiplier using residue logarithmic number system algorithm. The International Journal of Electrical Engineering & Education, 57(4), 361–375.
- [30] Y. Wang and M. Lieberman, “Thermodynamic Behavior of Molecular-Scale Quantum-Dot Cellular Automata (QCA) Wires and Logic Devices,” IEEE Trans. Nanotechnology, vol. 3, no. 3, pp. 368-376, Sept. 2004.
- [31] A. Bharti and A. Sharma, "Implementation of Ex-OR gate using QCA with NNI logic," 2017 International Conference on Wireless Communications, Signal



Processing and Networking (WiSPNET), Chennai, 2017, pp. 2027-2031, doi: 10.1109/WiSPNET.2017.8300117.

[32] J.M. Seminario et al., "A Molecular Device Operating at Terahertz Frequencies: Theoretical Simulations," IEEE Trans. Nanotechnology, vol. 3, no. 1, pp. 215-218, Mar. 2004.

[33] Jancy RUBIA J, Babitha Lincy r, Al-Heety, "Moving vehicle detection from video sequences for Traffic Surveillance System," ITEGAM-JETIA, Vol 7, Issue 27, PP 41-48

[34] Jency Rubia J., Babitha Lincy R. (2021) Digital Image Restoration Using Modified Richardson-Lucy Deconvolution Algorithm. In: Chen JZ., Tavares J., Shakya S., Iliyasu A. (eds) Image Processing and Capsule Networks. ICIPCN 2020. Advances in Intelligent Systems and Computing, vol 1200. Springer, Cham.



ISSN ONLINE: 2447-0228







RESEARCH ARTICLE

OPEN ACCESS

## DETERMINATION OF NATURALLY OCCURRING RADIOACTIVE MATERIALS-NORM (RA-226, RA-228) IN SYNTHETIC FLOWBACK DEVELOPED AT LABORATORY SCALE FROM ROCKS OF THE LA LUNA-1 WELL, COLOMBIA, AND BENCHMARKING WITH MARCELLUS AND EAGLE FORD SHALE PLAYS

Jenny Paola Rueda\*<sup>1</sup>, Javier Perez<sup>2</sup>, Alvaro Villar Garcia<sup>3</sup> and Jose Manuel Usuriaga<sup>4</sup>

<sup>1, 2, 3, 4</sup> Ecopetrol S.A, Innovation and Technology Center - Colombian Petroleum Institute (ICP), Piedecuesta, Santander, Colombia.

<sup>1</sup> <http://orcid.org/0000-0002-4243-2288> , <sup>2</sup> <http://orcid.org/0000-0003-2320-0200> , <sup>3</sup> <http://orcid.org/0000-0002-3555-1190> , <sup>4</sup> <http://orcid.org/0000-0002-8827-2021> 

Email: \*jennypa.rueda@ecopetrol.com.co, javier.perez@ecopetrol.com.co, alvaro.garcia@ecopetrol.com.co, jose.usuriaga@ecopetrol.com.co

### ARTICLE INFO

#### Article History

Received: August 10<sup>th</sup>, 2021

Accepted: August 25<sup>th</sup>, 2021

Published: August 31<sup>th</sup>, 2021

#### Keywords:

Shale gas/oil,  
Hydraulic fracturing- Flowback,  
NORM,  
Ra-226 and Ra-228 Radioactivity,  
La Luna Formation.

### ABSTRACT

The current decade has been characterized by significant changes in global energy, among which the development of new hydrocarbon deposits, including Unconventional, stand out. In Colombia, the need for exploration of these deposits has been evidenced by the lack of reserves of conventional. One of the main problems identified in the production of these resources is the perception of direct negative effects on the environment, including water as a resource. As part of efforts aimed at identifying potential effects on future production of source rock deposits in Colombia, experiments have been conducted to detect the presence or increase of radioactive elements in the flowback water from hydraulic fracturing fluids, which is one of the main issues identified in currently producing fields in world. Samples from La Luna-1, the first stratigraphic Shale Gas/ Oil Well in Colombia were used. This experimental research was intended to obtain measurements of "NORM Test with Lower Detection Limits" from a synthetic flowback from the digestion of rock samples and fracture fluids (slick water) including HCl at 15%. The results show low concentrations of NORM from synthetic flowback; to contextualize this data was carried a benchmarking with two important unconventional deposits, Marcellus and Eagle Ford Shales.



Copyright ©2016 by authors and Galileo Institute of Technology and Education of the Amazon (ITEGAM). This work is licensed under the Creative Commons Attribution International License (CC BY 4.0).

### I. INTRODUCTION

According to the National Hydrocarbons Agency (2021) [1], Colombia currently has 2041 million barrels (Mbls) of crude oil (proven reserves), from which 300 Mbls are produced annually, with remaining production expected to last approximately 5 more years. On the other hand, an estimated 3163 Gcf are the remaining proven gas reserves, from which 400 Gcf are produced annually. According to the foregoing, Colombia has approximately 8 years of gas reserves left to be produced. Therefore, there is an obvious need to increase or incorporate new conventional reserves, increase production from recovery techniques, and venture into the

exploration and exploitation of unconventional resources. Ecopetrol is currently carrying out studies focused on the identification of potential unconventional resources in Colombia; hence, the company has conducted a well campaign in the Middle Magdalena Valley (MMV) aimed at defining areas for possible shale gas/oil production.

"Natural gas is poised to enter a golden age, but will do so only if a significant proportion of the world's vast resources of unconventional gas – shale gas, tight gas and coalbed methane – can be developed profitably and in an environmentally acceptable manner. The technologies and know-how exist for unconventional gas to be produced in a way that satisfactorily meets these

challenges, but a continuous drive from governments and industry to improve performance is required if public confidence is to be maintained or earned” [2]. A key guideline at Ecopetrol is to ensure that procedures and processes for exploitation of resources, in this case, unconventional, are carried out in accordance with national and international standards, including zero environmental impact and responsible use of water.

A major concern in the production of Shale gas/oil is the presence or increase of radioactive elements derived from the interaction of La Luna Formation fluids with brines from source rocks. An experiment in the MMV is propose to simulated such interaction as it would occur in bottom hole conditions. Therefore, the goal of this study is to identify from a laboratory scale experiment, obtaining a synthetic fluid resulting from HCl [15%] digestion and subsequent slick water addition from rock samples from the La Luna-1 Well, if it presents radioactive elements of natural origin and in what proportion, this fluid will be characterized based on the “NORM Test with Lower Detection Limits”, which identifies the amount of naturally occurring radioactive materials.

Given the importance of the topic for the scientific community and the community in general, it is necessary to approach the subject from the recognition of the hydraulic fracturing technique, the fluids that are generated, among them the flowback and associated to these the NORM, identifying how these radioactive elements originate. Finally, in order to understand the data generated with the synthetic fluid, it is necessary to make a benchmarking with two unconventional reservoirs, the first (Marcellus Shale) for its trajectory in the process and the second (Eagle Ford Shale) for being analogous to the La Luna Formation, one of the Formations of interest for the unconventional in Colombia.

### I.1 LOCATION

This study was carried out in the La Luna-1 Well, which is the first stratigraphic shale gas/oil well in Colombia. It is situated near the Cira-Infantas Field, MMV basin, with coordinates, 1,249,953.0m N/1,031,363.5m E, in the department of Santander (Figure 1).

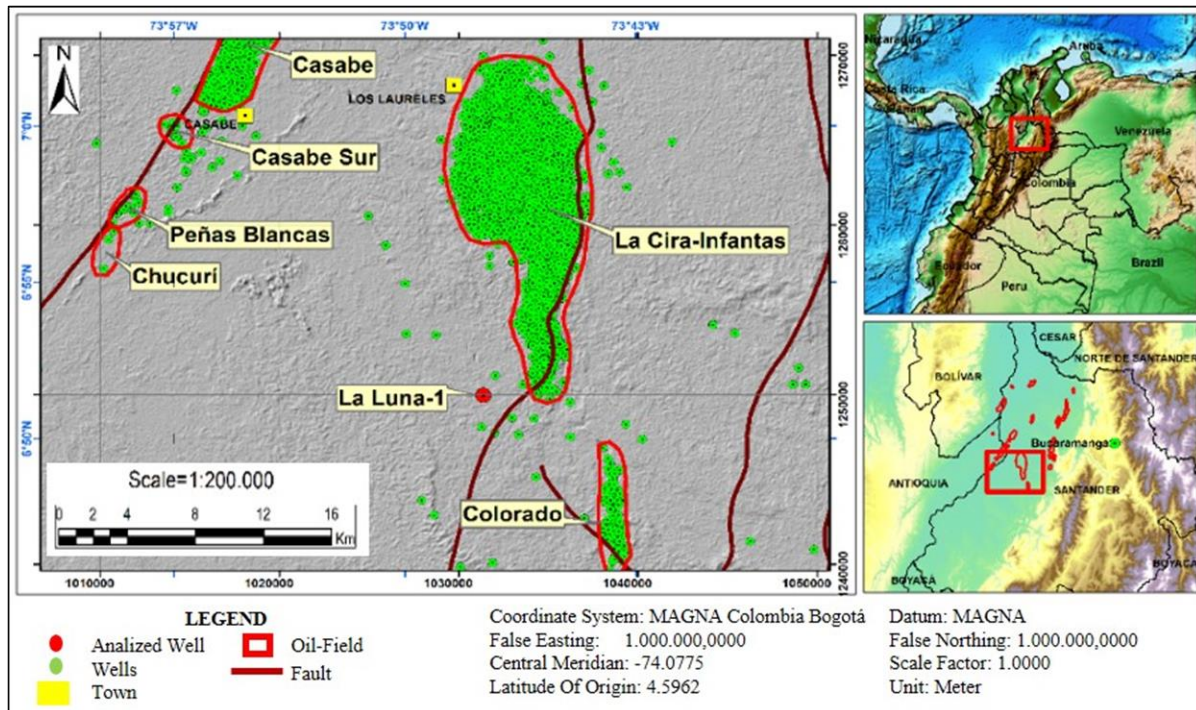


Figure 1: Location of the study area and La Luna-1 well in the Middle Magdalena Valley. Source: Authors, (2021).

## II. UNCONVENTIONAL DEPOSITS

Unconventional and conventional hydrocarbons are compositionally and genetically identical; they only differ in that the latter has migrated to a permeable reservoir rock (conventional reservoir), and the former remains in the source rock where shale gas/oil is generated or has migrated to a very compacted reservoir rock (tight gas) (Figure 2). Source rocks and tight rocks that contain hydrocarbons are called unconventional reservoirs [3].

These unconventional deposits are described as sedimentary rocks of very fine grain with low permeability, which limit the flow of fluids. As gas and oil are distributed in millions of microscopic pores that, unlike conventional reservoirs, are not interconnected and, therefore, cannot move inside the formation. Consequently, it is necessary to artificially generate pathways for fluid flow in the well [4].

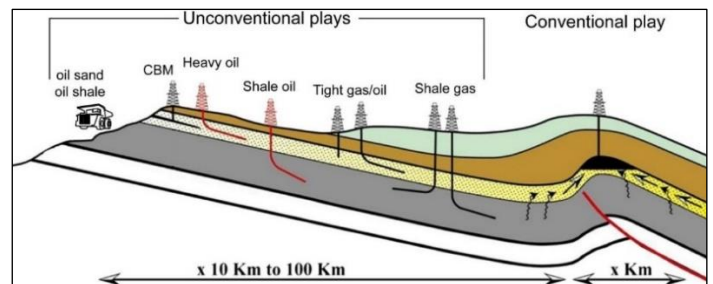


Figure 2: Generalised petroleum system for conventional and unconventional deposits. Source: [5].

The interest in the MMV is related to the trapped hydrocarbons in the shale gas/oil source rock. The main targets are the Olini Group (Upper Lidita, Lower Lidita), the La Luna



Formation (Galembó and Salada members) and the Tablazo Formation [6]. The risked, technically recoverable shale gas and shale oil resources in the combined Cretaceous La Luna and Tablazo shales of the Middle Magdalena Valley Basin are estimated to be 18 Tcf and 4.6 billion barrels, out of risked shale gas and shale oil in-place of 135 Tcf and 79 billion barrels. By comparison Ecopetrol has estimated the MMV Basin has 29 Tcf of shale gas potential [7].

**II.1 TECHNICAL REQUIREMENTS FOR THE EXPLOITATION OF SOURCE ROCK DEPOSITS**

The hydraulic stimulation technique, also called hydraulic fracturing or fracking, was developed almost 80 years ago, with the purpose of improving the permeability of specific deposits. This technique consists in opening tiny fibres of the source rock, where the hydrocarbons were generated and sealed over time by injecting fluids into the rock (water and sand 99.5% plus highly diluted chemicals 0.5%) (Figure 3) [4].

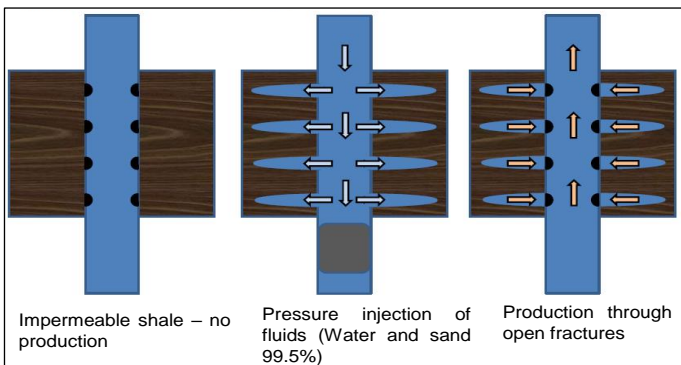


Figure 3: Diagram displaying the drilling design of shale gas/oil deposits. Source: [3].

For the exploitation of unconventional hydrocarbons, drilling must be carried out horizontally throughout the formation for hydraulic fracturing; this technique is developed in several stages. Horizontal drilling enables access to a wider surface of the source rock layer throughout the length of the deposit, thus, maximizing the amounts of shale gas/oil that can be recovered [8]. Further, horizontal drilling allows for multiple wells from a single wellpad, reducing surface footprint and capital investment, and improving shale gas/oil production and efficiency [9]; (Figure 4); hence, it is possible to maximize the Stimulated Reservoir Volume (SRV).

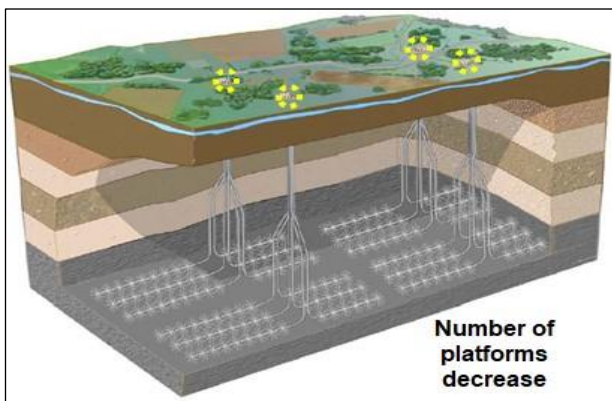


Figure 4: Diagram displaying the paddrilling. Source: [10].

Thus, a high-conductivity zone is artificially constructed within the rock to allow flowing of hydrocarbon from the reservoir to the wellbore. Quite often, before the main hydraulic fracturing operation, it is necessary to pump an acid treatment, usually 15% HCl, intended to clean the perforations and reduce the frictional pressure losses in the near-wellbore zone to thus reduce fracture pressure (this condition was simulated in this experimental protocol).

In conventional reservoirs (reservoir rock), hydrocarbons are stored in the porous rock matrix, which petrophysical properties allow the flow or movement of hydrocarbons and water from the reservoir to the wellbore for subsequent production to the surface, due to the thrust exerted by reservoir pressure. These wells are mostly vertical or deviated, which once drilled and completed can produce hydrocarbons without the need to use the hydraulic fracturing technique; nonetheless, this is widely used worldwide and in Colombia to accelerate production and to solve several production loss issues relative to various mechanisms of formation damage occurring throughout the productive life of the assets [11].

On the other hand, in unconventional reservoirs (source rock), the situation is different, as it is necessary to manage production of the hydrocarbon that did not migrate and was trapped in small pores in the rock. In the source rock, the porosity is very low and these small pores are not interconnected, so the permeability is almost zero (nano-darcies), and that is why in this type of reservoir it is essential to apply the hydraulic fracturing technique (Table 1) to create a network of complex fractures to contact the pores where the hydrocarbons are deposited, and thus create the reservoir in an artificial manner that enables profitable production.

Table 1: Hydraulic Fracturing Objectives in Conventional and Unconventional Reservoirs.

Conventional Reservoirs	Unconventional Reservoirs
To accelerate production	To artificially create the reservoir (VRS) to maximize rock contact and enable hydrocarbon production
Develop additional reserves	
Extend the productive life of assets	
Overcome formation damage	
Mitigate sanding problems	
Reduce organic scale precipitation problems	

Source: [11].

**II.1.1 Fracture Fluids**

The fracture fluids used are a mixture of water, chemicals and proppants (solid substances, such as sand) injected into the shale at high pressure in a well. This process creates a network of small fractures, held open by propagators, allowing oil or gas to flow into the well. Fracture fluids must achieve three main objectives: create a fracture, distribute the proppant and return to the surface avoiding damage of the conductivity of the proppant package [8].

The fluid is used to transmit enough high pressure from the surface to the well and to fracture the rock and place the proppant in the formation. Figure 5A shows the composition of the fracture fluid, which concentration of chemicals is very low. The purpose of the fluid includes mainly: control of bacterial growth, inhibition of clay, gelling agents, surfactants (interfacial tension reducers), emulsion prevention, pH buffer, scale inhibition, friction reduction, gel breakers, and crosslinkers, [13].



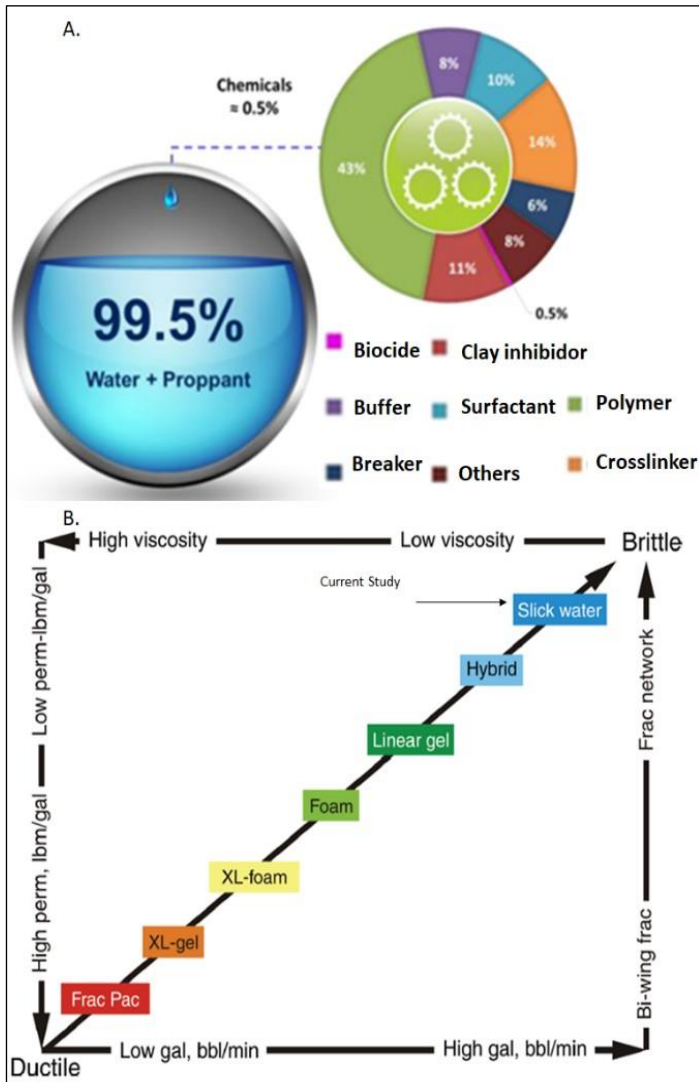


Figure 5: (A) Fluid composition of shale gas/oil fracturing. Water and sand (99,5%), plus additional extremely diluted chemicals (0,5%). (B) Classification of fracturing fluids according to their rock geomechanical characteristics. Source: [8], [14].

Different types of fracture fluids are used in hydraulic fracturing for unconventional reservoirs, according to the characteristics of the target rocks [14]. For this study, the slick water (SW) fluid was used. This fluid is described as having low viscosity mainly composed by water and other chemical additives of very low concentration such as biocides, clay controllers, friction reducers, and surfactants. It is suitable for use with fragile rocks with very low permeability, and rocks that hold pre-existing fractures (Figure 5B), as this enables the creation of denser and more complex fracture networks [15][16].

### II.1.2 Flowback

As they pass through the shale, fracking fluids dissolve many substances trapped naturally in the rock. The substances include particles of naturally occurring radioactive material (NORM), such as potassium (K) and radium (Ra). By dissolving chemicals trapped in the shale, the injected fluids can also become very salty. Some will return via the well to the surface and if they do so, are known as flowback fluids. Understanding their chemical composition is crucial to assessing whether they might have any impact on human health or the wider environment. [12].

## II.2 RADIOACTIVE MATERIALS OF NATURAL ORIGIN - NORM

All elements naturally found in the Earth's crust have different concentrations. However, only eight of them, namely oxygen (O), silicon (Si), aluminum (Al), iron (Fe), calcium (Ca), sodium (Na), magnesium (Mg) and potassium (K) - correspond to 98.5% (Figure 6A). Uranium and Thorium are relatively rare elements that form natural radioactive series (Figure 6B).

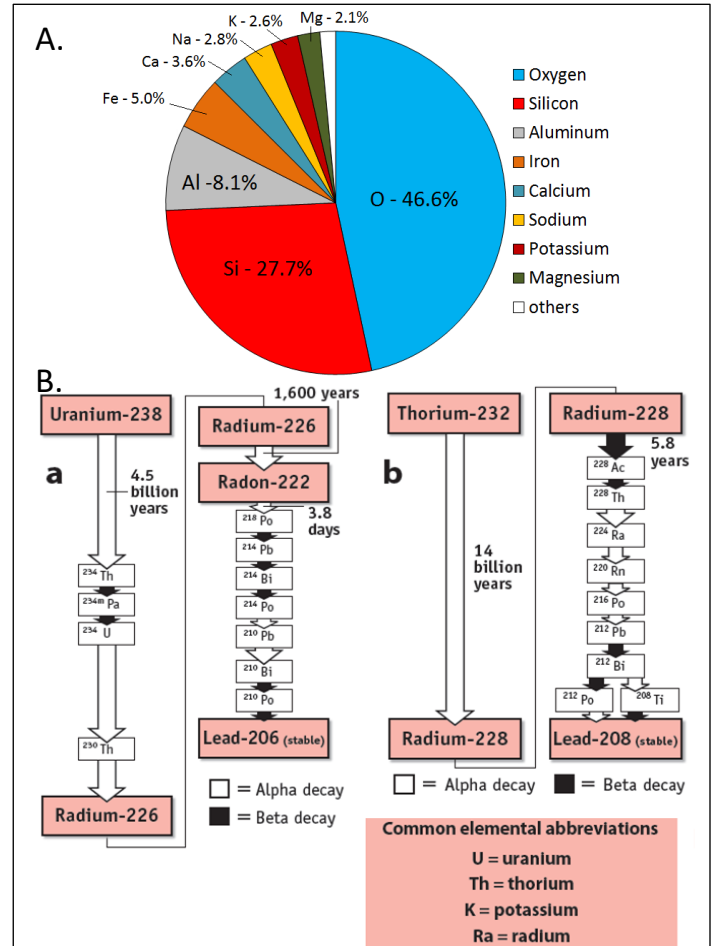


Figure 6: A. Main elements of continental crust. B. Decay sequence that leads to the main elements associated to radioactivity by decay a) U-238 and b) Th-232. Example for the shale gas of Marcellus, United States, one of the main source rocks for unconventional gas. Source: [17], [18].

Naturally occurring radioactive materials (NORM) are defined as materials that may contain any of the primary radionuclides or radioactive elements as they occur in nature, such as radium, uranium, thorium, potassium and its respective decomposition radioactive products. Energy and emitted particles as radioactive material disintegrate to achieve stable (Figure 6B; [19]). NORMs exist in all natural media and are widely distributed in the earth's crust, water, and air. It has been proven that mineral and hydrocarbon extraction processes produce some radioactive waste [20].

The components of the Earth's crust have radioactivity due, fundamentally, to the presence of radionuclides of the three natural radioactive series (from U-238, Th-232 and U-235) and to K-40, which were formed at some stage prior to the formation of the solar system. Since then, these components started to disintegrate, thus,

decreasing their concentration on Earth. Hence, in addition to original radioactive elements, the decay elements or products are also presented (Figure 6B). Uranium and Thorium generate very long radioactive families and Potassium is part of seawater salt and all living things. Basically, it is impossible to find a material or an environment in the Earth that is not radioactive; all of them are, to a greater or lesser extent, even ourselves [21].

**II.2.1 Radioactive Materials of Natural Origin Technologically Enhanced - TENORM**

Some of the injected fluids can dissolve NORM in shale deposits and transport them to the surface (TENORM); radioactive drilling wastes are identified as a form of TENORM (technologically enhanced naturally occurring radioactive material), which are a form of NORM that have been concentrated or placed for human exposure by anthropogenic means [20].

"Technologically Enhanced" means that the radiological, physical and chemical properties of the radioactive material have been further concentrated or altered as they have been processed, benefited or altered in a way that increases the potential for human and/or environmental exposure [19]. As previously mentioned, the shales must be hydraulically fractured to extract the hydrocarbons; this fracture requires high-pressure injection of fluid into the rock. Some of the injected fluids can dissolve the naturally occurring radioactive substances in the shale and transport them to the surface (Figure 7A).

Following the hydraulic fracturing, a mixture of oil, gas and formation water is pumped to the surface, where the water is separated from the gas and stored in tanks where it undergoes processes that concentrate the minerals present in it (Figure 7B). In addition to ions such as barium, strontium or bromine, these may include low concentrations of heavy metals and radioactive isotopes such as Ra-226 and Radio-228.

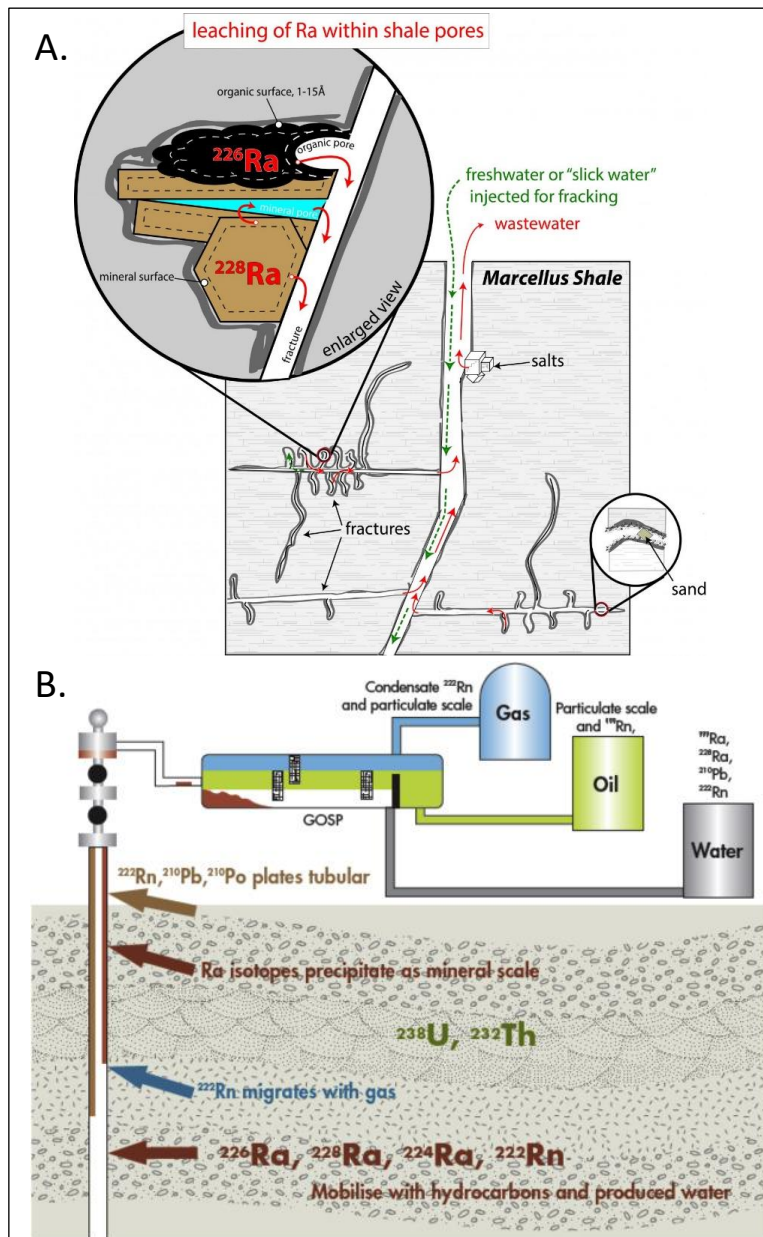


Figure 7: A. Fracturing involves the injection of fluid into the rock at high pressures; some of the injected fluids can dissolve the radioactive substances (Ra-226 and Ra-228) naturally found in the shale and transport them to the surface. B. A mixture of oil, gas and formation water is pumped to the surface; water is then separated from the gas and stored in tanks where it can undergo processes that concentrate the minerals present in it.

Source: [22], [23].

**II.2.2 Radioactive Materials in Sedimentary Rocks**

Sedimentary rocks were formed from igneous, sedimentary or metamorphic rocks. The amount of uranium and thorium present in sedimentary rocks is directly or indirectly related to igneous rocks. These radioelements are removed, by erosion and partial deposition due to their high density near the source rock or during transport, until they reach the sedimentary basin. When the radioactive elements are dispersed, sedimentary rocks generally contain less uranium and thorium than the source rock. A sedimentary rock affected by erosion results in less active sediments and, generally, each sedimentation cycle provides more rocks with less radioactive elements. Therefore, uranium and thorium from sedimentary rocks are, in most cases, in a diffuse state [24].

Among the different radioactive isotopes that can be found in rock formations, their ability to concentrate and come into contact with different materials depends on their mobility.

**II.2.3 Uranium**

Under reducing conditions, the uranium ion precipitates as complex primary oxides with organic matter or as insoluble hydroxides of iron or manganese. Under oxidizing conditions, secondary uranium minerals precipitate by evaporating uranium containing solutions and can form phosphates, arsenates, vanadate, and silicates, with copper, calcium, potassium and other metals.

In humid climates, uranium is transported by groundwater; however, the amount accumulated in seawater and carried by rivers is very low (Figure 8A). Most of the uranium precipitates as soon as it finds enough reducing conditions for conversion from U<sup>2+</sup> to U<sup>4+</sup>. These conditions are due to organic matter, which can be found both on the bottom of the restricted sedimentary basins, and in sediments where waters with uranium content circulate. Moreover, uranium is usually associated with coal, fossil wood, bituminous shales, oil and asphaltite. The form of uranium in these cases is either very finely subdivided UO<sub>2</sub>, or oxide in amorphous state.

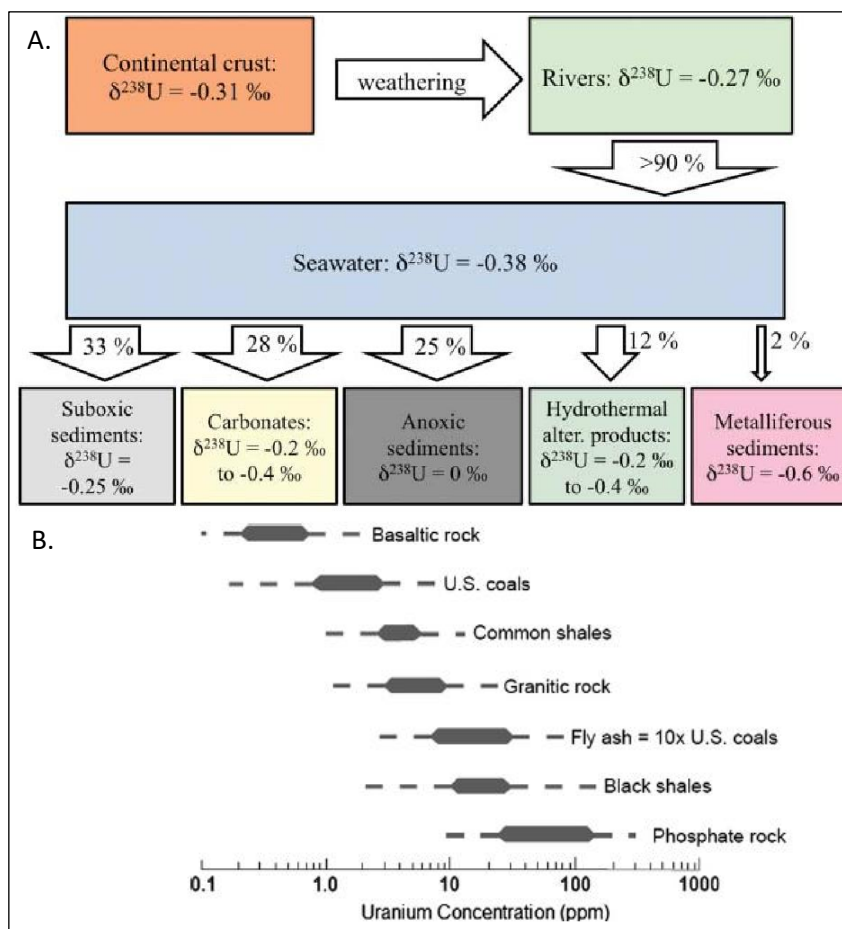


Figure 8: A. Uranium present in the continental crust showing its distribution in different environments. B. Amount of uranium in sedimentary and other types of rocks.

Source: [25], [26].

Black shales contain trace levels of U-238, U-235, K-40 and Th-232 in higher concentrations than those found in grey shales, sandstones or limestones, which are less rich in organic matter. This occurs because: 1) U-238 and U-235 bind better to organic matter, such as algae that die and settle at the bottom of the ocean; and 2) K-40 and Th-232 bind better to clays, which make up much of the sediment at the bottom of the ocean. Finally, as "black shales" contain more organic matter and clays, they are generally more radioactive than other shales or sedimentary rocks [18], (Figure 8B, Figure 9). Black shales and marine phosphates are

enriched with uranium and can often contain more 100 parts per million (ppm) [26].

**II.2.4 Radium**

The decomposition of uranium leads to the formation of radium (decayed isotope). Radium, it is usually found where uranium is produced, including rocks, soil and groundwater. However, sometimes radium can be found far from its uranium parent in the ground or in groundwater. These include soils derived from carbonated rocks, such as limestone, which is generally not



enriched in uranium. During the soil formation process, carbonates leaked resulting in enriched clay with residual materials, which include uranium. In addition, unlike uranium, radium is soluble in acidic or chloride-rich water [27, 28]. Reduced water can transport dissolved radium, just as hydrogen peroxide can transport the uranium in solution away from the area of origin.

The U-238 and Th-232 are part of the rock matrix and are linked to it, being essentially insoluble in the formation fluids under the typical anoxic conditions of black shales; however, the radium (decay product of U and Th) is easily dissolved and transported. The radium occurs naturally within black shales. Among radio isotopes, two of them, Ra-223 and Ra-224, have a short half-life (few days), while the average life of the other two isotopes, Ra-226 and Ra-228, is 1,622 and 5,75 years respectively. If they are dispersed in the environment, they will either endure for long periods or result in high doses. Examples of radium-containing water include wastewater from acid mines or brine waters associated with the extraction of oil, gas and methane [28].

Figure 9 summarizes radioactivity for sedimentary rocks according to the type of rock, with marine organic matter being the one with the highest radioactivity.

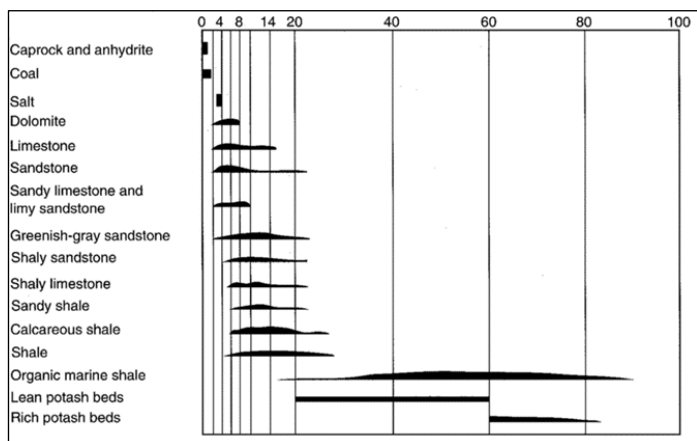


Figure 9: Relative radioactive distribution for several types of sedimentary rocks. Source: [29].

Several studies have shown the adsorption of Ra in organic matter. Their results suggest that Ra can be strongly adsorbed by organic material. It has been determined that the adsorption affinity of organic matter and clays is mainly due to its cation exchange capacity (CEC). It has also been identified that organic matter adsorbs approximately 10 times more Ra-226 than clays (Figure 9).

Organic matter is incorporated into the sediment in the following cases: 1. absorbed in mineral particles (clays and others), 2. dissolved in gel form into the pores of sediments and 3. by cellular material of organisms (phyto and zoo plankton) incorporated directly into the sediment.

In Figure 10, A) Shales are typically composed of clay minerals, quartz and calcium carbonate. Some shales contain organic matter, which, when heated sufficiently, will release gas, such as methane. NORM is commonly stuck (adsorbed) to the surface of the organic matter. B) In shale gas production, a well is drilled down into gas-rich shales, usually buried at depths of 1.5 km or more. A horizontal well is drilled into the shale, and fracking fluids forced into the rock at high pressure through holes in the well casing. The flowback fluid carries gas back up the well to the surface, but also picks up and transports some particles of NORM. [12].

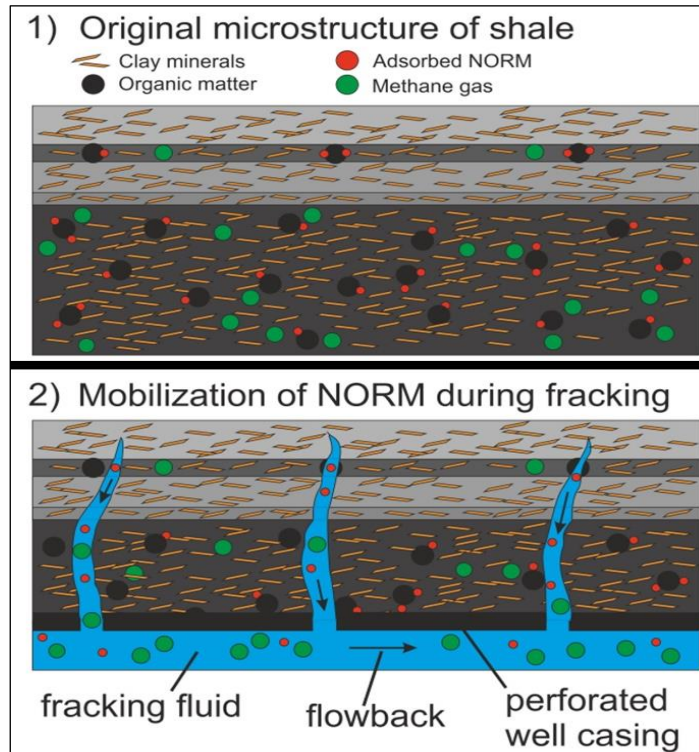


Figure 10: NORM schematic diagram in shales. Source: [12].

According to the information gathered by [30] although the first reports of NORM associated with oil and natural gas appeared in 1904 and, at least since the 1930s, the presence of radionuclides in oil reservoirs has been known. However, it was not until the 1980s, when NORMs were detected in British North Sea oil and gas operations, that knowledge of their presence became public. The U.S. oil and gas industry became aware of specific sources of NORM in 1986, when barium sulfate scale containing elevated levels of Radium-226 and Thorium-232 was discovered in pipelines being removed from a well in Mississippi.

Since unconventional gas development has the potential to generate large quantities of residues containing Ra-226 and Ra-228 in both solid and liquid form, a full analysis of the public exposure pathways should be performed as a prerequisite to the start of activities. Thus, wastewater contains heavy and radioactive metals that will include, mostly Ra-228 and Ra-226, which are soluble in water and may imply a health risk [30].

Both, the speed and scope of the natural gas drilling boom in the USA, have led to greater scrutiny of radioactive exposure and waste management issues [20]. This is currently focused on the formations with the highest production worldwide; however, in countries that are beginning the exploration of unconventional hydrocarbons, additional studies are required to support their exploitation to avoid direct impact for the people and the environment. Such is the case of Colombia, where Ecopetrol is currently analyzing the viability of the exploitation of this resource. This experiment is a great input to study the potential impact.

### III. MATERIALS AND METHODS

The experimental procedure is performed with the purpose of reproducing the physicochemical conditions that exist during the hydraulic fracturing process, which reproduce flowback waters. Currently, the NORM-TENORM present in these waters is being monitored in the deposits with highest production all over the world. The procedure to understand the interaction between rock



and fluid formations and fracturing fluids was carried out in the Optimization Laboratory for Production and Improved Recovery, in the experimental area of Production Chemistry at the Ecopetrol S.A, Innovation and Technology Center - Colombian Petroleum

Institute (ICP), using samples from the La Luna-1 Well (Table 2), which sedimentological characterization is shown in the stratigraphic column, Figure 11.

Table 2: Sample intervals from the La Luna-1 well. Source: Authors

Sample number	Identification	La Luna-1 Well Fm/Member	Depth
			(ft)
1	QP-18-149-11	Upper Lidita Fm (Kls)	9854.42
2	QP-18-149-12	Lower Lidita Fm (Kli)	10486.50
3	QP-18-149-13	Galemo Member	10854.83
4	QP-18-149-14	Salada Member	11892.50
5	QP-18-149-15	Tablazo Fm (Kt)	14755.83

Source: Authors, (2021).

Rock samples from the La Luna-1 Well (Table 1.), iron mortar, sieve mesh #10 and #18 grain size >1mm and <2mm, Slick Water, HCl [15%], oven, schott bottles, and nitric acid was the materials used.

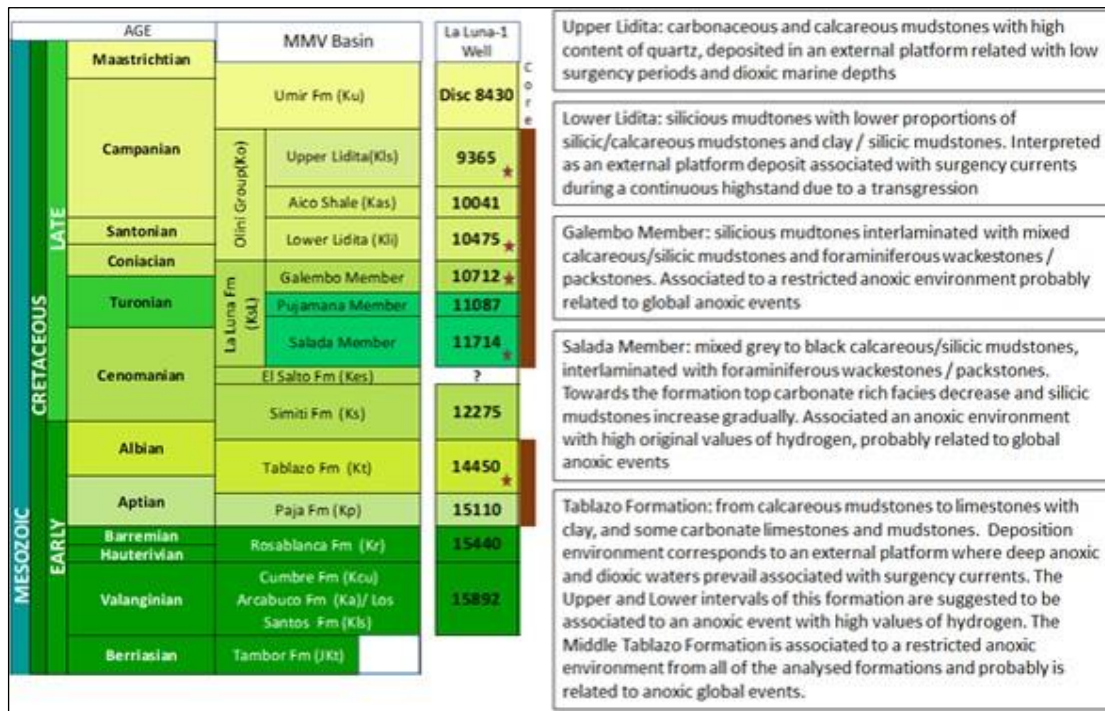


Figure 11: Stratigraphic column from the Cretaceous interval, Middle Magdalena Valley. The intervals are shown in red, and the star represents the interval NORM sample. Modified from.

Source: [6], [31].

### III.1 EXPERIMENTAL DEVELOPMENT

1. Sampling: sampling of approximately 120 g of rock for each interval of interest (Figure 12).

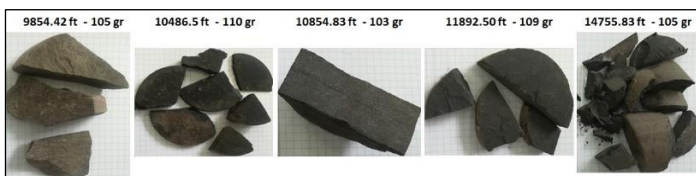


Figure 12: Selected samples for the NORM analysis in the Cretacic interval, MMV. Source: Authors, (2021).

2. Mash: For this procedure, an iron mortar was used, the samples are mashed seeking a grain size that allows best rock-fluid interaction, so as to have greater contact with the fluids.

3. Sieve: Sieves # 10 and 18 (ASTM) were used; the screened sample is larger than 1 mm and smaller than 2 mm. After screening, 100 g of the samples were weighed (Figure 13).

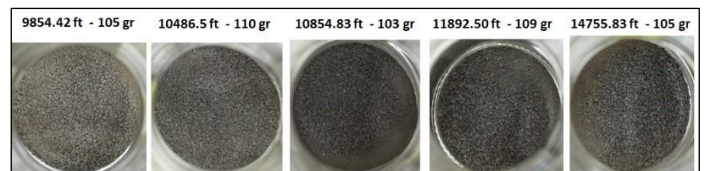


Figure 13: Sieve samples for the NORM analysis in the Cretacic interval, MMV. Source: Authors, (2021).

4. Acid digestion: The samples were placed in a schott bottle where 0.5 ml of [15%] HCl per gram was added. Thus, for 100 g, 50 ml of [15%] HCl were added, in order to simulate the previous treatment of acidification fracturing (Well stimulation operation

where an acid, usually hydrochloric [HCl], is injected into a carbonate formation at a higher pressure than the formation fracture pressure). The circulating acid tends to truncate the fracture faces according to a non-uniform pattern, forming conductive channels that remain open without a supporting or propping agent after the fracture is closed [32].

Pumping a volume of acid prior to fracturing (pre-flow) is an operational practice in hydraulic fracturing that is intended to clean perforations and reduce frictional pressure losses in the near-wellbore zone to ensure the success of the operation. Because a high reaction rate acid is required to dissolve part of the calcareous fraction present in the shale in the near-wellbore zone, the industry, based on the experience of unconventional reservoir development in the United States, has standardized the use of 15% HCl. However, in practice, 15% HCl is pumped as a general rule and it is not a concentration that is defined for each particular well or depending on the mineralogy of each zone or interval.

Based on the foregoing, from an operational and practical point of view, what the protocol used tried to represent was precisely the fact that most likely in Colombia pre-flows with HCl at 15% will also be used and thus determine what could be the concentration of the different parameters in the flowback, as the mineralogical compositions of the rock vary.

The scenario where acidic preflow pumping is used represents the most critical scenario from the perspective of maximum concentration of the different ions or parameters in the flowback. However, in scenarios where, due to operational issues, the use of acid pre-flows is not necessary, it is expected to have lower concentrations of the different parameters in the flowback, the expected concentrations of some ions could be lower than those identified.

5. The digested samples with HCl at [15%] were placed in an oven at 90 ° C, where they were left for interaction for nearly 45 minutes - temperature and approximate time for this treatment.

6. After 45 minutes, the samples were removed from the oven, and 1 liter of the slick water was added, emulating hydraulic fracturing. The fluid is composed, concentration per liter:

Water	Base fluid	982.5 ml
KCl	Clay inhibitor	22.454 g/l
Cla-Web	Clay inhibitor of clays	2 ml
LoSurf 300M	Surfactant	2 ml

From the left-over fluid from the latter mix, the pH is calculated previous to stirring (Table 3).

Table 3: Calculated pH from rock digestion of HCl-Slick Water in the La Luna-1 well.

ID Sample Lab ICP	Depth	Formation	pH
QP-18-149-11	9854.42'	Upper Lidita	6.36
QP-18-149-12	10486.50'	Lower Lidita	6.28
QP-18-149-13	10854.83'	Galembo	6.25
QP-18-149-14	11892.50'	Salada	6.22
QP-18-149-15	14755.83'	Tablazo	6.40

Source: Authors, (2021).

7. This fluid-rock interaction, which occurs on a large scale in the hydraulic fracturing process, is taken to the oven for 30 days at a temperature of 90°C (the schott bottle lid must be tightly secured to prevent the evaporation of fluids).

8. After 30 days, the samples are reduced, shaken and decanted (Figure 14). The fluid (1-liter, minimum amount required by the laboratory) is separated from the solid fraction of the rock and transferred to a bottle, adding 0.5 ml of nitric acid to preserve the sample in a liquid state (this is according to the Pace Analytical laboratory specifications). Finally, the five fluid samples (equivalent to the return fluid) were sent to the Pace Analytical laboratory in order to measure either the radioactive materials of NORM or the potential TENORM.

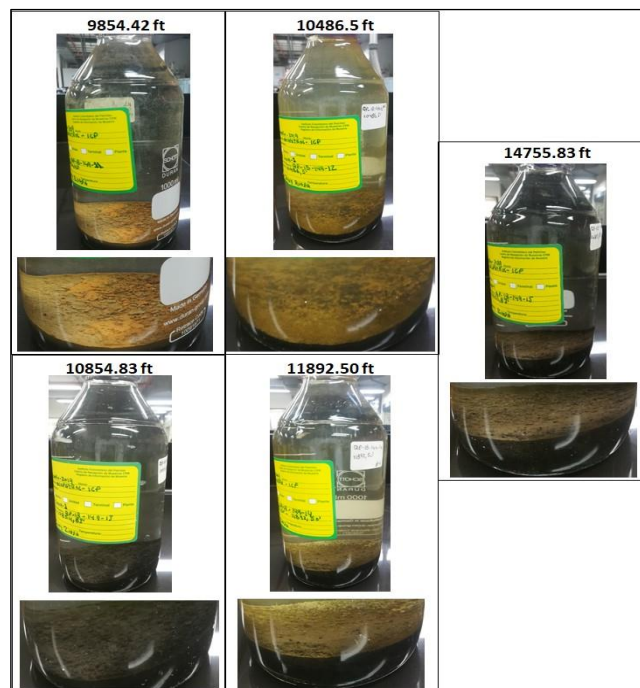


Figure 14: Digestion sample result: sieve sample (1-2mm) + HCl {15%} + Slick water, day 30. Source: Authors, (2021).

#### IV. RESULTS AND DISCUSSIONS

The analysis of fluid samples was carried out in the Pace Analytical laboratory located in Pennsylvania, USA. The laboratory followed the EPA 903 and EPA 904 nomenclature, which describes the procedure to measure Radio-226 and Radio-228 isotopes respectively according to the United States Environmental Protection Agency [33]. Table 4 displays the results obtained, which units are presented in pCi/L.

Where. Act: Activity/ Unc: Uncertainty: For Safe Drinking Water Act (SDWA) analyses, the reported Unc. Is the calculated

Count Uncertainty (95% confidence interval), using a coverage factor of 1.96. For all other matrices (non-SDWA), the reported Unc. is the calculated Expanded Uncertainty (aka Combined Standard Uncertainty, CSU), reported at the 95% confidence interval, using a coverage factor of 1.96./ MDC: Minimum Detectable Concentration/ Carr: C: Carrier Recovery (%)/Trac: T: Tracer Recovery (%).

Table 4: Isotopic results of Ra-226 and Ra-228, for the experimental return fluid from the La Luna-1 Well in the MMV, Colombia.

ID Sample Lab ICP	ID Sample Lab EHS	Depth	Formation	Parameter	Method	Results		Units
						Act ± Unc (MDC)	Carr Trac	
QP-18-149-11	BO1902506.001	9854.42'	Upper Lidita	Ra-226	EPA 903.0	7.27 ± 1.85 (1.25)	C:NA T:65%	pCi/L
QP-18-149-12	BO1902505.001	10486.50'	Lower Lidita	Ra-228	EPA 904.0	17.7 ± 3.39 (0.845)	C:73% T:79%	pCi/L
QP-18-149-13	BO1902506.002	10854.83'	Galembo	Ra-226	EPA 903.0	35.2 ± 5.36 (1.64)	C:NA T:35%	pCi/L
QP-18-149-14	BO1902505.002	11892.50'	Salada	Ra-228	EPA 904.0	8.53 ± 1.75 (0.828)	C:73% T:85%	pCi/L
QP-18-149-15	BO1902505.003	14755.83'	Tablazo	Ra-228	EPA 904.0	2.22 ± 0.753 (1.13)	C:69% T:81%	pCi/L

Source: Authors, (2021).

#### IV.1 NORM REGULATIONS

Compared to conventional hydrocarbon exploitation, on average, the concentrations of NORM in the water produced during unconventional methods can have a factor of approximately 1.5 higher than the water produced during conventional methods. So far, the reported concentration ranges are still within the reported ranges for conventional wells [34].

According to the International Commission for Radiation Protection (ICRP) and the International Atomic Energy Agency (IAEA) which raises the Basic Safety Standards (BSS), synchronized with the legislation of the European Union (EU), the extraction and processing of raw materials that involve exposure due to radioactive material, including the oil and gas industry, are treated as a practice in a planned exposure situation. The EU includes the oil and gas industry in a "list of 16 different industrial sectors involving NORM."

The ICRP stated that "natural radiation sources (e.g. NORM) can legitimately be completely excluded from the scope of their recommendations once the activity concentration of each NORM is less than 1 Bq [NORM] / g". This statement was implemented as per basic safety standards of the IAEA – EU, which states that "exemptions or authorization values for solid-state NORM-materials in secular equilibrium with their progeny" for members of the Th-232 decay series and U-238 will be 1 Bq [NORM] / g, which are equivalent to 27,03 pCi /g. Consequently, a substance or material with a concentration of NORM activity greater than 1 Bq/g, where the NORM must be a member of the Th-232 or U-238 decomposition series, can be defined as NORM.

The different chains of the oil and gas industry that produce solid materials with activity concentrations lower than those mentioned above, will be out of extend. However, for higher activity concentrations, the BSS provides a list of exempt activity concentrations. The BSS does not provide general exempt

concentrations for crude oil/water and natural gas. When the composition and salinity can be the determining factor for the production of water at large, the values provided for production water with concentrations below 10 Bq [Ra-228] / L, 10 Bq [Ra-226] / L can be treated as exempted, which are equivalent to 270 pCi / L [34]. According to the United States Nuclear Regulation Commission, the discharge limit for industrial effluents must be 60pCi / L. According to international standards such as the EPA, and national regulations for water quality in Colombia (NTC 813), the maximum limits for drinking water are equivalent to Ra-226, Ra-228 of 5 pCi/L.

According to the foregoing regulations and the results shown in Table 4 in synthetic flowback, the effluents generated would be treated as radioactive waste materials as they exceed 1 Bq [NORM] / g. Nonetheless, it is also suggested that they would be under the limits to be treated as exempt, as they are below 270 pCi / L, both for Ra-226 and Ra-228.

#### IV.2 COMPARISON BETWEEN THE RESULTS OBTAINED FROM THE LA LUNA-1 WELL AND A STANDARD WORLDWIDE SITE

In order to understand the results obtained from the La Luna-1 Well with respect to the NORM content, some parameters must be considered. One of the most important is the deposition environment of the rocks, which is directly associated with the content of TOC, Ro, Salinity and NORM of the intervals of interest, associated with the gamma ray log. Moreover, it is necessary to have a reference from another perspective, thus, the Marcellus Shale Play will be used, which one of the main shale gas/oil deposits worldwide (NORM deposits are widely distributed; Figure 15A, 15B) and is part of the deposits with the highest production in North America (Figure 15C, 15D).



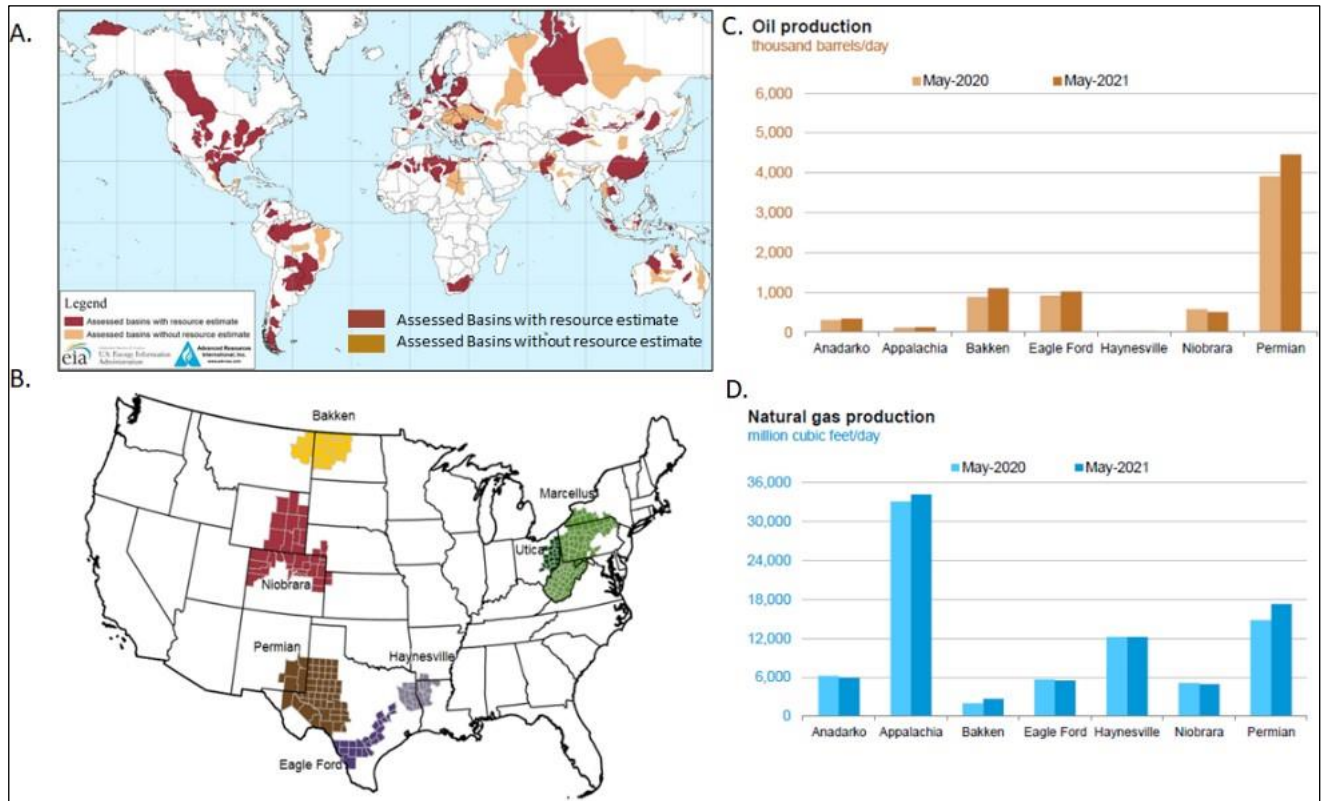


Figure 15: A. Global map of the evaluated basins with shale gas/oil formations. B. Main productive basins of shale gas/oil in USA. C and D Resources from Marcellus Shale. Source: [35], [36].

Table 5, figures 16 and 17, show data from the formations of interest in Colombia and the Marcellus Formation in the United States. Table 5 shows the global paleogeography established by Blakey Ron (2013) [37], identified to be Cretaceous, where the rocks in the VMM were deposited in an open shallow marine environment, under dysoxy and anoxic periods during cycles of major transgressions and regressions [38, 39].

Sediments rich in organic carbon are associated to oceanic anoxic events where large amounts of organic matter was generated and preserved [40]. These events are believed to represent important disturbances in the global carbon cycle [41, 42]. The Cretaceous is a period where organic rich sediments were extensively distributed all over the world in deep and shallow marine environments [43, 44].

Table 5: Comparison between the MMV basin and the Marcellus Formation (Located in the Appalachian basin, USA).

Formations of interest		Age	Environment of formation	Paleogeography, Blakey 2013.	TOC (%)			Ro (%)	Porosity (%)			NORM (pCi/L) (See Figure 17)
					Max	Avr	Min	Avr	Max	Avr	Min	
Olini Group	Upper Liditas	Upper Cretaceous - Campanian	Deposited in an external platform possibly associated with few periods of surgency with marine dioxic depths		4,90	3,24	1,20	0,65	10,81	7,00	0,81	7.27±1.85
	Lower Liditas	Upper Cretaceous - Santonian	Interpreted as a platform external deposit associated with surgency currents during a highstand followed by a transgression		5,02	4,12	3,30	0,72	17,77	12,18	8,71	17.7±3.39
La Luna Fm	Galembó Member	Upper Cretaceous - Coniacian	Associated to a restricted anoxic environment, probably related to global anoxic events		8,95	5,08	2,76	0,76	20,29	13,23	8,30	35.2±5.36
	Salada Member	Upper Cretaceous - Turonian	Associated to an anoxic environment, with high original values of hydrogen, probably related to global anoxic events		8,13	3,57	0,35	0,92	14,70	8,30	4,68	8.53±1.75
Tablazo Fm		Lower Cretaceous - Albian	External platform where anoxic and dioxic deep water conditions prevail with influence of current surgency deposits. The intervals of Lower and Upper Tablazo are suggested to be related to an anoxic environment with high hydrogen original values.		26,50	5,10	0,28	1,38	15,90	8,80	2,40	2.22±0.753
Marcellus FM		Middle Devonian	The paleogeographic reconstruction shows that system is rich in relation to the deposition of organic matter which took place in a three-way packing, almost closed. This geometry created a restriction in the marine circulation of the Appalachian basin during the middle Devonian		20,00	6,50	1,00	0,5/3,5	15,00	6,00	5,00	Depends on the analysed place, varying from 27 up to 13000

Source: [45], [6], [31].



For the Middle Magdalena Valley, in the La Luna-1 Well, Uranium is the element that contributes the most to the total gamma ray (Figure 16). On average, it corresponds to concentrations of 25 ppm, except for the Salada Member of the La Luna Formation, where some intervals reaching 80-100 ppm are observed. This follows maximum TOC values, greater deepening of the basin, and the lower contribution of terrestrial sediments. For the Salada Member specifically, Uranium enrichment could be produced by its incorporation into the sea through hydrothermal solutions associated with the subduction zone and the volcanic activity of the Early Cretaceous during the initial stages of the MMV basin, which is supported by the occurrence of volcanic ash layers in the Salada Member from the La Luna-1 Well [46].

According to Gomez (2014) [46], Uranium from the Salada Member was incorporated into the sediments by different mechanisms: 1) fixed to organic matter, 2) precipitated as uraninite evidenced by high contents of pyrite (obtained from DRX) and abundance of pyrite nodules (identified in the core), 3) chemically linked to phosphate nodules, as evidenced by the greater abundance of phosphate nodules in the Lower Salada Member (observed in

the core and outcrops), and 4) being part of heavy minerals, such as apatite, also evidenced in the description of the core.

The concentration of Uranium in the Marcellus Formation varies from 8 to 53 ppm (Figure 16), and in some studies it has been reported up to 100 ppm [47]. According to Taylor (2013) [48], the deposition of black shale from the Marcellus Formation took place when the basins were deeper, more restricted, and received less sediment. Furthermore, different authors have also proposed that Black Shale was deposited in an epicontinental sea of a shallow basin (Table 5), which enabled the preservation of organic material under anaerobic conditions in an almost closed environment where ocean circulation was restricted due to paleoclimatic and paleogeographic limitations. With regard to the Marcellus Formation, the enrichment or high concentration of metals in the shale has been identified, where the total organic carbon concentration generally increases. It is suggested that this is likely due to the conditions that favor the preservation of organic matter during the shale and during the deposition of metals in a reduced state [47].

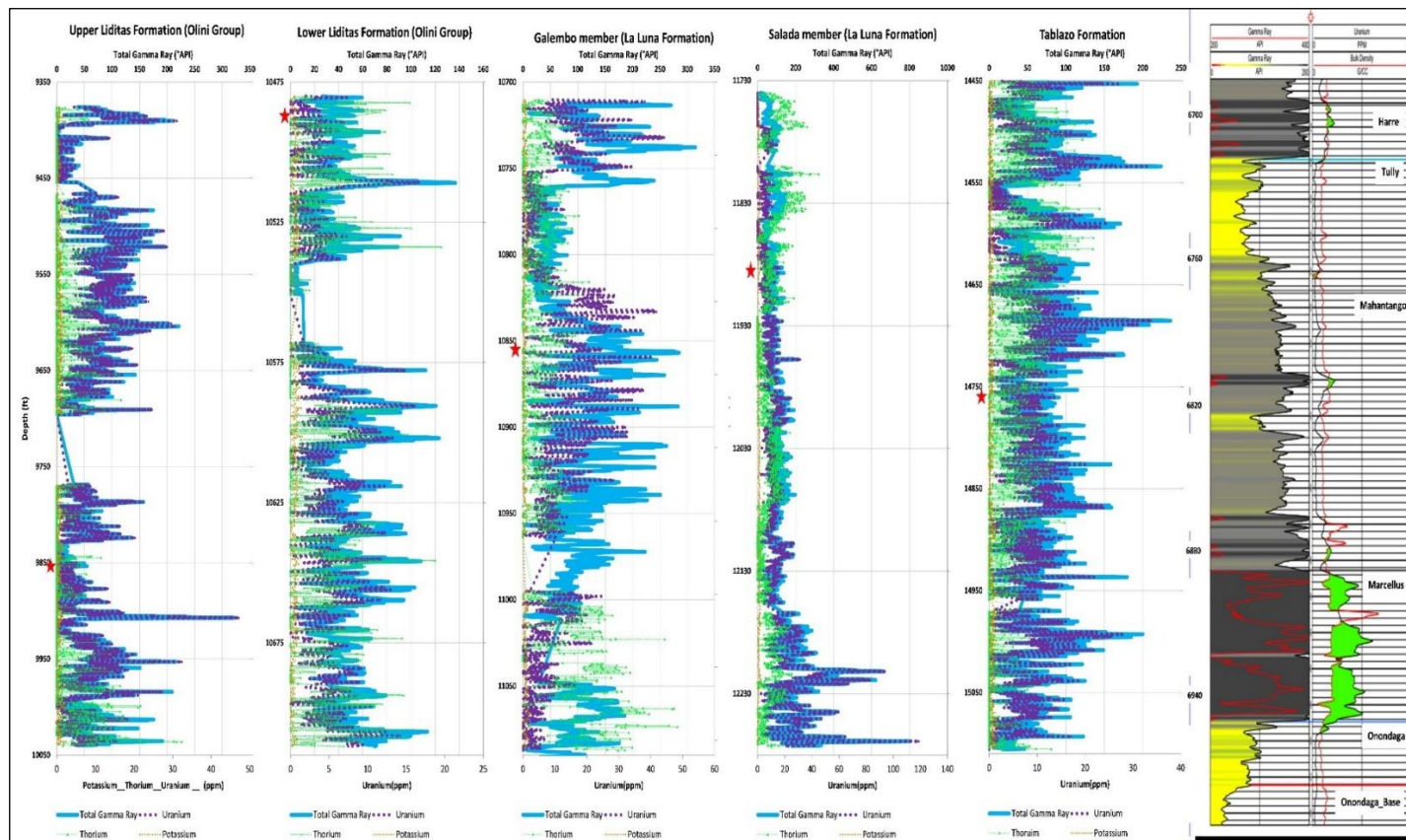


Figure 16: Core Gamma Ray Log obtained for the La Luna-1 well cores (Potassium, Thorium, Uranium and total Gamma Ray). From left to right, Upper Liditas fm, Lower Liditas fm, Galembó Member, Salada member, Tablazo fm, Marcellus Fm. (The curve of gamma ray is plotted in two tracks, from 0 to 200 API, and when Gamma ray exceeds 200 API it is indicated by the red line in the second track).

Source: [49], [6], [31].

The values that have been reported for the Marcellus Formation in Flowback water for the Ra-226 range from 551 to 25500, and average 8490 pCi / l [50] (Figure 17). Experimentally, the highest value for the MMV was 35.2 pCi / l (Figure 17). According to the regulations, the NORM values for the Marcellus Formation are higher than the exception level. Thus, the higher Marcellus values and lower MMV values are determined by the

formation conditions for each respective reservoir. However, it is necessary to pursue the analyses, either at laboratory or pilot scale, in order to obtain thorough knowledge of the different parameters that may increase the NORM contents in the formations of interest. The Marcellus has elevated NORM levels because it is generally more organic-rich than other shales and radioactive elements bond to organic matter [18].

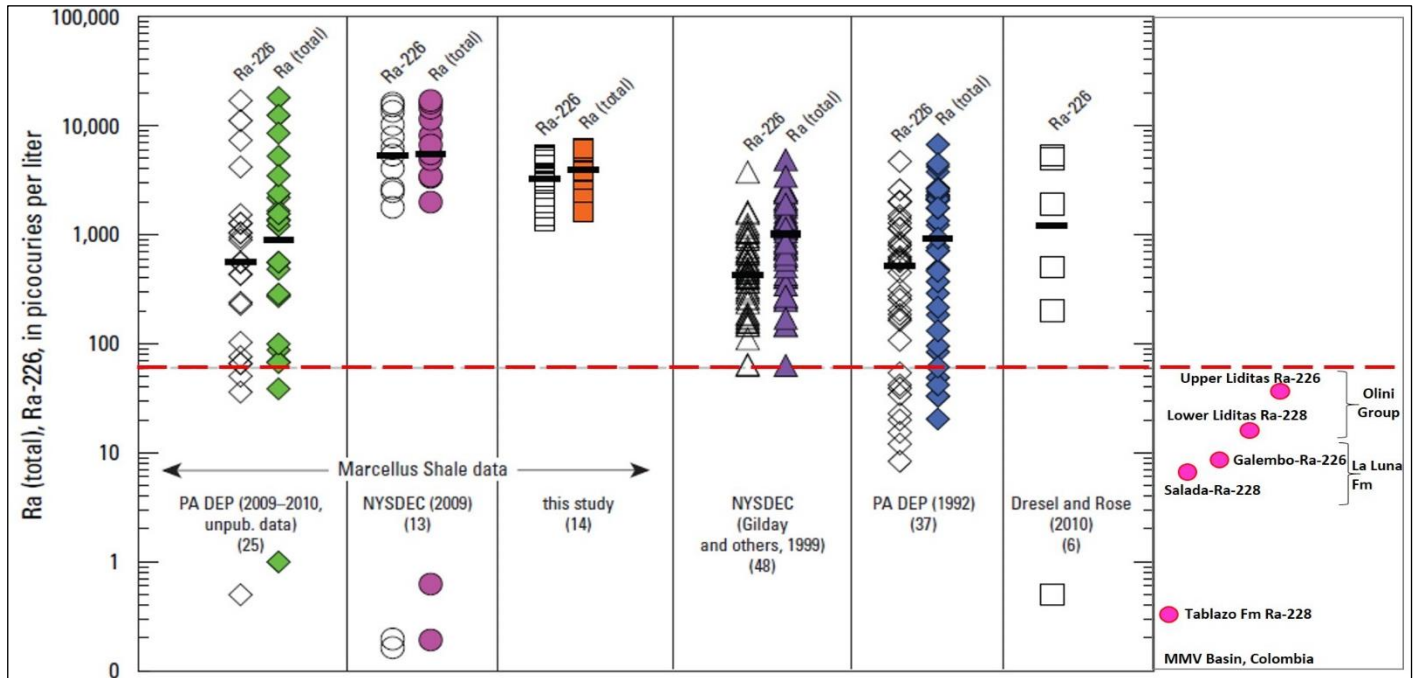


Figure 17: Comparison of data of total Ra-226 (Ra-226 + Ra-228) and Ra-226 in return waters for the Marcellus shale gas deposits and the Olini Group, the La Luna Formation, and the Tablazo Formation as the potential deposits in Colombia. In the case of Marcellus, the number of points in each data set is shown in brackets and the average value is plotted as a black line. For reference purposes, the dotted line shows the discharge limit to industrial effluents (60 pCi/l) for Ra-226, according to the U.S. Nuclear Regulatory Commission (<http://www.nrc.gov/reading-rm/doc-collections/cfr/part020/appb/Radium-226.html>).

Source: Adapted from [51].

### IV.3 COMPARISON WITH HYPOTHETICAL ANALOGUE

A foreign formation similar to a Colombian formation must be identified to correlate the physicochemical features of the flowback [52]. According to some data [52, 53] it was determined that the La Luna formation located in the Magdalena Valley (VMM) and the Shale Eagle Ford, showed similarities in their petrophysical and geologic features; in order to establish the similarities, the following features were taken into account: permeability, porosity, TOC, type of hydrocarbons, type of kerogen, temperature and vitrinite reflectance (Ro) [52].

The Eagle Ford formation consists of organic-rich calcareous mud rock with mineralogy ranging from 40-90% carbonate minerals, 15-30% clay, and 15-20% silica (quartz). The total-organic-carbon content (TOC) ranges from 2-12%, thermal maturity (%Ro) 0.45-1.4%, API gravity 28-62°, porosity 8-12%,

and pressure gradient 0.5-0.8+ (psi/ft), Depth 6500ft-14000 ft, Thickness 75ft-300ft [54].

The Eagle Ford Shale is a hydrocarbon-producing geological formation of significant importance due to its capability of producing both natural gas and more oil than other traditional shale play, the shale play trends across Texas from the Mexican border into East Texas [55] (Figure 15A, 15B). It was deposited approximately 93 million years ago in a marine continental shelf environment [56] (Figure 18), during a period of enhanced volcanism, which resulted in an abrupt rise in temperature due to an influx of CO<sub>2</sub> into the atmosphere, OAE2 Oceanic Anoxic Event [42, 57]. In short, deposition occurred mostly under the influence of: An oxic-suboxic water column before or after the onset of an OAE, an anoxic and possibly sporadically euxinic water column during the onset of an OAE A euxinic water column with available H<sub>2</sub>S during the late phase of an OAE [57].



Figure 18: Paleogeographic reconstruction of North America during the Late Cretaceous. Eagle Ford deposition is shown.

Source: [37].

The formation is divided into two units: an upper unit, characterized by interlayered light and dark gray calcareous mudrock deposited during a regressive interval (sea level falling), and a lower unit of mostly dark gray mudstone deposited during a transgressive interval (from rises in sea levels) [56].

Based on chemostratigraphic data, changing paleoceanographic conditions were documented, anoxic conditions associated with the Lower Eagle Ford Formation, suboxic conditions associated with most of the upper Eagle Fords, and then a return to normal marine conditions at the top of the Eagle Ford Formation. The high TOC content of the lower Eagle Ford was most likely caused by high productivity which in turn drove conditions to anoxia [58].

According to Fertl et al 1980 [59] and recent studies, this formation may vary from a typical dark, organic-rich shale response (i.e., high potassium, excessively high uranium, and high thorium) to a response of low potassium, low thorium, and excessively high uranium in the brittle, calcareous, fractured, and often productive Eagle Ford formation. Uranium concentrations ranging as high as 7 to 15 ppm are frequently observed [56]. In the Upper Eagle Ford, the Uranium values are highly scattered, although ranging from near 0 up to near 30 ppm [60]. The lower Eagle Ford is characterized by high gamma-ray values (90 to 135 API units), predominantly from high U, and many ash beds marked by Th and an upward-coarsening trend; the upper Eagle Ford Formation, interpreted as part of the high-stand systems tract, is characterized by generally low gamma-ray values (45 to 75 API units) with decrease in U and rarely Th, and an upward-fining trend [61, 62].

#### **IV.3.1 Reported Norm and Regulations in the Eagle Ford Shale Region**

Once the shale Eagle Ford formation was identified as the foreign formation analogue to the Colombian La Luna, it is assumed that the physic chemical composition of the flowback resulting from this formation in the United States is the base composition of the flowback in a non-conventional reservoir in the Colombian area [52].

The Eagle Ford Shale is 50 miles wide and 400 miles long; it has been a significant source of both gas and oil production ever since Petrohawk drilled its first wells in 2008 [63]. The increase in drilling activity could be an issue, because chemicals that flow back out of oil and gas wells during extraction could potentially cause groundwater contamination with toxic materials [63]. Due to the significant amount of oil and gas production, Texas has some of the most comprehensive laws and regulations in the country [55].

Jurisdiction over oil and gas NORM waste is split between the Texas Department of State Health Services (DSHS) and the Railroad Commission. The DSHS regulates the possession, use, transfer, transport, and storage of NORM, and the Railroad Commission regulates the activities associated with disposal of oil and gas NORM waste [55].

#### **IV.3.2 Limits From Texas Regulations for Control of Radiation (Above Background)**

Texas uses the term NORM instead of TENORM, under both the general radiation provisions and the oil and gas NORM disposal provisions. Texas defines NORM as “[naturally occurring radioactive] materials not regulated under the AEA whose radionuclide concentrations have been increased by or as a result of human practices,” which often meets the definition of TENORM. Oil and gas NORM waste disposal limits: [64].

For protection of general public:	100 mRem/yr
For radium in water:	30 pCi/liter
For radium in drinking water:	5 pCi/liter
Uranium	30 µg/l
Alpha particles	15 pCi/l

Considering that the levels are typically so low, NORM in produced waters and natural gas is not a problem in Texas, unless it becomes concentrated in some manner. Through temperature and pressure changes that occur in the course of oil and gas production operations, radium 226 and 228 found in produced waters may coprecipitate with barium sulfate scale in well tubulars and surface equipment. Concentrations of radium 226 and 228 may also occur in sludge that accumulates in oilfield pits and tanks. These solids become sources of oil and gas NORM waste [55]. This is explained by the behavior of the Radium, although Ra prefers the aqueous phase, leading to somewhat naturally enhanced concentrations, Ra will follow the aqueous produced water stream, and because Ra is chemically similar to barium (Ba), strontium (Sr), calcium (Ca) and magnesium (Mg) becomes incorporated in group II sulfate or carbonate deposits and scale [34].

Drinking water supplies come from several sources including surface water and aquifers. To identify possible affectation by radioactivity in water, such as Ra 226, numerous studies have been conducted in Texas about aquifers of this region. The Gulf Coast aquifer region has a history of uranium mining and several mines are active today. Currently, all the active mines obtain Uranium using in-situ methods whereby they inject fluids into the ground to dissolve the minerals, which are then brought to the surface in the fluid and sent for processing [65]. A 1989 survey showed the average radium-226 concentration in uranium-mine overburden to be about 0.9 kBq/kg (25 pCi/g) [66]. Very high in-situ gamma radiation from potassium-40, thorium, and uranium have been observed [59, 60].

At the surface, the RRC reports that one Eagle Ford drilling field in Wood County documented radiation greater than 500 microrentgen/hour (µR/hr); these contamination cases are related to historical uranium mining and waste disposal. Additionally, some records indicate concentrations above the EPA MCL (from 0.0 to 1120 pCi/l) Figure 19A, but it is unclear whether these last data points were taken in response to a contamination event, or whether they represent unaffected background data [63]. Figure 19B, shows the Map of some counties considered: those in dark gray counties had Ra-226 over the legal limit and those in light gray counties consistently had Ra-226 under the legal limit set by the US EPA, while those in white had no reported values. Excess figures varied from 1 to 195 times for all water systems within the county [65].

According to some studies [63], in light of the potential for groundwater contamination to occur in the Eagle Ford shale region, it is worth assessing the strength of existing background water quality datasets in accurately predicting a regional baseline of water quality. “Background” water or baseline quality refers to the chemical characteristics of water before a change introduced to the water body that could affect its chemical characteristics. Further, oil and gas companies (industry) are aware of the opportunity for landowners to falsely claim that contamination has occurred when water quality problems already exist. On the other hand, landowners have been unable to obtain compensation for groundwater remediation when no comparison to background water quality is available to indicate the source of contamination.



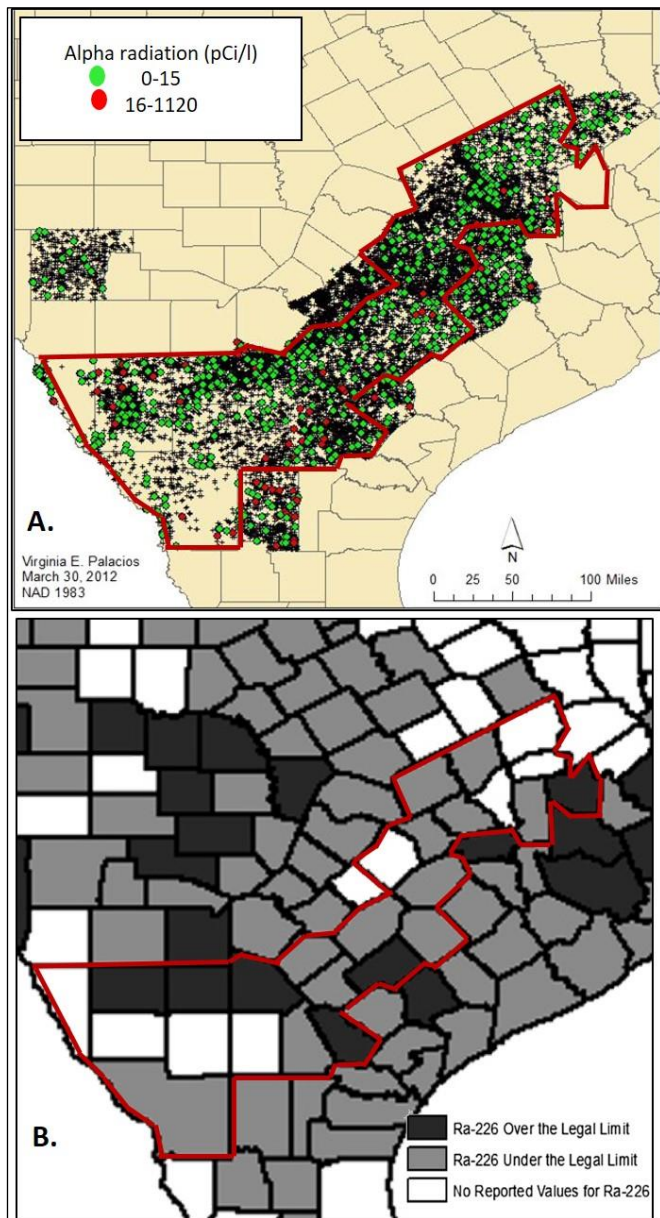


Figure 19: A. Alpha particle concentrations in the counties of interest. Red points represent values greater than the EPA MLC. B. Map of the counties considered: those in dark gray counties had Ra-226 over the legal limit and those in light gray counties consistently had Ra-226 under the legal limit set by the US EPA, while those in white had no reported values.

Source: [63], [65].

\*Note in red the Eagle Ford boundaries.

## V. CONCLUSIONS

The methodology simulated at laboratory scale the possible scenarios of rock-fluid contact (fracturing fluid) that occur in the hydraulic fracturing process (contact time, in this case with acid preflow), to obtain "synthetic flowback" samples. This fluid was called synthetic because although it used real rock samples from the La Luna formation, it is obtained in laboratory conditions; the importance of this experiment was to estimate or have indications of what could be the expected concentrations of NORM in this flowback in order to make risk management and mitigation plans based on this data for the possible development of unconventional in Colombia.

Based on the results obtained from the synthetic flowbacks in the Geologic formations of interest of the La Luna-1 well in the

MMV basin in Colombia to identify NORM in flowback water, would be treated as Radioactive Waste Materials, as they exceed 1 Bq [NORM] / g, nevertheless, they are below the limits to be treated as exempted as they are below 270 pCi / L, both for the Radio-226 as for the Ra-228. However, it is necessary to pursue the analyses, either at laboratory or pilot scale, in order to obtain thorough knowledge of the different parameters that may increase the NORM contents in the formations of interest.

Uranium and Radium 226 values measured in the La Luna-1 Well compared to the measured averaged values in the Marcellus Formation are present in lower concentrations, suggesting that the NORM enrichment in the Marcellus Formation and the low NORM values in Colombia are related to the content of uranium according to this results.

Uranium and Radium 226 values measured in the La Luna-1 Well compared to the measured averaged values in the Eagle Ford Formation exist in lower concentrations; however, it is not clear whether data from Eagle Ford were taken in response to an Oil and gas industry contamination event, or other influence such a uranium mining.

It is advisable to conduct a "Background" water or baseline quality assessment in the Middle Magdalena Valley Basin, intended to identify if another factor exists that could increase contamination in surface and underground water, as it occurred in the Eagle Ford Shale Play.

## VI. AUTHOR'S CONTRIBUTION

**Conceptualization:** Jenny Paola Rueda and Jose Manuel Usuriaga.

**Methodology:** Javier Perez and Jose Manuel Usuriaga.

**Investigation:** Jenny Paola Rueda.

**Discussion of results:** Jenny Paola Rueda, Javier Perez, Jose Manuel Usuriaga and Alvaro Villar Garcia.

**Writing – Original Draft:** Jenny Paola Rueda.

**Writing – Review and Editing:** Jenny Paola Rueda, Javier Perez, Jose Manuel Usuriaga and Alvaro Villar Garcia.

**Resources:** Jenny Paola Rueda, Javier Perez, Jose Manuel Usuriaga and Alvaro Villar Garcia.

**Supervision:** Javier Perez and Jose Manuel Usuriaga.

**Approval of the final text:** Jenny Paola Rueda, Javier Perez, Jose Manuel Usuriaga and Alvaro Villar Garcia.

## VII. ACKNOWLEDGMENTS

We thank the experimental area of production chemistry of Innovation and Technology Center - Colombian Petroleum Institute (ICP), for their support in carrying out the tests.

## VIII. REFERENCES

- [1] Agencia Nacional de Hidrocarburos, ANH, "Reservas de crudo y gas del país Corte a 31 de diciembre de 2020". [www. Anh.gov.co](http://www.anh.gov.co). accessed on 12 July 2021. [https://www.anh.gov.co/Operaciones-Regal%  
Participaciones/SiteAssets/estadisticas-del-sector/modulo-de-gestion-de-reservas/Presentacio%  
reservas/Presentacio%cc%81n%20Balance-Reservas\\_IRR2020\\_Prelim\\_10-06-2021.pdf](https://www.anh.gov.co/Operaciones-Regal%c3%adas-y-Participaciones/SiteAssets/estadisticas-del-sector/modulo-de-gestion-de-reservas/Presentacio%cc%81n%20Balance-Reservas_IRR2020_Prelim_10-06-2021.pdf)
- [2] EIA, "Golden Rules for a Golden Age of Gas", World Energy Outlook Special Report on Unconventional Gas. International Energy Agency, Paris. 2012. [www.worldenergyoutlook.org](http://www.worldenergyoutlook.org).
- [3] Schneider Frederic., Beicip Franlap. "Yacimientos No Convencionales. Foro "Preguntas y respuestas sobre el fracking", Agencia Nacional de Hidrocarburos. ANH Colombia. 2014. <https://www.anh.gov.co/Seguridad-comunidades-y-medio-ambiente/Estrategia-ambiental/Proyectos/Yacimientos-no-convencionales/Paginas/default.aspx>



- [4] Skalany Miriam., "Informe estimulación por fractura hidráulica en formaciones no convencionales. Experiencia en Mendoza sobre Vaca Muerta", Secretaria de ambiente y Ordenamiento territorial, Gobierno Mendoza. 2018. <https://www.mendoza.gov.ar/dpa/wp-content/uploads/sites/34/2018/04/Informe-Estimulaci%C3%B3n-Hidraulica-Mendoza-Vaca-Muerta.pdf>
- [5] Euzen, Tristan, "Shale Gas: An Overview", Ifp Technologies Canada Inc., Calgary. Technical Report, 2011. DOI: 10.13140/RG.2.1.2236.6242
- [6] Ecopetrol. Metodología de Estratigrafía de Secuencias aplicada a la evaluación de yacimientos No Convencionales. Internal Report. 2014.
- [7] EIA, "Technically Recoverable Shale Oil and Shale Gas Resources: Northern South America". 2013. [https://www.eia.gov/analysis/studies/worldshalegas/pdf/Northern\\_South\\_America\\_Columbia\\_Venezuela\\_2013.pdf](https://www.eia.gov/analysis/studies/worldshalegas/pdf/Northern_South_America_Columbia_Venezuela_2013.pdf)
- [8] Usuriaga, J., Bravo, O., Casas, O., Cardona, J., "Water Management Alternatives for Hydrocarbon Production from Source Rocks in Colombia", ACGGP. 2018.
- [9] Hughes, J. D. "Energy: A reality check on the shale revolution", Nature, vol 494, pp 307-308. February 2013.
- [10] Álvarez-Fernández I, Arenillas-González A, Cayola-Cortés FJ, Cienfuegos-Suárez P, García de la Noceda-Márquez C, Loredo-Pérez J, Martínez-Orio R, Mazadiego-Martínez LF, Vázquez-Teijeira D, Vicuña-Irusta JC, Tarín-Egoscobal I. "Gas no Convencional en España, una Oportunidad de Futuro", Consejo Superior de Colegios de Ingenieros de Minas. 2013.
- [11] Usuriaga Torres Jose Manuel. "Diseño de un fluido entrecruzado Guar\_Boro Compatible con Agua de Producción y Flowback para el fracturamiento hidráulico en Yacimiento en Roca Generadora en el Valle Medio del Magdalena", énfasis en Ingeniería de Producción de Hidrocarburos. Universidad Industrial de Santander, Tesis de Grado para optar el Título de Maestría. 2019.
- [12] Almond, S., Clancy, S.A., Davies, R.J. Worrall F., "The flux of radionuclides in flowback fluid from shale gas exploitation". Environmental Science and Pollution Research, vol 21, pp 12316-12324. 2014. DOI: <https://doi.org/10.1007/s11356-014-3118-y>. How radioactive is fracking flowback water? REFINE Briefing Note.
- [13] Kaufman, P., Penny, G.S., Paktinat, J., SPE 119900. "Critical evaluations of additives used in shale slickwater fracs." SPE Shale Gas Production Conference, Irving, Texas. 2008.
- [14] Chong, K. K., Grieser, W. V., Passman, A., Tamayo, C. H., Modeland, N., Burke, B. "A Completions Guide Book to Shale-Play Development: A Review of Successful Approaches Towards Shale-Play Stimulation in the Last Two Decades". Canadian Unconventional Resources & International Conference, Calgary, 19-21 October. CSUG / SPE 133874. 2010.
- [15] Cipolla, Craig L., Warpinski, Norman Raymond, Mayerhofer, Michael J., Lolon, Elyezer, and Michael C. Vincent. "The Relationship between Fracture Complexity, Reservoir Properties, and Fracture Treatment Design" Paper presented at the SPE Annual Technical Conference and Exhibition, Denver, Colorado, USA, September 2008, DOI: <https://doi.org/10.2118/115769-MS>
- [16] Houseworth James. "Chapter 2, Advanced Well Stimulation Technologies In: An Independent Scientific Assessment of Well Stimulation in California". Volume I, Well Stimulation Technologies and their Past, Present, and Potential Future Use in California. 2015.
- [17] Earle, S. "Physical Geology" – 2nd Edition. Victoria, B.C.: BCcampus. 2019. Retrieved from <https://opentextbc.ca/physicalgeology2ed/>.
- [18] Perry, S. A. "Understanding naturally occurring radioactive material in the Marcellus Shale". Marcellus Shale. Issue no 4. pp 1-8. August 2011.
- [19] EPA, United States Environmental Protection Agency. "Technologically Enhanced Naturally Occurring Radioactive Materials From Uranium Mining, Volume 1: Mining and Reclamation Background, Volume 2: Investigation of Potential Health, Geographic, and Environmental Issues of Abandoned Uranium Mines". 2008.
- [20] Brown, Valeria. "Radionuclides in Fracking Wastewater: Managing a Toxic Blend". Environmental health perspectives. vol. 122. no. 2. Pp 50-55. February 2014. DOI: <http://dx.doi.org/10.1289/ehp.122-A50>
- [21] Núñez Lagos Roglá, R. "La radioactividad ambiental". Revista Logos Ciencia & Tecnología, vol. 2 no. 2. pp 50-61. 2011. DOI: <https://doi.org/10.22335/rclt.v2i2.82>
- [22] Landis, Joshua, Sharma, Mukul, Renock, Devon, Niu, Danielle. "Rapid desorption of radium isotopes from black shale during hydraulic fracturing. 1. Source phases that control the release of Ra from Marcellus Shale". Chemical Geology, vol. 496, pp 1-13 2018. DOI: <https://doi.org/10.1016/j.chemgeo.2018.06.013>
- [23] OGP Report No. 412, "Guidelines for the management of Naturally Occurring Radioactive Material (NORM) in the oil & gas industry", September 2008, [www.ogp.org.uk](http://www.ogp.org.uk)
- [24] Liendo Perales Ana Maria, "Prospección geofísica de los radioelementos uranio, torio, potasio y minerales paragenéticos asociados. Estudio al suroeste del estado Aragua para demostrar la capacidad de las técnicas de espectrometría de radiación gamma, en la exploración y evaluación preliminar de recursos minerales y energéticos". Tesis Universidad Central de Venezuela. 2003.
- [25] Noordmann J., Weyer S., Georg R. B., Jöns S., Sharma M., "238U/235U isotope ratios of crustal material, rivers and products of hydrothermal alteration: New insights on the oceanic U isotope mass balance. Isotopes in Environmental and Health Studies". vol. 52. pp 141-163. 2016. DOI: [10.1080/10256016.2015.1047449](https://doi.org/10.1080/10256016.2015.1047449)
- [26] Baykal, Gökhan, Saygılı, Altug. "A new technique to reduce the radioactivity of fly ash utilized in the construction industry". Fuel. Vol. 90. pp 1612-1617. 2011. DOI: 10.1016/j.fuel.2011.01.006.
- [27] Felmlee, J. K., and Cadigan, R. A., "Determination of radium in source rocks by using radium in Crystal Springs, Great Salt Lake area, Utah: U.S". Geological Survey, Open-file Report 78-102. 1978. DOI: <https://doi.org/10.3133/ofr78102>
- [28] Gundersen, L. C. S., and Szabo, Z., "Natural radionuclides in earth, air, and water, and the effect on human health; in, Energy and the Environment—Application of Geosciences to Decision-making", L. M. H. Carter, ed.: U.S. Geological Survey, Circular 1108. 1995.
- [29] Bigelow, E.L. "Introduction to Wireline Log Analysis". Houston, Texas: Western Atlas International. 1992.
- [30] Eguilior, S., Hurtado, A., Recreo, F. "Riesgos asociados a la radioactividad natural en los proyectos de extracción de gas no convencional". Congreso Nacional del Medio Ambiente, CONAMA 2014, 20 pp. 2014.
- [31] Ecopetrol. Columna estratigráfica Valle Medio del Magdalena\_ actualización de topos pozo La Luna 1. Internal Report. 2019
- [32] Schlumberger, [https://www.glossary.oilfield.slb.com/es/Terms/f/fracture\\_acidizing.aspx](https://www.glossary.oilfield.slb.com/es/Terms/f/fracture_acidizing.aspx)
- [33] EPA, United States Environmental Protection Agency. "Method 903.0: Alpha-Emitting Radium Isotopes in Drinking Water". 1980. [www.epa.gov](http://www.epa.gov).
- [34] Evans, Peter, Jonkers, Gert, Steffan, Ernst-Michael, Campbell, John, Lloret, Carla. "Guidelines for the Management of Naturally Occurring Radioactive Material (NORM) in the Oil and Gas Industry", 2016. DOI: 10.2118/179272-MS.
- [35] EIA, U.S. Energy Information Administration, "Independent Statistics & Analysis. Shale oil and shale gas resources are globally abundant. Basins with assessed shale oil and shale gas formations". 2014.
- [36] EIA, U.S. Energy Information Administration, "Independent Statistics & Analysis. Drilling Productivity Report. For key tight oil and gas shale gas regions", 2021.
- [37] Blakey, R., "Paleogeographic Maps". 2013. <http://cpgeosystems.com/paleomaps.html>
- [38] Torres, E. "Unconventional Gas Shale Assessment of La Luna Formation, In the Central and South Areas of the Middle Magdalena Valley Basin, Colombia". M.S Thesis, University of Oklahoma. 2013.
- [39] Casadiego-Quintero, E., Ríos-Reyes, C. A. "Lithofacies analysis and depositional environment of The Galembó member of La Luna Formation". CT&F - Ciencia, Tecnología y Futuro, vol 6. no 4. pp 37 - 56. 2016. DOI: <https://doi.org/10.29047/01225383.02>

- [40] Liborius, Andreina, Slatt, Roger. "Geological Characterization of La Luna Formation as an Unconventional Resource in Lago De Maracaibo Basin, Venezuela". Conference Paper. Unconventional Resources Technology Conference (URTeC). 2016. DOI: 10.15530/urtec-2016-2461968
- [41] Mort, Haydon. "Biogeochemical changes during the Cenomanian-Turonian Oceanic Anoxic Event (OAE 2)". Thesis Doctorate in Science. Universidade de Neuchâtel, Suíssa. 2020. [https://doc.rero.ch/record/7944/files/these\\_MortH.pdf](https://doc.rero.ch/record/7944/files/these_MortH.pdf)
- [42] Jenkyns, Hugh. "Geochemistry of Oceanic Anoxic Events". *Geochemistry Geophysics Geosystems – Geochemistry geophysics geosystems*. vol. 11. no. 3. March 2010. DOI:10.1029/2009GC002788.
- [43] Perez-Infante, J., Paul, F., Max., F. "Global and local controls influencing the deposition of the La Luna Formation (Cenomanian-Campanian), western Venezuela". Elsevier, *Chemical Geology*, vol. 130. pp 271-288. 1996.
- [44] Evenick, Jonathan. "Late Cretaceous (Cenomanian and Turonian) organofacies and TOC maps: Example of leveraging the global rise in public-domain geochemical source rock data". *Marine and Petroleum Geology*. Vol 111. pp 301-308. 2020. DOI: <https://doi.org/10.1016/j.marpetgeo.2019.08.037>
- [45] EIA, U.S. "Marcellus Shale Play, Geology review". 2017.
- [46] Gomez, A. "Integrated geological characterization and distribution of the salada Member, La Luna Formation, in the central area of the Middle Magdalena Basin, Colombia". Norman, Oklahoma: M.S Thesis The University of Oklahoma. 2014.
- [47] Bank, T. "Uranium geochemistry in the Marcellus shale: effects on metal mobilization". Hydraulic Fracturing Technical Workshop 1 - 08 presentation by Tracy Bank, Department of Geology at the University of Buffalo. 2010. <https://www.epa.gov/hfstudy/trace-metal-geochemistry-and-mobility-marcellus-shale>
- [48] Taylor, Ty. "Lithostratigraphic and Petrophysical Analysis of the Middle Devonian Marcellus Shale at the Mamont Prospect, Westmoreland County, Pennsylvania". 2013. All Theses. 1775. [https://tigerprints.clemson.edu/all\\_theses/1775](https://tigerprints.clemson.edu/all_theses/1775)
- [49] Boyce, Matthew, Carr, Timothy. "Lithostratigraphy and Petrophysics of the Devonian Marcellus Interval in West Virginia and Southwestern Pennsylvania". *Unconventional Energy Resources: Making the Unconventional Conventional* vol 29. 2009. DOI: <https://doi.org/10.5724/gcs.09.29.0254>
- [50] Allard David. "An Investigation of the Radiological Aspects of Pennsylvania's Oil and Gas Activities", APHL Meeting. 2019. <https://www.aphl.org/conferences/proceedings/Pages/APHL-2019-Proceedings.aspx>
- [51] Rowan, E.L., Engle, M.A., Kirby, C.S., and Kraemer, T.F. "Radium content of oil- and gas-field produced waters in the northern Appalachian Basin (USA)— Summary and discussion of data". U.S. Geological Survey Scientific Investigations Report 2011–5135, 31 p. 2011. <http://pubs.usgs.gov/sir/2011/5135/>
- [52] Aranguren-Campos, Fabian, A., Calderón-Carrillo, Zuly, Usuriaga-Torres, José, M. "A selection methodology of Flowback treatment technologies and Water reuse in Hydraulic Fracturing in source rocks - A strategy to reduce the Environmental Impacts in Colombia". *CT&F- Ciencia, Tecnología y Futuro*, vol. 7. No. 1. pp 5-30. 2017.
- [53] Rengifo, J., Calderon Z., Perez E. "Estudio de analogías y sus posibles aplicaciones en las formaciones del Valle Medio del Magdalena, a partir del análisis histórico del desarrollo de los shale plays en Estados Unidos". XVI Congreso Colombiano de Petróleo y Gas. Acipet. 2015.
- [54] Za Za Energy Company Corporation, Presentation, Investor Presentation December 2014, p. 14., <http://www.zazaenergy.com/>
- [55] <http://www.rrc.texas.gov/oil-and-gas/major-oil-and-gas-formations/eagle-ford-shale/>, April 2021.
- [56] EIA, U.S. "Updates to the EIA Eagle Ford". 2014.
- [57] Kearns Timothy. "Chemostratigraphy of the Eagle Ford formation". Master Degree Thesis. UTA. 2011. <https://rc.library.uta.edu/uta-ir/handle/10106/9590>
- [58] Boling, Kenneth. "Controls on the accumulation of organic matter in the Eagle Ford Group". Thesis Master Degree. Central Texas, USA. 2014. <https://www.researchgate.net/publication/309126984>
- [59] Fertl, W.H., Stapp, W.L., Vaello, D.B., W.C. Vercellino. "Spectral Gamma-Ray Logging in the Texas Austin Chalk Trend." *Journal of Petroleum Technology*. 32. pp 481–488. March 1980. DOI: <https://doi.org/10.2118/7431-PA>
- [60] Brunick, J. "Depositional Dynamics of the Upper Eagle Ford (Upper Cretaceous): Karnes and Gonzales Counties, South Texas". 2017. Graduate Theses and Dissertations Retrieved from <https://scholarworks.uark.edu/etd/1889>
- [61] Hendershott, Zachary Paul. "Evaluation of the depositional environment of the Eagle Ford Formation using well log, seismic, and core data in the Hawkville Trough, LaSalle and McMullen counties, south Texas". 2012. LSU Master's Theses. 863. [https://digitalcommons.lsu.edu/gradschool\\_theses/863](https://digitalcommons.lsu.edu/gradschool_theses/863)
- [62] Pope, Michael, Wehner, Matthew, Peavey, Eric, Conte, Roy, Donovan, Art. "Surface to Subsurface Correlation of Eagle Ford Equivalent Strata From West to South Texas". Paper presented at the SPE/AAPG/SEG Unconventional Resources Technology Conference, Austin, Texas, USA. 2017. DOI: 10.15530/urtec-2017-2716442.
- [63] Palacios, Virginia E. "Baseline groundwater quality testing needs in the Eagle Ford shale region". Master's project, Duke University. 2012. <https://hdl.handle.net/10161/5370>.
- [64] Geltman, Elizabeth and LeClair, Nichole. "Regulation of Radioactive Fracking Wastes". *Vermont Journal of Environmental Law*, vol. 19, 2018. Available at SSRN: <https://ssrn.com/abstract=3030255>
- [65] S.G. Landsberger, G. George. "An evaluation of 226 Ra and 228 Ra in drinking water in several counties in Texas, USA", *Journal of Environmental Radioactivity*, vol. 125. 2013. ISSN 0265-931X, <https://doi.org/10.1016/j.jenvrad.2013.02.016>
- [66] National Research Council. "Evaluation of Guidelines for Exposures to Technologically Enhanced Naturally Occurring Radioactive Materials". Washington, DC: The National Academies Press. 1999. <https://doi.org/10.17226/6360>.



## ISOLATION, MOLECULAR IDENTIFICATION AND ENZYME ACTIVITY OF AMYLASE PRODUCING THERMOPHILIC BACTERIA FROM HOT SPRINGS

Edy Fachrial<sup>1</sup>, Vincentia Ade Rizky\*<sup>2</sup>, Harmileni<sup>3</sup>, I Nyoman Ehrich Lister<sup>4</sup>, Chrismis Novalinda Ginting<sup>5</sup>, Titania T Nugroho<sup>6</sup> and Saryono<sup>7</sup>








<sup>1</sup> Laboratory of Molecular Biology, Faculty of Medicine, Universitas Prima Indonesia, Jl. Belanga No.1, Medan 20118, North Sumatera, Indonesia.

<sup>2</sup> Graduate Program of Biomedical Science, Faculty of Medicine, Universitas Prima Indonesia, Jl. Belanga No.1, Medan 20118, North Sumatera, Indonesia.

<sup>3</sup> Politeknik Teknologi Kimia Industri Medan, Jl. Medan Tenggara No.7, Medan 20228, North Sumatera, Indonesia.

<sup>4,5</sup> Faculty of Medicine, Universitas Prima Indonesia, Jl. Belanga No.1, Medan 20118, North Sumatera, Indonesia.

<sup>6,7</sup> Departement of Chemistry, Universitas Riau, Jl. Bina Widya Km 12,5, Simpang Baru, Pekanbaru 28293, Riau, Indonesia.

<sup>1</sup> <http://orcid.org/0000-0002-5237-5803> , <sup>2</sup> <http://orcid.org/0000-0002-2866-1236> , <sup>3</sup> <http://orcid.org/0000-0002-1872-8222> ,  
<sup>4</sup> <http://orcid.org/0000-0003-1325-5208> , <sup>5</sup> <http://orcid.org/0000-0003-2269-2717> , <sup>6</sup> <http://orcid.org/0000-0001-9825-7549> ,  
<sup>7</sup> <http://orcid.org/0000-0002-4246-7042> 

Email: fachrial\_edy@yahoo.co.id, \*vincentiarizky@gmail.com, harmieni16@gmail.com, yysunpri@gmail.com, ermigirsang@unprimdn.ac.id, titania.nugroho@lecturer.unri.ac.id, saryono@lecturer.unri.ac.id

### ARTICLE INFO

#### Article History

Received: August 16<sup>th</sup>, 2021

Accepted: August 26<sup>th</sup>, 2021

Published: August 31<sup>th</sup>, 2021

#### Keywords:

Amylase,  
Enzyme Activity,  
Hot Springs,  
Molecular Identification,  
Thermophilic.

### ABSTRACT

In this era, enzyme exploration in Indonesia continues to increase, and the amylase enzyme of about 30% of the total production is used worldwide. The great needs for amylase enzyme and its uses in several industrial and health fields lead to the search for potential natural resources in its production, including hot springs, which are very promising because of their thermophilic and thermostable properties. The aim of this study was to isolate, determine the activity and molecular identification of amylase-producing thermophilic bacteria from natural hot springs Dolok Tinggi Raja, Simalungun, North Sumatera. This study includes measurement of enzyme activity using the DNS method and molecular identification. The results were obtained from 20 isolated isolates, 6 isolates had amylase activity with the highest activity, namely the UTMTR VAR A10 isolate with an amylase enzyme activity of 0.2733 Unit/mL. Based on the molecular identification using 16SrRNA gene amplification based on the BLAST program and phylogenetic analysis with the MEGA X program, it was shown that the UTMTR VAR A10 isolate is a bacterium *Bacillus licheniformis* strain UTMTR VAR A10. Further research is needed to purify the enzyme in such a way that it can be applied to the industrial world.



Copyright ©2016 by authors and Galileo Institute of Technology and Education of the Amazon (ITEGAM). This work is licensed under the Creative Commons Attribution International License (CC BY 4.0).

### I. INTRODUCTION

In this era, research on enzyme producing microbes in Indonesia continues to increase. Enzyme are widely used in various fields, such as diagnostic techniques, biotechnology industry, textile and paper industry, sewage and waste treatment, as well as food industry [1]. The application of enzymes in the field of biotechnology places increasing demand for thermophilic

(active at high temperatures) and thermostable (stable at high temperatures) enzymes. Furthermore, this is due to high-temperature reactions, which can minimize the risk of contamination, increase mass transfer rates, and can shift the equilibrium towards product formation [2]. In addition, enzymes act as biocatalysts, namely accelerating the rate of chemical reactions without being involved in the reaction. Also, it convert substrate molecules into reaction (products), and its uses as



catalysts can reduce environmental pollution, which are non-toxic. The application of enzymes as catalysts is widely used in industry and health, one of which is the amylase enzyme [3].

The amylase enzyme is a type that can degrade starch, and its uses in the industrial sector is quite high, that is in the food, textile, paper, and detergent industries. Also, the use of amylase enzymes in the health sector such as pharmacy, medicine, and the environment. The amylase requirements used in the food and beverage industry are of great value, and it is one of the most important and widely used enzymes. Furthermore, this enzyme represents the second largest market group after proteases, and the amylase enzyme of about 30% of the total enzyme production is used in the world. The high need for amylase enzyme and its uses in several industrial and health fields lead to the search for potential natural resources in its production [4].

Enzymes derived from microorganisms, especially thermophilic microorganisms such as bacteria, are more demanding in the industry because they are stable at high temperatures, easy to produce in large quantities, can work on several substrates, have high reaction rates, do not require a bioreactor cooling system and the possibility of low contamination. Thermophilic bacteria can survive and thrive in high-temperature conditions because the content of enzymes, ribosomes, and proteins is more stable. The lipid membrane of thermophilic bacteria is also rich in saturated fatty acids and

therefore forms a much stronger hydrophobic bond than mesophilic bacteria [5].

The natural habitat of thermophilic bacteria is widespread throughout the earth's surface, especially in geothermal areas such as hot springs, volcanic craters, and volcanic areas. Indonesia is one of the most active tectonic areas in the world with more than 70 active volcanoes and numerous geothermal areas. However, hot springs are the easiest places to sample bacterial isolates. This study aims to explore microorganisms from geothermal habitats, namely hot springs that have the potential to produce thermostable amylase enzymes to be developed as thermophilic microorganisms for industrial and health purposes. This exploration is carried out at the Dolok Tinggi Raja Simalungun geothermal hot spring, North Sumatra, which is a hot spring that has not been widely used for this purpose [6].

## II. MATERIALS AND METHODS

### II.1 STUDY SITE

This research was conducted in the Molecular Biology Laboratory of the Faculty of Medicine, Universitas Prima Indonesia, Medan, Indonesia. The samples were obtained from Dolok Tinggi Raja hot spring, Silau Kahean district, Simalungun Regency. Furthermore, geographically, Dolok Tinggi Raja is located between 3° 13' 30" North latitude and 98° 30' 49" East Longitude (Figure 1).



Figure 1: Sampling Location of Dolok Tinggi Raja, Simalungun, North Sumatra, Indonesia.  
Source: Authors, (2020).

### II.2 SAMPLING PROCEDURE

Hot water sampling at the Dolok Tinggi Raja Natural Hot Springs was performed at a depth of approximately 1-2 meters. Water samples of about  $\pm 100$  mL was taken and the sediment of about  $\pm 10$  grams was obtained from several different points in which the temperature and pH of the sampling point were previously measured. Then a water sample is placed in a sterile Winkler bottle and the sediment is placed in a sterile bottle that has been prepared and labeled. Furthermore, the samples were stored in cold boxes to be taken to the laboratory for further analysis [7].

### II.3 MICROBIAL ISOLATION

Water samples of about 4 mL was taken from 3 different location and placed in a centrifuge tube then mixed until

homogeneous. Furthermore, 2 grams of sediment samples were taken from 4 locations and place in a petridish then mixed until homogeneous. The two samples prepared were then isolated on the enrichment media by taking 1 mL or 1 gram of the sample, and then poured into a test tube containing 9 mL of median nutrient broth and homogenized, incubate at a temperature of  $\pm 50^{\circ}\text{C}$  for 2x24 hours. The microbes isolated on the enrichment media are then inoculated on the nutrient agar media. The sample was diluted at a concentration of  $10^4$ , and inoculated with the spread plate method. A sample of 0.1 mL (100  $\mu\text{L}$ ) was taken using micropipettes, and placed on the surface of the Nutrient Agar medium, and was spread using a spreader. The procedure was performed aseptically, and incubate at a temperature of  $\pm 50^{\circ}\text{C}$  for 2x24 hours, and the isolates were ready for further testing [8], [9].



## II.4 AMYLASE ENZYME SCREENING

The microbial isolates were inoculated in Nutrient Agar media containing 1% starch, and incubated for 24-48 hours at a temperature of  $\pm 50^{\circ}\text{C}$ . Then, a drip of Lugol reagents [(w/ v) 1% iodine in 2% potassium iodide] was added on the surface of the media until it was distributed, and let it stand for  $\pm 1$  minute, then the remaining liquid on the surface of the media was discarded. The clear zones on the surface of the media was observed, and the presence of clear zones showed that microbes produced amylase [10].

## II.5 PREPARATION OF GLUCOSE STANDARD CALIBRATION CURVES

A standard glucose solutions was prepared using glucose solutions at various concentrations ranging from 50-300  $\mu\text{g}/\text{mL}$ . Furthermore, 1 mL of glucose solution was taken at each concentration and 1.5 mL of DNS solution was added, vortexed, then boiled for 5 minutes. The mixture was cooled under running water for 15 minutes and 20 mL of aquabidest was added, and vortexed. The mixture was then measured for its absorbance at a wavelength of 540 nm. Each absorbance result of each glucose solution with different concentrations was plotted on a regression line showing a linear relationship between absorbance and glucose level [11].

## II.6 MEASUREMENT OF ENZYME ACTIVITY

The amylase enzyme activity was tested using the DNS method, and the test was carried out using 1 mL of bacterial sample inoculated on 25 mL of production media (2.55 g/L rice flour; 8.4 g/L yeast extract; 8.1 g/L NaCl) at a temperature of  $\pm 50^{\circ}\text{C}$  for 48 hours. After incubation, the media is centrifuge at a speed of 10,000 rpm for 15 minutes. The results of the supernatant (crude enzymes) are used to determine the activity of the enzymes. Then a mixture of reactions containing 1 mL substrate (1% starch in 0.1 M buffer phosphate pH 7) and 1 mL crude enzyme (supernatant) was incubated at a temperature of  $50^{\circ}\text{C}$  for 10 minutes. Furthermore, 1 mL substrate was added 1% starch in a phosphate buffer of 0.1 M pH 7) in an empty tube and then incubated at a temperature of  $50^{\circ}\text{C}$  for 10 minutes. Each tube is filled by adding 2 mL of 3,5-dinitrosalicylic (DNS) acid reagents, then heated for 5 minutes, and cool under running water for 15 minutes, then 20 mL aquabidest was added. Each solution in the tube was tested for color intensity by absorbent at a wavelength of 540 nm using a Spectrophotometer UV-Vis. One unit of an enzyme (Unit/mL) is equivalent to the amount of enzyme required to release 1  $\mu\text{mol}$  reduced sugar per minute in test conditions [10], [11], [12]. To see the size of one unit of enzyme activity, the following formula was used: Formula Activity Enzyme.

$$AE = \frac{Mg \times 100}{BMg \times MI} \quad (1)$$

Information:

AE: Enzyme Activity (Unit/mL Enzyme Filtrate)

Mg: Miligrams of Glucose resulting from the Hydrolysis of starch (mg)

BMg: Mr Glucose = 180

MI: Incubation period = 10 minutes

## II.7 MORPHOLOGICAL AND BIOCHEMICAL CHARACTERIZATION

The components of the isolates were assigned to the macroscopic and microscopic morphological characteristics of the isolates and the biochemical components. For the macroscopic morphological characteristics, the colony shape, surface, color, margins, and edges were observed, while microscopic morphological characteristics were carried out with gram staining. The characteristics of the isolates were also determined biochemically by testing catalase, motility, gelatinase, TSIA, and Simon's citrate [13].

## II.8 MOLECULAR IDENTIFICATION

Bacterial isolates planted or isolated overnight are transferred to a 1.5 ml microtube, and a 1 mL TE buffer was introduced and become homogeneous, and centrifuges at a speed of 11,000 rcf for 15 minutes. Furthermore, lysozyme was poured into the tube and incubated for 30 minutes at a temperature of  $37^{\circ}\text{C}$ . After that, 125  $\mu\text{L}$  ammonium acetate 7.5 M was added in the tube and then homogenized and placed on ice for 10 minutes. Then 500  $\mu\text{L}$  chloroform was added to the tube and shaken firmly. The sample was crossed at 11,000 rcf for 10 minutes. The supernatant is taken and placed in a new tube, then isopropanol was added to the supernatant at ratio = 1/2:1. Also, the tubes were homogeneously reversed up and down several times, and centrifuge back at 18,000 rcf for 10 minutes. The supernatant was removed and 500  $\mu\text{L}$  ethanol 70% was added, and then centrifuged again at 18,000 rcf for 10 minutes. The supernatant was discarded and the pellets was dried. Furthermore, 50  $\mu\text{L}$  free water nuclease was added to the tube, and the solution was used as a DNA template for PCR. The PCR program used includes; pre-denaturation at  $95^{\circ}\text{C}$  for 90 seconds, followed by 30 cycles consisting of denaturation at  $95^{\circ}\text{C}$  for 30 seconds, annealing at  $55^{\circ}\text{C}$  for 30 seconds, extension at  $72^{\circ}\text{C}$  for 90 seconds, and a final extension at  $72^{\circ}\text{C}$  for 3 minutes [14]. The primers used were primer 27 F: 5'AGA GTT TGA TCC TGG CTC AG-3 and Primer 1492 R: 5' GGT TAC CTT GTT ACG ACT T-3.

## II.9 PHYLOGENETIC ANALYSIS

The sequencing results were trimmed and compiled using the BioEdit program (<http://www.mbio.ncsu.edu/BioEdit/bioedit.html>). The sequential data assembled is then registered in BLAST along with the genomic data registered at the NCBI/National Center for Biotechnology Information (<http://www.ncbi.nlm.nih.gov/BLAST>) to determine taxon or species with homology or a largest and closest molecular similarity. Then an alignment was carried out using the CLUSTAL W program and a phylogenetic tree was created using the MEGA X program [15].

## III. RESULTS AND DISCUSSIONS

### III.1 AMYLASE ENZYME SCREENING

Based on the results of the research that has been carried out, from 20 isolates taken from hot springs Dolok Tinggi Raja, 6 isolates were able to produce amylase enzymes (Table 1). This is evidenced by the formation of a clear zone around the colony on nutrient agar containing 1% starch (Figure 2).

Table 1: Amylase Enzyme Screening Results.

No	Isolates	Amylase Enzyme
1	UTMTR VAR A1	+
2	UTMTR VAR A2	-
3	UTMTR VAR A3	-
4	UTMTR VAR A4	+
5	UTMTR VAR A5	+
6	UTMTR VAR A6	-
7	UTMTR VAR A7	-
8	UTMTR VAR A8	-
9	UTMTR VAR A9	-
10	UTMTR VAR A10	+
11	UTMTR VAR S1	-
12	UTMTR VAR S2	-
13	UTMTR VAR S3	-
14	UTMTR VAR S4	-
15	UTMTR VAR S5	+
16	UTMTR VAR S6	-
17	UTMTR VAR S7	-
18	UTMTR VAR S8	-
19	UTMTR VAR S9	+
20	UTMTR VAR S10	-

Source: Authors, (2020).

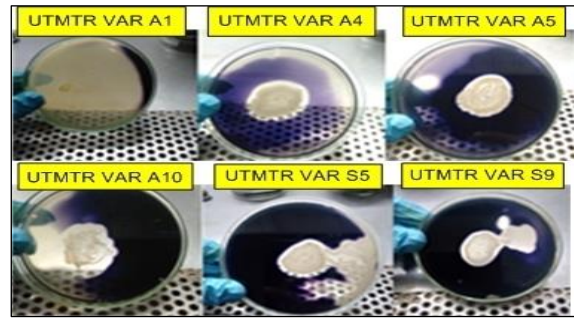


Figure 2: Isolates of UTMTR VAR A1, A4, A5, A10, S5 and S9 which can produce amylase enzymes are characterized by the formation of a clear zone around the colony.

Source: Authors, (2020).

In the amylase enzyme screening results, 6 isolates showed positive results with the formation of a clear zone on the addition of a lugol/iodine solution to starch [16].

### III.2 ENZYME ACTIVITY

The results of the isolation of thermophilic bacteria from hot springs Dolok Tinggi Raja were discovered to be 6 isolates that produced amylase enzyme. Furthermore, the 6 isolates were subjected to further test in order to determine the enzyme activity. The results of enzyme activity can be seen in Table 2.

Table 2: Enzyme Activity Results based on Growth Time (Incubation Time).

Isolate	Incubation Time (Hours)	Glucose Concentration (mg/mL)	Enzyme Activity Unit (Unit/mL)
UTMTR VAR A1	0 Hours	1.397	0.0776
	4 Hours	2.8667	0.1593
	8 Hours	4.2347	0.2353
UTMTR VAR A4	0 Hours	1.22055	0.0678
	4 Hours	2.150	0.1194
	8 Hours	2.7528	0.1529
UTMTR VAR A5	0 Hours	1.4706	0.0817
	4 Hours	2.7478	0.1527
	8 Hours	4.6782	0.2599
UTMTR VAR A10	0 Hours	1.2911	0.0717
	4 Hours	3.1359	0.1742
	8 Hours	4.9202	0.2733
UTMTR VAR S5	0 Hours	1.53105	0.0851
	4 Hours	1.8012	0.1001
	8 Hours	3.81835	0.2121
UTMTR VAR S9	0 Hours	1.71655	0.0954
	4 Hours	2.4988	0.1388
	8 Hours	3.67725	0.2043

Source: Authors, (2020).

In Table 2, it can be seen that these 6 bacterial isolates have different enzymatic activities. The activity of the amylase enzyme is determined based on the concentration of reducing sugars produced by hydrolysis of starch by the amylase enzyme in bacterial isolates. Based on the research on measuring enzyme activity as a function of growth time, it can be seen that the time for amylase enzyme production is increasing. This is in line with previous studies showing that the production time increased from 0 hours until the maximum production time was 36 hours [17]. Also, other studies stated that the incubation time for enzyme production in *Bacillus licheniformis* bacteria at 0, 4, and 8 hours also increased [18].

Based on the results of the amylase enzyme activity test, the graph shows that the highest amylase enzyme activity was shown by the UTMTR VAR A10 isolate (Figure 3). The activity of the UTMTR VAR A10 isolate at the 0 hour was 0.0717 Unit/mL, the 4 hour was 0.1742 Unit/mL and the 8 hour was 0.2733 Unit/mL. The influence of incubation time on production of enzymes is very important. This is because in the field of biotechnology time-saving is needed [19]. This result is in line with the results of previous studies, which state that *Bacillus sp.* RSII-1b begins to have an adaptation phase after 0 to 12 hours and the growth increases with increasing fermentation time. The amylase enzyme was secreted during the 15 hours resulting in an

enzyme activity of 0.0319 Unit/mL and increased at the 24 hours with the enzyme activity of 0.1323 Unit/mL. And the increase again resulted in the highest amylase enzyme activity of 0.0711 Units/mL at 33 hours [20]. Another study reported that the highest  $\alpha$ -amylase enzyme activity was at the 36 hours of 3832.08 U/mg. When the incubation time changed from 36 to 72 hours, the enzyme production activity decreased by 49.17%. The activity of this enzyme decreases as the growth of microbes in the medium increases, but the nutrients become less numerous, which in addition to the secondary metabolites leads to a nutrient deficiency of the bacteria [21].

The growth of cells and amylase products *Bacillus sp.* reported depends on the strain, media composition and concentration, cultivation method, cell growth, nutrient requirements, pH temperature, incubation time, and thermostability. The production of amylase is influenced by the composition and concentration of the media, because the media a source of carbon. Furthermore, carbon is needed during fermentation because it increases the carbon used in the flour of rice and starch as a stimulator for the production of the enzyme.

Starch and rice flour are slowly metabolized by bacteria as a source of complex carbohydrates and as an inductor for amylase secretion [22]. The enzyme activity decreases with increasing incubation time and after the maximum production time. This is because bacteria are no longer a source of carbon and therefore nutrients are reduced. Also, it is due to enzyme denaturation due to interactions with other compounds in the fermentation media [23].

According to Elmansy [22], the 72 hours observation was reported the optimal growth period for *Bacillus* strains and as the incubation time, which would result in more time for the number of colonies that cause the activity of the much weaker enzyme. The incubation period or the long growth period greatly reduced the  $\alpha$ -amylase due to exhaustion of nutrients that causes the death of the microorganism, and the collection of the product side contained in the media products such as toxins, inhibitors, and proteolytic  $\alpha$ -amylase by the enzyme protease, as well as the cells can reach the phase of decline and show the synthesis of amylase were reduced.

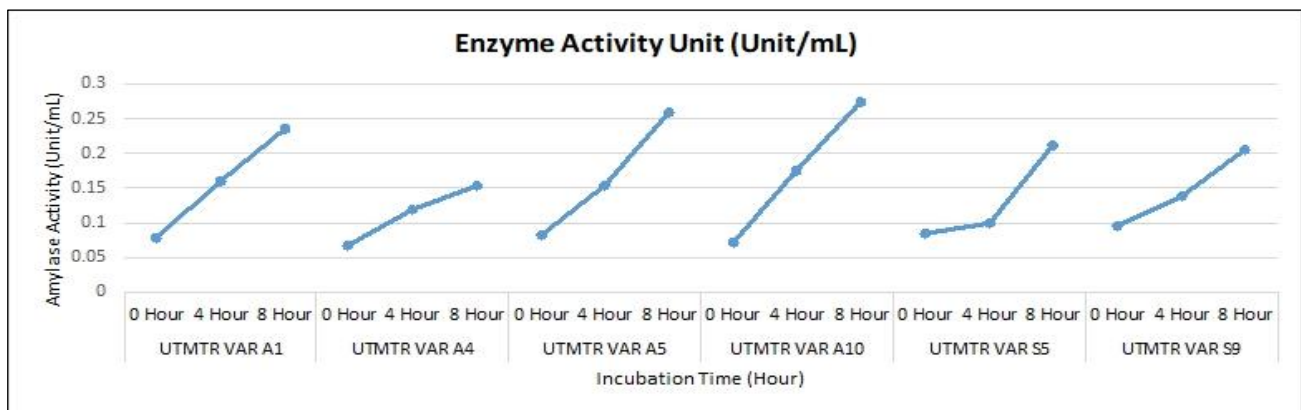


Figure 3: Amylase Enzyme Activity Test Results. Source: Authors, (2020).

### III.3 MORPHOLOGICAL AND BIOCHEMICAL CHARACTERIZATION

The selected isolates with the highest amylase enzyme activity were subjected to macroscopic, microscopic, and biochemical characterization tests. The results are shown in Table 3.

Table 3: Enzyme Activity Results based on Growth Time (Incubation Time).

Characteristics	Result
<b>Macroscopic</b>	
• Shape	Circular
• Edge	Undulate
• Elevation	Flat
• Color	Cream
<b>Microscopic</b>	
• Gram stain	Gram (-) Bacil (+)
<b>Biochemistry</b>	
• Catalase	+
• Motility	-
• Gelatin	-
• TSIA	K/A, H <sub>2</sub> S:-, Gas:-
• Simon's citrate	-

Source: Authors, (2020).

The morphological characteristics of the UTMTR VAR A10 isolate were carried out macroscopically and microscopically. The colonies were reported to be cream colored and circular by macroscopic observation. Meanwhile, microscopically, it was observed that the colony of UTMTR VAR A10 isolates were gram-negative rod-shaped bacteria (Figure 4.A). Also, identification was carried out by biochemical characteristics as shown in Table 3. The results of the catalase test on this isolate were positive (Figure 4.B), as indicated by the presence of gas bubbles in the bacterial colony reaction to which 3% H<sub>2</sub>O<sub>2</sub> reagent was added, the ability to convert H<sub>2</sub>O<sub>2</sub> which was to oxygen and water decomposes [17], with the exception of the results of negative mobility tests, gelatin and citrate (Figure 4.C). The TSIA test shows that the Slant is red because the formation of the basic compound shows that *Bacillus* does not ferment lactose, maltose, and sucrose. Meanwhile, the color of the TSIA media on the butt is yellow, which means that *Bacillus* can ferment glucose. According to Cappucino [24] *Bacillus* can ferment glucose as an energy source, besides that TSIA shows that these bacteria are not able to produce sulfur and gas. Based on the results of the macroscopic, microscopic, and biochemical characteristic tests obtained by comparing the results in the Bergey's Manual of Systematic Bacteriology, it can be concluded that the UTMTR VAR A10 isolate was identified as *Bacillus sp.* Bacteria of the genus *Bacillus sp.* are the most widely reported as thermostable enzyme-producing bacteria [25]. Furthermore,



molecular identification was carried out to determine the species of these bacterial isolates.

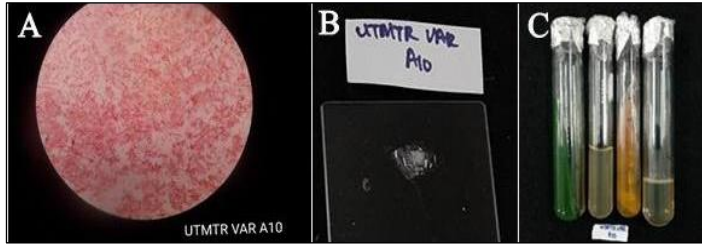


Figure 4: A. Microscopic isolate UTMTR VAR A10; B. Catalase Test Results; C. Biochemical Characteristics Test Results: 1) Simon's Citrate; 2) Gelatin; 3) Triple Sugar Iron Agar (TSIA); 4) Motility  
Source: Authors, (2020).

### III.4 MOLECULAR IDENTIFICATION

Isolates UTMTR VAR A10 which has the highest amylase enzyme activity in further identification using 16SrRNA gene sequence analysis with primer 27 F: 5' --AGA GTT TGA TCC TGG CTC AG – 3' and Primer 1492 R: 5' – GGT TAC CTT GTT ACG ACT T – 3'. The results of the 16SrRNA sequencing analysis obtained were compared with the gene sequences in GenBank using BLAST search (Basic Local Alignment Search Tool) on NCBI. The 16SrRNA gene sequence alignment database showed that the UTMTR VAR A10 isolate had the highest 99.78% similarity to *Bacillus licheniformis* strain MPF 22 [26].



Figure 5: UTMTR VAR A10 Phylogenetic Chart / Tree with 7 related *Bacillus* species based on the 16SrRNA gene  
Source: Authors, (2020).

### IV. CONCLUSIONS

Based on the research results, it can be concluded this is the first report on the isolation of amylase-producing thermophilic bacteria from Hot Springs Dolok Tinggi Raja, Simalungun, North Sumatra. Molecular identification based on 16SrRNA gene amplification and sequencing stated that the UTMTR VAR A10 isolate was a bacterium *Bacillus licheniformis* strain UTMTR VAR A10. This thermophilic bacterium showed the amylase enzyme activity at the 8 hours of 0.2733 Unit/mL. Further research is needed to purify the enzyme so that it can be applied in the industrial world.

### V. AUTHOR'S CONTRIBUTION

**Conceptualization:** Saryono, Titania T Nugroho and Edy Fachrial.

**Methodology:** Edy Fahrial, Saryono, and Harmileni.

**Investigation:** I Nyoman Ehrich Lister and Chrismis Novalinda Ginting.

**Discussion of results:** Edy Fachrial, Harmileni, and Vincentia Ade Rizky.

### III.5 PHYLOGENETIC ANALYSIS

Based on the phylogenetic tree, the bacteria *Bacillus sp* isolates UTMTR VAR A10 has the closest homology/similarity to the *Bacillus licheniformis* strain MPF22 (Figure 5). These results are based on the alignment of the base pairs to determine the phylogenetic relationships between the sequences. The phylogenetic of this bacterial isolate used the neighbor-joining tree method with bootstrap analysis of 1000 replications to test the phylogenetic tree branches. The higher the bootstrap repetition used, the better and more accurate the phylogenetic tree [17]. Therefore, based on the results obtained, it can be determined that the UTMTR VAR A10 isolate is a *Bacillus licheniformis* bacterium designated as strain UTMTR VAR A10.

The bacterium *Bacillus licheniformis* produces an amylase enzyme, a thermostable enzyme that is widely used in biotechnology. Amylase is an enzyme that can hydrolyze the starch. The enzyme can hydrolyze starch molecules to produce products that varies such as maltose, dextrin, and especially the molecules of glucose as the smallest unit. Furthermore, amylase is one of the enzymes widely used in industry, biotechnology, and health. The use of the amylase enzyme in the industrial sector is quite high, in the food industry (Food and Beverage), textiles, paper and detergents. Also, the use of amylase enzyme in the health sector such as pharmacy, medicine, and the environment is high [4].

**Writing – Original Draft:** Edy Fachrial and Vincentia Ade Rizky.

**Writing – Review and Editing:** Harmileni and Vincentia Ade Rizky.

**Resources:** Chrismis Novalinda Ginting and Edy Fachrial.

**Supervision:** Saryono and I Nyoman Ehrich Lister.

**Approval of the final text:** Saryono and Titania T Nugroho.

### VI. ACKNOWLEDGMENTS

This study was supported by the Republic of Indonesian Ministry of Research and Technology/National Research and Innovation Agency through Collegiate Research Collaboration Grant between Universitas Prima Indonesia and Universitas Riau, Indonesia with contract number: 222/LL1/PG/2020.

### VII. REFERENCES

[1] R. Singh, M. Kumar, A. Mittal, and P. K. Mehta, "Microbial enzymes: industrial progress in 21st century," 3 Biotech, vol. 6, no. 2, pp. 1–15, 2016, doi: 10.1007/s13205-016-0485-8.



- [2] L. D. Unsworth, J. van der Oost, and S. Koutsopoulos, "Hyperthermophilic enzymes – stability, activity and implementation strategies for high temperature applications," {FEBS} J., vol. 274, no. 16, pp. 4044–4056, Aug. 2007, doi: 10.1111/j.1742-4658.2007.05954.x.
- [3] J. Boyle, *Lehninger principles of biochemistry* (4th ed.): Nelson, D., and Cox, M., vol. 33, no. 1. Wiley, 2005.
- [4] A. Z. Putri and T. Nakagawa, "Microbial  $\alpha$ -Amylases in the Industrial Extremozymes," Rev. Agric. Sci., vol. 8, no. 0, pp. 158–169, 2020, doi: 10.7831/ras.8.0\_158.
- [5] S. Barik, "Evolution of Protein Structure and Stability in Global Warming," Int. J. Mol. Sci., vol. 21, no. 24, p. 9662, Dec. 2020, doi: 10.3390/ijms21249662.
- [6] K. Amjad, "Isolation and characterization of three thermophilic bacterial strains (lipase, cellulose and amylase producers) from hot springs in Saudi Arabia," African J. Biotechnol., vol. 10, no. 44, pp. 8834–8839, Aug. 2011, doi: 10.5897/ajb10.1907.
- [7] E. Fachrial, V. Krisdianilo, Harmileni, I. N. E. Lister, T. T. Nugroho, and Saryono, "Isolation, characterization, activity test and molecular identification of thermophilic bacteria producing proteases from Dolok Tinggi Raja Natural Hot Springs, North Sumatra, Indonesia," *Biodiversitas*, vol. 22, no. 4, pp. 1725–1732, 2021, doi: 10.13057/biodiv/d220416.
- [8] P. Yadav, S. Korpole, G. S. Prasad, G. Sahni, J. Maharjan, and L. Sreerama, "Morphological, enzymatic screening, and phylogenetic analysis of thermophilic bacilli isolated from five hot springs of Myagdi, Nepal," J. Appl. Biol. Biotechnol., vol. 6, no. 3, pp. 1–8, 2018, doi: 10.7324/jabb.2018.60301.
- [9] S. Simandjuntak and M. Y. Samuel, "Isolation and identification of thermophilic bacteria, producer of amylase enzyme, from Lake Linow, North Sulawesi," J. Pure Appl. Microbiol., vol. 12, no. 2, pp. 543–554, 2018, doi: 10.22207/JPaM.12.2.13.
- [10] S. Kiran, A. Singh, C. Prabha, S. Kumari, and S. Kumari, "Isolation and Characterization of Thermostable Amylase Producing Bacteria from Hot Springs of Bihar, India," Int. J. Pharma Med. Biol. Sci., vol. 7, no. 2, pp. 28–34, Apr. 2018, doi: 10.18178/ijpms.7.2.28-34.
- [11] G. L. Miller, "Use of Dinitrosalicylic Acid Reagent for Determination of Reducing Sugar," Anal. Chem., vol. 31, no. 3, pp. 426–428, Mar. 1959, doi: 10.1021/ac60147a030.
- [12] S. S. Kumar, R. Sangeeta, S. Soumya, R. P. Ranjan, B. Bidyut, and D. M. P. Kumar, "Characterizing novel thermophilic amylase producing bacteria from Taptapani hot spring, Odisha, India," Jundishapur J. Microbiol., vol. 7, no. 12, pp. 1–7, 2014, doi: 10.5812/jjm.11800.
- [13] F. M. Gazali and I. N. Suwastika, "Thermostable  $\alpha$ -Amylase Activity from Thermophilic Bacteria Isolated from Bora Hot Spring, Central Sulawesi," J. Phys. Conf. Ser., vol. 979, p. 12001, Mar. 2018, doi: 10.1088/1742-6596/979/1/012001.
- [14] E. Fachrial, S. Anggraini, Harmileni, T. T. Nugroho, and Saryono, "Isolation and molecular identification of carbohydrase and protease producing *Bacillus subtilis* {JCM} 1465 isolated from Penen Hot Springs in North Sumatra, Indonesia," *Biodiversitas J. Biol. Divers.*, vol. 20, no. 12, Nov. 2019, doi: 10.13057/biodiv/d201205.
- [15] K. Pranay, S. R. Padmadeo, V. Jha, and B. Prasad, "Screening and identification of amylase producing strains of *bacillus*," J. Appl. Biol. Biotechnol., vol. 7, no. 4, pp. 57–62, 2019, doi: 10.7324/JABB.2019.70409.
- [16] D. Sukmawati, Z. Arman, G. A. Sondana, N. N. Fikriyah, R. Hasanah, Z.N. Afifah, M. Balqis, H. E. Enshasy, S. N. A. Husna, S. Rahayu, T. H. Kurniati, and R. Puspitaningrum, "Potential amylase-producing yeast isolated from indigenous fermented beverages originating from Bali, Indonesia," J. Phys. Conf. Ser., vol. 1402, p. 55021, Dec. 2019, doi: 10.1088/1742-6596/1402/5/055021.
- [17] A. Ardhi, A. N. Sidauruk, N. Suraya, N. W. Pratiwi, U. Pato, and Saryono, "Molecular identification of amylase-producing thermophilic bacteria isolated from Bukit Gadang Hot Spring, West Sumatra, Indonesia," *Biodiversitas J. Biol. Divers.*, vol. 21, no. 3, Feb. 2020, doi: 10.13057/biodiv/d210319.
- [18] Y. Li, H. Wang, L. Zhang, Z. Ding, S. Xu, Z. Gu, and G. Shi, "Efficient Genome Editing in *Bacillus licheniformis* Mediated by a Conditional {CRISPR}/Cas9 System," *Microorganisms*, vol. 8, no. 5, p. 754, May 2020, doi: 10.3390/microorganisms8050754.
- [19] S. Özdemir, F. Matpan, K. Güven, and Z. Baysal, "Production and Characterization of Partially Purified Extracellular Thermostable  $\alpha$ -Amylase By *Bacillus subtilis* in Submerged Fermentation (SmF)," Prep. Biochem. Biotechnol., vol. 41, no. 4, pp. 365–381, Oct. 2011, doi: 10.1080/10826068.2011.552142.
- [20] R. A. Arfah, A. Ahmad, M. N. Djide, M. Anis, and M. Zakir, "Production Optimization and Characterization of Amylase Enzyme Isolated from Thermophilic Bacteria *Bacillus sp* RSAIL-1b from Lejja Hot Spring South Sulawesi," Am. J. Biomed. Life Sci., vol. 3, no. 6, p. 115, 2015, doi: 10.11648/j.ajbls.20150306.13.
- [21] S. A. Fincan, S. Ozdemir, A. Karakaya, B. Enez, S. D. Mustafov, M. S. Ulutas, and F. Sen, "Purification and characterization of thermostable  $\alpha$ -amylase produced from *Bacillus licheniformis* So-B3 and its potential in hydrolyzing raw starch," Life Sci., vol. 264, p. 118639, Jan. 2021, doi: 10.1016/j.lfs.2020.118639.
- [22] E. A. Elmansy, M. S. Asker, E. M. El-Kady, S. M. Hassanein, and F. M. El-Beih, "Production and optimization of  $\alpha$ -amylase from thermo-halophilic bacteria isolated from different local marine environments," Bull. Natl. Res. Cent., vol. 42, no. 1, Dec. 2018, doi: 10.1186/s42269-018-0033-2.
- [23] Henshaw and S. M. Wakil, "Effect of Agitation Speed and Incubation Time on Amylase Production by *Bacillus* Species Isolated from Malted and Fermented Maize (*Zea mays*)," Microbiol. Res. J. Int., pp. 1–7, Apr. 2019, doi: 10.9734/mrji/2019/v27i330097.
- [24] J. G. Cappucino, "Microbiologi : A Laboratory Manual", Reading, Mass Addison Wesley Publishing, 1983
- [25] B. T. Mohammad, H. I. Al Daghistani, A. Jaouani, S. Abdel-Latif, and C. Kennes, "Isolation and Characterization of Thermophilic Bacteria from Jordanian Hot Springs: *Bacillus licheniformis* and *Thermomonas hydrothermalis* Isolates as Potential Producers of Thermostable Enzymes," Int. J. Microbiol., vol. 2017, pp. 1–12, 2017, doi: 10.1155/2017/6943952.
- [26] S. Alrumman, Y. S. M. Mostafa, S. Al-Qahtani, and T. H. T. Taha, "Hydrolytic Enzyme Production by Thermophilic Bacteria Isolated from Saudi Hot Springs," Open Life Sci., vol. 13, no. 1, pp. 470–480, 2018, doi: 10.1515/biol-2018-0056.



ISSN ONLINE: 2447-0228



## CATCHMENT SCALE ASSESSMENT OF POLLUTION THREATS TO WATER QUALITY IN RELATION TO PREVALENCE OF WATER-BORNE DISEASES IN SOME COMMUNITIES IN OMU-ARAN, NIGERIA

Omotoso Toyin\*<sup>1</sup> and O. Ibitoye<sup>2</sup>

<sup>1</sup> Civil Engineering Department, Ekiti State University, Ado-Ekiti, Nigeria.

<sup>2</sup> Department of Civil Engineering, College of Engineering, Landmark University Omu-Aran, Nigeria.

<sup>1</sup> <http://orcid.org/0000-0002-5305-6978> , <sup>2</sup> <http://orcid.org/0000-0001-7206-3172> 

Email: \*toyintoso@yahoo.com, ibitoye.olanrewaju@lmu.edu.ng

### ARTICLE INFO

#### Article History

Received: June 25<sup>th</sup>, 2021

Accepted: August 25<sup>th</sup>, 2021

Published: August 31<sup>th</sup>, 2021

#### Keywords:

Water quality,  
Prevalence of waterborne diseases,  
Contamination risk,  
Hygiene practices.

### ABSTRACT

Water quality assessment, especially in relation to prevalent waterborne diseases is necessary to ensure that clean and safe drinking water is delivered and sustained to reduce water-borne disease and other public health issues that are associated with the use of unsafe water. Little has been documented about the relationship between water quality and prevalence of waterborne diseases in Omu-Aran, Nigeria. In this wise, eighteen (18) water samples were collected from the available drinking water sources in the three densely populated communities in the study area, Ifaja, Ihaiye and Aran. The microbiological analysis of the water samples was performed by the determination of total coliform, according to the modified methods while the physicochemical parameters were determined by Standard Methods (APHA, 2005). Questionnaires were administered to 100 respondents in the selected communities to elicit information on water sourcing, collection, storage, treatment and prevalence of waterborne diseases treatment. Eighteen (18) water quality parameters cutting across physico-chemical and biological traits were investigated. All parameters were found to be within the WHO limit except microbial parameter (coliform count). The contamination risk from the household activity assessment were found to be severe for water source and water storage while it is moderate for water collection and water treatment and hygiene practices. The prevalence of common waterborne diseases are 9%, 35% and 56% for cholera, typhoid and Diarrhea respectively. The correlation coefficient between microbial parameter and prevalence waterborne diseases are 0.02, -0.5 and 0.86 for cholera, typhoid and cholera respectively. This is indicative of the water quality potential to be inherently laddened with waterborne diseases.



Copyright ©2016 by authors and Galileo Institute of Technology and Education of the Amazon (ITEGAM). This work is licensed under the Creative Commons Attribution International License (CC BY 4.0).

### I. INTRODUCTION

Perhaps, the most significant environmental problem and threat to public health in developing countries today is inadequate access to clean water and poor sanitation practices. More than 2.6 billion people across the globe were reported [1] to lack access to improved sanitation facilities consequent upon traditional poverty, economic poverty, and degradation of the water sources. In the developing countries, prevalent diseases are water-related, ranging from skin infections to organs damage. According to [2-3], the

shortage or even lack of water affects more than 40 % of the world population due to political, economic and climatological reasons. Despite the millennium development goal (MDG) plans of United Nations (UN) on quality water supply, [4] indicates that more than 25 % of the population still suffers from water-related health problems especially in the developing countries of Africa, Asia and Latin America with attendant loss in productivity. The total global water available for consumption was estimated to be only 0.7% of

the worldwide water resources of which 97.5% is salt water and 2.5% is fresh water according to a release by [5].

The quality and “net availability” of water is reported to be predicated on anthropogenic “pressure” occasioned by industrialization, urbanization and demographic growth [6]. The United Nations’ World Water Development Report [7] details the pressures that impair the water body’s capacity against self-cleansing, ecological integrity, sustenance and other beneficial uses. The beneficial uses of water in a river reach are defined by [8] to include municipal or domestic supply, propagation of aquatic and wildlife, irrigation, watering of livestock, and recreation activities. The effects of these pressures in sub-Saharan African countries have resulted in “economic water scarcity” which in the context of water resources studies is a result of poor management of the available water resources and lack of coordinated efforts to integrate riparian management into aquatic ecology preservation. Slash and burn agricultural procedures coupled with deforestation underscore the traditional poverty being experienced. The consequent erosion effects produced heavily silted and turbid rivers that are inherently laddened with disease vectors. There are also the associated problems of increased salinity and nutrient enrichment in the water bodies which are known factors for the growth and propagation of eutrophication. Eutrophication is another pathway of measuring the health of surface water body. [9-10] explained that eutrophication is a symptom that an aquatic ecosystem has exceeded its assimilative capacity of nutrients from anthropogenic inputs. There is equally a burden of “economic” water scarcity which can be measured by examining the physical existence of water in nature and by laboratory analysis of the biochemical

composition as fit for sustaining both aquatic and terrestrial lives. Once this objective cannot be met in space and time, the situation can be classified as experiencing scarcity. The scarcity pressure requires an objective analysis of historic and future scenarios of the water quality, availability and water management practices to sustain life. Hence, the submission of [11] on the assessment of future needs and water crisis issues as things of great concern. The implications of the above thoughts were strengthened by strategic desires in most developed and developing countries to develop a Water Framework with the basic goal to achieve “good status” of both surface and ground waters with a strong focus on the ecological criteria and by strategic integrated management. This involves management and research activities that clearly focus on integrated water resources management and the development of harmonised tools to support it. The European Union determined its long-term policy of water resource management within the river basins in Europe by a fundamental document “European Water Framework Directive 2000/60/EC, 2000” (WFD) with the basic principle encompassing harmonization of legal regulations, institutional organization regarding water and environmental protection, provision of finances etc., to concrete plans regarding preventive measures, water resources and ecosystem rehabilitation and realization of water use projects in accordance with sustainable development principles. This Framework has since be the target of many countries, which they replicate in part or in whole, through establishing water agencies at various administrative levels. This is equally in use to promote and enforce water quality policies and by extension to protect public health which has direct consequences on economic security.

**Table 1: Pollution sources and pollution stressors.**

Section	Affected Environment	Water Quality	Facility Sitting	Protect Species	Effluent Disposal
i	Climate	✓	✓	✓	✓
ii	Soil, relief and gradient	✓	✓		✓
iii	Water Resources	✓	✓	✓	✓
iv	Water Quality	✓	✓	✓	✓
v	Ecological Habitat	✓	✓	✓	✓
vi	Urbanisation	✓	✓	✓	✓
vii	Recreation	✓	✓		✓
viii	Land-use and Planning	✓	✓	✓	✓

Source: Authors, (2021).

## II. THEORETICAL REFERENCE

### II.1 GLOBAL CHALLENGES

Major noted source of pollution in water bodies is the indiscriminate discharge of municipal wastes and industrial effluents into the environment. Over recent decades, [12] observed that stricter environmental regulations and drastically reduced sewage discharge into river systems have led to significant improvements in water quality of some studied UK rivers and lakes. However, there are still some river sites, such as the Lauffen weir of the River Neckar in Germany, as noted by [13] that is well-known for high level of contamination with specific pollutants such as cadmium. The Mississippi river in the United States is considered genuinely the most polluted river as it lacks the diluting action [14].

The United Kingdom Department of Environment Food and Rural Affairs [15] remarked that the implementation of the

European Union Water Framework Directive (WFD) (2000/60/EC) has given added impetus to efforts requiring catchment scale assessment of threats to ecology and water quality, and the formal development of management strategies (River Basin Plans) to address pollution. [16] noted that the US geological survey (USGS) began using an innovative, continuous estimate of real-time nutrient and bacteria concentrations to establish and monitor total maximum daily load (TMDL) in their waterways as mandated by the Clean Water Act of 1972 [17] said quantifying sources of pollution is becoming increasingly important when characterising river catchments in their entirety as a prerequisite for environmental management.

Cost assessment of environmental management and river water quality issue has been kept throughout in a context of environment health and disease burden especially on the developing countries of the world [18]. There is a need to expand the horizon to cover productivity and economic effects on society

as depicted in the Conceptual loop on Environmental, health and economic security in Figure 1.

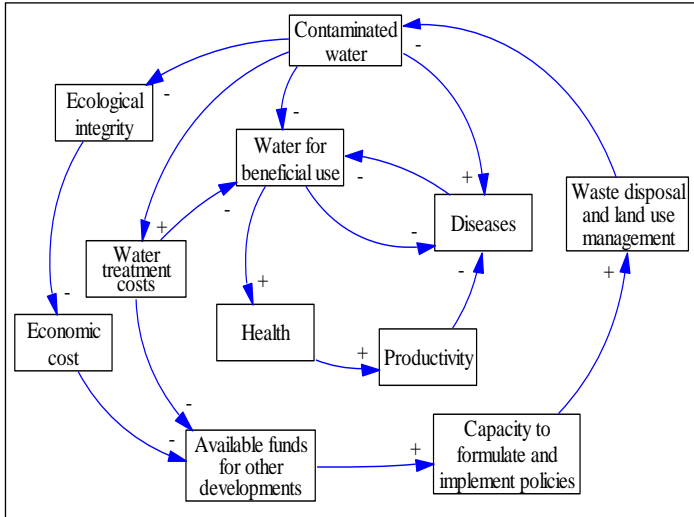


Figure 1: Causal loop on Environmental health and Economic security (The concept of adaptive system dynamics depicting impact of waste disposal and land management on health and economic security.

Source: [18].

This concept reflects the interaction between catchment environment and the cost of quality water within the context of policy issues. Therefore, it is being proposed here that the problem of water quality should be outlined in the context of socio-economic development and possibly should equally be quantified on the basis of an economic index.

### III.2 LOCAL CONSIDERATION AND MOTIVATION FOR STUDY

There are issues with availability and accessibility water of satisfactory quality to meet human and environmental needs in Irepodun Local Government [19-20]. Households are often compelled to travel long distances to collect water to be stored in vessels or containers for use. Since the water is mostly stored in plastic drums, metal tanks and barrels over long periods, it is susceptible to contamination by harmful bacteria and hazardous chemicals due to poor water handling practices, poor sanitation and poor waste management practices with the attendant effect of water-borne diseases such as dysentery, cholera, typhoid etc., when consumed. According to [21], the water in Omu-Aran is prone to pollution from unhygienic disposition of wastes on land and into water bodies. The streams were reported to be highly contaminated with heavy metals such as Cd, Mn and Fe [22] (Abdus-Salam et al., 2016). The high prevalence of cases of water borne diseases, most especially cholera outbreak, within the corridor of study is alarming. In 2001, cholera epidemic claimed not less than 40 lives and many others were hospitalized [23]. In June 2017, another reported episode had 12 deaths recorded in less than 5 days [24]. It is in view of these factors that this study seeks to assess the quality water in relation to prevalence waterborne diseases in Omu-Aran and its environs. The study seeks to help in devising a policy framework that is beneficial to water resources stake holders in protecting usable sources of water from degradation by anthropogenic activities with the following considerations:

- assessment of the microbial and physio-chemical parameters in household drinking water sources.

- determination of the prevalence of common waterborne diseases in the study area.
- assessment of the relationship between the water quality and the prevalence waterborne diseases in the study area.

## III. MATERIALS AND METHODS

### III.1 THE STUDY AREA

This study was conducted in Omu-Aran, a metropolitan town with the third largest population, approximately 150,000 [25] in Kwara State, Nigeria. It is surrounded by some rural communities like Oko, Ipetu, Rore, Aran-Orin and Ilofa. The town lies between 8° 8' 0" North, 5° 6' 0" East of prime meridian [21]. The mean annual rainfall and temperature in area ranges from 1234.9mm-1468.5mm and 32.3 - 36.4 oC respectively, while the annual mean relative humidity ranges from 47.6-52.4 [26] (Sojobi et al., 2015). The major economic activities include farming, petty trading and small-scale businesses.

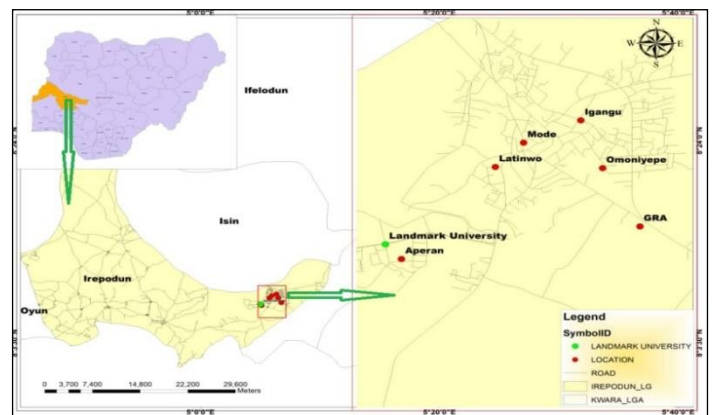


Figure 2: Map of the study area.

Source: Authors, (2021).

Six (6) communities, Latinwo, Mode, Igangu, GRA, Aperan and Omoniyepe in Omu-Aran were selected for the scheme. A multi-stage sampling technique including the administration of questionnaires was used to obtain samples and information in the study area. The six study areas were grouped into three (3) due to their vulnerability in terms of water availability and accessibility. The sample size was calculated using equation (1) on the assumption that no work on water quality assessment in relation to prevalence waterborne diseases in the study area has ever been done

- Proportion with good knowledge, attitude and practice of water quality assessment = 85%
- Precision limit = 10%
- 95% level of significance.

$$N = \frac{Z^2}{\Delta^2} pq \quad (1)$$

where

N = Sample size;

Z = Confidence interval at 95% which is 1.96;

p = Proportion with good knowledge, attitude and practice of water quality assessment = 27.7%;

q = 1-p = 1-0.277 = 72.3%;

Δ = precision limit = 10%.

Therefore,



$$N = \frac{1.96^2}{0.1^2} \times 0.277 \times 0.723 = 77 \quad (2)$$

Sample size calculated for household was 77. For convenience, a total of 100 people from different household were interviewed and 25 water samples were taken from household water source.

**III.1.1 Methods of Assessment**

**Pre-testing of questionnaire, inclusion and exclusion criteria**

The questionnaires were verified for accuracies and comprehensiveness before administration. To minimize errors, pre-testing of the data collection tools was done on 10% of the sample size in a nearby community. Revision of the questionnaires was done based on the results of the pilot study. The findings of the pre-test were used to improve the validity of the data collection tools and the reliability of the research findings. The inclusion criteria were households that formed part of the random sample within the six (6) selected communities in the study area. These are the people that were available at the time of sampling. The exclusion criteria were households with individuals who for some reasons would not be available during the questionnaire administration.

**Laboratory analyses**

Sample analysis was carried out in duplicates and the data presented as means. Turbidity, pH, electrical conductivity (EC), total dissolved solids (TDS) and temperature were tested in-situ for physical parameters, while chemical parameters included nitrate, arsenic, fluoride, iron and manganese. Bacteriological samples (E. coli and thermotolerant coliform, TTC) analysis were transported on ice pack in an ice chest to the laboratory within 6 hours of

collection and stored in a refrigerator at 4 °C prior to analysis. The assessment of the levels of microbial contaminants in the sample was by membrane filtration (MF) technique. This technique gives an immediate tally of thermotolerant and total coliforms that may be present in given water sample. A measured volume of water is filtered through a membrane filter comprising a cellulose compound with a uniform pore size of 0.45µm or 0.2µm in diameter. After the filtration procedure, bacteria are retained on the surface of the membrane filter. The membrane filter was placed in a Petri-dish containing a selective differential culture medium and incubated at a suitable temperature. Characteristic colonies indicating thermotolerant coliforms develop and are directly tallied.

An Erlenmeyer flask with side-arm was connected to a vacuum source and the porous support placed in position. The filtration unit was assembled by placing a sterile membrane filter on the porous support, using forceps sterilized by flaming and the upper container positioned to secure it. 10 mL of water sample was poured into the upper container and filtered by applying the vacuum. After filtration the membrane filter was placed in the Petri dish containing Chromogenic coliform agar with the grid side up using the sterile forceps and making sure that no air bubbles were trapped between the pad and the filter. The Petri dish was left at room temperature ranging between 35 and 37 °C for 2–4 hours, for resuscitation of stressed microbes. It was then transferred into an incubator at 44 ± 0.5 °C for 24 hours with 100% humidity for thermotolerant coliforms [27]. The colonies of thermotolerant coliform bacteria were identified from their characteristics on the medium used. The number of thermotolerant coliforms per 100 ml was given by: Thermotolerant coliforms per 100 mL = No. of thermotolerant coliform counted x 100 Vol in (mL) of sample filtered.

Table 2: Physical analysis of water samples.

Parameter	Iharye		Ifaja		Aran		WHO
	Igangu	GRA	Mode	Latinwo	Aperan	Omoniyepe	
Turbidity	2.3±0.6	1.3±0.0	2.0±0.0	1.3±0.0	0.0±0.0	0.0±0.0	5.0
Conductivity	630±5	70.3±0.3	469.3±0.6	96.4±0.1	130.9±0.1	498.0±0.0	1000
TDS	313±2.6	35.4±0.2	234.3±0.6	123.7±0.3	65.5±0.1	249.0±0.0	500
Ph	6.5±0.0	6.7±0.0	6.1±0.0	6.5±0.0	7.2±0.0	6.1±0.0	6.5-8.5

Source: Authors, (2021).

Table 3: Chemical analysis of some water samples collected from the sampling points.

Parameter	Ihaiye		Ifaja		Aran		WHO
	Igangu	GRA	Mode	Latinwo	Aperan	Omoniyepe	
T. Hardness	91.0±1.0	64.3±0.6	60.0±0.0	60.3±0.6	77.7±0.6	84.0±.0	150
Magnesium	47.7±2.3	20.3±0.6	41.3±0.6	16.0±0.0	27.3±0.6	77.7±0.6	75
Sulphate	13.3±1.5	7.7±0.6	7.0±0.0	16.0±0.0	6.0±0.0	8.0±0.0	100
Nitrate	10.3±0.6	5.0±1.0	6.0±0.0	11.7±0.6	4.7±0.6	10.0±0.0	50
Chloride	41.7±2.9	4.9±0.1	32.0±0.0	1.2±0.1	5.3±0.1	36±0.0	250
Phosphate	2.8±0.1	2.3±0.1	1.5±0.1	4.1±0.0	1.3±0.1	2.0±0.1	250
COD	72.0±2.6	120.0±1.0	110.0±0.0	170.0±0.0	80.0±0.0	75.0±0.0	1000
BOD	26.0±3.6	39.7±1.5	33.0±0.0	55.0±5.0	23.0±0.0	25.0±0.0	0
Calcium	16.3±0.6	27±0.0	18.3±0.6	24.3±0.6	31.3±0.6	35.0±0.0	250
E. Coli	62.3±1.2	34.7±8.5	38.3±7.6	34.0±4.0	10.3±4.5	34.0±4.0	0

Source: Authors, (2021).

Table 4: Compliant of some Water quality sampling data for the study area.

SN	Quality Variable	Total Samples	WHO guideline value	%Compliant
1	Bacteriologic Pipe-borne	200	<1 cfu/100ml	83
2	Coliform count in lined well	150	<1 cfu/100ml	30
3	Commercial water tankers	100	<1 cfu/100ml	52
3	Arsenic	550	0.01mg/L	60
4	Nitrate as NO <sub>3</sub>	550	50mg/L	62
5	Fluoride	550	1.5mg/L	85
6	Iron	550	0.3mg/L	82
7	Turbidity	550	<5NTU	45
8	pH	550	6.5-8.5	72
9	Electrical Conductivity	550	1400µS/cm	55

Source: Authors, (2021).

#### IV. RESULTS AND DISCUSSIONS

A total of 100 respondents participated in the survey pertaining to water quality, sanitation and hygiene. The corresponding responses are Ihaye (39%), Ifaja (31%) and Aran (30%). Majority of the local community rely on two major water sources (boreholes and hand dug wells) with percentage reliance on bore-hole, 45.1%; hand-dug wells, 43.1% public water supply, 9.8%; rain harvesting and streams, 2.0 %. The general practice involves water collection and storage in all manner of containers in a bit to gain ready access and forestall scarcity. This is done with little or no preference for treatment prior to consumption. In general, 1.2 % of borehole users report that they have experienced one or more water related illness within the last three years, 34.1 % of respondents who make use of shallow wells and 30% of use public water supply reported related illness. However, none of the respondents with reported use of rain water had related illness.

In the survey result, (Table 3) the general compliance with the WHO standard was lowest for turbidity with an average value of 45%, and a value of 30.0 % for thermo-tolerant coliforms in lined wells in the survey of conventional water supply options (pipe-borne water, borehole, hand-dug lined well, vehicle tanker) that were examined.

#### V. AUTHOR'S CONTRIBUTION

**Conceptualization:** Omotoso Toyin.

**Methodology:** Omotoso Toyin.

**Investigation:** Omotoso Toyin and O Ibitoye.

**Discussion of results:** Omotoso Toyin.

**Writing – Original Draft:** Omotoso Toyin and O Ibitoye.

**Writing – Review and Editing:** Omotoso Toyin and O Ibitoye.

**Resources:** Omotoso Toyin and O Ibitoye.

**Supervision:** Omotoso Toyin.

**Approval of the final text:** Omotoso Toyin and O Ibitoye.

#### VI. ACKNOWLEDGMENTS

The author sincerely appreciate the contributions of Engr. Obasanjo for his resourcefulness in driving the data feed for this research and the team of laboratory personnel at Landmark University, Omu-Aran, Kwara State for their invaluable support.

#### VII. REFERENCES

[1] WHO (2011) Guidelines for drinking-water: fourth edition. Site (<http://www.who.int>) Accessed 2012.

[2] WHO (2013) document on water quality and health strategies 2013-2020. Consultation on the Development of a Strategy on Water Quality and Health.

[3] [http://www.who.int/water\\_sanitation\\_health/dwq/en/](http://www.who.int/water_sanitation_health/dwq/en/). Retrieved from the net 2020.

[4] United Nations (UN) Commission on Sustainable Development. Comprehensive assessment of the freshwater resources of the World. Report of the Secretary General. New York, UN, 1997.33p.

[5] University of Michigan (2000). Human appropriation of World's fresh water supply. Science 271:785.

[6] Sharma, M.P., Singal, S.K and Patral, S (2008). Water Quality Profile of Yamuna River, India. Hydro Nepal. Issue No 3; 27-32.

[7] United Nations' World Water Development Report 4; Managing water under uncertainty and risk (2012). United Nations' World Water Development Report (2012) Open access publication of UNESCO. Retrieved 2020

[8] Pahl, R. (2004). History of Carson River Water Quality Standards- A supporting document for the Carson River Report Card. Carson City, NV, Nevada Division of Environmental Protection, Bureau of Water Quality Planning: 20.

[9] Campolo M., Andreussi P., Soldati A. (2002). Water quality control in the River Arno, technical note: Water Res. 36, 2673–2680.

[10] Heisler J., Glibert, P.M., Burkkolder, J.M., Anderson, D.M., Cochlan, W., Dennison, W.C., Dortch, Q., Gobler, C.J., Heil, C.A., Humphries, E., Lewtus, A., Magnien, R., Marshall, H.G., Sellner, K., Stockwell, D.A., Stoecker, D.K. and Suddleson M. (2008). Eutrophication and harmful algae blooms: A scientific consensus. Harmful algae8: 3-13.

[11] Herath Strikantha. (2008). Role Playing game approach to introduce complex water resources decision making process. United Nations University.

[12] Foster, I. D. L., and Charlesworth, S. M. (1996). Heavy metals in the hydrological cycle: Trends and explanation. Hydrological Processes, 10, 227–261.

[13] Haag, I., Kern, U., and Westrich, B. (2000). Assessing in-stream erosion and contaminant transport using the end member mixing analysis (EMMA). IAHS Publications, 263, 293–300.

[14] <https://www.environmentbuddy.com/the..calledfrom> the web .Mar 07, 2021.

[15] Department of Environment Food and Rural Affairs DEFRA (2014) Water Framework Directives implementation in England and Wales: new and updated standards to protect the water environment. <https://www.gov.uk/government/publications>.

[16] Christensen, V.G Bamussen, P.P and Ziegler, A.C (2008) Real-Time Water quality Monitoring and Regression Analysis to Estimate Nutrient and Bacteria Concentration in Kansas Stream. USGS Science for a Changing World.

[17] Gozzard, E, Mayes, I, W.M. Potter, H.A.B. Jarvis, A.P. (2011) Seasonal and spatial variation of diffuse (non-point) source zinc pollution in a historically metal mined river catchment, UK Journal of environmental pollution.

[18] Toyin Omotoso, 2016. Water quality profiling of Rivers in a data-poor region. PhD thesis submitted to the School of Mechanical Aerospace and Civil Engineering, The University of Manchester, UK.

[19] Asiedu, J.I (2014). A Preliminary Safety Evaluation of Polyhexamethylene Guanidine Hydrochloride. Interanational Journal of Toxicology.

[20] Ifabiyi, I. P., and Adedeji, A. O. (2014). Analysis of water poverty for Irepodun local government area (Kwara State, Nigeria). *Geography, Environment, Sustainability*, 7(4), 81-93.

[21] Elemile, O. O., Raphael, D. O., Omole, D. O., Oloruntoba, E. O., Ajayi, E. O., and Ohwavorua, N.A. (2019). Assessment of the impact of abattoir effluent on the quality of groundwater in a residential area of Omu-Aran, Nigeria. *Environmental Sciences Europe*, 31(1), 16.

[22] Abdus-Salam, N. (2016). Comparative Studies of Water and Sediment Qualities of Some Dams in Kwara State. *Fountain Journal of Natural and Applied Sciences*, 5(1).

[23] [www.thecable.ng/cholera-kwara-environmentalist](http://www.thecable.ng/cholera-kwara-environmentalist)

[24] [www.who.int/csr/don/12-july-2017-cholera-nigeria/en/](http://www.who.int/csr/don/12-july-2017-cholera-nigeria/en/).

[25] Nigeria Population Commission, (2018).

[26] Sojobi, A. O., Dahunsi, S. I., and Afolayan, A. O. (2015). Assessment of the efficiency of disinfection methods for improving water quality. *Nigerian Journal of Technology*, 34(4), 907-915.

[27] WHO and UNICEF, 2012. Progress on Drinking Water and Sanitation 2012.



ISSN ONLINE: 2447-0228



### RESEARCH ARTICLE

### OPEN ACCESS

## LIFE-CYCLE COST ANALYSIS (LCCA) COMPARISON OF PAVEMENTS (FLEXIBLE, RIGID AND RIGID-ADMIXED WITH COW BONE ASH)






Ariyo Adanikin<sup>\*1</sup>, Funsho Falade<sup>2</sup>, Adewale Olutaiwo<sup>3</sup>, Temi Ajibade<sup>4</sup> and Itunuoluwa Adeoye<sup>5</sup>

<sup>1,2,3</sup>Department of Civil and Environmental Engineering, University of Lagos, Akoka, Nigeria.

<sup>1</sup>Department of Civil Engineering, Elizade University, Ilara Mokin, Ondo State, Nigeria.

<sup>4</sup>Department of Accounting, Dominican University, Samonda Ibadan, Oyo State, Nigeria.

<sup>5</sup>Department of Business Admin., Elizade University, Ilara Mokin, Ondo State, Nigeria.

<sup>1</sup> <http://orcid.org/0000-0001-8455-1202> , <sup>2</sup> <http://orcid.org/0000-0003-1980-2014> , <sup>3</sup> <http://orcid.org/0000-0002-8097-9890> ,  
<sup>4</sup> <http://orcid.org/0000-0002-1657-7870> , <sup>5</sup> <http://orcid.org/0000-0002-5777-9233> 

Email: \*nukee02@gmail.com, ffallade@hotmail.com, adewaleolutaiwo@gmail.com, ajibade.t@dui.edu.ng, itunuoluwa63@gmail.com

### ARTICLE INFO

#### Article History

Received: May 14<sup>th</sup>, 2021

Accepted: August 25<sup>th</sup>, 2021

Published: August 31<sup>th</sup>, 2021

#### Keywords:

Life-Cycle Cost Analysis,  
Net Present Value,  
Cow Bone Ash,  
Cost Analysis,  
Pavement.

### ABSTRACT

Life Cycle Cost Analysis (LCCA) acts as a decision support tool in economic evaluation of cost (agency and user) during pavement type selection, maintenance and rehabilitation strategy. The Life cycle cost analysis was done using the Present worth of Cost method. Technical Recommendations for Highway (TRH) 12 (pavement rehabilitation investigation and design) analysis was used for calculating the agency cost which entailed the initial rehabilitation, maintenance, future and salvage cost. The LCCA analysis period for this study was taken as 40 years as the analysis period have to be sufficiently long to reflect long-term cost differences associated with reasonable design strategies. The result of the study shows that the present worth cost for the varying Pavement presents the options available for decision making. The result revealed that the initial cost of Rigid pavement is the highest followed by the initial cost of Rigid pavement with 15% CBA while flexible Pavement has the lowest initial cost. However, considering the result showing the present worth cost for the varying pavement types present worth cost of flexible pavement is the highest followed by Rigid pavement and Rigid pavement with 15% CBA has the lowest life cycle cost. The study recommended that Rigid pavement with 15% CBA should be considered because it gives the lowest life cycle cost and the initial cost is relatively low.



Copyright ©2016 by authors and Galileo Institute of Technology and Education of the Amazon (ITEGAM). This work is licensed under the Creative Commons Attribution International License (CC BY 4.0).

### I. INTRODUCTION

Road networks and transportation infrastructures play a significant role in the development of many countries across the globe. The increase in population growth and need for economic development had significantly contributed in the expansion of the road networks in particular highways road. Recently, road pavement construction, maintenance and rehabilitation costs are rising sporadically. As such, many highway agencies have employed tools and approaches that facilitate appropriate judgment making by applying economics and research like Life-Cycle Cost Analysis (LCCA) to attain economically reasonable long-run investments [1]. Accordingly, with respect to road construction,

life-cycle cost analysis (LCCA) is seen to having a higher priority than merely investments. Sustainability of transportation infrastructure is vital in enriching economy of developing countries hence the need for roads with long service life which requires less maintenance and able to sustain the country's traffic demands [2]. LCCA acts as a decision support tool in economic evaluation of cost (agency and user) during pavement type selection, maintenance and rehabilitation strategy. LCCA further provides better understanding on factors that influences cost effectiveness in pavement construction.

A pavement is a structure that comprises of superimposed layers of processed materials over a characteristic soil sub-grade, with the basic purpose of appropriating vehicle loads to the sub-



grade. There exists basically two types of pavements based on design considerations namely flexible and rigid pavements. Flexible pavements are pavements constructed from asphaltic or bituminous materials and aggregates while rigid pavements are pavement constructed from concrete or reinforced concrete slabs. Flexible pavements offers benefits such as low initial construction cost, absence of thermal stresses due to the pavements ability to expand and contract freely, does not require expansion joint, ability to be opened to traffic within a short time after construction, its surface can be milled and recycled for rehabilitation, it can be strengthened and improved in stages with the growth of traffic [3-6]. Construction of rigid pavements offer benefits such as reduction in greenhouse gas emissions (GHGs) due to use of pozzolanic materials such as cow bone ash (CBA), improves fuel saving [7-8], reduces accident due to less hydroplaning and enhanced night vision, and less traffic obstruction during frequent maintenance and rehabilitation works associated with flexible pavements [9]. [10] in their study considering vehicle type, annual average daily traffic, number and percentage vehicle composition stated that when a pavement condition is improved, an average of 124.41 minutes/day is saved annually by road users. [10] further revealed that for a 40 years pavement, 2.5 years is spent on maintenance and rehabilitation when it is a rigid pavement while 14 years is spent on maintenance and rehabilitation when it is a flexible pavement. This makes the effective years for the rigid pavement to be 37.5 years while that of the flexible pavement becomes 26 years.

Rigid pavements regardless suffer from Alkali-Silica Reaction (ASR) which is an internal expansion in concrete that leads to concrete deterioration. However, several studies such as [11-15] have shown using CBA to replace cement even in aggressive soil environments is good. [16] in their study reveals that replacement of cement with 15% CBA in concrete (rigid) pavements influences the densification of the rigid pavement at the transition zone, resulting in a much lower porosity. This further results in the rigid pavement having a tightly bound layer that repels ingress of water and thereby inhibiting cracks and gel formation as water is a contributing factor to the ASR in pavement. It is on this basis that this study evaluates rigid pavement with 15% CBA.

## II. LITERATURE REVIEW

LCCA according to [17] is defined as the process of accessing the economic performance of a structure over its entire life. Life cycle cost analysis (LCCA) according to [18] is defined as an evaluation technique that builds on the principles of economic analysis to determine the overall long term economic efficiency of alternative investment opportunities by trying to identify the best cost value for investment expenses. [19] defined LCCA as an early stage economic feasibility tool used to select an alternative pavement design which will result in reduction of costs of construction and maintenance and will also offer sufficient serviceability over the entire design life of the road. [20] stated that LCCA is used to explore trade-offs between low initial costs and long-term cost savings, identify the most cost-effective system, and determine how long incremental costs for infrastructural developments will be paid back. Costs evaluated using LCCA consists of agency and user costs. Agency costs includes preliminary engineering, contract administration, initial construction, construction supervision, maintenance costs, rehabilitation costs, administrative costs, salvage value and sunk costs. User costs includes road user cost, vehicle operating costs

and crash costs. Enhancing pavement condition offers various benefits for road users, socio-economic growth, vehicle time savings amongst several other benefits. [19] noted that economic assessment of alternatives that considers all of the significant costs of ownership over the useful life is essential. This includes; initial costs financing costs and maintenance costs.

LCCA is particularly necessary when project alternatives that fulfill the same performance requirements, but differ with respect to initial costs and operating costs. Life cycle cost analysis explains the economic assessment of highway upgrades during the initial stage and also for highway investment decisions overtime [1]. [21] states that LCCA includes all the phases, starting from materials procurement, through to design production, construction, maintenance, restoration, transportation, costs in the work zone, and ending with the recycling phase. The LCCA considered the costs related to raw materials, machinery, manpower, traffic management, and costs involved in lane closure. LCCA utilizes recycled asphalt which is economical and has eco-friendly benefits [22]. However, the cycle of cash flow is not restricted to the production of material and the materials' transportation, but it includes all life recycling and rehabilitation phases during the construction of pavements.

According to [23], the cost of road construction consists of design expenses, material extraction, construction equipment, maintenance and rehabilitation strategies, and operations over the entire service life. An economic analysis process known as Life-Cycle Cost Analysis (LCCA) is used to evaluate the cost-efficiency of alternatives based on the Net Present Value (NPV) concept. It is essential to evaluate the above-mentioned cost aspects in order to obtain optimum pavement life-cycle costs. However, pavement managers are often unable to consider each important element that may be required for performing future maintenance tasks. Over the last few decades, several approaches have been developed by agencies and institutions for pavement Life-Cycle Cost Analysis (LCCA). Findings from the study of [24] indicate that the estimation of initial bid prices is the major source of uncertainty, despite the regression analysis to reduce it. This can be a function of JPCP pavement which traditionally comes at a larger up-front cost, although it is expected to have significantly less rehabilitation costs than other pavement alternatives.

Posit that in order to determine the managerial consequences of the increase in operational and maintenance costs, the costs must be assessed using an asset management perspective [25]. Also, [26] posits that a life cycle costing system should include major variables that drive future costs in order to provide a framework for reducing the risk of under or overestimating the future costs for maintenance and rehabilitation aspects. In the same vein, [27] explained the economic aspects of Slovakia's pavement management system (PMS) - Road Network Management System (RNMS). The study revealed that economic efficiency is the criterion that enables the creation of insightful outputs like strategy for allocation of limited funds between particular road sections or the total funding amount is necessary.

## III. MATERIALS AND METHODS

The Life cycle cost analysis was done using the Present worth of Cost method. Technical Recommendations for Highway (TRH) 12 (pavement rehabilitation investigation and design) analysis was used for calculating the agency cost which entailed the initial rehabilitation, maintenance, future and salvage cost. Table 1 show the parameters used in the study.

Table 1: Parameters considered for the LCCA.

S/N	Pavement Parameters	Dimension
1	Road length	1000 m
2	Road width	7.3 m
3	Wearing course	40 mm (thick)
4	Binder course	60 mm (thick)
5	Base course	200 mm (thick)
6	Sub-base course	200 mm (thick)
7	Concrete surface course	225 mm (thick)

Source: Authors, (2021).

Cost calculations were based on the pavement layers and their dimensions. After cost determination of pavement initial, maintenance, rehabilitation, and salvage value costs for one kilometer, the present worth costs of the rigid and flexible pavements is calculated. The Net Present Worth formula which was used is shown in equation 1 and as used by [5].

$$PWC = I_c + [\sum_n^N M_c] \left[ \frac{1}{(1+i)^n} \right] + [\sum_n^N R_c] \left[ \frac{1}{(1+i)^n} \right] + [\sum_n^N F_c] \left[ \frac{1}{(1+i)^n} \right] - S_v \left[ \frac{1}{(1+i)^n} \right] \quad (1)$$

Where:  $I_c$  = Initial construction cost;  $M_c$  = Maintenance cost;  $R_c$  = Rehabilitation cost;  $F_c$  = Future cost;  $n$  = Number of years;  $N$  = Analysis period in years (40);  $i$  = Interest rate (5%).

The Life Cycle Cost Analysis (LCCA) analysis period for this study was taken as 40 years as the analysis period have to be

Table 2: Summary of Initial Cost for Pavements for road length of 9.413 KM.

Bill Nos.	Description	Total Cost (₹)		
		Flexible Pavement	Rigid Pavement	Rigid Pavement (with 15% CBA)
1	Preliminaries	110,000,000.00	110,000,000.00	110,000,000.00
2	Clearing and Earthworks	193,269,951.60	193,269,951.60	193,269,951.60
3	Pavement and Surfacing	802,173,086.00	1,286,803,426.08	1,177,659,690.08
	<b>Total</b>	<b>1,105,443,037.60</b>	<b>1,590,073,377.68</b>	<b>1,480,929,640.08</b>
	<b>Cost per km</b>	<b>117,437,909.91</b>	<b>168,923,125.22</b>	<b>157,328,125.00</b>

Source: Authors, (2021).

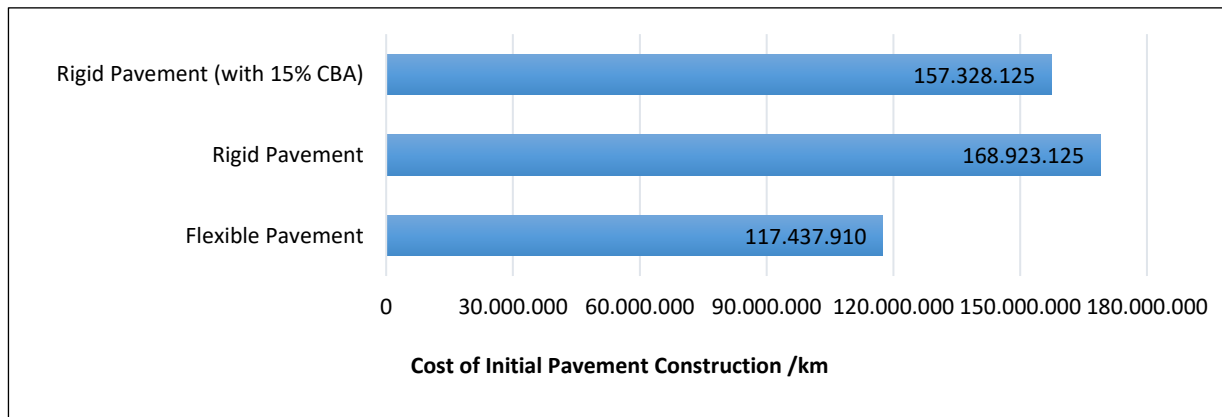


Figure 1: Initial cost comparison between Flexible and Rigid Pavement for a 1KM road section.

Source: Authors, (2021).

Figure 1 shows that the initial construction cost for flexible pavement (₹117,437,909.91) was lower than that of the rigid pavement without CBA replacement (₹168,923,125.22) by 30.5%.

sufficiently long to reflect long-term cost differences associated with reasonable design strategies. Furthermore, the analysis period should always be longer than the pavement design period which is usually 20 years for flexible pavements and 30 years for rigid pavements [28-29]. The FHWA’s September 1996 Final LCCA Policy statement recommends an analysis period of at least 35 years for all pavement projects, including new or total reconstruction projects as well as rehabilitation, restoration, and resurfacing projects [30].

Discounting factor  $\frac{1}{(1+i)^n}$  obtained at the end of the 40 years analysis period is 17.2.

Salvage cost was estimated based on the results of rehabilitation, maintenance, and future cost. Salvage cost was calculated using formula:

$$\text{Salvage Cost} = S_v = \left[ 1 - \left( \frac{A}{B} \right) \right] \times \text{Cost of overlay}$$

$S_v$  = Salvage value;  $A$  = Age of the overlay;  $B$  = Expected life of overlay

#### IV. RESULTS AND DISCUSSIONS

##### IV.1 DETERMINATION OF AGENCY COSTS

The initial construction cost of pavements was calculated after determining the materials quantity and cost breakdown for a 1km and 7.3 meter width road based on the typical road section of both pavement types. Summary of initial construction costs for the Flexible, Rigid and Rigid with 15% CBA replacement pavements is as shown in Table 2 and Figure 1.

Also, the initial construction cost of the flexible pavement is lower than that of the rigid pavement with 15% CBA replacement (₹157,328,125.00) by 25.4%.

**IV.2 FLEXIBLE PAVEMENT - AGENCY COST**

**IV.2.1 Rehabilitation Cost**

Rehabilitation Cost = Base + Sub-base + Binder + Wearing Cost  
 = 8,679,349.60 + 5,621,700.80 + 18,490,244.46 + 15,987,584.00  
 = ₺ 48,778,878.90

**IV.2.2 Maintenance Costs**

Asphalt Resurfacing (Once every decade = 4times) = ₺ 63,950,336.00

**IV.2.3 Future Cost**

Asphalt Resurfacing (After 1<sup>st</sup> decade, 2<sup>nd</sup> decade, 3<sup>rd</sup> decade and on the 35<sup>th</sup> year)  
 Total Future Cost= Rehabilitation Cost + Resurfacing(s)  
 = ₺ (48,778,878.90 + 63,950,336) = ₺ 112,729,215.00

**IV.2.4 Salvage Cost**

Total salvage cost = Conventional Rehabilitation + Conventional Maintenance Cost + Conventional Future Cost  
 Total Salvage Cost = ₺ (12,194,719.70 + 15,987,584 + 28,182,303.8) = ₺ 56,364,607.50

$$PWC = I_c + \left[ \sum_n^N M_c \right] \left[ \frac{1}{(1+i)^n} \right] + \left[ \sum_n^N R_c \right] \left[ \frac{1}{(1+i)^n} \right] + \left[ \sum_n^N F_c \right] \left[ \frac{1}{(1+i)^n} \right] - S_v \left[ \frac{1}{(1+i)^n} \right] \quad (2)$$

Flexible Pavement Initial Construction Cost = ₺117,437,909.91  
 PWC = 117,437,909.91 + [(48,778,878.90 + 63,950,336 + 112,729,215)(17.2)] - (56,364,607.5 × 17.2)  
 PWC = 117,437,909.91 + [(225, 458,430 × 17.2)] - (56,364,607.5 × 17.2)  
 PWC = 117,437,909.91 + 3,877,885,000 - 969,471,249  
 PWC = 3,995,322,909.91 - 969,471,249  
 PWC = ₺3,025,851,660.91

**IV.3 RIGID PAVEMENT - AGENCY COST**

**IV.3.1 Rehabilitation Cost**

Rehabilitation Cost = Base + Surface course costs  
 = ₺ (8,679,349.60 + 31,332,330.00) = ₺ 40,011,679.60

**IV.3.2 Maintenance Costs**

Concrete resurfacing (After 15<sup>th</sup>, 30<sup>th</sup> and on the 40<sup>th</sup> year) = ₺ 16,710,576.00

**IV.3.3 Future Cost**

Concrete resurfacing (After 15<sup>th</sup>, 30<sup>th</sup> and on the 40<sup>th</sup> year)  
 Total future cost = Rehabilitation cost + Resurfacing  
 = ₺ (40,011,679.60 + 16,710,576.00) = ₺ 56,722,255.60

**IV.3.4 Salvage Cost**

Total salvage cost = Conventional Rehabilitation + Conventional Maintenance Cost + Conventional Future Cost  
 Total Salvage Cost = ₺ (10,002,919.90 + 4,177,644.00 + 14,180,563.90) = ₺ 28,361,127.80

Rigid Pavement Initial Construction Cost = ₺ 168,923,125.22k

PWC = ₺[168,923,125.22+ [(40,011,679.60 + 16,710,576.00 + 56,722,255.60)(17.2)] - (28,361,127.80) (17.2)]  
 PWC = ₺ [168,923,125.22+ (113,444,511)(17.2) - (28,361,127.80) (17.2)]  
 PWC = ₺ [168,923,125.22+ 1,951,245,590 - 487,811,398]  
 PWC = ₺ [2,120,168,720 - 487,811,398]  
 PWC = ₺ 1,632,357,320

**IV.4 RIGID PAVEMENT WITH CEMENT AND 15% CBA - AGENCY COST**

**IV.4.1 Rehabilitation Cost**

Rehabilitation Cost = Base + Surface course costs  
 = ₺ (8,679,349.60 + 24,992,280.00) = ₺ 33,671,629.60

**IV.4.2 Maintenance Costs**

Concrete resurfacing (After 15<sup>th</sup>, 30<sup>th</sup> and on the 40<sup>th</sup> year) = ₺ 13,329,216.00

**IV.4.3 Future Cost**

Concrete resurfacing (After 15<sup>th</sup>, 30<sup>th</sup> and on the 40<sup>th</sup> year)  
 Total future cost = Rehabilitation cost + Resurfacing  
 = ₺(33,671,629.60 + 13,329,216.00) = ₺ 47,000,845.60

**IV.4.4 Salvage Cost**

Total salvage cost = Conventional Rehabilitation + Conventional Maintenance Cost + Conventional Future Cost  
 Total Salvage Cost = ₺ (8,417,907.40 + 3,332,304.00 + 11,750,211.40)  
 = ₺ 23,500,422.80

Rigid Pavement Initial Construction Cost = ₺ 157,328,125.00k  
 PWC = ₺ [157,328,125.00 + [(33,671,629.60 + 13,329,216.00 + 47,000,845.60)(17.2)] - (23,500,422.80) (17.2)]  
 PWC = ₺ [157,328,125.00 + (94,001,691.20)(17.2) - (23,500,422.80) (17.2)]  
 PWC = ₺ [157,328,125.00 + 1,616,829,090 - 404,207,272]  
 PWC = ₺ [1,774,157,220 - 404,207,272]  
 PWC = ₺ 1,369,949,950.00

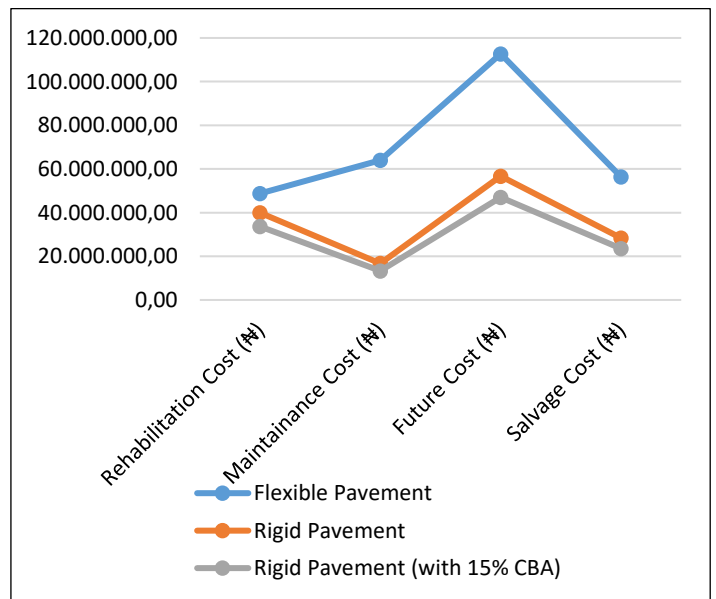


Figure 2: Agency costs for varying pavement types. Source: Authors, (2021).

Figure 2 show that the rehabilitation cost for flexible pavement was higher than that of the rigid pavement without CBA replacement and with 15% CBA replacement by 18.0% and 31.0% respectively. The maintenance cost for the flexible pavement was also higher by 73.9% and 79.2% for the rigid pavement without CBA replacement and with 15% CBA replacement respectively. The future and salvage costs also show an increase of 49.7% and 58.3% when comparing the flexible pavement and rigid pavement without CBA replacement and with 15% CBA replacement

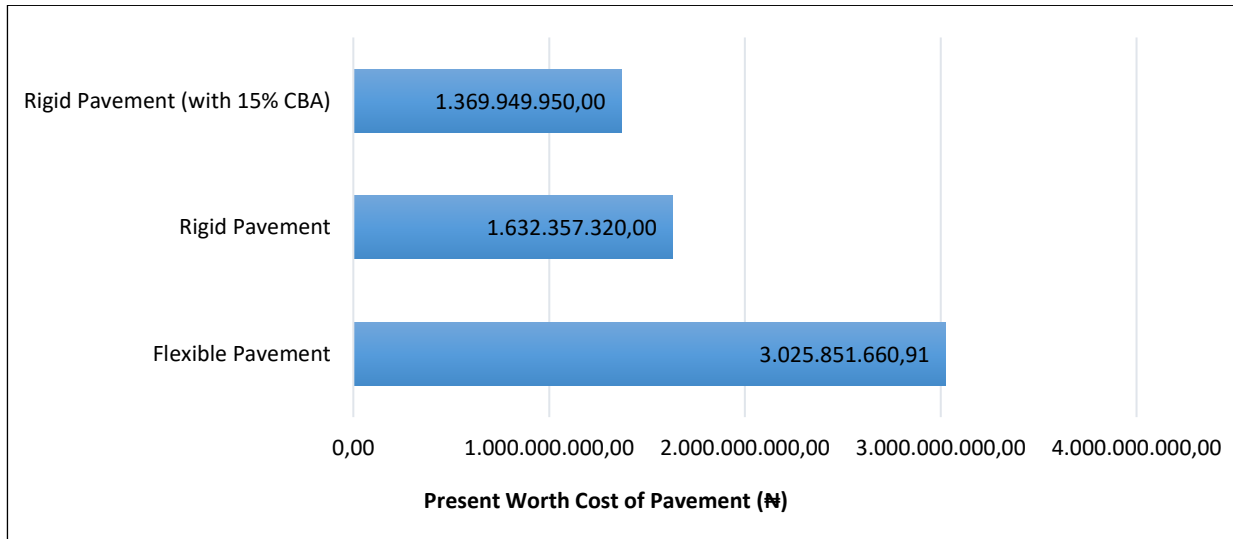


Figure 3: Present worth cost for the varying pavement types.  
Source: Authors, (2021).

The study reveals that the frequent periodic maintenance of flexible pavement causes its life cycle cost to increase significantly whereas rigid pavements do not need costly periodic maintenance. Furthermore, according to [2] rigid pavements follow the build and forget concept which eventually make it economically viable and sustainable type of pavement especially for developing countries such as Nigeria. The findings of this study supports the findings of [4] that posit that flexible pavements have lower initial construction cost, they require higher maintenance cost and lower life span when compared to rigid pavement. The findings of this study negates the findings of [31] whose economic analysis slightly shows higher lifecycle costs for rigid pavement when compared with flexible pavements.

## V. CONCLUSIONS

The study evaluated the life cycle costs analysis (LCCA) of three different pavements (flexible, rigid and rigid with 15% replacement of cement CBA). The result of the study shows that the present worth cost for the varying Pavement presents the options available for decision making. The result revealed that the initial cost of Rigid pavement is the highest followed by the initial cost of Rigid pavement with 15% CBA while flexible Pavement has the lowest initial cost. However, considering the result from Figure 3 present worth cost of flexible pavement is the highest followed by Rigid pavement and Rigid pavement with 15% CBA has the lowest life cycle cost. The reason for the high cost of flexible pavement is due to the fact that the frequent periodic maintenance of flexible pavement causes its life cycle cost to increase significantly whereas rigid pavements do not need costly periodic maintenance. Furthermore, rigid pavements follow the build and forget concept which eventually make it economically viable and sustainable type of pavement especially for developing

countries such as Nigeria. Therefore the study recommends rigid pavement with 15% CBA because it gives the lowest life cycle cost. Further studies should be extended to the life cycle assessment analysis (LCAA) by considering fuel consumption, CO<sub>2</sub> emissions, and pavement condition ratings for both flexible and rigid pavements.

Figure 3 reveals that the present worth cost of the flexible pavement (₦3,025,851,660.91) is 46.05% higher than the cost of the rigid pavement without CBA (₦ 1,632,357,320.00). The flexible pavement present worth cost is also 54.73% higher than the cost of the rigid pavement with 15% CBA (₦ 1,369,949,950.00).

countries such as Nigeria. Therefore the study recommends rigid pavement with 15% CBA because it gives the lowest life cycle cost. Further studies should be extended to the life cycle assessment analysis (LCAA) by considering fuel consumption, CO<sub>2</sub> emissions, and pavement condition ratings for both flexible and rigid pavements.

## VI. AUTHOR'S CONTRIBUTION

**Conceptualization:** Adanikin Ariyo and Falade Funsho.

**Methodology:** Ajibade Temi and Adewale Olutaiwo.

**Investigation:** Adanikin Ariyo and Adeoye Itunuoluwa.

**Discussion of results:** Adanikin Ariyo and Adeoye Itunuoluwa.

**Writing – Original Draft:** Adanikin Ariyo.

**Writing – Review and Editing:** Ajibade Temi and Adeoye Itunuoluwa.

**Resources:** Adanikin Ariyo and Falade Funsho.

**Supervision:** Falade Funsho and Adewale Olutaiwo.

**Approval of the final text:** Adanikin Ariyo and Falade Funsho.

## VII. REFERENCES

- [1] Gour, P., & Yadav, S. (2020). Pavement life cycle cost analysis: review and analysis by meta computing techniques. *International Journal of Core Engineering & Management*, 6(9), 23-41.
- [2] Hamim, O.F., Aninda, S.S., Hoque, M.S. & Hadiuzzaman, M. (2020). Suitability of pavement type for developing countries from an economic perspective using life cycle cost analysis. *International Journal of Pavement Research and Technology*, 14, 259-266. <https://doi.org/10.1007/s42947-020-0107-z>
- [3] Jain, S., Joshi, Y. P. & Goliya, S. S. (2013). Design of Rigid and Flexible Pavements by Various Methods & Their Cost Analysis of Each Method. *Int. Journal of Engineering Research and Applications*, 3(5), 119-123.



- [4] Mohod, M. V. & Kadam, K. N. (2016). A Comparative Study on Rigid and Flexible Pavement: A Review. *IOSR Journal of Mechanical and Civil Engineering (IOSR-JMCE)*, 13(3), 84-88. <https://doi.org/10.9790/1684-1303078488>
- [5] Yonas, K., Emer, T. Q. & Getachew, K. (2016). Cost and Benefit analysis of Rigid and Flexible Pavement: A case study at Chanco-Derba-Becho Road project. *International Journal of Scientific & Engineering Research*, 7(10), 181-188.
- [6] Skrzypczak, I., Radwański, W., and Pytlowany, T. (2018). Durability vs technical - the usage properties of road pavements. *E3S Web of Conferences*, 45, 1-8. <https://doi.org/10.1051/e3sconf/20184500082>
- [7] Bienvenu, M. & Jiao, X. (2013). Comparison of fuel consumption on rigid versus flexible pavements along I-95 in Florida. Paper presented at Florida International University, 1-15.
- [8] Indian Road Congress - IRC (2008). Tentative Guidelines for Conventional, Thin and Ultra-Thin White-Topping. IRC: SP: 76-2008, Indian Roads Congress, New Delhi.
- [9] Czarnecki, B., Bouteillier, C., & Gustafson, W. (2017). Life Cycle Cost Analysis Considerations in Pavement Type Selection in Red Deer and Construction Challenges. Conference of the Transportation Association of Canada, 1-7.
- [10] Katema, Y., Quezon, E. T. & Kebede, G. (2016). Cost and Benefit Analysis of Rigid and Flexible Pavement: A Case Study at Chanco –Derba-Becho Road Project. *International Journal of Scientific & Engineering Research*, 7(10), 181-188.
- [11] Akinyele, J. O., Adekunle, A. A., & Ogundaini, O. (2016). The Effect of Partial Replacement of Cement with Bone Ash and Wood Ash in Concrete. *Annals of Faculty Engineering Hunedoara – International Journal of Engineering*, 14(4), 199-204.
- [12] Lamidi I. O., Olomo R. O., Mujedu K. A. and Alao M. O. (2017). Evaluation of Rice Husk Ash and Bone Ash Mixed as Partial Replacement of Cement in Concrete. *International Conference of Science, Engineering & Environmental Technology*, 2(34), 258-264.
- [13] Okeyinka, O. M., Olutoge, F. A. & Okunlola, L. O. (2018). Durability Performance of Cow-Bone Ash (CBA) Blended Cement Concrete in Aggressive Environment. *International Journal of Scientific and Research Publications*, 8(12), 37-40.
- [14] Olutaiwo, A. O., Yekini, O. S. & Ezegbunem, I. I. (2018). Utilizing Cow Bone Ash (CBA) as Partial Replacement for Cement in Highway Rigid Pavement Construction. *SSRG International Journal of Civil Engineering*, 5(2), 13-19.
- [15] Modupe, A. E., Olayanju, T. M. A., Atoyebi, O. D., Aladegboye, S. J., Awolusi, T. F., Busari, A. A., Aderemi, P. O., & Modupe, O. C. (2019). Performance evaluation of hot mix asphaltic concrete incorporating cow bone ash (CBA) as partial replacement for filler. *IOP Conf. Series: Materials Science and Engineering*, 640, 1-18. <https://doi.org/10.1088/1755-1315/665/1/012057>
- [16] Adanikin, A., Falade, F. & Olutaiwo, A. (2020). Microstructural Analysis of Concrete Using Cow Bone Ash for Alkali-Silica Reaction (ASR) Suppression. *Journal of Casting & Materials Engineering*, 4(2), 34-40. <https://doi.org/10.7494/jcme.2020.4.2.34>
- [17] Gaikwad, T., Patil, L.R., Zinjade, R., Sisode, V., Rajput, S., & Mahajan, S. (2020). Life cycle cost analysis of road pavements. *International Journal of Engineering Research & Technology*, 8(12), 700-702. <http://dx.doi.org/10.17577/IJERTV8IS120311>
- [18] FHWA SA-98-079 (2000). Life-cycle cost analysis in pavement analysis. Retrieved from: [www.fhwa.dot.gov/infrastructure/asstmgmt/lcca.htm](http://www.fhwa.dot.gov/infrastructure/asstmgmt/lcca.htm).
- [19] Akhai, M. M. S., Ahmed, A. S. & Siddesh, K. P. (2016). Life Cycle Cost Analysis of Road Pavements in Rural Areas. *International Journal of Science Technology and Management*, 5(8), 260 - 267.
- [20] Kale, P. B., Aher, M. C. & Aher, P. D. (2016). Life Cycle Cost Analysis of Rigid and Flexible Pavements. *International Journal of Advanced Technology in Engineering and Sciences*, 4(12), 340-348.
- [21] Rafiq, W.; Musarat, M.A.; Altaf, M.; Napiyah, M.; Sutanto, M.H.; Alaloul, W.S.; Javed, M.F.; Mosavi, A. (2021) Life Cycle Cost Analysis Comparison of Hot Mix Asphalt and Reclaimed Asphalt Pavement: A Case Study. *Sustainability*, 13(4411), 1-14. <https://doi.org/10.3390/su13084411>
- [22] Qiao, Y.; Dave, E.; Parry, T.; Valle, O.; Mi, L.; Ni, G.; Yuan, Z.; & Zhu, Y. (2019). Life Cycle Costs Analysis of Reclaimed Asphalt Pavement (RAP) Under Future Climate. *Sustainability*, 11, 5414. <https://doi.org/10.3390/su11195414>
- [23] Babashamsi, P. Md Yusoff, N. Halil Ceylan, H. Md Nor, N. Hashem Salarzadeh Jenatabadi, H. S. (2016). Evaluation of pavement life cycle cost analysis: Review and analysis, *International Journal of Pavement Research and Technology*, 9(4), 241-254.
- [24] Swei, O., Gregory, J. & Kirchain, R. (2015). Probabilistic life-cycle cost of pavements: Drivers of Variation and Implications of Context. Transportation research record: *Journal of the Transportation Research Board*, 2523(1), 47-55.
- [25] Rasane, K., & Ambre, H. (2019). A study on life cycle cost analysis for roads. *International Research Journal of Engineering and Technology (IRJET)*, 6(5), 7652-7655.
- [26] Mirzadeh, I., Butt, A. A., Toller, S. & Birgisson, B. (2014). Life cycle cost analysis based on the fundamental cost contributors for asphalt pavement. *Structure and Infrastructure Engineering*, 10(12), 1638-1647 <http://dx.doi.org/10.1080/15732479.2013.837494>
- [27] Mikolaj, J., & Remek, L. (2014). Life cycle cost analysis- Integral part of Road network management system. *Procedia Engineering*, 91, 487 – 492. <http://dx.doi.org/10.1016/j.proeng.2014.12.031>
- [28] Anderson, R. O. (2020). Rigid versus flexible pavement design. Retrieved from: <https://www.roanderson.com/2011/12/22/rigid-versus-flexible-pavement-design/#:~:text=Design%20life%20typically%2010%20E2%80%9320,Hig her%20maintenance%20costs>
- [29] Mugdha, P. (2020). Highway Pavements: Design, Types, Flexible and Rigid Pavement and Notes. Retrieved from: <https://www.engineeringenotes.com/transportation-engineering/highway-pavement/highway-pavements-design-types-flexible-and-rigid-pavement-and-notes/48847>.
- [30] Walls, J. and M. R. Smith. (1998). Life-Cycle Cost Analysis in Pavement Design—Interim Technical Bulletin. Federal Highway Administration, Washington, DC.
- [31] Kristowski, A., Grzyl, B., Kurpinska, M. & Pszczola, M. (2018). The rigid and flexible road pavements in terms of life cycle costs. *Proceedings of the Creative Construction Conference*, 226-233. <http://dx.doi.org/10.3311/CCC2018-030>